Scuola Internazionale Superiore di Studi Avanzati - Trieste

Scuola Internazionale Superiore di Studi Avanzati

The Abdus Salam
International Centre for Theoretical Physics

Higgs Mass and QCD Axion Properties at High Precision

Candidate: Javier Pardo Vega

Supervisor: Prof. Giovanni Villadoro

Thesis submitted for the degree of
Doctor Philosophiae

Trieste, Italy, August 2016.

SISSA - Via Bonomea 265 - 34136 TRIESTE - ITALY

Scuola Internazionale Superiore di Studi Avanzati

The Abdus Salam
International Centre for Theoretical Physics

Higgs Mass and QCD Axion Properties at High Precision

Candidate: Javier Pardo Vega

Supervisor: Prof. Giovanni Villadoro

Thesis submitted for the degree of
Doctor Philosophiae

Trieste, Italy, August 2016.

Acknowledgements

First of all, I would like to thank my supervisor Giovanni Villadoro. I have learned a lot from him about physics and how to do scientific research. These years of collaboration have been a great experience for me.

I would like to thank Emanuele Bagnaschi, Giovanni Grilli di Cortona, Edward Hardy and Pietro Slavich for fruitful collaborations.

I would also like to thank Luis Aparicio and Juan Carlos Vasquez Carmona for useful discussions.

I would like to thank Fernando Quevedo for being very supportive with all the students. I would also like to thank the ICTP family for creating an excellent environment and to the SISSA profesors for his teachings.

Special thanks to my family and friends which are an essential source of inspiration and motivation for me.

Abstract

This thesis is dedicated to study the physical properties at high precision of two scalars of well-motivated beyond the standard model theories: the Higgs boson in the Minimal Supersymmetric Standard Model (MSSM) and the axion of the Peccei-Quinn mechanism. The discussion is divided in two parts. We make use of the advantages of the effective field theory framework.

In the first part, we consider the state-of-the-art of the effective field theory computation of the MSSM Higgs mass, improving the existing ones by including extra threshold corrections. We perform a detailed estimate of the theoretical uncertainty. We study the large $\tan\beta$ region and we put emphasis on the allowed parameter space reproducing the experimental value of the Higgs mass. We present SusyHD, a fast computer code that computes the Higgs mass and its uncertainty for any supersymmetry (SUSY) scale, from the TeV to the Planck scale, even in Split SUSY, both in the $\overline{\text{DR}}$ and in the on-shell (OS) schemes. Finally, we apply our results to derive bounds on some well motivated SUSY models, in particular we show how the value of the Higgs mass allows to determine the complete spectrum in minimal gauge mediation.

In the second part, we discuss how to extract several properties of the axion of Quantum Chromodynamics (QCD) with great accuracy using only first principle QCD computations. We obtained the axion potential, the mass and the coupling to photons by combining next to leading order (NLO) calculations in chiral perturbation theory (ChPT) with recent Lattice QCD results. Axion-nucleon interactions are also derived reliably. The method we have followed allows to further improve the precision as uncertainties on the light quark masses and the effective field theory couplings are reduced. We have also studied the finite temperature dependence of the axion potential and its mass, in connection with its role in determining the axion relic abundance.

Original material contained in this thesis is based on the results published in refs. [1, 2]. Some recent improvements on the Higgs mass calculation in the effective field theory approach presented here are in preparation for publication.

Contents

Part I

MSSM Higgs mass

Introduction

With the recent discovery of the Higgs boson the last missing piece of the Standard Model (SM) has been unveiled and all the parameters of the theory measured. The success of the Standard Model in describing all the measured observables at colliders contrasts with the failure of the theory to explain some non-collider observations, such as Dark Matter (DM), matter-antimatter asymmetry, etc.

Among the various completions of the Standard Model proposed so far, supersymmetric (SUSY) theories remain the most attractive option. Not only they screen the electroweak (EW) scale from ultraviolet (UV) sensitivity to new physics thresholds but they successfully predict the unification of gauge couplings and may provide with a natural WIMP dark matter candidate.

Indirect hints for a small hierarchy between the scales of electroweak and supersymmetry restoration (e.g. flavor observables, searches for electric dipole moments (EDMs)), have found stronger support from the recent discovery of a moderately heavy SM-like Higgs [3, 4] and from the absence of any evidence of superpartners at run I of the LHC (see e.g. [5, 6]).

While the scale of supersymmetry may still be low (there are still various arguments in favor of this scenario), hopefully within the reach of the LHC run II, it is fair to say that our confidence in predicting the new physics scale based on naturalness arguments weakened substantially [7, 8]. The suspicion that other mechanisms may explain the strength of the weak interactions is becoming stronger and alternative scenarios to low energy SUSY already exist [9, 10]. It is thus useful to look for different (more-experimentally-driven) methods to infer the scale of the superpartners. One natural candidate is the value of the Higgs mass, which in supersymmetry is calculable in terms of the couplings and the soft SUSY breaking parameters.

In particular, in the Minimal Supersymmetric Standard Model (MSSM) the tree-level Higgs mass is predicted to lie below the Z-boson mass up to quantum corrections logarithmically sensitive to the SUSY breaking scale. Therefore the measured value of the Higgs mass gives non-trivial constraints on the spectrum

and couplings of the MSSM, allowing to shrink the allowed energy range for the superpartners.

The Higgs mass has been measured experimentally with a great accuracy $m_h = 125.09(24)$ GeV [11]. Radiative corrections are needed to reproduce this value within the MSSM. When applying the Higgs mass constraint to reliably determine the allowed parameter space of the theory, one needs a high precision calculation. Indeed there has been exceptional progress in the Higgs mass computation, using different methods and renormalization schemes. Some of the calculations are performed at fixed order, thus they are not valid for a SUSY scale above the TeV where the logarithmic terms need to be resummed. Besides, some of the calculations and computer codes disagree among themselves, and in some cases the differences can not be explained in terms of the estimated theoretical uncertainties.

Motivated by the important role of the Higgs mass in constraining SUSY models, the limitations of the existing codes compared to the allowed parameter space and the disagreements in the literature, we decided to revisit the computation. Particular attention is dedicated to the relevant parameter space consistent with the Higgs mass value, to the analysis of the uncertainties and to the possible origin of the differences with other methods. Exploiting the mass gap suggested by the absence of superpartners at the LHC and the largish value of the Higgs mass, we recompute the Higgs mass in the MSSM using the effective field theory (EFT) approach. This method allows to systematically resum large logarithms, to have arbitrary large hierarchies in the spectrum and to have simple physical understanding of the results as one neglects subleading effects suppressed by the SUSY scale.

This part contains three chapters. In the first chapter, we present basic topics on the MSSM. It is followed by a more specific analysis on the state of the art of the MSSM Higgs mass calculation in chapter 2. These two chapters help to understand chapter 3 where the original results are presented.

Chapter 1

Aspects of the MSSM

In this chapter we describe some basic topics of the minimal supersymmetric standard model which are useful for this part of the thesis. We do not aim to present a detailed discussion, since there are excellent reviews and books about SUSY in general (see eg. [12, 13]), and about the MSSM and its phenomenology (see eg. [14]).

We start presenting some motivations of why supersymmetry may be realized in nature in section 1.1. In section 1.2 we describe how invariance under supersymmetry transformations determine the general form of the Lagrangian in renormalizable theories. In section 1.3 we review the minimal supersymmetric extension of the Standard Model (SM). In particular we present how the SM particles are accommodated into representations of SUSY, the particle interactions fixed by SUSY, the effective Lagrangian containing the soft SUSY breaking terms whose existence is required by observations, the renormalization group equations and the mass spectrum.

In section 1.4 we consider how SUSY breaking may be communicated to the observable sector and discuss some models that have interesting phenomenology. Finally, in section 1.5 we describe the current experimental limits on SUSY. They are based on direct searches at the Large Hadron Collider (LHC), measurements of low energy observables, and the role that may play the MSSM in providing a dark matter candidate.

1.1 Motivation for Supersymmetry

One of the current theoretical hints suggesting physics beyond the Standard Model comes from the approximate gauge couplings unification in the SM. With

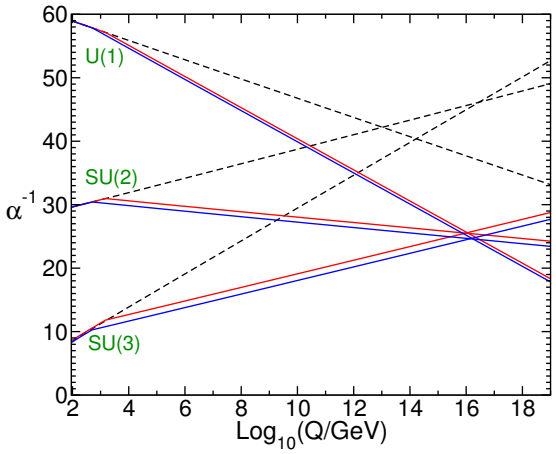

Figure 1.1: Evolution of the inverse gauge couplings in the Standard Model (dashed lines) and the MSSM (solid lines) according to the two loop renormalization group equations. To draw the MSSM curves, the supersymmetric particles are treated as a common threshold varied between 0.5 TeV and 1.5 TeV, and the input value $\alpha_3(m_Z)$ is varied between 0.117 and 0.121 (figure taken from [14]).

only the SM matter content they do not really unify, because α_2 and α_3 meet at $\sim 10^{16}$ GeV, while α_1 meets α_2 at $\sim 10^{13}$ GeV as shown in fig. 1.1; and perturbative threshold corrections can not cure the lack of unification unless they are anomalously large. For instance, the minimal $SU(5)$ grand unified theory (GUT) faces this problem, together with a prediction of too short proton lifetime, i.e. excluded experimentally. Then, one needs additional field content in the theory which handles unification and a consistent prediction for proton decay.

The MSSM naturally predicts unification of the gauge couplings at a scale $M_U \sim 2\times 10^{16}$ GeV within threshold effects (see fig. 1.1) and renders proton decay compatible with the experimental limits. In particular, fermion superparticles with masses near the TeV guarantees unification regardless of the scalar masses.

Another important implication of SUSY is that it may provide a well-motivated dark matter candidate. At present, the existence of dark matter is well established. We have convincing evidence from the observation of luminous objects (stars, gas clouds, globular cluster, or galaxies) moving faster than one would expect if they only felt the gravitational attraction of other visible objects. The lightest neutralino, usually the lightest supersymmetric particle (LSP), in models with exact R-parity (which guarantees its stability) is a weakly interacting massive particle (WIMP) that generically leads to the correct order of magnitude of the observed dark matter relic density.

There are also more theoretical reasons for SUSY. The direct product of the supersymmetric version of the Poincaré group (known as super-Poincaré) and some internal symmetry group is the most general symmetry of the $S-$matrix (see more details in section 1.2). One could expect that all possible kind of allowed symmetries might be realized in nature.

Among the first works on Supersymmetry are those which appeared in the context of the foundations of String Theory [15]. In fact, SUSY is an essential ingredient for superstring theory.

In the absence of clear experimental inputs, physicists need a guiding principle when trying to construct new theories and make predictions. The naturalness criterion has played a significant role in particle physics. A possible definition of the naturalness criterion by 't Hooft [16] is as follows. Consider a theory valid up to a maximum energy Λ and make all its parameters dimensionless by measuring them in units of Λ. One such parameters is allowed to be much smaller than unity only if setting it to zero increases the symmetry of the theory. If this does not happen, the theory is unnatural.

In the Standard model, the potential for the Higgs doublet is

$$V(H) = \frac{\lambda}{2}\left(H^\dagger H - \frac{v^2}{2}\right)^2, \tag{1.1}$$

which implies a non-vanishing vacuum expectation value (VEV) denoted as v for H at the minimum and a mass squared of the physical Higgs field $m_h^2 = \lambda v^2$. With this normalization the value of the Higgs VEV is $v \approx 246$ GeV. Nowadays we know the experimental value of the Higgs mass with a precision better than 0.2%, $m_h = 125.09 \pm 0.24$ GeV [11]. Note that no symmetry is recovered when the Higgs mass is set to zero in the SM.

The squared mass of the Higgs field receives quantum corrections, which are quadratically sensitive to new mass thresholds at high scale. For example, consider a heavy complex scalar S with mass m_S that couples to the Higgs through the interaction term $-\lambda_S |H|^2 |S|^2$ in the Lagrangian. One-loop corrections induced by the scalar S are given by

$$\Delta m_h^2 = \frac{\lambda_S}{16\pi^2}\left[-2m_S^2 \ln\left(\frac{Q}{m_S}\right)\right], \tag{1.2}$$

where we have used the $\overline{\text{MS}}$ scheme and Q is the renormalization scale.

As a consequence of this quadratic sensitivity to new physics at high scale, the large separation between the Planck scale $M_p = (8\pi G_{\text{Newton}})$ and the electroweak (EW) scale is a disturbing fact, known as the hierarchy problem [17]. However this is not an inconsistency of the theory. But for a natural theory one would

expect new physics at the TeV scale or even below, at energies already explored at the Large Hadron Collider (LHC). The lack of experimental signatures at the TeV scale already leads to a little hierarchy problem.

If there are no new degrees of freedom with masses $M \gg$ TeV then there is no hierarchy problem. This seems in contradiction with the the hints of physics at high scales such as neutrino masses, gauge coupling unification and the need of a UV completion of gravity.

There are some possible solutions to the hierarchy problem. If the Higgs boson is not a fundamental scalar but a composite instead, the radiative corrections to its mass would be cutoff by the compositeness scale. However, if it is fundamental, a solution of the hierarchy problem needs the existence of a symmetry that protects the Higgs mass from quantum corrections. Supersymmetry provides a solution; it transforms a bosonic state into a fermionic state (whose mass is protected by chiral symmetry) and arranges the cancellation of quadratically sensitive corrections to scalar masses.

Despite the naturalness principle has worked for most of the phenomena in nature, it has failed to explain the smallness of the cosmological constant which produces a hierarchy of at least 60 orders of magnitude more severe. Similarly to the cosmological constant problem, the naturalness principle might not be applicable to the Higgs mass and a different kind of explanation might exist for the hierarchy problem. This idea is also suggested by the absence of new physics at the TeV scale. In this thesis we explore a different method to infer the new physics scale based on the constrain imposed by the Higgs mass on SUSY models.

1.2 Construction of SUSY Lagrangians

In relativistic quantum field theory, the most general group of bosonic symmetries of the $S-$matrix is the direct product of the Poincaré group with an internal symmetry group. Moreover, the internal symmetry group must be the direct product of a compact semisimple group with some abelian factors. This result is known as the Coleman-Mandula theorem [18]. Its proof is based on general physical assumptions and considers only Lie groups of symmetries. Therefore, it does not exclude the possibility of fermionic generators, although severely restricts them. Allowing for fermionic generators, it was shown by Haag, Lopuszanski and Sohnius [19] that the most general graded Lie algebra of symmetries of the S-matrix is the super-Poincaré group times the algebra of internal symmetries.

The supersymmetry algebra is classified in terms of the number of fermionic generators $\mathcal{N}$. We focus on the case $\mathcal{N} = 1$ of simple or unextended supersymmetry. In that case, the R-symmetry stands out, which is a $U(1)$ (chiral) symmetry

group characterized for being the only internal symmetry non-commuting with the generators of the supersymmetry transformations.

There are excellent reviews and books on SUSY in general (see e.g. [12] and [13]). For a comprehensive and pedagogical lectures notes, see for instance [20]. The most used introduction to the MSSM and its phenomenology is presented in Martin's review [14].

There is an elegant and powerful framework to formulate supersymmetric theories in terms of an extension of space-time known as superspace. Points in superspace are labeled with coordinates x^μ, associated to the generators of translations, and 2+2 additional anticommuting Grassman coordinates θ_α, $\overline{\theta}_{\dot{\alpha}}$, associated with the supersymmetry generators Q_α, $\overline{Q}_{\dot{\alpha}}$. This makes a total of eight coordinates $(x^\mu, \theta_\alpha, \overline{\theta}_{\dot{\alpha}})$. The representation of fields in superspace, which are functions of the coordinates $(x^\mu, \theta_\alpha, \overline{\theta}_{\dot{\alpha}})$, are known as superfields. Then, supersymmetric actions can be written as integrals over the superspace. We do not describe this formalism here, but we focus on the implications of SUSY for field theories.

In $\mathcal{N} = 1$ global supersymmetry there are two types of supermultiplets: the chiral or matter multiplet and the gauge or vector multiplet. If the theory includes gravity, it contains in addition the gravitino and the graviton multiplet.

A chiral supermultiplet Φ_i consists of a complex scalar ϕ_i and a left-handed Weyl fermion ψ_i as physical degrees of freedom, plus a non-propagating complex auxiliary field F_i that guarantees that SUSY closes off-shell, $\Phi_i = (\phi_i, \psi_i, F_i)$. We suppose that we have a collection of chiral superfields labeled by the index i, representing all flavor and gauge degrees of freedom. The matter fields of the SM are contained in chiral supermultiplets.

A vector or gauge supermultiplet V is the supersymmetric analogue of a spin one field. It contains as physical degrees of freedom a massless gauge boson A^a_μ, a Weyl fermion λ^a called gaugino, and one real scalar auxiliary field D^a, necessary for consistency of the supersymmetry algebra off-shell, $V = (A^a_\mu, \lambda^a, D^a)$. The index a runs over the adjoint representation of the gauge group. In the MSSM there is one vector superfield for each simple factor of the SM group $SU(3) \times SU(2) \times U(1)$.

Consider chiral supermultiplets $\Phi_i = (\phi_i, \psi_i, F_i)$ transforming under the gauge group in a representation with hermitian matrices $(T^a)^j_i$. All the field components of the chiral superfields must transform in the same representation because gauge transformations and supersymmetry commute. Under supersymmetry transformations the fields transform as

$$\delta\phi_i = \epsilon\psi_i \,, \tag{1.3}$$

$$\delta\psi_{i\alpha} = -i(\sigma^\mu\epsilon^\dagger)_\alpha\, \nabla_\mu\phi_i + \epsilon_\alpha F_i\,, \tag{1.4}$$

$$\delta F_i = -i\epsilon^\dagger\overline{\sigma}^\mu\nabla_\mu\psi_i \;+\; \sqrt{2}g(T^a\phi)_i\,\epsilon^\dagger\lambda^{\dagger a}\,, \tag{1.5}$$

$$\delta A^a_\mu = -\frac{1}{\sqrt{2}}\left(\epsilon^\dagger\overline{\sigma}_\mu\lambda^a + \lambda^{\dagger a}\overline{\sigma}_\mu\epsilon\right)\,, \tag{1.6}$$

$$\delta\lambda^a_\alpha = \frac{i}{2\sqrt{2}}(\sigma^\mu\overline{\sigma}^\nu\epsilon)_\alpha\, F^a_{\mu\nu} + \frac{1}{\sqrt{2}}\epsilon_\alpha\, D^a\,, \tag{1.7}$$

$$\delta D^a = \frac{i}{\sqrt{2}}\left(-\epsilon^\dagger\overline{\sigma}^\mu\nabla_\mu\lambda^a + \nabla_\mu\lambda^{\dagger a}\overline{\sigma}^\mu\epsilon\right)\,, \tag{1.8}$$

where ϵ^α is an infinitesimal, anticommuting, two-component Weyl fermion parameterizing the supersymmetry transformation and $\overline{\sigma}^\mu \equiv (\mathbb{I}, -\sigma^1, -\sigma^2, -\sigma^3)$, where $\mathbb{I}$ is the 2×2 identity matrix and σ^j are the Pauli matrices. We denote the covariant derivative by ∇, e.g. acting on the scalars it gives

$$\nabla_\mu\phi_i = \partial_\mu\phi_i - ig_a A^a_\mu T^{aj}_i\phi_j. \tag{1.9}$$

The most general renormalizable Lagrangian for chiral and gauge supermultiplets invariant under SUSY transformations has the form

$$\begin{aligned}\mathcal{L} =& \nabla^\mu\phi^{*i}\nabla_\mu\phi_i + i\psi^{\dagger i}\overline{\sigma}^\mu\nabla_\mu\psi_i - \frac{1}{4}F^a_{\mu\nu}F^{\mu\nu a} + i\lambda^{\dagger a}\overline{\sigma}^\mu\nabla_\mu\lambda^a \\ &- \left(\frac{1}{2}W^{ij}\psi_i\psi_j + \text{h.c.}\right) - \sqrt{2}g(\phi^*T^a\psi)\lambda^a - \sqrt{2}g\lambda^{\dagger a}(\psi^\dagger T^a\phi) - V(\phi,\phi^*)\,,\end{aligned} \tag{1.10}$$

with scalar potential

$$V(\phi,\phi^*) = F^{*i}F_i + \frac{1}{2}D^aD^a = W^*_iW^i + \frac{1}{2}g_a^2(\phi^*T^a\phi)^2\,. \tag{1.11}$$

Here we have used the classical equations of motion to write the auxiliary fields F_i, F^{*i} and D^a in terms of the scalar fields, there is an implicit sum over repeated indices i, and the index a is summed over all the simple factors with different gauge couplings g_a of the gauge group of the theory. The non-gauge interactions for chiral supermultiplets (invariant under SUSY transformations) are determined by a single holomorphic function of the complex scalar fields (or the chiral superfields), called the superpotential W. A general renormalizable superpotential reads

$$W = L^i\phi_i + \frac{1}{2}M^{ij}\phi_i\phi_j + \frac{1}{6}y^{ijk}\phi_i\phi_j\phi_k, \tag{1.12}$$

where the couplings L^i have $(\text{mass})^2$ dimension, M^{ij} is a symmetric mass matrix for the fermions, and y^{ijk} is a Yukawa coupling $\psi_i\psi_j\phi_k$ which is totally symmetric in all its indices. The linear superpotential term can only exists if there is a gauge

singlet, thus it is not relevant for the MSSM where there are no gauge singlet chiral multiplets. We also use the notation

$$W^i = \frac{\delta W}{\delta \phi_i}\,, \qquad W^{ij} = \frac{\delta^2 W}{\delta \phi_i \delta \phi_j}\,. \tag{1.13}$$

The first line in eq. (1.10) contains the kinetic terms and the ordinary gauge interactions determined by the covariant derivative. Recall that we neglect the linear term in the superpotential (1.12), then the terms in brackets in the second line of eq. (1.10) generate mass matrices for the fermions and Yukawa couplings, and the next two terms are the gaugino-scalar-fermion interactions fixed by gauge invariance in SUSY. As we see in eq. (1.11) the scalar potential receives *F-term* and *D-term* contributions and it is always non-negative. The *F-term* contribution induces (scalar)^4 and (scalar)^3 interactions proportional to the Yukawa couplings y^{ijk} and the product of the Yukawa couplings and the fermion mass matrices respectively; while the *D-term* produces quartic interactions controlled by the gauge couplings.

1.3 The MSSM

Supersymmetric extensions of the SM requires that each known fundamental particle belongs to a chiral or a gauge supermultiplet and have associated a superpartner with spin differing by half. Here we describe how the SM particles are accommodated into supermultiplets (or superfields). The SM fermions (quarks and leptons) must pertain to chiral supermultiplets because their left-handed components transform differently under the gauge group than their right-handed ones, and there must be a separate chiral supermultiplet for each component. The spin-0 partners of the SM fermions are named by prepending an "s" which stands for scalar. That is, they are called squarks and sleptons, or sfermions to refer to all of them. We denote the superpartners of SM particles with the same symbol but with a tilde added.

The Higgs scalar boson must be a member of a chiral superfield because it has spin 0. However, one needs necessarily to introduce another chiral supermultiplet for two reasons. First, the fermionic partner of the Higgs chiral superfield will spoil the cancellation of the gauge anomalies of the SM because it is a weak isodoublet with hypercharge $Y = 1/2$ or $Y = -1/2$. One can preserve the cancellation of gauge anomalies by introducing two Higgs supermultiplets with opposite hypercharge $Y = \pm 1/2$. Second, the structure of supersymmetry implies that one needs two different chiral supermultiplets to give masses to up-type

Chiral supermultiplets				
Names		spin 0	spin 1/2	$SU(3)_C$, $SU(2)_L$, $U(1)_Y$
squarks, quarks	Q	$(\widetilde{u}_L \;\; \widetilde{d}_L)$	$(u_L \;\; d_L)$	$(\mathbf{3}, \mathbf{2}, \frac{1}{6})$
(3 families)	$\overline{u}$	$\widetilde{u}^*_R$	$u^\dagger_R$	$(\overline{\mathbf{3}}, \mathbf{1}, -\frac{2}{3})$
	$\overline{d}$	$\widetilde{d}^*_R$	$d^\dagger_R$	$(\overline{\mathbf{3}}, \mathbf{1}, \frac{1}{3})$
sleptons, leptons	L	$(\widetilde{\nu} \;\; \widetilde{e}_L)$	$(\nu \;\; e_L)$	$(\mathbf{1}, \mathbf{2}, -\frac{1}{2})$
(3 families)	$\overline{e}$	$\widetilde{e}^*_R$	$e^\dagger_R$	$(\mathbf{1}, \mathbf{1}, 1)$
Higgs, higgsinos	H_u	$(H_u^+ \;\; H_u^0)$	$(\widetilde{H}_u^+ \;\; \widetilde{H}_u^0)$	$(\mathbf{1}, \mathbf{2}, +\frac{1}{2})$
	H_d	$(H_d^0 \;\; H_d^-)$	$(\widetilde{H}_d^0 \;\; \widetilde{H}_d^-)$	$(\mathbf{1}, \mathbf{2}, -\frac{1}{2})$
Gauge supermultiplets				
Names		spin 1/2	spin 1	$SU(3)_C$, $SU(2)_L$, $U(1)_Y$
gluino, gluon		$\widetilde{g}$	g	$(\mathbf{8}, \mathbf{1}, 0)$
winos, W bosons		$\widetilde{W}^\pm \;\; \widetilde{W}^0$	$W^\pm \;\; W^0$	$(\mathbf{1}, \mathbf{3}, 0)$
bino, B boson		$\widetilde{B}^0$	B^0	$(\mathbf{1}, \mathbf{1}, 0)$

Table 1.1: Supermultiplets of the Minimal Supersymmetric Standard Model.

quarks, and to down-type quarks and charged leptons; they are denoted by H_u and H_d respectively. The fermionic superpartners are called appending "-ino" to the name of the corresponding SM particle, thus the higgsinos are the superpartners of the two Higgses.

Finally, the gauge bosons of the SM must belongs to gauge supermultiplets. Their fermionic superpartners are called gauginos. The superpartners of the gluon, the W-boson and the B-boson are called gluino, wino and bino respectively. After electroweak symmetry breaking (EWSB) the mass eigenstates are the Z-boson and the photon whose superpartners are the zino and the photino. The chiral and gauge supermultiplets of the MSSM are summarized in table 1.1.

1.3.1 The SUSY-preserving Lagrangian

The MSSM superpotential reads

$$W_{\text{MSSM}} = \overline{u}\mathbf{y_u}QH_u - \overline{d}\mathbf{y_d}QH_d - \overline{e}\mathbf{y_e}LH_d + \mu H_u H_d \,, \tag{1.14}$$

where Q, L, $\overline{u}$, $\overline{d}$, $\overline{e}$, H_u, H_d are the chiral superfields containing the SM matter content summarized in table 1.1, and $\mathbf{y_u}$, $\mathbf{y_d}$, $\mathbf{y_e}$ are 3×3 dimensionless matrices in family space representing the MSSM Yukawa couplings. To simplify the notation, we have suppressed the gauge and family indices. Since the superpotential is holomorphic in the chiral superfields, we appreciate why we needed both H_u and H_d to generated the SM Yukawa couplings.

The last term in eq. (1.14) is known as the μ term and it is the supersymmetric analogous of the Higgs boson mass. It generates mass terms for the Higgs scalars and the higgsinos. The superpotential Yukawa terms give rise to interactions of the form (scalar-fermion-fermion) and (scalar)^4. There are also important (scalar)^3 interactions generated by the combination of the μ term and Yukawa couplings. Since the quarks and charged lepton of the third generation are the heaviest fermions of the SM, for collider physics it is a good approximation to neglect all the entries of the MSSM Yukawa matrices except the $(3,3)$ one, i.e.

$$\mathbf{y_u} \approx \mathrm{diag}(0,0,y_t), \qquad \mathbf{y_d} \approx \mathrm{diag}(0,0,y_b), \qquad \mathbf{y_e} \approx \mathrm{diag}(0,0,y_\tau). \tag{1.15}$$

Most often production and decay processes for superpartners in the MSSM are dominated by the supersymmetric gauge interactions because all the Yukawa couplings are comparably small with except of the third generation ones. As usual, the couplings of the MSSM particles to the SM gauge bosons is determined by gauge invariance of the kinetic terms in the Lagrangian. Supersymmetry also requires couplings of the gauginos to the (squark,quark), (slepton,lepton) and (Higgs,higgsino) pairs dictated by their transformation properties under the corresponding gauge group and controlled by the gauge couplings. These interactions yields to the decay channels $\widetilde{q} \to q\widetilde{g}$, $\widetilde{q} \to q\widetilde{W}$ and $\widetilde{q} \to q\widetilde{B}$, when the squarks are sufficiently heavy for the process to be kinematically allowed, just to mention an example.

SUSY also implies the existence of scalar quartic interactions fixed by gauge invariance, arising from the D-term contribution to the scalar potential (1.11). The interactions of the form (Higgs)^4 proportional to g^2 and g'^2, generalizes the SM Higgs quartic interaction.

The μ term generates both a mass term for the higgsinos

$$\mathcal{L}_{\text{higgsino mass}} = -\mu(\widetilde{H}_u^+ \widetilde{H}_d^- - \widetilde{H}_u^0 \widetilde{H}_d^0) + \text{h.c.} \tag{1.16}$$

and squared masses with positive sign for the Higgs scalars

$$\mathcal{L}_{\text{SUSY Higgs mass}} = -|\mu|^2 \left(|H_u^0|^2 + |H_u^+|^2 + |H_d^0|^2 + |H_d^-|^2\right). \tag{1.17}$$

We will see in section 1.3.2 that there are additional contributions to the Higgs squared masses.

There are other terms which are allowed in the superpotential that violate either total lepton number (L) or baryon number (B)

$$W_{\Delta \mathrm{L}=1} = \frac{1}{2}\lambda^{ijk} L_i L_j \overline{e}_k + \lambda'^{ijk} L_i Q_j \overline{d}_k + \mu'^i L_i H_u + \frac{1}{2}\lambda''^{ijk} \overline{u}_i \overline{d}_j \overline{d}_k, \tag{1.18}$$

with the family indices $i = 1, 2, 3$. The couplings λ and λ'' must be antisymmetric in the last two indices because so it is the corresponding operator. The assignment of the baryon number to the chiral superfields attribute $B = +1/3$ for Q_i, $B = -1/3$ for $\overline{u}_i, \overline{d}_i$, and $B = 0$ for the rest, while the lepton number assignment are $L = +1$ for L_i, $L = -1$ for $\overline{e}_i$, and $L = 0$ for the rest. The first three terms in eq. (1.18) violate the lepton number by one unit and the third one violate the baryon number also by one unit.

These operators are dangerous because baryon and lepton number violating processes are highly constrained experimentally, e.g. by the non-observation of proton decay, the smallness of the neutrino masses, etc. [21]. For instance, if both couplings λ' and λ'' are unsuppressed, some decays channels for the proton are opened like $p^+ \to e^+\pi^0$ or e^+K^0 or $\mu^+\pi^0$ or μ^+K^0 or $\nu\pi^+$ or νK^+, leading to large contributions to the proton decay width. This is in conflict with the current experimental limits, in particular the constrains from Super-Kamiokande for the channels $p \to e^+\pi^0$ and $p \to \overline{\nu}K^+$ are [22, 23]

$$\tau(p \to e^+\pi^0) > 8.2 \times 10^{33}\,\mathrm{yrs}, \qquad \tau(p \to \overline{\nu}K^+) > 5.9 \times 10^{33}\,\mathrm{yrs}\,. \tag{1.19}$$

How can we suppress or possibly kill these B- and L- violating terms? One way would be to propose baryon and lepton number as symmetries of the theory, but they are broken at the non-perturbative level [24]. Moreover, it is very nice that baryon and lepton number emerge as accidental symmetries in the SM. Then one adds a new symmetry known as *R-parity* [25] or equivalently as *matter-parity* [26], which forbids the dangerous operators in eq. (1.18).

For each particle, the matter-parity P_M and the $R-$parity P_R are defined as

$$P_M = (-1)^{3(B-L)}, \qquad P_R = (-1)^{3(B-L)+2s}\,, \tag{1.20}$$

where s is the spin of the particle. They are multiplicative quantum numbers and both are equivalent since they differ only by the angular momentum which is conserved in any interaction vertex of the theory. In principle, they can be an exact symmetry because they are not violated non-perturbatively. All the SM fields have $P_R = 1$ while all SUSY partners have $P_R = -1$. $R-$parity conservation implies that there is no mixing between the SM particles and the sparticles (sfermions, gauginos and higgsinos).

$R-$parity (or equivalently matter-parity) has relevant phenomenological consequences:

- Baryon and lepton number are conserved.
- The lightest supersymmetric particle is stable. If it interacts only weakly with the other particles it can be a good candidate for dark matter.
- The sparticles can only be produced in even numbers at colliders, typically in pairs.
- Any sparticle but the LSP, must decay into an odd number of LSPs. Typically one expects just one LSP at the end of the decay chain.

We adopt the definition of the MSSM as the most general renormalizable $\mathcal{N} = 1$ gauge theory with the gauge group of the SM $SU(3) \times SU(2) \times U(1)$, chiral content as in the SM and R-parity (or equivalently matter-parity) conserved.

1.3.2 Soft supersymmetry breaking

If Supersymmetry were an exact symmetry of nature, it would predict that the superpartners have the same masses as the corresponding SM particles in the same supermultiplet. For example, the gluino and the photino would be massless, the stop masses would be determined by the top mass $m_t = 173.34$ GeV, and similar for other sparticles. Therefore, if supersymmetry is realized in nature it must be broken.

We recall that one of the motivations for SUSY was the cancellation of the quadratic sensitivity of scalar squared masses. If SUSY is intended to solve or alleviate the hierarchy problem it should be broken without reintroducing quadratic sensitivity. This leads to the idea of soft SUSY breaking, which means that all the SUSY-violating operators in the Lagrangian, denoted as $\mathcal{L}_{\text{soft}}$, should have positive energy dimension. The models we will discuss in section 1.4 lead to effective Lagrangians with terms of this type. The Higgs mass receives corrections proportional to m^2_{soft}, where m_{soft} is the scale defined by the parameters appearing in $\mathcal{L}_{\text{soft}}$. In a natural theory one expects m_{soft} to be below the TeV scale.

It is very useful to parametrize the breaking of Supersymmetry in terms of an effective MSSM Lagrangian, hiding the details of the mechanism of breaking. Specific models will be discussed in section 1.4. The possible terms with positive energy dimension are

$$\mathcal{L}_{\text{soft}} = -\left(\frac{1}{2}M_a\,\lambda^a\lambda^a + \frac{1}{6}a^{ijk}\phi_i\phi_j\phi_k + \frac{1}{2}b^{ij}\phi_i\phi_j + \text{h.c.}\right) - (m^2)^i_j\phi^{j*}\phi_i, \quad (1.21)$$

where M_a are the gaugino masses for each gauge group (i.e. the index a is summed over each group), b^{ij} and $(m^2)^i_j$ are scalar squared-mass terms, and

a^{ijk} are the scalar cubic couplings. There are also other operators with positive energy dimension which one can write, they are the tadpoles ϕ^i, a cubic scalar interaction $\phi^{*i}\phi_j\phi_k$, and a Dirac mass term between the gauginos and a fermion ψ_a if it belongs to a chiral supermultiplet which is a singlet or in the adjoint representation of a simple factor the gauge group. However, they are not present in the MSSM.

For the MSSM, the soft SUSY breaking Lagrangian in eq. (1.21) becomes

$$\begin{aligned}\mathcal{L}_{\text{soft}}^{\text{MSSM}} = &-\frac{1}{2}\left(M_1\widetilde{B}\widetilde{B} + M_2\widetilde{W}\widetilde{W} + M_3\widetilde{g}\widetilde{g} + \text{h.c.}\right)\\ &-\left(\widetilde{\overline{u}}\,\mathbf{a_u}\,\widetilde{Q}H_u - \widetilde{\overline{d}}\,\mathbf{a_d}\,\widetilde{Q}H_d - \widetilde{\overline{e}}\,\mathbf{a_e}\,\widetilde{L}H_d + \text{h.c.}\right)\\ &-\widetilde{Q}^\dagger\,\mathbf{m_Q^2}\,\widetilde{Q} - \widetilde{L}^\dagger\,\mathbf{m_L^2}\,\widetilde{L} - \widetilde{\overline{u}}\,\mathbf{m_{\overline{u}}^2}\,\widetilde{\overline{u}}^\dagger - \widetilde{\overline{d}}\,\mathbf{m_{\overline{d}}^2}\,\widetilde{\overline{d}}^\dagger - \widetilde{\overline{e}}\,\mathbf{m_{\overline{e}}^2}\,\widetilde{\overline{e}}^\dagger\\ &-\ m_{H_u}^2 H_u^\dagger H_u - m_{H_d}^2 H_d^\dagger H_d - (B_\mu H_u H_d + \text{h.c.})\,. \end{aligned} \tag{1.22}$$

Here M_1, M_2 and M_3 are the bino, wino and gluino masses, the second line corresponds to the scalar cubic interactions , the third line contains the squark and slepton masses, while in the last line $m_{H_u}^2$ and $m_{H_d}^2$ are terms of the type $(m^2)_j^i$ in eq. (1.21) and B_μ is of the type b^{ij} in eq. (1.21). The symbols $\mathbf{a_u}$, $\mathbf{a_d}$, $\mathbf{a_e}$, $\mathbf{m_Q^2}$, $\mathbf{m_{\overline{u}}^2}$, $\mathbf{m_{\overline{d}}^2}$, $\mathbf{m_L^2}$, $\mathbf{m_{\overline{e}}^2}$ denote 3×3 matrices in family space which are complex in general. The soft SUSY breaking Lagrangian introduces 105 new independent parameters, which cannot be rotated away by field redefinitions.

Most of the new parameters in $\mathcal{L}_{\text{soft}}^{\text{MSSM}}$ contribute to flavor mixing or CP-violating processes which are tightly constrained by experiments (see references in section 6.4 of [14]), thus some of these parameters are very suppressed. For instance, the off-diagonal elements of the slepton mass matrix $\mathbf{m_{\overline{e}}^2}$ produces mixing that violates the individual lepton number. In particular, there is a strong constrain from the experimental upper limit on the branching ratio $\text{Br}(\mu\to e\gamma)$ [27]. Also the scalar cubic interactions $\widetilde{\overline{e}}\,\mathbf{a_e}\,\widetilde{L}H_d + \text{h.c.}$ can produce slepton mixing once the Higgs field H_d is put on the VEV, so the off-diagonal entries of the matrix $\mathbf{a_e}$ are constrained by the experimental limits on $\text{Br}(\mu\to e\gamma)$ [27], $\text{Br}(\tau\to e\gamma)$ or $\text{Br}(\tau\to\mu\gamma)$ [28]. Limits on the parameters Δm_K, ϵ and ϵ'/ϵ of the neutral Kaon effective Hamiltonian put severe constraints on the $\widetilde{d}_{L,R}$-$\widetilde{s}_{L,R}$ mixings and CP-violating complex phases [29]. There are also weaker constraints on the $\overline{u}-\overline{c}$, $\overline{d}-\overline{b}$, $\overline{s}-\overline{b}$ squark mixings from the $D^0-\overline{D}^0$, $B_d^0-\overline{B}_d^0$ and $B_s^0-\overline{B}_s^0$ systems respectively. Finally, the experimental limits on the electric dipole moments of the neutron [30, 31] and electron [32] put strong bounds on the CP-violating phases in the gaugino masses and scalar cubic couplings. These constraints will be described in section 1.5.2.

1.3.3 Renormalization group equations

Generically, the soft SUSY breaking terms are generated at a scale much higher than the EW scale, then they should be evolved to the low scale using the renormalization group equations (RGEs). This also requires the knowledge of the RGEs of the SUSY parameters. An important technical observation is that the most common regularization procedure used in loop computations in the SM, dimensional regularization, is not appropriate in the context of the MSSM because it introduces spurious violation of SUSY. Preferably one should use a SUSY preserving regularization, among which dimensional reduction [33] is the most popular one. Usually dimensional reduction is combined with renormalization in the minimal subtraction scheme, this regularization-renormalization procedure is known as $\overline{\text{DR}}$ for short.

In supersymmetric theories the shape of the RGEs is determined by the non-renormalization theorems [34, 35]. They imply that logarithmically divergent contributions can always be written only in terms of wave-function renormalizations.

The RGEs for softly broken SUSY are known up to 3-loop order, even some partial 4-loop results are available (see references in [14]). In practice such level of precision is not required since the soft terms are not known at such accuracy.

In order to highlight some features about the evolution of the MSSM parameters we consider the one-loop RGEs with real quantities. For the gauge couplings they read

$$\beta_{g_a} \equiv \frac{d}{dt} g_a = \frac{1}{16\pi^2} b_a g_a^3, \quad (b_1, b_2, b_3) = \begin{cases} (41/10,\ -19/6,\ -7) & \text{SM} \\ (33/5,\ 1,\ -3) & \text{MSSM} \end{cases} \tag{1.23}$$

where $t = \ln Q/Q_0$ with Q representing the renormalization scale and Q_0 a reference scale.

The β-functions for the superpotential parameters, considering among the Yukawa couplings only the one of the top quark, are given by

$$\beta_{y_t} \equiv \frac{d}{dt} y_t = \frac{y_t}{16\pi^2} \Big[6y_t^2 - \frac{16}{3} g_3^2 - 3g_2^2 - \frac{13}{15} g_1^2 \Big], \tag{1.24}$$

$$\beta_\mu \equiv \frac{d}{dt} \mu = \frac{\mu}{16\pi^2} \Big[3y_t^2 - 3g_2^2 - \frac{3}{5} g_1^2 \Big]. \tag{1.25}$$

As a consequence of non-renormalization theorems, these β-functions are proportional to the supersymmetric parameters themselves. They do not depend on the soft SUSY breaking parameters. Radiative corrections to μ do not change its order of magnitude with respect to the tree-level value.

Each gaugino mass runs as the corresponding gauge coupling squared, i.e. the ratio M_a/g_a^2 is RGE invariant at one-loop as can be seen from

$$\beta_{M_a} \equiv \frac{d}{dt}M_a = \frac{1}{8\pi^2}b_a g_a^2 M_a \qquad (b_a = 33/5,\ 1,\ -3). \tag{1.26}$$

In the context of SUSY GUT theory and in the absence of large SUSY breaking thresholds, it is common to assume that the gaugino masses unify near the GUT scale with a value $m_{1/2}$ in analogy to the gauge couplings that are unified with a value g_U. Then the relation

$$\frac{M_1}{g_1^2} = \frac{M_2}{g_2^2} = \frac{M_3}{g_3^2} = \frac{m_{1/2}}{g_U^2} \tag{1.27}$$

holds at any scale up to NLO effects.

The RGEs of the soft SUSY breaking trilinear couplings and B_μ are not protected by the supersymmetric non-renormalization theorems

$$16\pi^2\frac{d}{dt}a_t = a_t\Big[18y_t^2 - \frac{16}{3}g_3^2 - 3g_2^2 - \frac{13}{15}g_1^2\Big] + y_t\Big[\frac{32}{3}g_3^2M_3 + 6g_2^2M_2 + \frac{26}{15}g_1^2M_1\Big], \tag{1.28}$$

$$16\pi^2\frac{d}{dt}B_\mu = B_\mu\Big[3y_t^2 - 3g_2^2 - \frac{3}{5}g_1^2\Big] + \mu\Big[6a_ty_t + 6g_2^2M_2 + \frac{6}{5}g_1^2M_1\Big]. \tag{1.29}$$

Here we only included the stop-stop-Higgs trilinear coupling for simplicity. Even if the cubic couplings and B_μ are zero or negligible at the high scale, they will be attracted by the gaugino masses when they are evolved to the electroweak scale. It is usual to define $A_t = a_t/y_t$, $A_b = a_b/y_b$, $A_\tau = a_\tau/y_\tau$ and we will also use this notation later.

For the squared soft masses of the Higgses the RGE are

$$16\pi^2\frac{d}{dt}m_{H_u}^2 = 6y_t^2(m_{H_u}^2 + m_{Q_3}^2 + m_{\overline{u}_3}^2) + 6a_t^2 - 6g_2^2|M_2|^2 + \ldots, \tag{1.30}$$

$$16\pi^2\frac{d}{dt}m_{H_d}^2 = -6g_2^2|M_2|^2 + \ldots, \tag{1.31}$$

where the ellipses represent subleading corrections proportional to the gauge coupling g_1 or other Yukawa couplings. The squared mass $m_{H_u}^2$ tends to run smaller in the infrared because of the terms proportional to y_t^2 or a_t^2 in eq. (1.30), which are typically positive and dominates over the other contributions. As a result $m_{H_u}^2$ often runs negative, driving EWSB.

Under the approximation of diagonal squared-mass matrices for squarks and sleptons, the RGEs of the soft squared masses read

$$16\pi^2\frac{d}{dt}m_{Q_3}^2 = 6y_t^2(m_{H_u}^2 + m_{Q_3}^2 + m_{\overline{u}_3}^2) + 6a_t^2 - \frac{32}{3}g_3^2M_3^2 - 6g_2^2M_2^2 + \ldots, \tag{1.32}$$

$$16\pi^2 \frac{d}{dt} m^2_{\overline{u}_3} = 4y_t^2 (m^2_{H_u} + m^2_{Q_3} + m^2_{\overline{u}_3}) + 4a_t^2 - \frac{32}{3} g_3^2 |M_3|^2 + \dots , \tag{1.33}$$

$$16\pi^2 \frac{d}{dt} m^2_{\overline{d}_3} = -\frac{32}{3} g_3^2 M_3^2 + \dots \tag{1.34}$$

$$16\pi^2 \frac{d}{dt} m^2_{L_3} = -6 g_2^2 M_2^2 + \dots , \quad 16\pi^2 \frac{d}{dt} m^2_{\overline{e}_3} = \dots \tag{1.35}$$

Here we have omitted corrections proportional to g_1 or Yukawa couplings different than the one for the top quark; these terms are represented generically by the ellipses. The RGEs for squarks and sleptons of the first and second families can be obtained by obvious replacements. Generically, sfermion masses are attracted by the gaugino masses when they are evolved to the low scale. In particular, the squark squared masses of the third generation get a large positive contribution proportional to M_3^2, which typically dominates.

More complete expressions for the MSSM RGEs can be found in [14] and references therein.

1.3.4 The mass spectrum

Electroweak Symmetry Breaking

Electroweak symmetry breaking in the MSSM involves two Higgs doublets: $H_u = (H_u^+, H_u^0)$ and $H_d = (H_d^0, H_d^-)$. Using $SU(2)_L$ gauge transformation one can set $H_u^+ = H_d^- = 0$ at the minimum of the potential, then focus on the minimization of the potential of the neutral components

$$\begin{aligned} V = &(|\mu|^2 + m^2_{H_u})|H_u^0|^2 + (|\mu|^2 + m^2_{H_d})|H_d^0|^2 - (B_\mu \, H_u^0 H_d^0 + \text{h.c.}) \\ &+ \frac{1}{8}(g^2 + g'^2)(|H_u^0|^2 - |H_d^0|^2)^2 . \end{aligned} \tag{1.36}$$

Through field redefinition and $U(1)_Y$ gauge transformations, it is easy to show that CP cannot be spontaneously broken by the scalar potential, then the Higgs scalar mass eigenstates have well defined CP quantum numbers at tree level. Anyway, we will assume in this work that the MSSM parameters introduce negligible CP violation, which is a good approximation given the experimental constraints.

Requiring the potential to be bounded from below implies

$$2B_\mu < 2|\mu|^2 + m^2_{H_u} + m^2_{H_d} , \tag{1.37}$$

while the condition to have EWSB reads

$$B_\mu^2 > (|\mu|^2 + m^2_{H_u})(|\mu|^2 + m^2_{H_d}) . \tag{1.38}$$

Neglecting EW effects with respect to the MSSM dimensionful parameters the EWSB condition implies [36]

$$\det \begin{pmatrix} |\mu|^2 + m_{H_u}^2 & -B_\mu \\ -B_\mu^* & |\mu|^2 + m_{H_d}^2 \end{pmatrix} \approx 0\,. \tag{1.39}$$

Models of SUSY breaking that generate $m_{H_u}^2 = m_{H_d}^2$ at leading order at the high scale are incompatible with eqs. (1.37) and (1.38). However when the soft masses are evolved to the electroweak scale, the RGEs drive $m_{H_u}^2$ negative, such that $m_{H_u}^2 < m_{H_d}^2$. In this case EWSB is caused by quantum corrections, a mechanism known as *radiative electroweak symmetry breaking*. For a detail analysis of how the tuning for EWSB can be achieved, see e.g. [36].

Spontaneous symmetry breaking $SU(2)_L \times U(1)_Y \to U(1)_{\rm em}$ occurs when the Higgs scalars develop a non-zero VEVs

$$\langle H_u^0 \rangle = v_u, \qquad \langle H_d^0 \rangle = v_d\,, \ \text{with} \tag{1.40}$$

$$v_u^2 + v_d^2 = v^2 = 4m_Z^2/(g^2 + g'^2) \approx (246\ \text{GeV})^2. \tag{1.41}$$

It is useful to define the angle $0 < \beta < \pi/2$ as

$$\tan\beta \equiv \frac{v_u}{v_d} = \sqrt{\frac{m_{H_d}^2 + |\mu|^2}{m_{H_u}^2 + |\mu|^2}}\,. \tag{1.42}$$

This is a tree level relation, quantum corrections require different definitions at higher order. The minimization of the scalar potential also leads to a expression of the $Z-$boson mass in terms of the MSSM parameters, which at large $\tan\beta$ reads

$$m_Z^2 = -2(m_{H_u}^2 + |\mu|^2) + \frac{2}{\tan^2\beta}(m_{H_d}^2 - m_{H_u}^2) + \mathcal{O}(\tan^{-4}\beta). \tag{1.43}$$

This shows the μ *problem*: without accidental cancellations the Higgs squared soft masses and $|\mu|^2$ should be of order m_Z^2. However the current collider bounds already require significant cancellation between $m_{H_u}^2$ and $|\mu|^2$, because of the radiative corrections to $m_{H_u}^2$ proportional to the stop and gluino squared masses. The SUSY preserving mass μ and the SUSY breaking soft mass terms are apparently unrelated. Then, why should $|\mu|^2$ be approximately of the same order of the soft squared mass terms? In section 1.4.3 we will study the Giudice-Masiero mechanism [37] as an example of a possible solution to the μ problem.

Mass eigenstates

The two Higgs doublets contains eight reals scalars. Three of them are the would be Nambu-Goldstone bosons eaten by the gauge bosons. The other five physical mass eigenstates are two CP-even neutral scalars h^0 and H^0 (h^0 is the lightest one that plays the role of the SM Higgs boson), one CP-odd neutral scalar A^0, and single charged scalars $H^\pm$. They are related to the interaction eigenstates by the rotation

$$\begin{pmatrix} H_u^0 \\ H_d^0 \end{pmatrix} = \frac{1}{\sqrt{2}} \begin{pmatrix} v_u \\ v_d \end{pmatrix} + \frac{1}{\sqrt{2}} R_\alpha \begin{pmatrix} h^0 \\ H^0 \end{pmatrix} + \frac{i}{\sqrt{2}} R_{\beta_0} \begin{pmatrix} G^0 \\ A^0 \end{pmatrix} \tag{1.44}$$

$$\begin{pmatrix} H_u^+ \\ H_d^{-*} \end{pmatrix} = \frac{1}{\sqrt{2}} R_{\beta^+} \begin{pmatrix} G^+ \\ H^+ \end{pmatrix}, \tag{1.45}$$

where R_α, R_β^0 and R_β^+ are orthogonal matrices, in particular the rotation R_α that diagonalizes the mass matrix of the neutral CP-even scalars is given by

$$R_\alpha = \begin{pmatrix} \cos\alpha & \sin\alpha \\ -\sin\alpha & \cos\alpha \end{pmatrix}. \tag{1.46}$$

The mixing angle α ranges from $-\pi/2 < \alpha < 0$. Then, the tree level masses for the Higgs scalars reads

$$m_{A^0}^2 = 2b/\sin(2\beta) \;=\; 2|\mu|^2 + m_{H_u}^2 + m_{H_d}^2 \tag{1.47}$$

$$m_{h^0,H^0}^2 = \frac{1}{2}\Big(m_{A^0}^2 + m_Z^2 \mp \sqrt{(m_{A^0}^2 - m_Z^2)^2 + 4m_Z^2 m_{A^0}^2 \sin^2(2\beta)}\Big), \tag{1.48}$$

$$m_{H^\pm}^2 = m_{A^0}^2 + m_W^2. \tag{1.49}$$

The mass of the light CP-even neutral Higgs scalar h^0, which plays the role of the SM Higgs boson, must satisfy the tree-level bound

$$m_{h^0}^2 < m_Z^2 \cos^2 2\beta. \tag{1.50}$$

As a result, one needs to rely on the radiative corrections to reproduce the experimental value of the Higgs mass.

There is an important situation with $m_A \gg m_Z$, favored by the current constraints, known as the *decoupling limit*. In this case the tree level bound (1.50) is saturated; and the particles A^0, H^0, and $H^\pm$ are much heavier than the Higgs and almost degenerate in mass, so they decouple from low energy experiments. Furthermore, the mixing angle α is roughly $\alpha \approx \beta - \pi/2$ and the Higgs couplings are very close to the SM ones.

We proceed with the mass matrices for squarks and sleptons. Any sfermions with the same quantum numbers (electric charge, color, R-parity) can mix with each other in the general case. Then, there would be 6×6 squared mass matrices for up-type squarks ($\widetilde{u}_L$, $\widetilde{c}_L$, $\widetilde{t}_L$, $\widetilde{u}_R$, $\widetilde{c}_R$, $\widetilde{t}_R$), down-type squarks ($\widetilde{d}_L$, $\widetilde{s}_L$, $\widetilde{b}_L$, $\widetilde{d}_R$, $\widetilde{s}_R$, $\widetilde{b}_R$), and charged sleptons ($\widetilde{e}_L$, $\widetilde{\mu}_L$, $\widetilde{\tau}_L$, $\widetilde{e}_R$, $\widetilde{\mu}_R$, $\widetilde{\tau}_R$), and one 3×3 matrix for sneutrinos ($\widetilde{\nu}_e$, $\widetilde{\nu}_\mu$, $\widetilde{\nu}_\tau$). As a way to evade the bounds from flavor physics mentioned at the end of section 1.3.2, we make the simplifying assumption that the soft parameters are flavor blind such that there is no significant mixing between sfermions of different generations. Thus, only left and right components of a given sfermion flavor ($\tilde{f}_L, \tilde{f}_R$) can mix, with mass matrices

$$\mathbf{M}^2_{\tilde{f}} = \begin{pmatrix} m^2_{\tilde{f}_L} + m^2_f + m^2_Z \cos 2\beta \, (T^3_f - Q_f s^2_w) & m_f X_f \\ m_f X_f & m^2_{\tilde{f}_R} + m^2_f + m^2_Z \cos 2\beta \, Q_f \, s^2_w \end{pmatrix}, \tag{1.51}$$

where $m_{\tilde{f}_L}$ and $m_{\tilde{f}_R}$ are the soft masses for the doublet (that contains the left component) and the right handed sfermions respectively, Q_f and T^3_f denote electric charge and isospin of the corresponding fermion in the same supermultiplet, and m_f is the mass of the fermion. This sfermion mixing breaks EW symmetry, thus it is automatically suppressed by the fermion masses. The mixing parameters X_f are given by $X_t = A_t - \mu \cot\beta$, $X_b = A_b - \mu \tan\beta$, and $X_\tau = A_\tau - \mu \tan\beta$ for the stops, sbottoms and staus respectively; while one can generically neglect the mixing for the other sfermions due to the smallness of the corresponding Yukawa couplings.

Finally, we are left to consider the mass eigenstates composed of a mixture of the fermion superpartners (gauginos and higgsinos). The gluino cannot mix with other MSSM fermions because it is the only one carrying color, so its mass is fixed by the soft parameter M_3. The charged higgsinos ($\widetilde{H}^+_u$, $\widetilde{H}^-_d$) and winos ($\widetilde{W}^+$, $\widetilde{W}^-$) combine in two mass eigenstates named charginos. The neutral components of gauginos ($\widetilde{B}$, $\widetilde{W}^0$) and higgsinos ($\widetilde{H}^0_u$, H^0_d) associate to form four mass eigenstates known as neutralinos. Ordered by ascending mass, the charginos and neutralinos are denoted as $\widetilde{\chi}^\pm_i$ ($i = 1, 2$) and $\widetilde{\chi}^0_i$ ($i = 1, 2, 3, 4$). In the gauge-eigenstate basis $\psi^\pm = (\widetilde{W}^\pm, \widetilde{H}^\pm_u)$ for the charged fermions and $(\widetilde{B}, \widetilde{W}^0, \widetilde{H}^0_d, \widetilde{H}^0_u)$ for the neutral ones, the chargino and neutralino mass matrices are given by

$$\mathbf{M}^2_{\tilde{\chi}^\pm} = \begin{pmatrix} M_2 & g v_u \\ g v_d & \mu \end{pmatrix} = \begin{pmatrix} M_2 & \sqrt{2} s_\beta m_W \\ \sqrt{2} c_\beta m_W & \mu \end{pmatrix}, \tag{1.52}$$

$$\mathbf{M}^2_{\tilde{\chi}^0} = \begin{pmatrix} M_1 & 0 & -c_\beta s_W m_Z & s_\beta s_W m_Z \\ 0 & M_2 & c_\beta c_W m_Z & -s_\beta c_W m_Z \\ -c_\beta s_W m_Z & c_\beta s_W m_Z & 0 & -\mu \\ s_\beta s_W m_Z & -s_\beta c_W m_Z & -\mu & 0 \end{pmatrix}. \tag{1.53}$$

The mixing between gauginos and higgsinos is an electroweak effect. In a situation with relatively heavy gaugino masses and μ parameter the mixing is suppressed. Then the charginos are very nearly wino-like and higgsino-like, and the neutralinos are very nearly bino-like, wino-like and higgsino-like $(\widetilde{H}^0_u \pm \widetilde{H}^0_d)/\sqrt{2}$. Their masses are almost completely determined by the value of the gaugino masses and the μ parameter. Usually one assumes that the lightest neutralino is the LSP, except when there is a lighter gravitino, because it is the only MSSM particle that can be a viable dark matter candidate.

1.4 Models of SUSY breaking

We will discuss models of spontaneous SUSY breaking which lead to the Lagrangian $\mathcal{L}^{\text{MSSM}}_{\text{soft}}$ as the low energy effective field theory. In these models the vacuum state $|0\rangle$ is not invariant under supersymmetry transformations ($Q_\alpha|0\rangle \neq 0$ and $Q^\dagger_\alpha|0\rangle \neq 0$). The Hamiltonian of a theory with global supersymmetry can be written in terms of the generators

$$H = P^0 = \frac{1}{4}\left(Q_\alpha Q^\dagger_\alpha + Q^\dagger_\alpha Q_\alpha\right). \tag{1.54}$$

When supersymmetry is exact $H|0\rangle = 0$ and the vacuum state has zero energy. For spontaneously broken supersymmetry the vacuum state has positive energy due to positivity of the Hilbert space

$$\langle 0|H|0\rangle = \frac{1}{4}\sum_\alpha \left(||Q^\dagger_\alpha|0\rangle||^2 + ||Q_\alpha|0\rangle||^2\right) > 0. \tag{1.55}$$

In perturbative models, the energy of the vacuum state is determined by the scalar potential since $\langle 0|H|0\rangle = \langle 0|V|0\rangle$. This implies that supersymmetry can be spontaneously broken when the F- or/and D- terms have a non-zero VEV. Of course, when supersymmetric vacua exist they are global minima of the potential. Acceptable vacua can be either stable or metastable but sufficiently long-lived.

The extended Nambu-Goldstone theorem states that when a global symmetry is spontaneously broken there is a massless mode with the same quantum numbers as the broken generator. Since supersymmetry is a fermionic symmetry and the

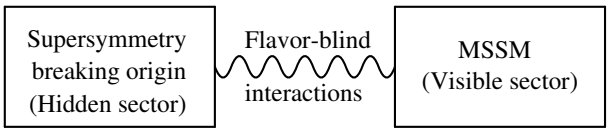

Figure 1.2: Expected paradigm of how SUSY breaking should be realized [14].

broken generator is the fermionic charge Q_α, the associated Nambu-Goldstone particle is a massless neutral Weyl fermion known as the goldstino. Theories with spontaneous SUSY breaking also satisfy a sum rule for the tree-level squared mass matrices

$$\mathrm{STr}(m^2) = \mathrm{Tr}(\mathbf{m}_S^2) - 2\mathrm{Tr}(\mathbf{m}_F^\dagger \mathbf{m}_F) + 3\mathrm{Tr}(\mathbf{m}_V^2) = -2g_a \mathrm{Tr}(T^a) D^a = 0. \quad (1.56)$$

In the equation above $\mathrm{STr}(m^2) \equiv \sum_j (-1)^{2j}(2j+1)\mathrm{Tr}(m_j^2)$ is the supertrace of the tree level squared mass matrices and we suppose that the traces of the $U(1)$ charges over the chiral superfields vanishes, which is satisfied by the $U(1)_Y$ of the MSSM and as well as any anomaly free gauge symmetry.

Within the MSSM field content, a D-term VEV for $U(1)_Y$ would produce an unsatisfactory spectrum because of the supertrace mass formula (1.56) and there is no gauge singlet whose F-term could develop a VEV. Then there should exists additional field content responsible for supersymmetry breaking and its communication to the MSSM. On top of that, it is difficult to find a phenomenologically suitable model which communicates SUSY breaking to the observable sector only through renormalizable interactions at tree level, because there is not any scalar-gaugino-gaugino operator which could give rise to the gaugino masses when the scalar gets a VEV. Also, after taking into account the bounds from flavor there will be sum rules analogous to (1.56) which predicts too light fermion superpartners.

According to the arguments above, one expects the following paradigm to fulfill the constraints from the mass sum rules and flavor violation. The MSSM soft terms are generated radiatively, rather than from tree-level couplings to the SUSY-breaking sector. Thus SUSY breaking takes place in a so called *hidden sector* of particles that have no or very small direct couplings to the *observable* or *visible sector* determined by the MSSM. This is illustrated in fig. 1.2. The main proposals communicate SUSY breaking to the observable sector through gravity or gauge interactions.

The spontaneous breaking of global supersymmetry implies the existence of the goldstino, the fermionic component of the supermultiplet whose auxiliary field gets a VEV. In a theory including gravity, supersymmetry must be promoted to a local symmetry. This theory, which unifies the spacetime symmetries of general

relativity with local supersymmetry transformations, is known as supergravity. In supergravity, the graviton multiplet contains, in addition to the spin-2 graviton, a spin-3/2 fermion superpartner called the gravitino. The gravitino should be thought of as the gauge field of local supersymmetry transformations. If SUSY is not broken, the graviton and the gravitino are massless, each with two spin helicity states. When SUSY is spontaneously broken, the gravitino acquires a mass by eating the goldstino, which becomes its longitudinal components. The massive gravitino now has four helicity states, two of which were part of the would-be goldstino. This is called the super-Higgs mechanism in analogy with the Higgs mechanism in the SM. The gravitino mass, denoted as $m_{3/2}$, can be estimated in the presence of F-term breaking using dimensional analysis

$$m_{3/2} \sim \frac{F}{M_P}. \tag{1.57}$$

Here we have used that $m_{3/2}$ must vanish in the limits when SUSY is restored ($F \to 0$) and when gravity is turned off ($M_P \to \infty$).

1.4.1 Gravity mediation

We describe a scenario in which SUSY breaking is communicated to the MSSM sector through gravitational interactions. One can parametrize the effect with a effective theory at low energy in terms of higher dimensional operators suppressed by the Planck mass M_P with the following superpotential, Kähler potential and gauge kinetic function

$$W = W_{\text{MSSM}} - \frac{1}{M_P}\left(\frac{1}{6}y^{Xijk}X\Phi_i\Phi_j\Phi_k + \frac{1}{2}\mu^{Xij}X\Phi_i\Phi_j\right) + \ldots, \tag{1.58}$$

$$K = \Phi^{*i}\Phi_i + \frac{1}{M_P}\left(n_i^j X + \overline{n}_i^j X^*\right)\Phi^{*i}\Phi_j - \frac{1}{M_P^2}k_i^j XX^*\Phi^{*i}\Phi_j + \ldots, \tag{1.59}$$

$$f_{ab} = \frac{\delta_{ab}}{g_a^2}\left(1 - \frac{2}{M_P}f_a X + \ldots\right), \tag{1.60}$$

where Φ_i denotes the chiral superfields of the visible sector, y^{Xijk}, k_i^j, n_i^j, $\overline{n}_i^j$ and f_a are dimensionless couplings, and μ^{Xij} has the dimension of mass. The superfield X represents a spurion whose F-term acquires a non-zero VEV F

$$X = \theta\theta F, \qquad X^\dagger = \bar{\theta}\bar{\theta}\,\overline{F}. \tag{1.61}$$

After performing the integral over the superspace one gets the following SUSY breaking Lagrangian

$$\mathcal{L}_{\text{soft}} = -\frac{F}{2M_P}f_a\lambda^a\lambda^a - \frac{F}{6M_P}y^{Xijk}\phi_i\phi_j\phi_k - \frac{F}{2M_P}\mu^{Xij}\phi_i\phi_j - \frac{F}{M_P}n_i^j\phi_j W^i_{\text{MSSM}} + \text{h.c.}$$

$$-\frac{|F|^2}{M_P^2}(k^i_j + n^i_p \overline{n}^p_j)\phi^{*j}\phi_i\,. \tag{1.62}$$

On the other hand, the MSSM superpotential is given by

$$W_{\rm MSSM} = \frac{1}{6}y^{ijk}\Phi_i\Phi_j\Phi_k + \frac{1}{2}\mu^{ij}\Phi_i\Phi_j. \tag{1.63}$$

This leads to the following soft terms

$$M_a = \frac{F}{M_P}f_a, \tag{1.64}$$

$$a^{ijk} = \frac{F}{M_P}(y^{Xijk} + n^i_p y^{pjk} + n^j_p y^{pik} + n^k_p y^{pij}), \tag{1.65}$$

$$b^{ij} = \frac{F}{M_P}(\mu^{Xij} + n^i_p \mu^{pj} + n^j_p \mu^{pi}), \tag{1.66}$$

$$(m^2)^i_j = \frac{|F|^2}{M_P^2}(k^i_j + n^i_p \overline{n}^p_j). \tag{1.67}$$

Also the operator $\phi^{*i}\phi_j\phi_k$ is generated from non-renormalizable terms in the Kähler potential, but its coupling is of order $F^2/M_P^3 \sim m^2_{\rm soft}/M_P$, i.e. it is very suppressed. To explain the absence of $\mathcal{O}(1)$ flavor changing neutral current (FCNC) effects in gravity mediation additional structure is needed. The parameters f_a, k^i_j, n^j_i, y^{Xijk} and μ^{Xij} may be determined from the theory of ultraviolet completion. In principle the gravitino mass is comparable to other soft masses. But the details of the spectrum are model-dependent.

Related to this context, a setup in which all supersymmetric particles have masses around a common mass scale $m_{\rm SUSY}$, that can be generically much larger than the electroweak scale, has received some interest in the literature. This scenario is known as *High-Scale SUSY*. For simplicity, sometimes we will assume that all supersymmetric particles are degenerate in mass.

1.4.2 Gauge mediation

Supersymmetry breaking can be communicated to the observable sector through gauge interactions leading to the so-called gauge mediated supersymmetry breaking (GMSB) models. One introduces new chiral superfields, called messengers, that couple to the SUSY breaking sector and are charged under the SM group. In the simplest GUT version, the messenger fields are a set of left-handed chiral supermultiplets q, $\bar{q}$, ℓ, $\bar{\ell}$ with the following charges under $SU(3)_C \times SU(2)_L \times U(1)_Y$

$$q \sim (\mathbf{3},\mathbf{1},-\frac{1}{3}), \qquad \overline{q} \sim (\overline{\mathbf{3}},\mathbf{1},\frac{1}{3}), \qquad \ell \sim (\mathbf{1},\mathbf{2},\frac{1}{2}), \qquad \overline{\ell} \sim (\mathbf{1},\mathbf{2},-\frac{1}{2}). \tag{1.68}$$

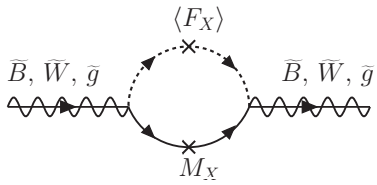

Figure 1.3: One-loop diagrams generating the MSSM gauginos masses in GMSB.

The messengers acquire their masses from a superpotential coupling to a spurion superfield X

$$W \supset y_2 X \ell \,\overline{\ell} + y_3 X q \overline{q}, \tag{1.69}$$

whose scalar component and its $F-$term have a non-zero VEV,

$$\langle X \rangle = M_X + \theta^2 \langle F_X \rangle. \tag{1.70}$$

While masses of the fermion component of the messengers $(\psi_\ell, \psi_{\overline{\ell}}, \psi_q, \psi_{\overline{q}})$ receives only supersymmetric contribution from the Yukawa type interaction with the spurion, the scalars $(\phi_\ell, \phi_{\overline{\ell}}, \phi_q, \phi_{\overline{q}})$ receive both supersymmetric and non-supersymmetric contributions from the potential

$$m_{\psi_\ell, \psi_{\overline{\ell}}} = y_2 M_X, \quad m^2_{\phi_\ell, \phi_{\overline{\ell}}} = |y_2 M_X|^2 \pm |y_2 \langle F_X \rangle| \tag{1.71}$$

$$m_{\psi_q, \psi_{\overline{q}}} = y_3 M_X, \quad m^2_{\phi_q, \phi_{\overline{q}}} = |y_3 M_X|^2 \pm |y_3 \langle F_X \rangle|. \tag{1.72}$$

The MSSM gaugino masses are generated at one-loop from the diagrams in fig. 1.3, where the internal lines represents the scalar and fermion component of the messengers and the vertex arises from the supersymmetric gauge interactions. These one-loop diagrams give

$$M_a = \frac{\alpha_a}{4\pi} \Lambda, \tag{1.73}$$

where Λ is a mass parameter defined as

$$\Lambda \equiv \frac{\langle F_X \rangle}{M_X}. \tag{1.74}$$

The leading contribution to the scalar masses starts at two-loops (see fig. 1.4), with messenger fermions (represented by heavy solid lines), messenger scalars (heavy dashed-lines) and ordinary gauge bosons (wavy lines) and gauginos (solid lines with wavy lines on top) around the loops. The result reads

$$m^2_{\phi_i} \;=\; 2\Lambda^2 \left[\left(\frac{\alpha_3}{4\pi} \right)^2 C_3(i) + \left(\frac{\alpha_2}{4\pi} \right)^2 C_2(i) + \left(\frac{\alpha_1}{4\pi} \right)^2 C_1(i) \right], \tag{1.75}$$

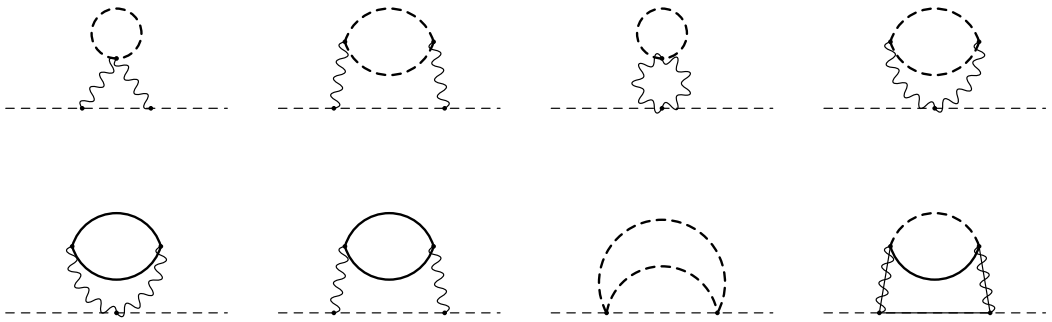

Figure 1.4: Two-loop diagrams inducing the scalar soft masses in GMSB at leading order, with messenger fermions (represented by heavy solid lines), messenger scalars (heavy dashed-lines), ordinary gauge bosons (wavy lines) and gauginos (solid lines with wavy lines on top) around the loops.

where $C_a(i)$ are the quadratic Casimir invariants, defined in terms of the Lie algebra generators T^a by $(T^a T^a)^j_i = C_a(i)\delta^j_i$. The scalar cubic couplings $\mathbf{a_u}, \mathbf{a_d}, \mathbf{a_e}$ are generated at two-loops, but they have dimension of (mass)^1 so they are suppressed with respect to the gaugino and scalar masses. For practical purposes, it is a very good approximation to assume

$$\mathbf{a_u} = \mathbf{a_d} = \mathbf{a_e} = 0. \tag{1.76}$$

Note that the MSSM soft masses and cubic couplings are running parameters and the eqs. (1.73)–(1.76) holds at the renormalization scale corresponding to the average characteristic mass of the messengers, i.e. $M_{\rm mess} \sim y_I M_X$ with $I = 2, 3$. Also these equations have been obtained under the assumption $\langle F_X \rangle / (y_I M_X^2) \ll 1$ when the mass splittings within each messenger supermultiplet are small compared to the overall messenger scale.

The model can be generalized to have a different messenger sector with chiral superfields $\Phi_I, \overline{\Phi}_I$ coupled to the spurion X by

$$W_{\rm mess} = \sum_I y_I X \Phi_I \overline{\Phi}_I. \tag{1.77}$$

The left-handed supermultiplet $\overline{\Phi}_I$ transforms as the complex conjugate representation of Φ_I, also a left-handed supermultiplet. When the spurion X is substituted by the VEV, the masses for the components of the messenger superfields develop. Then the MSSM soft masses have the following form

$$M_a = \frac{\alpha_a}{4\pi} \Lambda \sum_I n_a(I), \quad (a = 1, 2, 3) \tag{1.78}$$

$$m_{\phi_i}^2 = 2\Lambda^2 \sum_I \left[\left(\frac{\alpha_3}{4\pi}\right)^2 C_3(i) n_3(I) + \left(\frac{\alpha_2}{4\pi}\right)^2 C_2(i) n_2(I) + \left(\frac{\alpha_1}{4\pi}\right)^2 C_1(i) n_1(I) \right], \tag{1.79}$$

where $n_a(I)$ is the Dynkin index for $\Phi_i + \overline{\Phi}_i$, with the normalization in which $n_3 = 1$ for a $\mathbf{3} + \overline{\mathbf{3}}$ of $SU(3)_C$, $n_2 = 1$ for a $\mathbf{2} + \overline{\mathbf{2}}$ of $SU(2)$ and for $U(1)_Y$ the Dynkin index is $n_1 = 6Y^2/5$ for each pair with weak hypercharges $\pm Y$. In order to keep the prediction of unification of gauge couplings, if the messengers have masses below the GUT scale, they should appear in complete representations of the $SU(5)$ group that contains the Standard Model gauge group, and the various components should have similar masses. Therefore, often it is consider that the messenger sector is composed by N_5 copies of the $\mathbf{5} + \overline{\mathbf{5}}$ of $SU(5)$. In this case the Dynkin indices are given by $\sum_I n_a(I) = N_5$ for $a = 1, 2, 3$. The minimal model corresponds to $N_5 = 1$.

Solutions to the μ problem in GMSB theories generically introduce a $\mu - B_\mu$ problem [38]: both μ and B_μ are generated at the same order in perturbation theory (say one-loop), which produces a hierarchy $B_\mu \gg \mu^2$ inconsistent with EWSB. There are solutions to the $\mu - B_\mu$ problem (see e.g. [38–40] and references therein) but they require excessive model building.

One of the most attractive features of gauge mediation models is that the masses of the scalar superpartners depend only on their gauge quantum numbers, thus the flavor-violating mixings are automatically suppressed.

Minimal Gauge Mediation (MGM)

GMSB scenarios do not necessarily predict the values of μ and B_μ. Natural implementations of GMSB have to deal with the μ and the $\mu - B_\mu$ problems. Minimal gauge mediation (MGM) scenario does not try to address these problems. Instead it is driven by minimality.

The soft masses for scalars and gauginos are generated as explained above. On the other hand, MGM does not predict a value for the superpotential parameter μ, it is rather treated as an independent parameter whose value is fixed by the EWSB condition. The parameter B_μ and the trilinear scalar couplings are negligible at the messenger scale where SUSY breaking MSSM parameters originate. This is a plausible assumption because in gauge mediation the A-terms are generated at two loops and there is no compelling argument to forbid vanishing tree level B_μ term. Both the values of the A-terms and B_μ are generated by radiative corrections when they are evolved to the electroweak scale. Since B_μ violates both Peccei-Quinn symmetry and R-symmetry, in order to generate a non-zero

value from the RGEs in eq. (1.29), non-zero values are required for μ and at least one of the trilinear couplings or the electroweakino masses.

MGM has interesting phenomenological consequences [41, 42], as will be shown in section 3.5.1. We will also see that requiring the model reproduces the observed value of the Higgs mass is a very powerful constraint.

Lopsided Gauge Mediation

Lopsided gauge mediation models [43] propose a solution to the $\mu - B_\mu$ problem of gauge mediation, where both μ and B_μ are generated at one-loop order. The soft masses are generated as in minimal gauge mediation through messenger loops. On the other hand, μ and B_μ are generated by adding direct couplings of the Higgs doublets to two (additional) pairs of messenger fields ($D, \bar{D}$ and $S, \bar{S}$)

$$W = \lambda_u H_u D S + \lambda_d H_d \bar{D} \bar{S} + X_D D \bar{D} + X_S S \bar{S}, \tag{1.80}$$

with

$$X_{D,S} = M_{D,S}(1 + \Lambda_{D,S}\, \theta^2)\,. \tag{1.81}$$

Then, the calculation of the soft parameters of the Higgs sector yields

$$m^{2\,(l)}_{H_{u,d}} = \frac{\lambda^2_{u,d}}{16\pi^2} \Lambda_D^2\, P(x,y) \tag{1.82}$$

$$\mu = \frac{\lambda_u \lambda_d}{16\pi^2} \Lambda_D\, Q(x,y) \tag{1.83}$$

$$B_\mu = \frac{\lambda_u \lambda_d}{16\pi^2} \Lambda_D^2\, R(x,y) \tag{1.84}$$

$$A_{u,d} = \frac{\lambda^2_{u,d}}{16\pi^2} \Lambda_D\, S(x,y)\,, \tag{1.85}$$

with $x = M_S/M_D, y = \Lambda_S/\Lambda_D$ and the (P, Q, R, S) functions defined as

$$P(x,y) = \frac{x^2(1-y)^2}{(x^2-1)^3} \left[2(1-x^2) + (1+x^2)\log x^2\right] \tag{1.86}$$

$$Q(x,y) = \frac{x}{(x^2-1)^2} \left[(x^2-1)(1-y) + (y-x^2)\log x^2\right] \tag{1.87}$$

$$R(x,y) = \frac{x}{(x^2-1)^3} \left\{(1-x^4)(1-y)^2 + \left[2x^2(1+y^2) - y(1+x^2)^2\right]\log x^2\right\} \tag{1.88}$$

$$S(x,y) = \frac{1}{(x^2-1)^2} \left[(x^2-1)(1-x^2 y) - x^2(1-y)\log x^2\right]\,. \tag{1.89}$$

Unfortunately, one finds R and P satisfy $|R(x,y)| \geq 2P(x,y)$ for any x and y. This relation is *problematic* for EWSB because for small value of μ it implies

$$m_{H_u}^2 m_{H_d}^2 - B_\mu^2 \propto P^2(x,y) - R^2(x,y) < 0 \tag{1.90}$$

at the messenger scale. Namely, EWSB takes place at the messenger scale, leading to a spectrum with too light sparticles. In the original proposal [43], this difficulty was overcome by complicating the model. We re-examine the simplest versions of lopsided gauge mediation in chapter 3 (section 3.5.2) and analyze whether the EWSB condition can be satisfied without adding new degrees of freedom.

The phenomenology of some enlarged versions of the model was discussed in detail in ref. [43]. As it is often the case in gauge mediation, the LSP is the gravitino. Since μ and B_μ originate at the same order in perturbation theory, generically they satisfy $\mu \ll B_\mu$ and the EWSB condition imply that μ is smaller than the scale of the soft masses. Then, the model is characterized by a light higgsino which is typically the next-to-lightest supersymmetric particle (NLSP), although the possibility of sneutrino NLSP was also considered in [43].

1.4.3 Anomaly mediation

We discuss a model known as (un-sequestered) anomaly-mediated supersymmetry breaking (AMSB) [44]. Scalar masses are generated by gravity-mediated contribution of order the gravitino mass $m_{3/2}$. Gaugino masses are protected by R-symmetry and the leading contribution comes from one-loop anomaly mediation effects [44, 45]

$$M_a = \frac{\beta_{g_a}}{g_a} m_{3/2}, \tag{1.91}$$

where β_{g_a} is the β-function of the gauge coupling g_a. Similarly, the trilinear couplings also receive their main contribution from anomaly mediation

$$a_f = -\beta_{y_f} m_{3/2}, \tag{1.92}$$

with β_{y_f} being the β-function corresponding to the top Yukawa y_f of the fermion f. The eqs. (1.91) and (1.92) hold at any renormalization scale to all orders in perturbation theory since they resulted from the conformal anomaly. The spectrum naturally has a one-loop splitting between the scalars and gauginos. The values of μ and B_μ depend on the details of the hidden sector and its interactions with the Higgses.

To completely specify the model one should define how μ and B_μ are generated. Both μ and B_μ can be generated compatible with EWSB by supergravity

effects through the Giudice-Masiero mechanism [37]. This is triggered by the operators

$$\int d^4\theta \frac{X^\dagger X}{M_P^2} H_u H_d, \quad \int d^4\theta \frac{X^\dagger}{M_P} H_u H_d, \tag{1.93}$$

with chiral superfield $X = M_P + \theta^2 F$. The integrals produce $B_\mu \sim |\mu|^2 \sim m_{3/2}^2$. In this case the tuning of EWSB can be achieved through either μ or B_μ and $m_{H_u}^2$ can run negative (see eg. [36]). Another possibility corresponds to $B_\mu \sim m_{3/2}^2 > |\mu|^2$, where the tuning of EWSB must be carried out through B_μ and $m_{H_u}^2$ must stay positive. This can also be accomplished by the Giudice-Masiero mechanism, assigning a VEV to X smaller than M_P and R-charge to X different from to 2 such that the second operator in eq. (1.93) is forbidden.

Without an alignment mechanism, $\mathcal{O}(1)$ flavor violations are expected from the gravity mediated contributions to the scalar masses and FCNCs bound the scalar masses to lie above few 10^3 TeV [46]. Given the high scale of mediation, additional constraints exist from the RGE evolution of the soft spectrum potentially leading to unwanted tachyonic states [36]. The LHC phenomenology depends on the origin μ/B_μ and the solution to the flavor problem. In the absence of an alignment mechanism of the soft masses, the gravitino mass should be sufficiently large implying that gauginos are not accessible at the LHC, although higgsinos may be light. If the flavor problem is addressed, gauginos and in particular the gluino may be accessible at the LHC.

1.4.4 Split SUSY

Supported by the failure of the naturalness principle in explaining the smallness of the cosmological constant, one can consider theories in which SUSY is broken at scales much higher than the TeV. Moreover the absence of experimental evidence of sparticles already introduces a little hierarchy problem. Split SUSY [9, 10] models are characterized by scalar superparticles with masses around m_0 well above the TeV scale, while fermionic superparticles are lighter as they are protected by R-symmetry, with masses of order $m_{1/2}$ possibly near the weak scale. The AMSB model considered in the previous section leads to a Split-SUSY spectrum. Other examples such as $U(1)'$ mediation, Split-gauge mediation and triplet mediation are discussed in [36].

Fermions near the TeV scale are convenient in order to preserve the successful gauge coupling unification. In particular, higgsinos should be below 100 TeV. On the other hand, scalars come in almost complete representations of $SU(5)$ and do not affect unification at one loop order. The heavy Higgs doublet gives a small contribution to the running of the gauge couplings. Another reason to expect

gauginos and higgsinos to be near the TeV scale is to provide a good dark matter candidate.

This pattern of SUSY breaking is exempt from the usual difficulties of the MSSM: the absence of sparticles, dimension five proton decay, SUSY flavor and CP problems, and the cosmological gravitino problem. It is important to note that the scalar superparticles can not be arbitrarily heavy with respect to the fermions, as their masses are constrained to be below 10^5 TeV [36, 47, 48] by the measured value of the Higgs mass. Having correct electroweak symmetry breaking and the renormalization group evolution of the scalar masses also constrain Split model building.

The phenomenology of Split SUSY has a golden channel of gluino decaying into a quark, antiquark and the LSP. Since the scalar masses has to lie below 10^5 TeV in order to reproduce the Higgs mass, the gluino lifetime is generically less than 10^{-8} s. Therefore, if the gluinos are produced at the LHC, they will show up as displaced vertices or prompt decays unless the scalars are above 10^4 TeV, as discussed in [36].

In case the gluino is the LSP, it decays directly, for example into a gravitino and a gluon. Then the gluino lifetime is not related to the scalar masses but still its decay leads to interesting phenomenology. There are other channels involving the gauginos and higgsinos but the best LHC search strategy depends on the details of the spectrum. A light bino with no other accessible states is undetectable. More optimistic appears the production of light higgsinos, light winos or an admixture of electrowikinos and/or higgsinos.

1.5 Experimental searches for SUSY

1.5.1 Direct searches at colliders

After two years of maintenance and upgrading, the LHC has started its second three-year run. It is operating at collision energy of 13 TeV, a substantial increase with respect to the run I, which began at 7 TeV, rising to 8 TeV.

As mentioned before, R-parity implies that sparticles are produced in pairs. The production of colored particles is dominated by the strong interactions, the processes at the partonic level has the form

$$gg \to \widetilde{g}\widetilde{g}, \quad \widetilde{q}_i\widetilde{q}_j^*, \tag{1.94}$$

$$gq \to \widetilde{g}\widetilde{q}_i, \tag{1.95}$$

$$q\overline{q} \to \widetilde{g}\widetilde{g}, \quad \widetilde{q}_i\widetilde{q}_j^*, \tag{1.96}$$

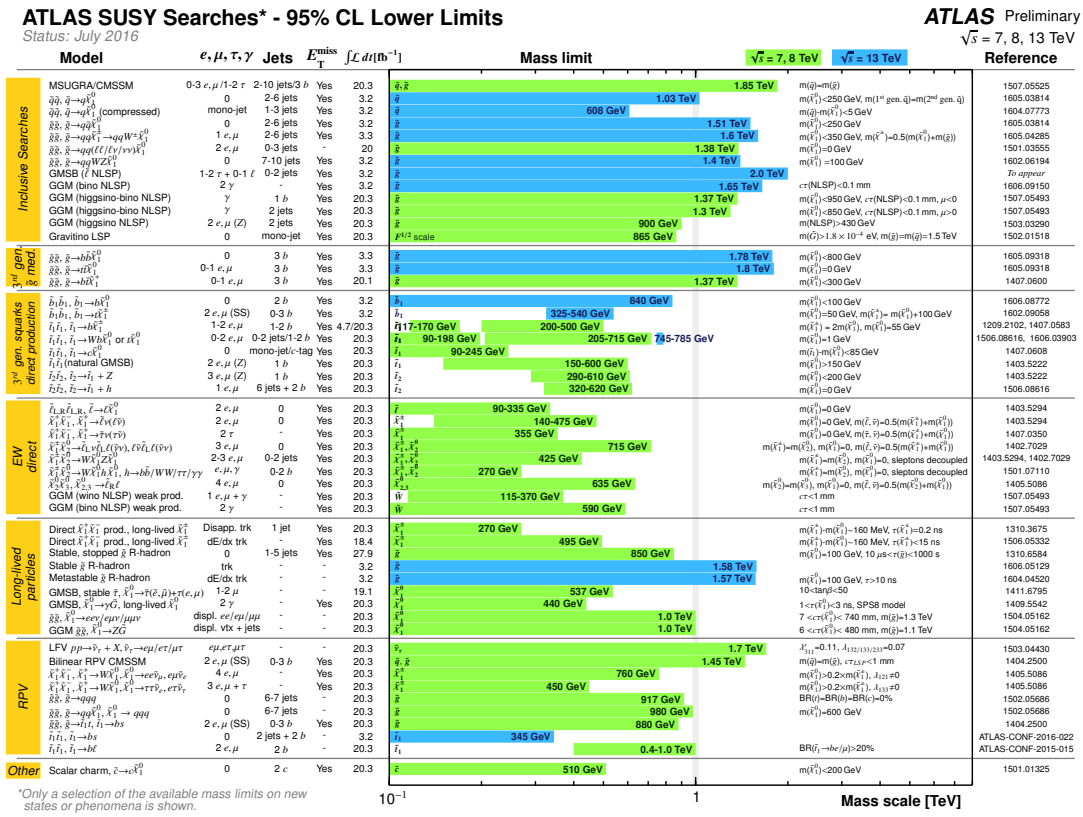

Figure 1.5: Summary results of SUSY searches of the ATLAS experiment [5].

$$qq \to \widetilde{q}_i \widetilde{q}_j, \tag{1.97}$$

while the production of other sparticles are controlled by the electroweak gauge couplings

$$q\overline{q} \to \widetilde{C}_i^+ \widetilde{C}_j^-, \quad \widetilde{N}_i \widetilde{N}_j, \qquad u\overline{d} \to \widetilde{C}_i^+ \widetilde{N}_j, \qquad d\overline{u} \to \widetilde{C}_i^- \widetilde{N}_j, \tag{1.98}$$

$$q\overline{q} \to \widetilde{\ell}_i^+ \widetilde{\ell}_j^-, \quad \widetilde{\nu}_\ell \widetilde{\nu}_\ell^* \qquad u\overline{d} \to \widetilde{\ell}_L^+ \widetilde{\nu}_\ell \qquad d\overline{u} \to \widetilde{\ell}_L^- \widetilde{\nu}_\ell^*. \tag{1.99}$$

Loosely speaking, the LHC can be considered as a gluon-gluon and gluon-quark collider given the shape of the parton distribution functions. Of course, the signals are an inclusive combination of all the possible parton collisions.

One expects the produced sparticles to decay to states with two LSPs, which escape the detector; this leads to the typical SUSY signature at colliders of missing energy $\not{E}_T$ (or transverse momenta). The standard observable signals for SUSY at hadron colliders are final states of the form n jets + m leptons + $\not{E}_T$, where either the number of jets n or the number of leptons m can be zero. These signals

have a large SM background, in particular from processes involving production and decay of W and Z bosons decaying to neutrinos, which also leads to missing energy. Hence it is essential to apply specific signal region cuts in order to reduce the background.

Experimental limits on SUSY are presented in the framework of *full models* or *simplified models*. The *full models* are characterized by a small number of parameters that completely (or almost completely) specify the spectrum, e.g. the GMSB and AMSB models described in section 1.4. In such models the production cross sections and branching ratios of every particle are fixed and events can be realized in many different ways. In this approach the results are difficult to generalize to other models or event topologies. On the other hand, the presentation of SUSY limits in the context of *simplified models* assumes a single production mode and one-step or occasionally two-step decay chain, e.g. $p\,p \to \widetilde{q}\,\widetilde{q} \to q\,\widetilde{\chi}_1^0\,q\,\widetilde{\chi}_1^0$. This has the advantage that the limits can often be re-interpreted for a full model. ATLAS and CMS experiments [5] provide useful summary plots which provide an idea of the current reach on sparticles masses in various channels, see figures 1.5 and 1.6. A good review on the status of SUSY after the first run of the LHC is given in ref. [6].

The current picture of the SUSY bounds is roughly the following. ATLAS and CMS experiments at the run I of LHC at 8 TeV with 20 fb^{-1} luminosity had a sensitivity to sparticle production at the level of $\sigma \times \mathrm{Br} \sim$ few 10 fb. Then, the present limits on sparticles are: $\sim$ TeV on first and second generation squarks and gluinos, $\sim$ 650 GeV on third generation squarks, $\sim$ 250 GeV on sleptons, and $\sim$ 350 GeV on electroweakinos without sleptons and it improves to 500 GeV including light sleptons. These bounds should improve during the second LHC run.

When the gluino and the light-flavor squarks have comparable masses, the squark-gluino associated production is available, with a cross section approximately an order of magnitude larger that gluino pair production. This leads to an improved sensitivity with respect to separate squarks and gluino scenarios, which results in improved limits of around 2 TeV.

These limits on sparticle masses rely on the assumption of kinematically available decays to the lightest neutralino, whose mass is well separated from the decaying particles. The bounds worsen in compressed regions of the parameter space, but there is no clear symmetry argument that motivates such degeneracy.

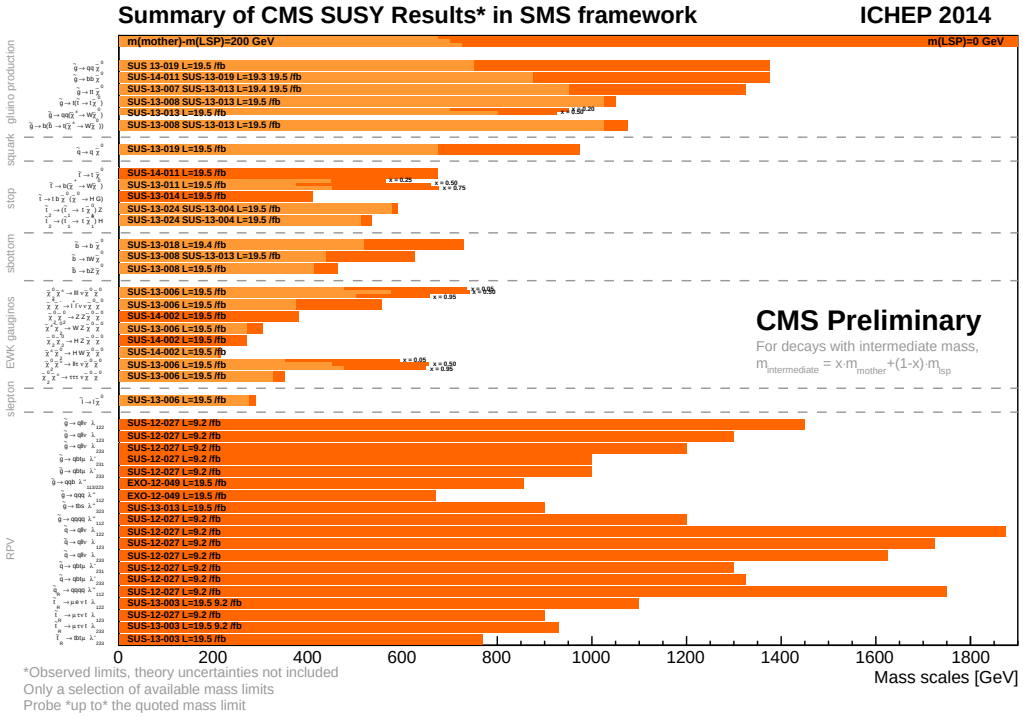

Figure 1.6: Summary of SUSY results of the CMS experiment in the simplified model framework [5].

1.5.2 Low energy observables

As it was already mentioned at the end of section 1.3.2, there are indirect constrains on SUSY from processes that are suppressed or forbidden in the SM but receive quantum corrections from sparticles, like those that imply flavor mixing or CP violation. Among them are included $\mu \to e\,\gamma$ [27], $B \to X_s\gamma$ [49], $B_s \to \mu^+\mu^-$ [50], neutral meson mixing [29, 51], electric dipole moments for the neutron [31] and the electron [32], proton decay [22, 23], etc. Some models are also tightly constrained by the deviation from the SM prediction induced in the muon anomalous magnetic moment and the branching ratio of hadronic Z decays with $b\,\bar{b}$ (see [52], [53] and references therein). To give an idea, if there is mass mixing between the first and second generations, FCNC, in particular $K^0 - \overline{K}^0$ mixing, constrains the scalar superpartners to lie above ∼few 100 TeV in the absence of CP violating phases, and the bounds become one order of magnitude stronger in the presence of such phases [29].

We comment as an example, on some experimental bounds from B physics that has been recently improved [49, 50]. $B \to X_s\gamma$ receives contribution from

the stop-higgsino loop that constrains $A_t \mu \tan\beta / m_{\tilde{t}}^2 <$ few (analytic expressions can be found in [54]). There is also a charged Higgs-top quark loop correction typical from the two Higgs doublet model (2HDM). If there are not accidental cancellations it implies $m_{H^\pm} \gtrsim 300$ GeV, which is complementary to the direct 2HDM searches [55, 56] in the region of low $\tan\beta$. Another important constraints come from $B_s \to \mu^+\mu^-$; the MSSM contribution is dominated by the Penguin diagram involving the exchange of the heavy scalar H and pseudoscalar A with their one-loop induced flavor changing $b \to s$ couplings (see ref. [54]). These corrections decouple as $1/m_A^2$ but put important constraints in the large $\tan\beta$ region because they scale like $\tan^3\beta$.

Aside from the experimental searches, there are strong constraints from the existence of charge and color breaking (CCB) minima in the scalar potential deeper than the realistic minimum and directions in field space along which the potential becomes unbounded from below [57, 58]. In particular, absolute stability requires that the trilinear couplings A_f cannot be much larger than the relevant soft masses for the scalar potential. Allowing the vacuum to be metastable but with lifetime longer than the age of the universe relaxes the bounds only slightly (see [58], or more recently e.g. [59]).

1.5.3 Dark matter direct detection

At the moment the most accurate determination of the dark matter mass density comes from global fits of cosmological parameters. From measurements of the anisotropy of the cosmic microwave background and of the spatial distribution of galaxies the density of cold, non-baryonic matter is given by [51, 60]

$$\Omega_{\rm nbm} h^2 = 0.1186 \pm 0.0020\,, \tag{1.100}$$

where h is the Hubble constant in units of 100 km/(s·Mpc). While the baryonic matter density reads [51]

$$\Omega_b h^2 = 0.02226 \pm 0.00023\,, \tag{1.101}$$

which may also receive a contribution from baryonic dark matter.

The LSP in SUSY models with R-parity conservation may be a viable thermal dark matter candidate. A stable LSP must be neutral from searches for exotic isotopes, see [51] and references therein. Then, the possible candidates among the sparticles are the gravitino, the sneutrino and the lightest neutralino. A sneutrino LSP as primary component of the dark matter halo in our galaxy has been ruled out by various WIMP searches. In many GMSB models the gravitino is the

LSP. Gravitinos may be produced from other sparticle decays or from reheating after inflation. In principle they could account for the observed dark matter relic density, but unfortunately they interact too weakly to be detected directly. The lightest neutralino remains the best option.

If the lightest neutralino is mostly higgsino or mostly wino, it could account for all the observed relic density of dark matter if the mass is 1.1 TeV or 3.2 TeV respectively [61]. Bino-like LSP as dark matter is not possible because the annihilation cross section is too low, so the predicted relic density is too high. An interesting possibility is that the lightest neutralino is a mixture of two of the states bino, wino and higgsino.

In order to account for the observed rotational curves, WIMPs should have the appropriate density profile and should be gravitational trapped inside galaxies like the Milky Way. Their mean velocity inside our galaxy relative to its center should be similar to that of stars (few 100 km/s at the solar system). This implies that WIMPs interact with the ordinary matter on Earth through elastic scattering on nuclei. For masses in the range 10 GeV to 10 TeV, the nuclear recoil energies are of order of 1 to 100 keV, which can be detected by the present experiments. The Xenon100 collaboration [62] and the Large Underground Xenon (LUX) experiment [63] set interesting exclusion limits for the spin independent cross section of the scattering of dark matter off of nucleons. LUX is able to set a minimum upper limit on the cross section of $7.6 \times 10^{-46}\text{cm}^2$ at a WIMP mass of 33 GeV. Applying these constraints to the MSSM with neutralino dark matter, one probes important regions of the parameter space [54, 61].

Chapter 2

MSSM Higgs mass calculation: state of the art

In this chapter we review the state-of-art of the Higgs mass calculation in the MSSM. We also present simplified analytical formulas of the MSSM Higgs mass as a function of the MSSM parameters.

In section 2.1 we describe the main methods used for the MSSM Higgs mass calculation: the Feynman diagrammatic, the effective potential and the effective field theory approaches. We briefly comment on the advantages and disadvantages of each method. In section 2.2 we review the status of the calculation of the higher order corrections to the MSSM Higgs mass. Finally, in section 2.3 we obtain simplified analytical expressions, which facilitate a clear understanding of the dependence of the Higgs mass on the sparticle masses, in particular the gluino mass.

2.1 Calculational methods

There is a relation between the mass of the light CP-even Higgs boson of the MSSM and the other parameters of the model. At tree level, the Higgs boson mass squared has an upper bound, saturated in the decoupling limit $m_h^2 \approx m_Z^2 \cos^2 2\beta$, with $\tan\beta$ defined by the ratio of the Higgs VEVs. Radiative corrections are essential in order to raise the theoretical value predicted in the MSSM to the experimental one:

$$m_h^2 = m_Z^2 \cos^2 2\beta + \frac{3}{2\pi^2}\frac{m_t^4}{v^2}\left[\frac{X_t^2}{m_{\tilde{t}}^2} - \frac{X_t^4}{12 m_{\tilde{t}}^4} + \ln\frac{m_{\tilde{t}}^2}{m_t^2}\right] + \dots , \tag{2.1}$$

where m_t is the top mass, v is the electroweak VEV, X_t is the stop mixing, we have assumed degenerate stop masses $m_{\tilde{t}}$ for simplicity, and the ellipsis stands for other (subleading) corrections at one loop and higher order.

In the literature, radiative corrections to m_h^2 have been computed using three different techniques or combinations of them: direct diagrammatic calculation, effective potential method, and effective theory (or renormalization group) approach. The first one requires the computation of the Higgs self-energy diagrams. The complete expressions are complicated and huge beyond one-loop order. The second one consists of taking the second derivatives of the effective potential; this is equivalent to computing the pole mass from self-energy functions in the approximation that the external momentum is neglected. This has the advantage that calculations can be reduced to vacuum graphs, which can always be computed analytically through 2-loop order. The last method uses the effective Lagrangian formalism, with renormalization group running used to systematically incorporate the effects that are enhanced by logarithms of the ratio of the superpartner mass scale to the electroweak scale.

2.1.1 Feynman Diagrammatic Approach

The tree-level mass matrix for the neutral CP-even Higgs bosons in the interaction basis (S_1, S_2) is given by,

$$M_{\text{Higgs}}^{2,\text{tree}} = \begin{pmatrix} m_{S_1S_1}^2 & m_{S_1S_2}^2 \\ m_{S_1S_2}^2 & m_{S_2S_2}^2 \end{pmatrix} = \begin{pmatrix} m_A^2 \sin^2\beta + m_Z^2 \cos^2\beta & -(m_A^2 + m_Z^2)\sin\beta\cos\beta \\ -(m_A^2 + m_Z^2)\sin\beta\cos\beta & m_A^2\cos^2\beta + m_Z^2\sin^2\beta \end{pmatrix}, \tag{2.2}$$

where S_1 and S_2 are real components of the Higgs doublets $H_1 \equiv H_d$ and $H_2 \equiv H_u$ respectively. When the mass matrix is diagonalized one obtains the tree level masses m_h^{tree}, m_H^{tree}, as described in section 1.3.4.

Radiative corrections to the mass matrix are obtained in terms of the self-energies. The inverse propagator matrix in the interaction basis reads

$$(\Delta_{\text{Higgs}})^{-1} = -i \begin{pmatrix} p^2 - m_{S_1}^2 + \hat{\Sigma}_{S_1S_1}(p^2) & -m_{S_1S_2}^2 + \hat{\Sigma}_{S_1S_2}(p^2) \\ -m_{S_1S_2}^2 + \hat{\Sigma}_{S_1S_2}(p^2) & p^2 - m_{S_2}^2 + \hat{\Sigma}_{S_2}(p^2) \end{pmatrix}, \tag{2.3}$$

with p being the external momentum and $\hat{\Sigma}(p^2)$ the renormalized Higgs-boson self-energies. The latter is written in terms of unrenormalized self-energies $\Sigma(p^2)$, mass renormalization constants δm^2 and wave function renormalizations δZ as

$$\hat{\Sigma}_{S_1S_1}^{(i)}(p^2) = \Sigma_{S_1S_1}^{(i)}(p^2) + \delta Z_{S_1S_1}^{(i)}(p^2 - m_{S_1S_1}^2) - \delta m_{S_1S_1}^{2(i)} \tag{2.4}$$

$$\hat{\Sigma}^{(i)}_{S_2S_2}(p^2) = \Sigma^{(i)}_{S_2S_2}(p^2) + \delta Z^{(i)}_{S_2S_2}(p^2 - m^2_{S_2S_2}) - \delta m^{2(i)}_{S_2S_2} \tag{2.5}$$

$$\hat{\Sigma}^{(i)}_{S_1S_2}(p^2) = \Sigma^{(i)}_{S_1S_2}(p^2) + \delta Z^{(i)}_{S_1S_2}(p^2 - m^2_{S_1S_2}) - \delta m^{2(i)}_{S_1S_2}. \tag{2.6}$$

Here the index $i = 1, 2$ denotes the loop level. Requiring the corresponding renormalization conditions the counterterms are fixed.

Rotating the renormalized self-energies in the interaction basis into the physical (h, H) basis, where the tree-level propagator matrix is diagonal, one gets

$$\begin{pmatrix} \hat{\Sigma}_{HH} & \hat{\Sigma}_{hH} \\ \hat{\Sigma}_{hH} & \hat{\Sigma}_{hh} \end{pmatrix} = D(\alpha) \begin{pmatrix} \hat{\Sigma}_{S_1S_1} & \hat{\Sigma}_{S_1S_2} \\ \hat{\Sigma}_{S_1S_2} & \hat{\Sigma}_{S_2S_2} \end{pmatrix} D^T(\alpha) \tag{2.7}$$

where the rotation matrix is

$$D(\alpha) = \begin{pmatrix} \cos\alpha & \sin\alpha \\ -\sin\alpha & \cos\alpha \end{pmatrix}. \tag{2.8}$$

Then, the $CP-$even Higgs boson masses are given by the real part of the poles of the propagator matrix (or the zeros of the inverse propagator matrix)

$$(\Delta_{\text{Higgs}})^{-1} = -i \begin{pmatrix} p^2 - m^2_{H,\text{tree}} + \hat{\Sigma}_{HH}(p^2) & \hat{\Sigma}_{hH}(p^2) \\ \hat{\Sigma}_{hH}(p^2) & p^2 - m^2_{h,\text{tree}} + \hat{\Sigma}_{hh}(p^2) \end{pmatrix}, \tag{2.9}$$

which is equivalent to solve the equation

$$\left[p^2 - m^2_{h,\text{tree}} + \hat{\Sigma}_{hh}(p^2)\right]\left[p^2 - m^2_{H,\text{tree}} + \hat{\Sigma}_{HH}(p^2)\right] - \left[\hat{\Sigma}_{hH}(p^2)\right]^2 = 0. \tag{2.10}$$

This is a non linear equation which is usually solved iteratively. The solutions lead to the radiative corrected pole masses for the light (m_h) and heavy (m_H) CP-even Higgs bosons.

In the Feynman diagrammatic approach the full momentum dependence is included. As a consequence, the method is very convenient for low SUSY scale, close to the EW scale. The price to pay is that the complete expressions are complicated and huge beyond one-loop order. Moreover, the logarithmic resummation, required for a SUSY scale in the multi-TeV region, is much more involved than in mass-independent renormalization schemes.

2.1.2 Effective potential approach

The tree-level Higgs potential for the neutral components, introduced in section 1.3.4, is given by

$$V_0 = m_1^2 \left|H_1^0\right|^2 + m_2^2 \left|H_2^0\right|^2 + m_3^2 \left(H_1^0 H_2^0 + \text{h.c.}\right) + \frac{g^2 + g'^2}{8}\left(|H_1^0|^2 - |H_2^0|^2\right)^2. \tag{2.11}$$

Here we are using a slightly different notation: $H_1 \equiv H_d$, $H_2 \equiv H_u$, $m_1^2 = m_{H_1}^2 + |\mu|^2$, $m_2^2 = m_{H_2}^2 + |\mu|^2$ and $m_3^2 \equiv B_\mu$. The neutral Higgses can be decomposed into their vacuum expectation values plus their CP-even and CP-odd fluctuations

$$H_1^0 \equiv \frac{v_1 + S_1 + i\,P_1}{\sqrt{2}}\,, \qquad H_2^0 \equiv \frac{v_2 + S_2 + i\,P_2}{\sqrt{2}}\,. \tag{2.12}$$

The mass matrices are obtained, at every order in perturbation theory, by taking derivatives of the effective potential

$$\left(\mathcal{M}_P^2\right)_{ij} = \left.\frac{\partial^2 V_{\text{eff}}}{\partial P_i \partial P_j}\right|_{\text{min}}\,, \qquad \left(\mathcal{M}_S^2\right)_{ij} = \left.\frac{\partial^2 V_{\text{eff}}}{\partial S_i \partial S_j}\right|_{\text{min}}\,, \quad (i,j=1,2)\,, \tag{2.13}$$

where $V_{\text{eff}} = V_0 + V$ is the loop-corrected Higgs potential in the $\overline{\text{DR}}$ scheme, and the fields S_1, S_2, P_1 and P_2 have zero vacuum expectation value. By minimizing the effective potential one gets the two vevs v_1 and v_2

$$\frac{1}{v_1}\left.\frac{\partial V_{\text{eff}}}{\partial S_1}\right|_{\text{min}} = m_1^2 + m_3^2\,\frac{v_2}{v_1} + \frac{(g^2+g'^2)}{4}(v_1^2 - v_2^2) + \frac{1}{v_1}\left.\frac{\partial V}{\partial S_1}\right|_{\text{min}} = 0\,, \tag{2.14}$$

$$\frac{1}{v_2}\left.\frac{\partial V_{\text{eff}}}{\partial S_2}\right|_{\text{min}} = m_2^2 + m_3^2\,\frac{v_1}{v_2} + \frac{(g^2+g'^2)}{4}(v_2^2 - v_1^2) + \frac{1}{v_2}\left.\frac{\partial V}{\partial S_2}\right|_{\text{min}} = 0\,. \tag{2.15}$$

Using eqs. (2.11)–(2.15) the Higgs mass matrices can be written as

$$\left(\mathcal{M}_P^2\right)_{ij} = -m_3^2\,\frac{v_1 v_2}{v_i v_j} - \left.\frac{\delta_{ij}}{v_i}\frac{\partial V}{\partial S_i}\right|_{\text{min}} + \left.\frac{\partial^2 V}{\partial P_i \partial P_j}\right|_{\text{min}}\,, \tag{2.16}$$

$$\left(\mathcal{M}_S^2\right)_{ij} = (-1)^{i+j}\left[-m_3^2\,\frac{v_1 v_2}{v_i v_j} + \frac{(g^2+g'^2)}{2}v_i v_j\right] - \left.\frac{\delta_{ij}}{v_i}\,\frac{\partial V}{\partial S_i}\right|_{\text{min}} + \left.\frac{\partial^2 V}{\partial S_i \partial S_j}\right|_{\text{min}}\,. \tag{2.17}$$

Finally using eqs. (2.16) and (2.17) we can express the CP-even Higgs mass matrix in terms of the CP-odd one as

$$\left(\mathcal{M}_S^2\right)_{ij} = (-1)^{i+j}\left[\left(\mathcal{M}_P^2\right)_{ij} - \left.\frac{\partial^2 V}{\partial P_i \partial P_j}\right|_{\text{min}} + \frac{(g^2+g'^2)}{2}v_i v_j\right] + \left.\frac{\partial^2 V}{\partial S_i \partial S_j}\right|_{\text{min}}\,; \tag{2.18}$$

in turn the CP-odd mass matrix can be written in terms of the pseudoscalar mass m_A and of $\tan\beta$

$$\mathcal{M}_P^2 = \begin{pmatrix} \sin^2\beta & \sin\beta\,\cos\beta \\ \sin\beta\,\cos\beta & \cos^2\beta \end{pmatrix} m_A^2\,. \tag{2.19}$$

The effective potential calculation neglects the external momentum dependence. This has the advantage that calculations can be reduced to vacuum graphs, which can always be computed analytically through 2-loop order. There has been a lot of progress in the computation of the effective potential in the MSSM as well as in the Standard Model.

2.1.3 Effective Field Theory Approach

Effective field theory method is very convenient. It makes calculations easier, because one is forced to concentrate on the important physics (for excellent reviews on EFT see [64, 65]). The relevant parameter in particle physics is the distance scale, or equivalently the energy scale. Any features of the physics that are small compared to the relevant distance scale of the process under consideration is shrunk down to zero size. Then, these finite size effects can be incorporated as perturbations. For this procedure to work, a separation of energy scales is required. In the case of the MSSM, we assume the SUSY scale of the sparticle masses ($m_{\rm SUSY}$) is sufficiently heavy compared to the weak scale ($m_{\rm SUSY} \gg m_Z$).

Particles too heavy to be produced are integrated out and eliminated from the low energy EFT. Requiring the two effective theories describe the same physics lead to matching conditions between the couplings. The couplings of the EFT below $m_{\rm SUSY}$ receive threshold corrections (free of large logarithms), which need to be obtained by a loop computation. To avoid large logarithms, the matching conditions should be evaluated at a renormalization scale Q of order the mass of the particle being integrated out.

Ultraviolet regularization lead to renormalization group running of coupling constants with Q. Moreover, EFT changes the running of coupling constants, replacing the logarithmic dependence on heavy particle masses for scale dependence. The next step of the strategy consist of evolving the couplings from the matching scale down to the weak scale by solving the renormalization group equations (RGE). Finally the running couplings at low energy are related to physical observables. The EFT calculations are usually performed in mass-independent renormalization schemes like modified minimal subtraction $\overline{\rm MS}$.

For the High-Scale SUSY setup presented in section 1.4.1, where all the sparticles have masses around $m_{\rm SUSY}$, the MSSM theory is directly matched with the SM. While in the Split-SUSY scenario, where gauginos and higgsinos are much lighter than the scalars, an additional matching is applied at the intermediate scale $m_{1/2}$ of the fermionic superparticles. The intermediate theory between the mass scales of the scalars m_0 and the fermions $m_{1/2}$ contains the fermionic sparticles in addition to the SM ones. The Lagrangian contains additional terms

$$\begin{aligned}\mathcal{L}_{\rm split} \supset & -\frac{M_3}{2}\tilde{g}^A\tilde{g}^A - \frac{M_2}{2}\tilde{W}^a\tilde{W}^a - \frac{M_1}{2}\tilde{B}\tilde{B} \;-\; \mu\,\tilde{H}_u^T\epsilon\tilde{H}_d \;+ \\ & - \frac{H^\dagger}{\sqrt{2}}\left(\tilde{g}_{2\rm u}\sigma^a\tilde{W}^a + \tilde{g}_{1\rm u}\tilde{B}\right)\tilde{H}_u - \frac{H^T\epsilon}{\sqrt{2}}\left(-\tilde{g}_{2\rm d}\sigma^a\tilde{W}^a + \tilde{g}_{1\rm d}\tilde{B}\right)\tilde{H}_d \;+\; \text{h.c.}\,.\end{aligned} \tag{2.20}$$

Here σ^a are the Pauli matrices and it contains mass terms for the fermions and Higgs-higgsino-gaugino Yukawa interactions. Since gauginos and higgsinos are integrated out at the scale $m_{1/2}$, their contributions must be removed from the matching conditions at m_0, and instead they appear when matching the Split-SUSY theory into the SM at $m_{1/2}$. More details on this approach are given in section 3.1.

Effective field theory techniques require the existence of a hierarchy between the SUSY scale and the weak scale, therefore they are not applicable when $m_{\text{SUSY}} \sim \mathcal{O}(m_Z)$. But the EFT method has several advantages. The resummation of the logarithmic corrections is straightforward by solving the RGE, which allows to consider arbitrary heavy SUSY scale. The physical understanding of the dependence on the various parameters is simple because subleading effects suppressed by the SUSY scale are neglected, while the leading momentum dependence can be incorporated.

2.2 State of the art

For the MSSM (with real parameters) the status of higher-order corrections to the masses and mixing angles in the neutral Higgs sector is advanced (see the reviews [66–68] and references therein). There are several independent computations of the Higgs mass in the MSSM by various groups, using different renormalization conditions (OS, $\overline{\text{DR}}$, hybrid) and gauges (Feynman-'t Hooft, Landau). Some of them are included in computer codes.

The complete one-loop result is known [69, 70]. The dominant contribution is the $\mathcal{O}(\alpha_t)$ one due to top and stop loops. While the effect of sleptons and other squarks is subdominant due to the smallness of their Yukawa coupling relative to the top Yukawa (y_t). The variation of the Higgs mass with chargino and neutralino parameters is of order $2 \div 3$ GeV and decreases for larger values of M_1, M_2 and μ.

In the Feynman-diagrammatic approach the masses are the physical ones and the self-energies should be evaluated at external momentum equal to the poles of the (h, H)-propagator matrix. The momentum-independent parts are the dominant contributions (by momentum independent we mean contributions evaluated at zero external momenta). The prediction for the CP-even Higgs masses contains a dependence of the field renormalization constants which is formally of higher order because eq. (2.10) is solved by iteration. For this reason one can choose suitable renormalization conditions for the field renormalization constants, which can also be seen as different renormalizations of $\tan\beta$.

With respect to the two-loop corrections, all the dominant corrections are available. The $\mathcal{O}(\alpha_t\alpha_s)$, $\mathcal{O}(\alpha_t^2)$, $\mathcal{O}(\alpha_b\alpha_s)$, $\mathcal{O}(\alpha_t\alpha_b)$, $\mathcal{O}(\alpha_b^2)$, $\mathcal{O}(\alpha_\tau^2)$ and $\mathcal{O}(\alpha_b\alpha_\tau)$ contributions to the self-energies are known in the limit of vanishing electroweak gauge couplings (gaugeless) and vanishing external momenta in different renormalization schemes [71–84]. The main contributions are of $\mathcal{O}(\alpha_t\alpha_s)$, followed by the $\mathcal{O}(\alpha_t^2)$ ones.

All order resummation of the $\tan\beta$-enhanced terms, $\mathcal{O}(\alpha_b(\alpha_s\tan\beta)^n)$, have been also performed [85]. This is the dominant part of the contributions from the sbottom sector, which are only sizable for large $\tan\beta$, say $\tan\beta \gtrsim 30$. A similar situation occurs in the stau sector, where even larger values of $\tan\beta$ are needed to have sizable corrections.

A full 2-loop effective potential calculation has been published by Martin [86]. The expressions are quited complicated and difficult to interpret analytically. Moreover, purely electroweak corrections should be of similar order to omitted terms at finite external momentum. The calculation was done for mass-independent renormalization schemes and no computer code containing these terms is publicly available.

The inclusion of two-loop external-momentum effects is quite involved. The two-loop contributions to the Higgs self-energies involving the strong gauge coupling or the third-family Yukawa couplings, including $\mathcal{O}(\alpha\alpha_s)$, was presented by Martin [87]. More recently, the momentum dependent $\mathcal{O}(\alpha_t\alpha_s)$ [88–90] and $\mathcal{O}(\alpha\alpha_s)$[89] corrections have been computed.

The leading 3-loop calculation at $\mathcal{O}(\alpha_t\alpha_s^2)$ is available for vanishing external momentum, based on a $\overline{\text{DR}}$ or a hybrid renormalization scheme for the stop sector [91, 92]. The numerical evaluation depends on the mass hierarchies of the sparticles. This contribution has an effect of a few 100 MeV and is included in the computer code *H3m* [92].

Other efforts have been dedicated to the resummation of the logarithmic corrections, which is easily done in the EFT approach. It allows a high precision prediction for the Higgs mass with stop masses above the TeV scale. The calculation of the SM β-functions up to three loops have been completed (see [93] and references therein). They have been used for the EFT calculation of the Higgs mass in the MSSM at NNLO precision in [94]. The latest versions of the FeynHiggs code [95, 96], provides a combination of the full one-loop result, plus the dominant two-loop corrections and a resummation of the leading and subleading logarithmic corrections from the top-stop sector.

There are two types of uncertainties in the prediction of the light CP-even Higgs boson mass. One consists of the parametric uncertainties due to the experimental uncertainties of the input parameters. The dominant source is associated

to the experimental determination of the top quark mass. To give an idea, the experimental uncertainty on the top mass influences the prediction for the Higgs mass approximately as [97]

$$\frac{\delta m_h^{(m_t)}}{\delta m_t^{\rm exp}} \sim 1. \tag{2.21}$$

Therefore, high precision in the Higgs sector requires accurate measurements of the top mass.

The second type are the intrinsic theoretical uncertainties associated to unknown higher order corrections. Understanding them is very important in order to fix some differences found in the recent literature, presented in the next section.

The FeynHiggs code estimates the theoretical uncertainty in the computation of the Higgs masses and mixing, taking into account three effects: the variation of the renormalization scale from $m_t/2$ to $2m_t$, the use of $m_t^{\rm pole}$ instead of $m_t^{\rm run}$ in the two-loop corrections, and the exclusion of higher-order resummation effects in the sbottom sector. The inclusion of the resummation of the leading and subleading logarithms at all orders reduces the theoretical uncertainty related to the remaining unknown higher-order corrections. For a review on possible ways of estimating the uncertainty see for instance [98].

2.2.1 Discrepancies among existing computations

There have been some discrepancies among recent computations of the MSSM Higgs mass. The FeynHiggs code [95] implement the fixed-order result, including the full one-loop, and the two-loop corrections $\mathcal{O}(\alpha_s\alpha_t)$, $\mathcal{O}(\alpha_t^2)$, $\mathcal{O}(\alpha_b\alpha_s)$, $\mathcal{O}(\alpha_t\alpha_b)$, and $\mathcal{O}(\alpha_b^2)$ at zero external momentum evaluated in the effective potential approach. All order resummation of the $\tan\beta$-enhanced $\mathcal{O}(\alpha_b(\alpha_s\tan\beta)^n)$ and the momentum-dependent two-loop $\mathcal{O}(\alpha_t\alpha_s)$ corrections are also included. The latest versions [96] perform a combination of the fixed order result with a NLL resummation of the logarithmic corrections from the stop sector, allowing to compute the Higgs mass in the multi TeV region of the relevant sparticle masses.

Some computer codes: SoftSUSY [99, 100], SuSpect [101], and SPheno [102, 103], which compute the mass spectrum of the MSSM including the full one-loop and the dominant two-loop corrections to the Higgs masses in the $\overline{\rm DR}$ scheme at fixed order, are also available. They are expected to deviate from the results with logarithmic resummation for multi TeV stops.

Other recent calculations based on the EFT techniques have appeared [1, 94, 104]. They have achieved a good precision for stops around the TeV scale and above. The numerical results of the EFT computations are similar. Small differences in the computations are associated with subleading corrections to the

SUSY thresholds and the matching at the weak scale that are included in some and neglected in others.

It has been pointed out in [105] the presence of significant deviations between the Higgs mass calculation in the OS scheme implemented in FeynHiggs [95] and the $\overline{\text{DR}}$ calculations performed in SofSUSY [99], SuSpect [101], and SPheno [102]. It was also noticed that the deviations were larger for maximal stop mixing. However, the comparison in [105] was done for fixed-order calculations in what were considered natural regions of the parameter space and when the value of m_h was still unknown. Thus this comparison does not necessarily apply to computations with SUSY scale above the TeV, when RGE resummation is required.

In ref. [104] it was found that the EFT calculation of m_h gives values which are lower than those computed by other methods: CPSuperH [106], FeynHiggs [95], SoftSUSY [99], SPheno [102, 103], and H3M [92] for stop masses of ~ 1 TeV. Similar deviations were also found in [94] for two indicative scenarios. For heavy and degenerate SUSY masses $m_{\text{SUSY}} = 10$ TeV, no stop mixing $X_t = 0$ and $\tan\beta = 20$ the result of the EFT computation in [94] gives $m_h = 123.6$ GeV, while $m_h = 126.5$ GeV was obtained using FeynHiggs [95, 96]. In the case of vanishing stop mixing the radiative correction are expected to be under control. The other scenario corresponds to SUSY mass parameters all equal to $m_{\text{SUSY}} = 1$ TeV, maximal stop mixing and $\tan\beta = 20$. Here ref. [94] reported $m_h^{\max} \approx 123$ GeV in contrast with FeynHiggs $m_h^{\max} \approx 129 - 131$ GeV (depending on the code's setting). While SoftSusy, SuSpect and SPheno give values in between $m_h^{\max} \approx 124.5 - 126.5$ GeV.

We will discuss the origin of the discrepancies in detail and explain how to reconcile the existing results in section 3.1. We will see that discrepancies are mostly related to the high sensitivity of the Higgs mass to the values of the top mass and the top Yukawa coupling. More recently, subsequent versions of the available codes have taken into account the causes of discrepancies discussed in [1] and presented in section 3.1, and are now in better agreement.

2.3 Simplified analytical expressions

Full expressions of the radiative corrections to the Higgs mass squared, including the leading two-loop corrections are very long, which makes difficult to visualize the dependence on the various parameters. It is convenient to find analytical simplified expressions for m_h^2 with a more clear dependence on the MSSM parameters.

A simplified analytical formula which has been extensively used in the literature was provided by Carena et. al. [107]. It is easily derived by using EFT.

The formula contains the one-loop threshold at the scale of the (common) stop masses $m_{\tilde{t}}$ and the two-loop leading logarithmic corrections which are obtained by solving iteratively the two-loop RGE. It reads

$$m_h^2 = m_Z^2 \cos^2 2\beta \left(1 - \frac{3}{4\pi^2}\frac{\overline{m}_t^2}{v^2}\ln\frac{m_{\tilde{t}}^2}{m_t^2}\right) + \frac{3}{2\pi^2}\frac{\overline{m}_t^4}{v^2}\left[\frac{X_t^2}{m_{\tilde{t}}^2} - \frac{X_t^4}{12m_{\tilde{t}}^4} + \ln\frac{m_{\tilde{t}}^2}{m_t^2}\right] + \frac{3}{32\pi^4}\frac{\overline{m}_t^4}{v^2}\left(3\frac{m_t^2}{v^2} - 32\pi\alpha_3\right)\left[2\left(\frac{X_t^2}{m_{\tilde{t}}^2} - \frac{X_t^4}{12m_{\tilde{t}}^4}\right)\ln\frac{m_{\tilde{t}}^2}{m_t^2} + \ln^2\frac{m_{\tilde{t}}^2}{m_t^2}\right], \quad (2.22)$$

where $\overline{m}_t$ is the running top mass, and α_3 is the running strong coupling constant at the scale of the top mass.

The main radiative corrections can be obtained and resummed using renormalization group techniques. On the other hand, the finite non-logarithmic terms require a two-loop computation. The most important two-loop non-logarithmic contribution originate from the stop mixing dependent terms. It can increase the value of the Higgs mass up to 5 GeV [78], in a fixed order computation in the region of maximal mixing and for $m_{\tilde{t}} = 1$ TeV. Also the condition of maximal mixing $(X_t)_{\max} \approx \pm\sqrt{6}m_{\tilde{t}}$ gets slightly modified as $(X_t)_{\max} \approx \pm 2m_{\tilde{t}}$.

As it was pointed in ref. [80], in the simplified formula of eq. (2.22), m_h is symmetric under $X_t \to -X_t$ and has a minimum at $X_t = 0$. However, the two loop fixed order corrections are odd in X_t, leading to values of the Higgs mass which differ substantially for positive and negative mixing and also the local minimum is moved slightly away from the origin.

A logical extension of eq. (2.22), by including the $\mathcal{O}(\alpha_t\alpha_s)$ terms, has been obtained both by a diagrammatic computation [75] and the effective potential method [78, 79]. When the one-loop corrections are written in terms of OS parameters, including the top mass, the $\mathcal{O}(\alpha_t\alpha_s)$ expression reads

$$\Delta m_h^2 = \frac{\alpha_s m_t^4}{\pi^3 v^2}\left[-3\ln^2\frac{m_{\tilde{t}}^2}{m_t^2} - 6\ln\frac{m_{\tilde{t}}^2}{m_t^2} + 6\frac{X_t}{m_{\tilde{t}}} - 3\frac{X_t^2}{m_{\tilde{t}}^2}\ln\frac{m_{\tilde{t}}^2}{m_t^2} - \frac{3}{4}\frac{X_t^4}{m_{\tilde{t}}^4}\right]. \quad (2.23)$$

In the expression above it is assumed that the gluino mass is equal to the common stop mass $m_{\tilde{g}} = m_{\tilde{t}}$. There are other simplified expressions (for example [80, 108]), but eq. (2.23) works quite well and captures the asymmetry in X_t.

A simplified expression containing also the two loop top Yukawa corrections have been proposed by Espinosa and Zhang [79]. Using an effective potential approach, they computed the two-loop $\mathcal{O}(\alpha_t^2)$ radiative corrections to m_h^2 in the simplified case of degenerate soft masses (M_S) for the scalars (stops and pseudocalar Higgs), while the μ parameters is kept independent. The mass eigenvalues of the stops are $m_{\tilde{t}_{1,2}}^2 = m_{\tilde{t}}^2 \pm m_t X_t$, with $m_{\tilde{t}}^2 = M_S^2 + m_t^2$, and mixing angle

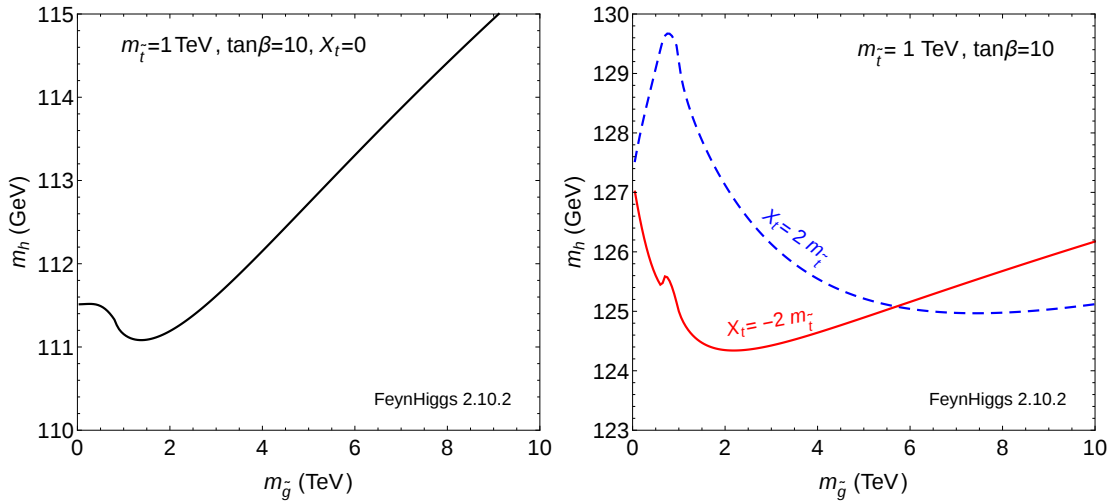

Figure 2.1: Dependence of the Higgs mass m_h on the gluino mass $m_{\tilde{g}}$ for no stop mixing $X_t = 0$ (left plot), and maximal mixing (right plot). We assumed a degenerate superparticle spectrum at $m_{\tilde{t}} = 1$ TeV and $\tan\beta = 10$. The plots are done with FeynHiggs 2.10.2. The asymmetry of m_h with respect to X_t is erased for $m_{\tilde{g}} \ll m_{\tilde{t}}$ or $m_{\tilde{g}} \approx 6m_{\tilde{t}}$, and for larger gluino mass the asymmetry is reversed.

$\sin^2\theta_{\tilde{t}} = \cos^2\theta_{\tilde{t}} = 1/2$ of the top squark squared mass matrix. These contributions are sizable for the maximal stop mixing case. They can increase m_h by as much as 5 GeV in a fixed order computation, assuming $m_{\tilde{t}} = 1$ TeV [79]. These analytical simplified formulas approximate well (with differences below GeV) the exact fixed order results.

2.3.1 Dependence on the gluino mass

It has been customary to assume the gluino mass satisfies $m_{\tilde{g}} \approx m_{\tilde{t}}$ to derive the simplified analytical expressions. This is done for simplicity and to avoid dealing with the additional scale set by $m_{\tilde{g}}$. But the gluino mass dependence of the Higgs can be important, as it is shown in figs. 2.1 and 2.2.

Fig. 2.1 shows m_h as a function of the gluino mass for $\tan\beta = 10$, $m_{\tilde{t}} = 1$ TeV and $X_t = 0, \pm 2m_{\tilde{t}}$. The plot was done using FeynHiggs 2.10.2, with default settings. For positive X_t the Higgs mass changes by almost 5 GeV in the range of the gluino mass $m_t < m_{\tilde{g}} < 6$ TeV, and the value of m_h is maximized for $m_{\tilde{g}} \approx m_{\tilde{t}}$. The asymmetry in $X_t \to -X_t$ is erased for $m_{\tilde{g}} \sim 6$ TeV and it is reversed for larger values of $m_{\tilde{g}}$. We also see in Fig. 2.2 that the dependence on

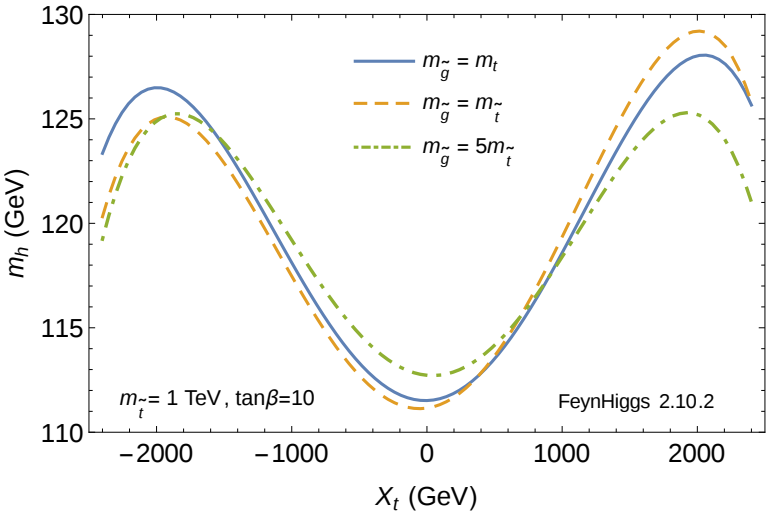

Figure 2.2: Higgs mass as a function of the stop mixing for some values of the gluino mass: $m_{\tilde{g}} = m_t$, $m_{\tilde{g}} = m_{\tilde{t}}$ and $m_{\tilde{g}} = 5m_{\tilde{t}}$. The plot have been done using FeynHiggs 2.10.2. The other parameters are $m_{\tilde{t}} = 1$ TeV and $\tan\beta = 10$.

the gluino is more relevant for large and positive values of X_t, though for zero mixing it is not negligible.

An analytical formula for the $\mathcal{O}(\alpha_t\alpha_s)$ two-loop corrections keeping the explicit dependence on $m_{\tilde{g}}$ was obtained in [81] with the use of the effective potential. In ref. [81] it was also discussed in detail the limit of heavy gluino, obtaining an approximate expression for the Higgs mass matrix in this limit for the simplified case of degenerate stop masses $m^2_{\tilde{t}_1} = m^2_{\tilde{t}_2} = m^2_{\tilde{t}}$, but without including the dependence on the stop mixing. Below we are going to find an extension of eq. (2.23) including the dependence on the gluino mass and the stop mixing, based on the results of [81]. We consider the parameters of the stop sector and the top mass in the OS scheme.

Limit values

In order to find a simple formula for the Higgs mass which includes the dependence on the gluino mass we need to make some assumptions because the full expression is intrinsically complicated. We consider three limit cases: $m_{\tilde{g}} \ll m_{\tilde{t}}$ (light gluino), $m_{\tilde{g}} \sim \mathcal{O}(m_{\tilde{t}})$ (comparable gluino and stop masses), and $m_{\tilde{g}} \gg m_{\tilde{t}}$ (heavy gluino). Our strategy consists of finding approximate expressions of the $\mathcal{O}(\alpha_t\alpha_s)$

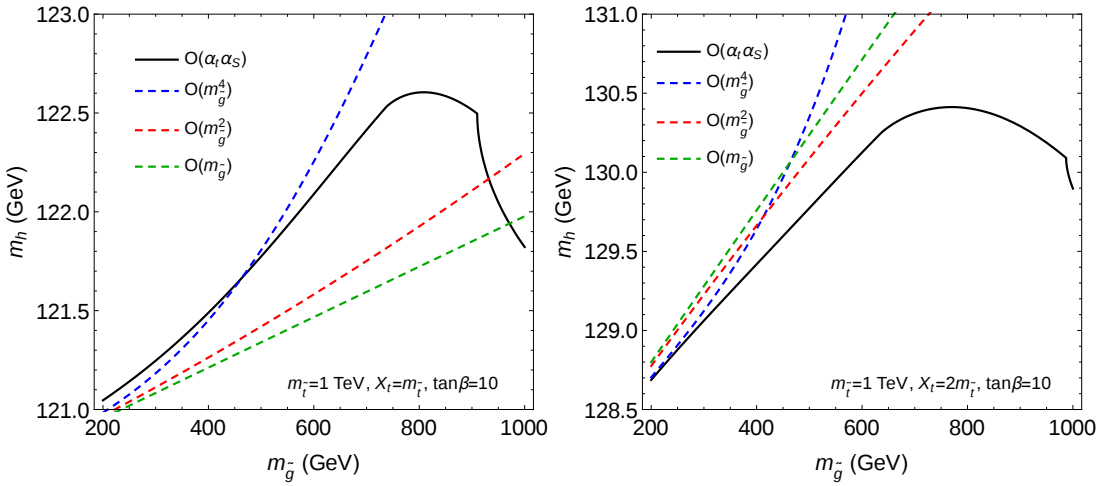

Figure 2.3: Comparison of the approximate formula with the exact result of the $\mathcal{O}(\alpha_t\alpha_s)$ corrections in the case of light gluino for $X_t = 1$ TeV (left) and $X_t = 2$ TeV (right). We use $\tan\beta = 10$ and $m_{\tilde{t}} = 1$ TeV. The black line corresponds to the analytic formula of [81], while the dashed-blue, dashed-red and dashed-green are obtained with the approximate expression truncated at the power $m_{\tilde{g}}^4$, $m_{\tilde{g}}^2$ and $m_{\tilde{g}}$.

corrections for these three cases, and based on that obtaining an interpolating formula valid for any gluino mass.

In the limit of light gluino, expanding in powers of $m_{\tilde{g}}/m_{\tilde{t}}$ we find (up to the quadratic term)

$$\Delta m_h^{2,(\alpha_t\alpha_s)} = \frac{\alpha_s m_t^4}{\pi^3 v^2}\left[\frac{3}{2} - 3\ln^2\frac{m_{\tilde{t}}^2}{m_t^2} - 6\ln\frac{m_{\tilde{t}}^2}{m_t^2} - \frac{7}{2}\frac{X_t^2}{m_{\tilde{t}}^2} - 3\frac{X_t^2}{m_{\tilde{t}}^2}\ln\frac{m_{\tilde{t}}^2}{m_t^2} + \frac{m_{\tilde{g}}}{m_t}\left(4\frac{X_t}{m_{\tilde{t}}} + 2\frac{X_t^3}{m_{\tilde{t}}^3}\right) + \frac{m_{\tilde{g}}^2}{m_{\tilde{t}}^2}\left(1 + \frac{X_t^2}{m_{\tilde{t}}^2} - \frac{X_t^4}{2m_{\tilde{t}}^2}\right) + \mathcal{O}(m_{\tilde{g}}^3)\right]. \quad (2.24)$$

We compare our approximate formula for light gluino with the two-loop $\mathcal{O}(\alpha_t\alpha_s)$ formula of [81] in fig. 2.3 [1]. The approximate expression (2.24) agrees well with the two-loop formula when the gluino mass is of the order of the top mass $m_{\tilde{g}} \sim \mathcal{O}(m_t)$, however it deviates for larger values of $m_{\tilde{g}}$. From fig. 2.3 (black line) we appreciate the behavior of m_h as a function of $m_{\tilde{g}}$ for $m_g \lesssim m_{\tilde{t}}$. It goes approximately linear for $m_{\tilde{g}} \lesssim 0.7 m_{\tilde{t}}$ and after, m_h remains almost constant

[1] For doing the plots we also took into account the tree level and the most important one-loop corrections. Since we are interested in the effect of the gluino mass contained in the two loop $\mathcal{O}(\alpha_t\alpha_s)$ corrections, the precise central value of m_h is not relevant in this analysis.

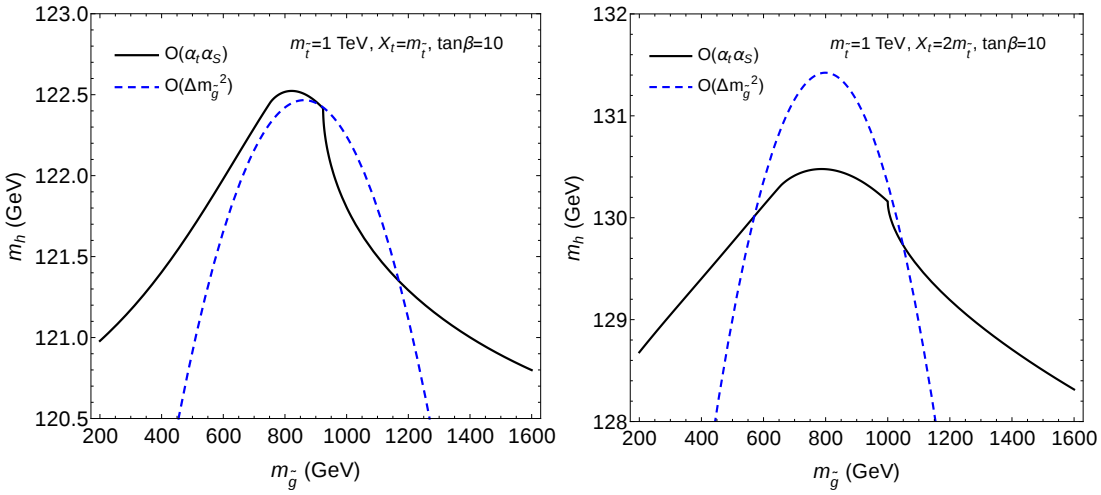

Figure 2.4: Higgs mass vs. gluino mass for $X_t = 1$ TeV (left) and $X_t = 2$ TeV (right) for comparison with the approximate formula for $m_{\tilde{g}} \sim \mathcal{O}(m_{\tilde{t}})$. We use $\tan\beta = 10$, $m_{\tilde{t}} = 1$ TeV. The black line corresponds to the analytic formula of [81] and the dashed-blue to the approximate expression quadratic in $\Delta m_{\tilde{g}} = m_{\tilde{g}} - m_{\tilde{t}}$.

around the region $0.7 m_{\tilde{t}} \leq m_{\tilde{g}} < m_{\tilde{t}}$. We will comment more about this behavior when we find the interpolating formula. Basically, the eq. (2.24) will be useful to extract the limit behavior of m_h^2 for vanishing gluino mass.

For the case $m_{\tilde{g}} \sim \mathcal{O}(m_{\tilde{t}})$ we assume that $(m_{\tilde{g}} - m_{\tilde{t}}) \ll m_{\tilde{t}}$. When we try to find an approximate formula for $m_g \sim \mathcal{O}(m_{\tilde{t}})$ we encounter some subtleties because in this regime we have to deal with physical thresholds at $m_{\tilde{g}} = m_{\tilde{t}_1} - m_t$ and $m_{\tilde{g}} = m_{\tilde{t}_2} - m_t$. We use the explicit expression for the Passarino-Veltmann function given in [109]. An approximate expression quadratic in $(m_{\tilde{g}} - m_{\tilde{t}})/m_{\tilde{t}}$ is given in appendix A.1.

The Higgs mass changes quickly its functional behavior in the region $m_{\tilde{g}} \approx m_{\tilde{t}}$. This is related to the physical thresholds at $m_{\tilde{g}} = m_{\tilde{t}_1} - m_t$ and $m_{\tilde{g}} = m_{\tilde{t}_2} - m_t$, when the stop decay channels $\widetilde{t}_{1,2} \to \widetilde{g}\, t$ open. For this reason the approximate expression does not capture well the functional dependence on $m_{\tilde{g}}$, in particular for large X_t, as we can see in fig. 2.4. When we take the limit $m_{\tilde{g}} \to m_{\tilde{t}}$ we recover the simplified expression of Espinosa and Zhang [79]. In the interpolating formula which we present later, valid for any gluino mass, we will simply consider m_h as a constant function of $m_{\tilde{g}}$ in the range $2/3 m_{\tilde{t}} \leq m_{\tilde{g}} \leq m_{\tilde{t}}$.

The case of heavy gluino is approximated by expanding in inverse powers of

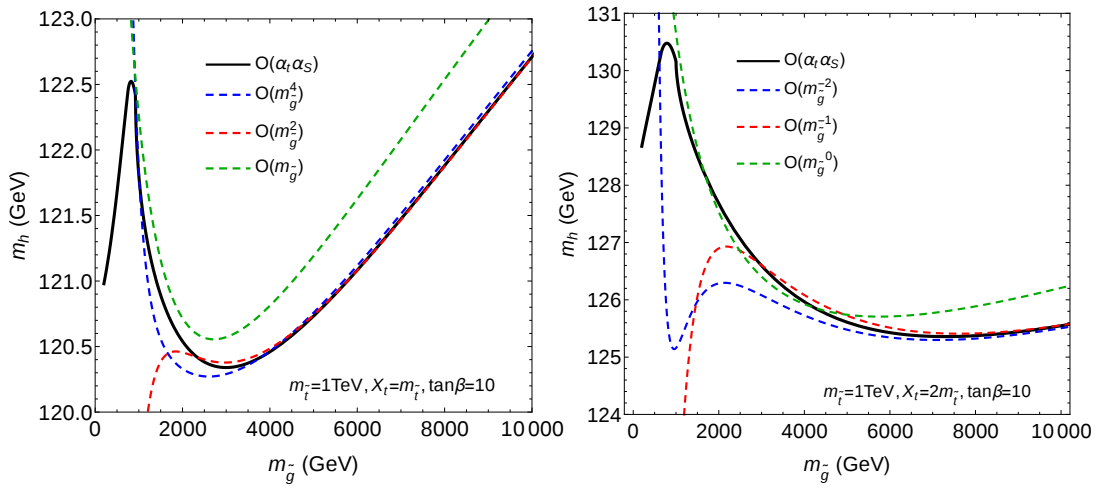

Figure 2.5: Heavy gluino limit for $X_t = 1$ TeV (left) and $X_t = 2$ TeV (right), $\tan\beta = 10$ and $m_{\tilde{t}} = 1$ TeV. The black line corresponds to the analytic formula of [81], while the dashed-blue, dashed-red and dashed-green to the approximate expressions truncated at $m_{\tilde{g}}^{-2}$, $m_{\tilde{g}}^{-1}$ and $m_{\tilde{g}}^{0}$ respectively. We find an excellent agreement among the black, blue and red curves for $m_{\tilde{g}} \gtrsim 4m_{\tilde{t}}$.

the gluino mass and it yields

$$\begin{aligned}\Delta m_h^{2,(\alpha_t\alpha_s)} = \frac{\alpha_s m_t^4}{\pi^3 v^2}\Bigg\{&\left[\frac{2\pi^2}{3} - 1 - 3\ln^2\frac{m_{\tilde{t}}^2}{m_t^2} - 6\ln\frac{m_{\tilde{t}}^2}{m_t^2} + 2\ln^2\frac{m_{\tilde{g}}^2}{m_{\tilde{t}}^2} - 6\ln\frac{m_{\tilde{g}}^2}{m_{\tilde{t}}^2}\right.\\ &\left. - 3\frac{X_t^2}{m_{\tilde{t}}^2}\ln\frac{m_{\tilde{t}}^2}{m_t^2} - 2\frac{X_t^2}{m_{\tilde{t}}^2}\ln\frac{m_{\tilde{g}}^2}{m_{\tilde{t}}^2} - \frac{X_t^4}{m_{\tilde{t}}^4}\right]\\ &+ \frac{m_{\tilde{t}}}{m_{\tilde{g}}}\left[\left(2 - \frac{4\pi^2}{3}\right)\frac{X_t}{m_{\tilde{t}}} - 4\frac{X_t}{m_{\tilde{t}}}\left(\ln^2\frac{m_{\tilde{g}}^2}{m_{\tilde{t}}^2} - 3\ln\frac{m_{\tilde{g}}^2}{m_{\tilde{t}}^2}\right) - 3\frac{X_t^3}{m_{\tilde{t}}^3} + 2\frac{X_t^3}{m_{\tilde{t}}^3}\ln\frac{m_{\tilde{g}}^2}{m_{\tilde{t}}^2}\right]\\ &+ \frac{m_{\tilde{t}}^2}{m_{\tilde{g}}^2}\left[\left(\frac{4\pi^2}{3} - \frac{14}{3}\right) + 4\ln^2\frac{m_{\tilde{g}}^2}{m_{\tilde{t}}^2} - 12\ln\frac{m_{\tilde{g}}^2}{m_{\tilde{t}}^2} + 4\frac{X_t^2}{m_{\tilde{t}}^2} - 4\frac{X_t^2}{m_{\tilde{t}}^2}\ln\frac{m_{\tilde{g}}^2}{m_{\tilde{t}}^2} - \frac{1}{3}\frac{X_t^4}{m_{\tilde{t}}^4}\right]\Bigg\}.\end{aligned} \tag{2.25}$$

The expression (2.25) is an excellent approximation for $m_{\tilde{g}} \gtrsim 4m_{\tilde{t}}$ as it is shown in fig. 2.5, and it works better and better as we increase the gluino mass. The asymptotic behavior is approached quickly keeping only the $m_{\tilde{g}}^{-1}$ power, so there is no need to include $m_{\tilde{g}}^{-2}$ terms. We will use the eq. (2.25) up to the $m_{\tilde{g}}^{-1}$ power for the interpolating expression. Note that the limit of heavy gluino and for general stop mixing given in eq. (2.25) is a new result not present in the

literature and can account for a shift of 5 GeV in the Higgs mass (for $m_{\widetilde{t}} = 1$ TeV) with respect to eq. (2.23).

All formulas in this section 2.3.1 are written in terms of OS parameters. In the $\overline{\text{DR}}$ scheme the two-loop corrections contain terms proportional to $m_{\widetilde{g}}$ and $m_{\widetilde{g}}^2$, which become very large in the limit of heavy gluino [81]. This issue is related to non-decoupling effects of mass-independent renormalization schemes. Additionally, as we will discuss in section 3.2.1, negative quadratic corrections proportional to the gluino mass in the expressions of the OS stop masses in terms of the $\overline{\text{DR}}$ masses, drive the stop masses tachyonic when the gluino mass is roughly a factor of four larger.

Interpolating Expression

Now we propose an interpolating formula valid for any value of the gluino mass. We require some general features: simplicity, continuity and accuracy. Of course, there is no unique choice for the interpolation.

For a gluino mass around the stop mass, m_h can be approximated by a constant function of $m_{\widetilde{g}}$, given by the first line of eq. (A.1). More specifically, we consider the interval $2/3\, m_{\widetilde{t}} \leq m_{\widetilde{g}} \leq m_{\widetilde{t}}$. The deviation from the exact contribution is always smaller than 0.4 GeV. In order to interpolate up to the region of light gluino it is enough to adopt a linear function. We use two points corresponding to vanishing gluino mass and to $m_{\widetilde{g}} = 2/3 m_{\widetilde{t}}$. The value of the Higgs mass for vanishing $m_{\widetilde{g}}$ is extracted from the limit formula (2.24) while the value at $m_{\widetilde{g}} = 2/3 m_{\widetilde{t}}$ is approximated by $m_h(m_{\widetilde{g}} = m_{\widetilde{t}})$. Finally, we consider the region $m_{\widetilde{g}} > m_{\widetilde{t}}$. Since the approximate expression (2.25) approaches very quickly the asymptotic behavior (see fig. 2.5), we can assume that the *heavy gluino* regime corresponds to not-so-large values $m_{\widetilde{g}} \gtrsim 3 m_{\widetilde{t}}$.

We require the interpolation to recover the expression for $m_{\widetilde{g}} \approx m_{\widetilde{t}}$ and eq. (2.25) up to the power $m_{\widetilde{g}}^{-1}$ for heavy gluino. We compare the limit expressions for $m_{\widetilde{g}} \approx m_{\widetilde{t}}$ and $m_{\widetilde{g}} \gg m_{\widetilde{t}}$ term by term. Depending on the importance of each term one chooses a function of interpolation which approaches faster or slower to the extremes. Then, the proposal for interpolating function valid for any value of the gluino mass has the form:

$$m_h^{2,(\alpha_t\alpha_s)} = \frac{\alpha_s m_t^4}{\pi^3 v^2}\Bigg\{ F_1(m_{\widetilde{g}}) - 3\ln^2\frac{m_{\widetilde{t}}^2}{m_t^2} - 6\ln\frac{m_{\widetilde{t}}^2}{m_t^2} + 6\frac{X_t}{m_{\widetilde{t}}} F_2(m_{\widetilde{g}}) - 3\frac{X_t^2}{m_{\widetilde{t}}^2}\ln\frac{m_{\widetilde{t}}^2}{m_t^2} + \frac{7}{2}\frac{X_t^2}{m_{\widetilde{t}}^2} F_4(m_{\widetilde{g}}) - \frac{3}{4}\frac{X_t^4}{m_{\widetilde{t}}^4} F_3(m_{\widetilde{g}}) + \Theta(m_{\widetilde{g}} - m_{\widetilde{t}})\left(2\ln^2\frac{m_{\widetilde{g}}^2}{m_{\widetilde{t}}^2} - 6\ln\frac{m_{\widetilde{g}}^2}{m_{\widetilde{t}}^2} - 2\frac{X_t^2}{m_{\widetilde{t}}^2}\ln\frac{m_{\widetilde{g}}^2}{m_{\widetilde{t}}^2}\right)$$

$$+\Theta(m_{\widetilde{g}}-m_{\widetilde{t}})\frac{m_{\widetilde{t}}}{m_{\widetilde{g}}}\left[-4\frac{X_t}{m_{\widetilde{t}}}\left(\ln^2\frac{m_{\widetilde{g}}^2}{m_{\widetilde{t}}^2}-3\ln\frac{m_{\widetilde{g}}^2}{m_{\widetilde{t}}^2}\right)-3\frac{X_t^3}{m_{\widetilde{t}}^3}F_5(m_{\widetilde{g}})+2\frac{X_t^3}{m_{\widetilde{t}}^3}\ln\frac{m_{\widetilde{g}}^2}{m_{\widetilde{t}}^2}\right]\Bigg\}, \tag{2.26}$$

where the functions F_i are defined in appendix A.1 and $\Theta(m)$ is the Heaviside step function.

The eq. (2.26) shows the influence of every term separately. If we want to improve the interpolating formula one can play with the functions F_i. The logarithmic terms in the first two lines of eq. (2.26) can be obtained from the RGE.

We have checked that the interpolating expression approximates very well the two-loop $\mathcal{O}(\alpha_t\alpha_s)$ result of [81], as can be seen in fig. 2.6. It performs properly, with a deviation from the analytic formula of $\Delta m_h \lesssim 0.5$ GeV in all the parameter space or even smaller for most of the parameter space.

2.3.2 Approximate formulas

Combining the dominant corrections, we can write an approximate fixed-order formula as

$$m_h^2 = m_h^{2,(\text{tree})} + \Delta m_h^{2,(\text{1-loop})} + \Delta m_h^{2,(\alpha_t\alpha_s)} + \Delta m_h^{2,(\alpha_t^2)}, \tag{2.27}$$

with the tree level and one loop corrections represented as

$$m_h^{2,(\text{tree})} = m_Z^2\cos^2 2\beta, \tag{2.28}$$

$$\Delta m_h^{2,(\text{1-loop})} = m_Z^2\cos^2 2\beta\left(-\frac{3}{4\pi^2}\frac{m_t^2}{v^2}\ln\frac{m_{\tilde{t}}^2}{m_t^2}\right)+\frac{3}{2\pi^2}\frac{m_t^4}{v^2}\left[\frac{X_t^2}{m_{\tilde{t}}^2}-\frac{X_t^4}{12m_{\tilde{t}}^4}+\ln\frac{m_{\tilde{t}}^2}{m_t^2}\right], \tag{2.29}$$

$\Delta m_h^{2,(\alpha_t\alpha_s)}$ given in eq. (2.26) and the two-loop correction $\Delta m_h^{2,(\alpha_t^2)}$ is well approximated analytically in ref. [79]. Unfortunately eq. (2.27) does not capture the momentum dependence, which is sizable at one loop. It also suffers from a large uncertainty due to large logarithms, that are not resummed in a fixed order result.

Using effective field theory techniques we also obtain a simple formula for the High Scale SUSY scenario with a degenerate spectrum of masses m_{SUSY}. The MSSM parameters such as the sparticle masses and stop mixing X_t are in the $\overline{\text{DR}}$ scheme while the couplings g_1, g_2, g_3, y_t and λ are the SM ones in the $\overline{\text{MS}}$ scheme. We present the solution of the RGE in two ways: fixed-order expression by iterative solution and a numeral solution which resums the logarithms at all

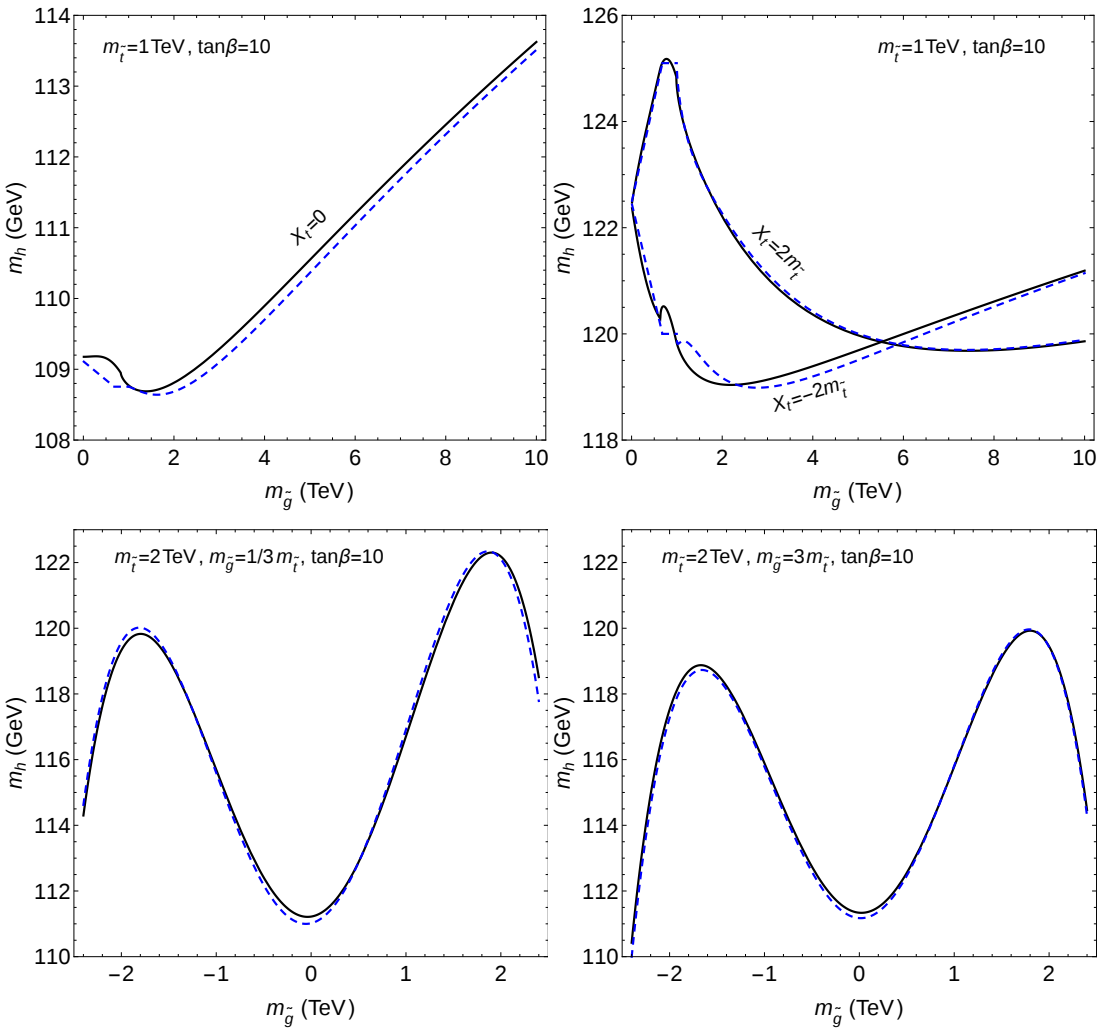

Figure 2.6: Comparison between the interpolating formula (blue-dashed line) for the gluino mass dependence of the Higgs mass and the exact $\mathcal{O}(\alpha_t\alpha_s)$ expression (black-solid line). We appreciate the good agreement between them.

orders. The calculation of the Higgs mass proceeds in three steps: matching at the high scale of the sparticle masses, evolving the quartic coupling between the high scale and the weak scale solving the coupled RGE, and relating SM parameters in the $\overline{\text{MS}}$ scheme to physical observables. For the parameters of the scalar potential we use the normalization presented in section 1.1.

The quartic coupling at the high scale depends on the various threshold corrections as

$$\begin{aligned}
\lambda(m_{\text{SUSY}}) = & \frac{1}{4}\left(\frac{3}{5}g_1^2 + g_2^2\right)\cos^2 2\beta \\
& + \frac{1}{(4\pi)^2}\left[6y_t^4\left(\hat{X}_t - \frac{\hat{X}_t^4}{12}\right) + \frac{1}{4}y_t^2\left(\frac{3}{5}g_1^2 + g_2^2\right)\hat{X}_t\left(3\cos 2\beta - \cos^2 2\beta\right)\right. \\
& + \frac{3}{800}(-89 + 8\cos 4\beta + 9\cos 8\beta - 62\sin 2\beta + 2\sin 6\beta)g_1^4 \\
& + \frac{1}{80}(-85 + 12\cos 4\beta + 9\cos 8\beta - 60\sin 2\beta + 4\sin 6\beta)g_1^2 g_2^2 \\
& \left. + \frac{1}{96}(-265 + 8\cos 4\beta + 9\cos 8\beta - 186\sin 2\beta + 6\sin 6\beta)g_2^4\right] \\
& + \frac{g_3^2 y_t^4}{96\pi^4}\left[-12\hat{X}_t - 6\hat{X}_t^2 + 14\hat{X}_t^3 + \frac{1}{2}\hat{X}_t^4 - \hat{X}_t^5\right], \qquad (2.30)
\end{aligned}$$

with $\hat{X}_t = X_t/m_{\tilde{t}}$. The first, second and the next three lines of eq. (2.30) represent the tree level contribution, one loop corrections enhanced by the stop mixing, and the corrections proportional to the electroweak gauge couplings. The last line corresponds to the leading two-loop $\mathcal{O}(\alpha_t\alpha_s)$ corrections [94].

We proceed to solve iteratively the RGE up to two loops (see e.g. refs. [108] and [104]). We denote the logarithms of the ratio of the low scale Q_l and high scale Q_h over a reference scale Q_0 as

$$t_l \equiv \log Q_l/Q_0, \qquad t_h \equiv \log Q_h/Q_0, \qquad L \equiv t_h - t_l = \log Q_h/Q_l > 0. \qquad (2.31)$$

For a generic running coupling λ, its β-function is defined as

$$\beta_\lambda(t) \equiv \frac{d\lambda}{dt}, \qquad (2.32)$$

where $t = \log Q/Q_0$ and Q is the renormalization scale. The β-function can be written as

$$\beta_\lambda(t_l) = \sum_{n=1}^{\infty}\kappa^n\beta_\lambda^{(n)}(t_l) = \sum_{n=1}^{\infty}\kappa^n\sum_{k=0}^{\infty}\frac{\beta_\lambda^{(n,k)}(t_h)}{k!}(t_l - t_h)^k, \qquad (2.33)$$

with the notation:

$$\kappa \equiv \frac{1}{16\pi^2}, \qquad \beta_\lambda^{(n,k)}(t) \equiv \frac{\mathrm{d}^k \beta_\lambda^{(n)}}{\mathrm{d}t^k}(t), \qquad \beta_\lambda^{(n,0)} \equiv \beta_\lambda^{(n)}. \tag{2.34}$$

Integrating eq. (2.33) from t_l to t_h yields

$$\lambda(Q_l) = \lambda(Q_h) + \sum_{n=1}^{\infty} \kappa^n \sum_{k=0}^{\infty} (-1)^{k+1} \frac{\beta_\lambda^{(n,k)}(t_h)}{(k+1)!}\, L^{k+1}. \tag{2.35}$$

In terms of the low energy scale it reads

$$\lambda(Q_h) = \lambda(Q_l) + \sum_{n=1}^{\infty} \kappa^n \sum_{k=0}^{\infty} \frac{\beta_\lambda^{(n,k)}(t_l)}{(k+1)!}\, L^{k+1}. \tag{2.36}$$

At two loops, with β-function coefficients evaluated at the top mass, the (fixed order) solution for the quartic coupling at the top mass reads

$$\lambda(m_t) = \lambda(m_{\mathrm{SUSY}}) - \kappa\beta_\lambda^{(1)}(m_t)\, L - \kappa^2 \beta_\lambda^{(2)}(m_t)\, L - \kappa \frac{\beta_\lambda^{(1,1)}(m_t)}{2!}\, L^2. \tag{2.37}$$

Terms proportional to the electroweak gauge couplings are included at the one-loop level only in our approximation, i.e.

$$\beta_\lambda^{(1)} = \lambda\left(12\lambda + 12y_t^2 - 9g_2^2 - \frac{9}{5}g_1^2\right) - 12y_t^4 + \frac{9}{4}g_2^4 + \frac{9}{10}g_1^2 g_2^2 + \frac{27}{100}g_1^4 \tag{2.38}$$

$$\beta_\lambda^{(2)} = -64 g_3^2 y_t^4 + 60 y_t^6 + \dots \tag{2.39}$$

$$\beta_\lambda^{(1,1)} = \frac{d\beta_\lambda^{(1)}}{dt} = \sum_X \frac{\partial \beta_\lambda^{(1)}}{\partial X} \kappa \beta_X^{(1)} = \kappa\left(768 g_3^2 y_t^4 - 576 y_t^6\right) + \dots, \tag{2.40}$$

where we represented all the SM couplings generically by X in the sum. The formulas for the SM β-functions can be found, for instance, in ref. [93].

We also need the value of the couplings at m_{SUSY} to calculate the threshold corrections to the quartic coupling. At the order we are working it is enough to use the exact one loop solution

$$y_t(m_{\mathrm{SUSY}}) = y_t(m_t)\left[1 + \kappa\left(9/2\, y_t^2 - 8 g_3^3 L\right)\right] + \dots \tag{2.41}$$

$$g_1^2(m_{\mathrm{SUSY}}) = g_1^2(m_t)\left[1 + \kappa\, 41/5\, g_1^2 L\right] \tag{2.42}$$

$$g_2^2(m_{\mathrm{SUSY}}) = g_2^2(m_t)\left[1 - \kappa\, 19/3\, g_2^2 L\right] \tag{2.43}$$

$$\tag{2.44}$$

Conversely, we consider the numerical solution of the coupled two-loop RGEs of λ, y_t, g_3, g_2, g_1. As boundary conditions we use the value of all the couplings at the top mass extracted from data, except the quartic coupling for which we use the value at $m_{\rm SUSY}$. Since the SM couplings are known with good precision, the result of evolving the quartic coupling from the high scale to the weak scale can be considered as a function of $\lambda(m_{\rm SUSY})$ and the logarithm of the ratio of scales

$$\lambda(m_t) = f\left(\lambda(m_{\rm SUSY}), L\right). \tag{2.45}$$

We present the numerical solution of the RGE as an interpolating polynomial[1] which depends on two variables $\lambda(m_{\rm SUSY})$ and L. We also need the solutions for $y_t(m_{\rm SUSY})$, $g_1(m_{\rm SUSY})$ and $g_2(m_{\rm SUSY})$; we propose interpolating polynomials for them. We write

$$\lambda(m_t) = \sum_n \sum_m C^{(\lambda)}_{n,m} \lambda(m_{\rm SUSY})^n L^m, \tag{2.46}$$

$$y_t(m_t) = \sum_{k=0} C^{(y_t)}_k L^k, \tag{2.47}$$

$$g_1^2(m_{\rm SUSY}) = \frac{g_1^2(m_t)}{1 - \kappa\, 41/5\, g_1^2(m_t) L} + \sum_k C^{(g_Y)}_k L^k, \tag{2.48}$$

$$g_2^2(m_{\rm SUSY}) = \frac{g_2^2(m_t)}{1 + \kappa\, 19/3\, g_2^2(m_t) L} + \sum_k C^{(g_2)}_k L^k, \tag{2.49}$$

with coefficients different from zero up to a given order. Their numerical values are given in appendix A.1.

Finally we need to do the matching at the electroweak scale. The value of the SM couplings extracted from experimental data are given, for instance, in [93]. The relation between the Higgs pole mass and the quartic coupling depends only on SM input (see [93] and references therein). It can be written as

$$m_h^2 = v^2 \left\{\lambda(m_t) + [0.0028 + 0.0093(\lambda(m_t) - 0.25)] + [0.0034]\right\}, \tag{2.50}$$

where the first term in brackets represent the one-loop corrections (expanded around $\lambda(m_t) = 0.25$) and the second one contains the two-loop QCD and electroweak corrections.

We illustrate the use of the approximate interpolated formula for m_h in fig. 2.7. It shows m_h as a function of the SUSY scale in the High scale SUSY scenario with

[1] The coefficients of the polynomial are chosen to fit the exact numerical solution, thus they are not directly related to the perturbative solution of the RGE.

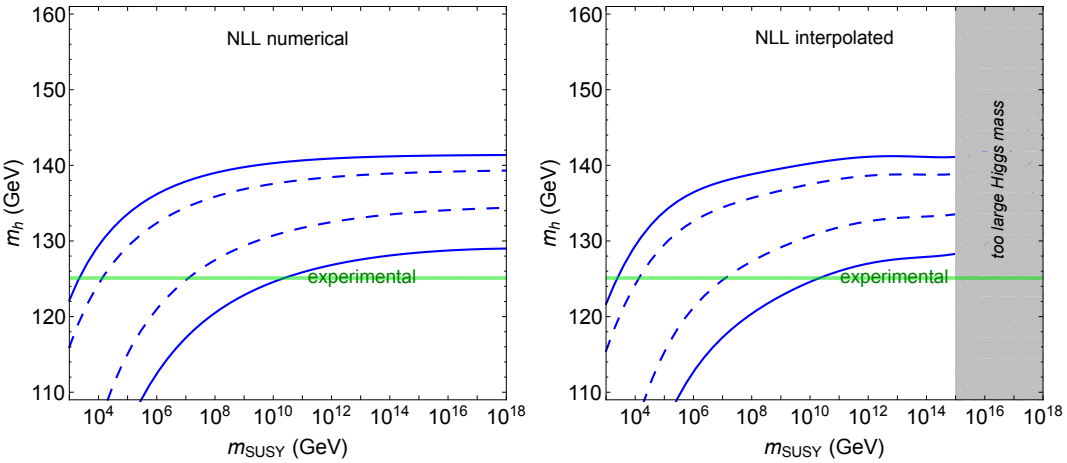

Figure 2.7: Higgs mass as a function of the SUSY scale $m_{\rm SUSY}$ with degenerate spectrum calculated with the exact numerical solution (left) or the approximate interpolated solution (right) of the RGE. The lines correspond to $\tan\beta = 1, 2$ and vanishing stop mixing (lower lines) and $\tan\beta = 4, 50$ and maximal mixing (upper lines). The green band represents to the experimental value of m_h.

degenerate sparticle masses for various values of $\tan\beta$. This plots are inspired on similar ones in refs. [47, 48, 94].

Although our efforts to find simplified analytical formulas are useful to understand the dependence on the various parameters, the complete expressions are intrinsically complicated and a precise calculation requires a full numerical study. That is the task in the next chapter, where a very precise calculation is performed including the estimate of the uncertainties.

Chapter 3

Higgs mass determination with EFT

Due to the logarithmic (in)sensitivity of the Higgs mass value to the SUSY scale, high precision is required in such calculation to reliably determine the allowed parameter space of the theory. This can be seen in fig. 3.1. Besides, the experimental value is now known with per mille accuracy $m_h = 125.09(24)$ GeV [11]. The effort in the Higgs mass calculation has been remarkable, reaching the two-loop and in some cases the three-loop level, with different techniques and schemes, see *e.g.* [47, 48, 71, 72, 74, 76, 78, 79, 81–84, 86, 92, 94, 104, 110]. Some of the computations, however, are only valid for small SUSY breaking scales, where log-corrections do not need resummation; in fact currently available computer codes have a very limited range of applicability compared to the allowed parameter space. Moreover, different computations and/or computer codes disagree among themselves, in some cases substantially more than the expected/claimed level of uncertainties.

Given the important role played by the Higgs mass in constraining supersymmetric models, the limitations of the existing codes and the disagreements in the literature, we felt the need to revisit the computation. We put special emphasis on the relevant parameter space to reproduce the experimental value of the Higgs mass, on the study of the uncertainties and on the possible origin of the differences with other methods. In this chapter we recompute the Higgs mass in the MSSM using the effective field theory (EFT) approach, which allows to systematically resum large logarithms and to have arbitrary big hierarchies in the spectrum, exploiting the mass gap hinted by the largish value of the Higgs mass and the absence of new physics at the LHC.

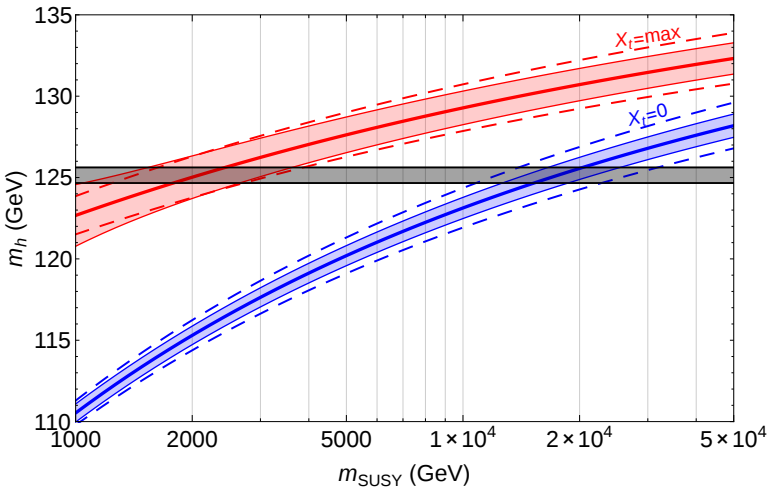

Figure 3.1: Logarithmic sensitivity of the Higgs mass to the SUSY scale. We consider a SUSY spectrum with degenerate masses $m_{\rm SUSY}$, $\tan\beta = 20$, and maximal (red) or vanishing (blue) stop mixing. The bands represent the total theoretical uncertainties, while the dashed lines correspond to the experimental uncertainty estimated by varying the top mass by 2σ around the experimental value.

Our computation follows very closely the ones in [9, 10, 47, 48, 94, 104, 110], providing independent checks of such computations. We improved them in various ways. We added all the dominant SUSY threshold corrections including the contributions from bottom and tau sectors, which become important at large $\tan\beta$. In this way we provide the state of the art in the EFT calculation of the Higgs mass. We performed the computation in both the $\overline{\rm DR}$ and the on-shell (OS) schemes, the latter has the advantages of ensuring the correct decoupling limits and keeping the theoretical errors under control in the whole parameter space. We point out that large logarithms arising from splitting the fermions from the scalar superpartners in split SUSY scenarios do not need resummation in the whole region of parameters space relevant for the observed Higgs mass. We also find that $m_h = 125$ GeV may not necessarily bound the SUSY scale to lie below 10^{10} GeV (and much below at large $\tan\beta$), but it might extend at arbitrarily high scales. Another outcome of our computation is that, even at maximal stop mixing, the average stop mass is required to be above the TeV scale in order to reproduce the correct Higgs mass in the MSSM. We also performed a study of the various possible uncertainties, showing that for most of the parameter space we are dominated by the experimental ones. We identified some of the sources of disagreement between existing computations/codes.

We implemented the computation in a new computer code, SusyHD, which we make public [111] and which allows to reliably compute the MSSM Higgs mass (and its uncertainties) even when big hierarchies are present in the spectrum. Avoiding slow numerical integrations, the code is fast enough to be used to set the experimental value of the Higgs mass as a constraint on any other SUSY parameter.

Finally we also explore the implications of the Higgs mass on two of the simplest SUSY scenarios: minimal gauge mediation (MGM) and anomaly mediation. In particular in the first case we show how the value of the Higgs mass allows to determine the complete spectrum of the superpartners.

The chapter is organized as follows. In section 3.1 we describe our computation of the Higgs mass in the effective field theory approach, we study the theoretical uncertainties and we compare our results with the existing ones. In section 3.2 we present the implications of our computation for the SUSY spectrum in different regimes, in particular we show the constraints from the Higgs mass in the parameter range relevant for SUSY searches at hadron colliders, we explored the region of very large $\tan\beta$ and we comment on the (non) importance of extra log resummation when the SUSY spectrum is split. In section 3.3 we briefly introduce SusyHD, a new code to compute the Higgs mass using the EFT technique. Recent progress, further reducing the theoretical uncertainty, is presented in section 3.4 . In section 3.5 we apply our results to some of the simplest SUSY models: minimal gauge mediation, lopsided gauge mediation and anomaly mediation. Finally, in appendix A.2, we provide the explicit expressions for some of the SUSY thresholds computed in this work and more details about the conventions used in the text.

3.1 The computation

In this section we review the computation that we presented in [1]. Recent progress in the EFT computation will be discussed in section 3.4. In that section, we will improve our computation by including the leading three-loop strong corrections to the matching of λ at the EW scale, the four-loop QCD contributions to the RGE of λ, y_t and g_3, and the two-loop SUSY thresholds proportional to the third generation Yukawa couplings in the general case. We will also consider the effect on the Higgs mass of the dimension-six operators of the SM EFT expansion. According to the inclusion of these corrections we will also modify our estimate of the theoretical uncertainty.

3.1.1 The Effective Field Theory technique

Whenever a theory presents a gap in its energy spectrum effective field theory techniques become a very powerful tool. They exploit the hierarchy of scales to allow a perturbative expansion in powers of the energy gap. This simplifies the theory getting rid of irrelevant degrees of freedom and couplings.

Applied to supersymmetry, as the scale of the superpartners is raised, the Standard Model becomes a better and better EFT, with corrections from higher dimensional operators decoupling fast, as powers of $v/m_{\rm SUSY}$, the ratio between the EW and the SUSY scale. At leading order in this expansion the presence of supersymmetry at low energy reduces to a boundary condition for the SM couplings evolved at the SUSY scale, where they have to match with the full supersymmetric theory.

From the bottom up the technique reduces to taking the measured SM couplings at low energy, evolving them up to the superpartner scale and matching them to the full supersymmetric theory living at high scales. The non-trivial relations between the couplings in the supersymmetric theory (in particular between the Higgs quartic, the gauge-Yukawa couplings and the soft terms) translates into a non-trivial condition on the soft SUSY parameters. Equivalently one can leave the physical Higgs mass as a free parameter to be determined as a function of the UV SUSY parameters. Imposing the physical value for the Higgs mass then gives the constraint.

The use of this technique in the computation of the Higgs mass in the MSSM is quite old [110], however its utility in natural SUSY spectra was limited since corrections from higher dimensional operators could not be neglected in that case. These techniques became more popular with the advent of Split SUSY scenarios [9, 10] and the recent LHC results [36, 48, 94, 104, 112].

In the rest of the chapter, unless specified otherwise, the gauge couplings $g_{1,2,3}$, the Yukawa couplings $y_{t,b,\tau}$ and the Higgs quartic coupling λ are assumed to be the SM ones in the $\overline{\rm MS}$ scheme while the soft parameters (masses and trilinear couplings) are in the $\overline{\rm DR}$ or OS schemes. In particular when we refer to our $\overline{\rm DR}$ or OS results it means that the soft masses are $\overline{\rm DR}$ or OS while the couplings are always taken to be the SM ones in the $\overline{\rm MS}$ scheme.

Our computation presented in [1] is organized as follows:

- The SM couplings (gauge, Yukawa and quartic) in the $\overline{\rm MS}$ scheme are extracted from the corresponding physical quantities at the EW scale at full

two-loop level [93]. In particular the matching between the top mass[1] and the top Yukawa coupling is done using full two-loop thresholds plus the leading three-loop QCD one[2] from [114].

- The couplings are then evolved from the weak scale to the superpartner scale using the full three-loop renormalization group equations (RGE) for these couplings[3] [93].

- At the SUSY scale the SM couplings are matched to those of the SUSY theory (converted from either $\overline{\text{DR}}$ or OS to the $\overline{\text{MS}}$ scheme) using the full one loop thresholds (from [94] and the $\mathcal{O}(\alpha_{b,\tau})$ corrections from appendix A.2) plus the leading two-loop thresholds $\mathcal{O}(\alpha_s\alpha_t)$ and $\mathcal{O}(\alpha_t^2)$. The former is computed for generic SUSY spectra while the latter (which is generically smaller) is only computed for degenerate scalars.

The final expression for the Higgs mass can thus be written as

$$m_h^2 = v^2[\lambda(m_t) + \delta\lambda(m_t)]\,, \tag{3.1}$$

where $v = 246.22$ GeV and $\delta\lambda(m_t)$ are the SM threshold corrections (here computed up to two loops) to match the Higgs pole mass to the $\overline{\text{MS}}$ running quartic coupling. The coupling $\lambda(m_t)$ is derived using the RGE and the boundary conditions at the SUSY scale (see below). The RGE for the Higgs quartic coupling are solved together with gauge and Yukawa couplings at three loops, in particular the top Yukawa y_t is extracted from

$$m_t = \frac{v}{\sqrt{2}}(y_t(m_t) + \delta y_t(m_t))\,, \tag{3.2}$$

where $\delta y_t(m_t)$ is the SM threshold correction matching the top pole mass with the $\overline{\text{MS}}$ top Yukawa coupling and here computed at NNLO, and N^{3}LO in the strong coupling. The matching at the SUSY scale Q is instead given by

$$\lambda(Q) = \frac{g^2(Q) + g'^2(Q)}{4}\cos^2 2\beta + \Delta\lambda^{(1)} + \Delta\lambda^{(2)}_{\alpha_t\alpha_s} + \Delta\lambda^{(2)}_{\alpha_t^2}\,, \tag{3.3}$$

[1] As usual we interpreted the experimental value $m_t = 173.34 \pm 0.76$[113] as the pole mass, systematic uncertainties coming from this choice can be estimated by rescaling the experimental error on the top mass.

[2] Since we do not perform a complete N^{3}LO computation this last correction is also used to evaluate the uncertainties from higher order terms.

[3] As for the three-loop top Yukawa threshold, the four-loop QCD corrections [115, 116] to the strong coupling RGE has been used to estimate the uncertainties.

where $\Delta\lambda^{(1)}$ contains the 1-loop thresholds matching the Higgs quartic coupling $\lambda(Q)$ in the $\overline{\rm MS}$-scheme with the one computed in full SUSY in terms of soft terms and couplings, in the $\overline{\rm DR}$ or OS schemes. $\Delta\lambda_i^{(2)}$ are the leading two loop threshold corrections further discussed below.

If some of the superpartners are light compared to the rest of the SUSY spectrum, as in the case of Split SUSY, a new mass threshold develops. In this case two matchings are in order, the first at the Split scale between the SM and the Split SUSY theory, and the second at the SUSY scale, between the Split theory and the MSSM. The evolution up to the Split scale is the same as in the previous case. We then used 1-loop thresholds to do the matchings and 2-loop RGEs to run the Split-SUSY theory [10, 47]. We will show in section 3.2.4 that the simplest approach also works in the Split case, i.e. the effect coming from the splitting of the fermions from the scalar superpartners do not need RGE resummation in the parameter region relevant for the observed Higgs mass.

Our computation is very close to the one in [94], in particular we added the contributions from the bottom and tau Yukawas, relevant at large values of $\tan\beta$, we recomputed the two-loop thresholds $\mathcal{O}(\alpha_t\alpha_s)$ using the effective potential in [77], and we also included $\mathcal{O}(\alpha_t^2)$ corrections computed for degenerate scalar masses.

The general expression for the two-loop $\mathcal{O}(\alpha_t\alpha_s)$ corrections is too long to be reported here, but can be accessed through the computer code SusyHD provided in [111] for $\overline{\rm DR}$ and OS schemes. Our computation in the $\overline{\rm DR}$ scheme agrees[1] with the one of [94]. In the limit $m_{Q_3} = m_{U_3} = m_{\tilde{t}}$ and vanishing gluino mass the OS expression takes the simple form

$$\Delta\lambda^{(2)}_{\alpha_t\alpha_s} = -\frac{y_t^4 g_3^2}{16\pi^4}\left[\frac{5}{2} - \frac{1}{2}\hat{X}_t^2 - \left(2 - 3\hat{X}_t^2\right)\ln\frac{m_{\tilde{t}}^2}{Q^2} + 3\ln^2\frac{m_{\tilde{t}}^2}{Q^2}\right], \qquad (3.4)$$

while for $M_3 = m_{Q_3} = m_{U_3} = m_{\tilde{t}}$

$$\Delta\lambda^{(2)}_{\alpha_t\alpha_s} = -\frac{y_t^4 g_3^2}{16\pi^4}\left[4 - 6\hat{X}_t - 4\hat{X}_t^2 + \frac{3}{4}\hat{X}_t^4 - \left(2 - 3\hat{X}_t^2\right)\ln\frac{m_{\tilde{t}}^2}{Q^2} + 3\ln^2\frac{m_{\tilde{t}}^2}{Q^2}\right], \qquad (3.5)$$

where $\hat{X}_t = X_t/m_{\tilde{t}}$, $X_t = A_t - \mu/\tan\beta$ and Q is the renormalization scale. The definition we used for X_t in the OS scheme is given in eq. (A.24) in appendix A.2.

The two-loop $\mathcal{O}(\alpha_t^2)$ supersymmetric threshold correction to the quartic coupling can be derived from the corresponding correction to the Higgs mass. We

[1] We thank the authors of [94] for providing the explicit expression of their result for the cross-check.

derived it under the simplifying assumption of degenerate scalars while the μ parameter and the renormalization scale are left free. We used the results in ref. [79] for the $\mathcal{O}(\alpha_t^2)$ correction to the Higgs mass calculated using the effective potential technique in $\overline{\text{DR}}$. Converting in the one-loop $\mathcal{O}(\alpha_t)$ correction the $\overline{\text{DR}}$ superpotential top Yukawa coupling and MSSM Higgs vev into the $\overline{\text{MS}}$ SM top Yukawa and EW vev will produce an additional shift contribution at two loops. Analogously for the OS computation there is an extra shift from converting the stop masses and mixings in the one-loop corrections. We subtract the $\mathcal{O}(\alpha_t^2)$ top-quark contribution because it already appears in the matching at the EW scale. Finally, it is important to notice that there is also a contribution to the matching of the Higgs mass (and the quartic coupling) at the SUSY scale induced by the one-loop contribution of the stops to the wave-function renormalization of the Higgs field, which is instead absent in the $\mathcal{O}(\alpha_t\alpha_s)$ corrections. The complete expression with the details of the calculation can be found in appendix A.2, a simplified expression in the OS scheme for the case $\mu = m_{\tilde{t}}$ and large $\tan\beta$ reads

$$\Delta\lambda^{(2)}_{\alpha_t^2} = \frac{9\,y_t^6}{(4\pi)^4}\left[3 + \frac{26}{3}\hat{X}_t^2 - \frac{11}{6}\hat{X}_t^4 + \frac{1}{6}\hat{X}_t^6 - \left(\frac{10}{3} - \hat{X}_t^2\right)\ln\frac{m_{\tilde{t}}^2}{Q^2} + \ln^2\frac{m_{\tilde{t}}^2}{Q^2}\right] + \mathcal{O}\left(\tan^{-2}\beta\right). \tag{3.6}$$

As a cross check we verified analytically that the two-loop $\mathcal{O}(\alpha_t\alpha_s)$ and $\mathcal{O}(\alpha_t^2)$ threshold corrections to the quartic coupling (under the assumption of degenerate scalars) cancel the dependence on the renormalization scale of the Higgs mass at the same order.

Finally we also included the 1-loop threshold corrections from the bottom (and tau) sector, which are relevant in the large $\tan\beta$ region. The explicit expressions can be found in the appendix A.2. At large $\tan\beta$, depending on the size and sign of other parameters, such as the μ term and the gaugino masses, the net effect is that of reducing the value of the Higgs mass. This effect may even cancel the tree-level contribution and allow for larger SUSY scales (see section 3.2.3).

The relevance of the supersymmetric thresholds decreases as the SUSY scale increases because of the evolution of the SM running couplings. Among the missing SUSY threshold corrections the most important are the two-loop $\mathcal{O}(\alpha_t^2)$ when the scalars are not degenerate, the two-loop $\mathcal{O}(\alpha_t\alpha, \alpha_s\alpha)$ proportional to the electroweak gauge couplings and the three-loop $\mathcal{O}(\alpha_t\alpha_s^2)$. In the case of large $\tan\beta$ and sizable μ parameter, the two-loop corrections proportional to the bottom Yukawa can also be relevant, they include the $\mathcal{O}(\alpha_b\alpha_s, \alpha_b\alpha_t, \alpha_b^2)$ corrections. The contribution of the missing SUSY thresholds to the Higgs mass is estimated to be below 1 GeV even for a spectrum of superparticles as low as 1 TeV, see the next section.

Further improvements of our computation are discussed in section 3.4.

3.1.2 Estimate of the uncertainties

In the EFT approach to the calculation of the Higgs mass in SUSY, the uncertainties can be recast into three different groups:

1. *SM uncertainties*: from the missing higher order corrections in the matching of SM couplings at the EW scale and their RG evolution;

2. *SUSY uncertainties*: from missing higher order corrections in the matching with the SUSY theory at the high scale;

3. *EFT uncertainties*: from missing higher order corrections from higher dimensional operators in the SM EFT and other EW suppressed corrections $\mathcal{O}(v^2/m^2_{\rm SUSY})$.

The estimate of the uncertainties in the Split-SUSY scenario is slightly different from the High-Scale one, because there are additional contributions from the extra matching at the Split scale and the evolution of the Split couplings between the mass scales of the fermion and scalar superpartners. Fortunately, one does not expects large stop mixing in Split-SUSY models, which renders the uncertainties under control. As we will discuss in section 3.2.4, the High-Scale SUSY EFT computation also gives excellent results when the fermion superpartners are lighter than the scalars. For these reasons we will focus on the estimate of the uncertainties in the High-Scale EFT calculation.

Fig. 3.2 summarizes the importance of the individual sources of uncertainty as a function of the SUSY scale. For definiteness we took the superpartners to be degenerate with mass $m_{\rm SUSY}$, the Higgs mass has been kept fixed at 125 GeV by varying either the stop mixing (with fixed $\tan\beta = 20$ for $m_{\rm SUSY} < 20$ TeV) or $\tan\beta$ (with vanishing stop mixing for $m_{\rm SUSY} > 20$ TeV). We will now discuss these uncertainties individually.

SM uncertainties

As described in the previous section, in our computation we employed full SM three-loop RGE and two-loop matching conditions at the EW scale to relate the pole masses m_h and m_t and the gauge couplings to the $\overline{\rm MS}$ running couplings at the high scale. We also included the 3-loop $\mathcal{O}(\alpha_s^3)$ corrections to the top mass matching. This is expected to be the leading higher-order correction and the missing 3-loop matching and 4-loop running corrections are not expected to

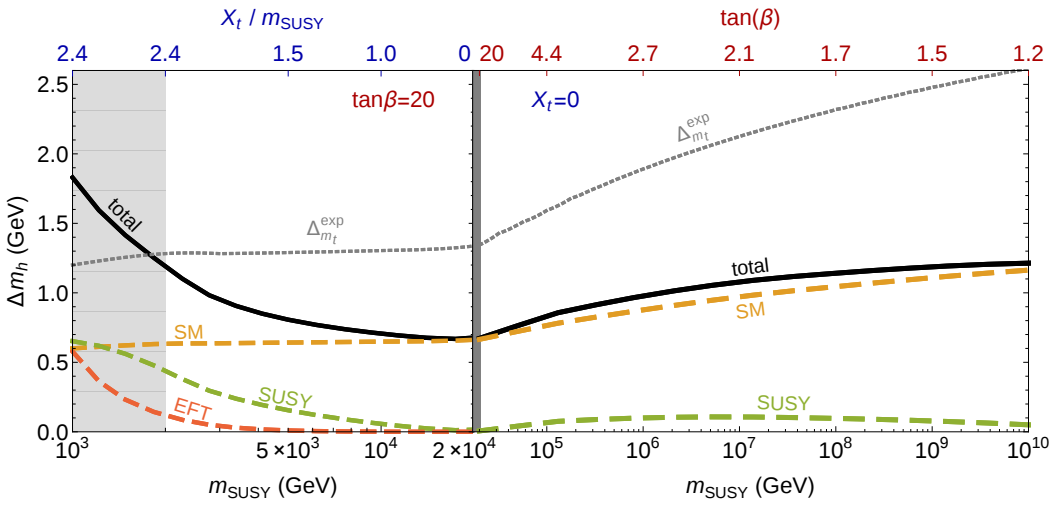

Figure 3.2: Breakdown of the uncertainties for a 125 GeV Higgs mass as a function of the (degenerate) superparticle masses $m_{\rm SUSY}$. The Higgs mass has been kept fixed at 125 GeV by varying either the stop mixing (with fixed $\tan\beta = 20$ for $m_{\rm SUSY} < 20$ TeV, left panel of the plot) or $\tan\beta$ (with vanishing stop mixing for $m_{\rm SUSY} > 20$ TeV, right panel of the plot. Note that for $m_{\rm SUSY} < 2$ TeV (the gray region) the 125 GeV value for the Higgs mass cannot be reproduced anymore but is within the theoretical uncertainties. The black "total" line is the linear sum of the theoretical uncertainties from SM, SUSY and EFT corrections (in dashed lines). The dotted line $\Delta_{m_t}^{\rm exp}$ corresponds to the 2σ experimental uncertainty on the top mass.

give larger effects. Still, we conservatively used the 3-loop $\mathcal{O}(\alpha_s^3)$ corrections to estimate the SM uncertainties from the higher-order missing corrections, although the latter are probably smaller[1].

The full SM uncertainty in fig. 3.2 has been computed by summing the effects from $\mathcal{O}(\alpha_s^3)$ corrections to the top mass and the $\sim$0.15 GeV estimate [93] of the 3 loop corrections to m_h^2. While the latter corrections would be formally of the same order as the corrections induced by the 2-loop SM corrections to the matching of the top Yukawa in a fixed order computation, in the EFT approach they are actually subleading because the 2-loop corrections from the top sector get enhanced by the RG logarithms and by the stop mixing (when this is large).

[1]For this reason our theoretical uncertainty from the SM calculation is somewhat larger than the one quoted for example in [93], which uses the same precision for the computation of the stability of the SM Higgs potential.

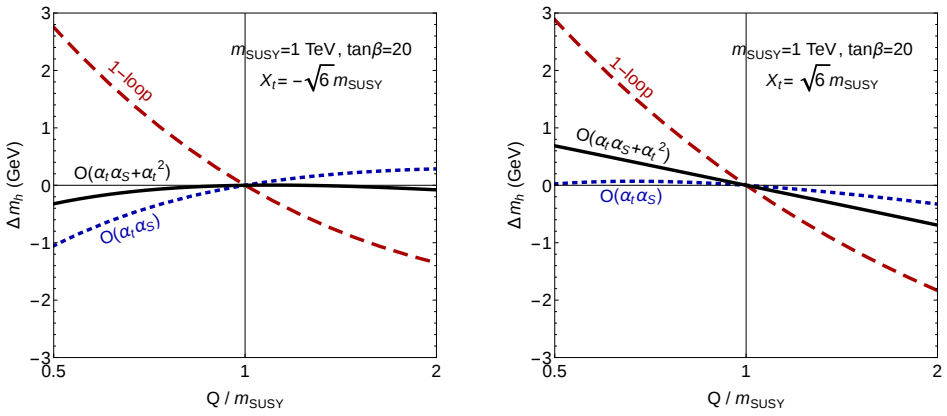

Figure 3.3: *The uncanceled scale dependence from higher order corrections is largest at maximal stop mixing and small stop masses (here taken 1 TeV). Including only 1-loop SUSY threshold it amounts to up to a 3 GeV shift of the Higgs mass, when the scale is changed by a factor of 2. It reduces to below 1 GeV when the leading 2-loop $\mathcal{O}(\alpha_t\alpha_s)$ and $\mathcal{O}(\alpha_t^2)$ corrections are included.*

The net effect from these SM corrections amount to a shift to the Higgs mass of order $0.5\div1$ GeV for $m_{\rm SUSY} \sim 1 \div 10^7$ TeV. The uncertainty slowly increases with the SUSY scale as a result of the longer RGE running.

How can the SM uncertainty be reduced? One can consistently include the next order in the strong corrections, in the matching at the electroweak scale and the RGE. It requires the expressions of the three-loop $\mathcal{O}(y_t^4 g_3^4)$ and $\mathcal{O}(y_t g_3^6)$ threshold corrections to λ and y_t respectively. For evolving the running couplings, one needs the four-loop $\mathcal{O}(y_t^4 g_3^6)$, $\mathcal{O}(y_t g_3^8)$, and $\mathcal{O}(y_t^4 g_3^9)$ contributions to the beta functions of λ, y_t and g_3. This is discussed in more detail in section 3.4.1, where also the estimate of the SM uncertainties is improved.

SUSY uncertainties

The matching between the SUSY soft parameters and the SM couplings includes full one-loop threshold corrections (including also bottom and tau Yukawa corrections) plus the leading two-loop corrections $\mathcal{O}(\alpha_t\alpha_s)$ and $\mathcal{O}(\alpha_t^2)$ (the latter only in the simplified case of degenerate scalar masses). While $\mathcal{O}(\alpha_t\alpha_s)$ can give large effects, the corrections from $\mathcal{O}(\alpha_t^2)$ are substantially smaller and other missing 2-loop thresholds are expected to be even smaller. Since a missing threshold produces an uncanceled renormalization scale dependence in the final Higgs mass, such dependence can be used to estimate the missing corrections. In the worst case (maximal stop mixing and small SUSY scale) the uncanceled scale depen-

dence from the 1-loop thresholds may shift the Higgs mass by roughly 3 GeV when the renormalization scale is changed by a factor of 2. $\mathcal{O}(\alpha_t\alpha_s)$ reduce the shift[1] to 1 GeV and $\mathcal{O}(\alpha_t^2)$ further down below 1 GeV, see fig. 3.3.

The uncertainty from SUSY thresholds in fig. 3.2 has been estimated by taking the maximum of the shifts induced by varying the SUSY matching scale by a factor of 2 or 1/2 with respect to $m_{\rm SUSY}$. The impact on the uncertainties from missing SUSY threshold corrections greatly reduces away from maximal stop mixing and when the stop masses are increased, the latter effects due to the reduction of the SM couplings from the RGE evolution. This fact is manifest in the EFT approach, less so in others, which require a careful resummation of logs.

In order to decrease the SUSY uncertainties one can include some of the missing SUSY threshold corrections, as those mentioned at the end of section 3.1.1. In particular, it is worth to compute the two loop $\mathcal{O}(\alpha_t^2)$ thresholds for non-degenerate scalars and the two loop corrections proportional to the bottom Yukawa coupling $\mathcal{O}(\alpha_s\alpha_b, \alpha_b\alpha_t, \alpha_b^2)$, important for large values of $\tan\beta$. That is precisely the task of section 3.4.2. The two loop $\mathcal{O}(\alpha_t\alpha, \alpha_s\alpha)$ proportional to the electroweak gauge couplings and the three loop $\mathcal{O}(\alpha_t\alpha_s^2)$ can also be important.

EFT uncertainties

The last source of uncertainties is intrinsic to the EFT approach and comes from neglecting higher dimensional operators below the SUSY scale; consistently with such approximation we also neglected EW corrections to the sparticle spectrum. These corrections decouple fast, as powers of the EW scale over the SUSY scale, however they could become important for light SUSY scale. Given the relatively high value of the Higgs mass and the bounds from the LHC, superpartners are expected to lie above the TeV scale, reducing the relevance of these corrections only to very particular corners of the parameter space.

At tree level the only source of power corrections comes from the heavy Higgs states—if m_A is close to the EW scale the mixing effects may become important and the tree-level expression in (3.3) gets corrections of order

$$\delta^{(\rm tree)}_{EFT}\lambda \sim -\lambda\frac{m_Z^2}{m_A^2}\sin^2(2\beta). \tag{3.7}$$

Such contributions become important only when m_A is particularly light, i.e. $m_A \lesssim 200$ GeV, in a region of the parameter space which is already disfavored by indirect bounds on the Higgs couplings [117].

[1] In the right plot of fig. 3.3 the scale dependence left after the inclusion of the $\mathcal{O}(\alpha_t\alpha_s)$ corrections seems to be smaller because of an accidental cancellation for those particular values of the parameters.

Corrections from higher dimensional operators induced by the other superpartners enter only at one loop (such as the other scalars and the EWinos) or at two loops (gluino). The most dangerous corrections are thus expected to come from the stops, they are of $\mathcal{O}(\alpha_t\, m_t^2/m_{\tilde{t}}^2)$ and can get enhanced at large stop mixing. We estimated such corrections by multiplying the one-loop corrections by $v^2/m_{\rm SUSY}^2$. Numerically, for stops above 1 TeV, even at maximal mixing, these corrections are below 1 GeV and rapidly decouple for heavier stop masses, see fig 3.2. Having lighter stops may require to take such corrections into account, although they start being too light to accommodate the observed value of the Higgs mass (see sec. 3.2.2).

The total EFT uncertainty in fig. 3.2 has been estimated by taking the sum of the single contributions to $\Delta\lambda$ from each SUSY particle with mass m_i multiplied by the corresponding factor[1] v^2/m_i^2.

In conclusion, for stops above the TeV scale power corrections are small, justifying the use of the EFT. A more detailed analysis is performed in section 3.4.3.

Combined uncertainties

Fig. 3.2 summarizes the impact of the various uncertainties to the determination of the Higgs mass as a function of the SUSY scale, $\tan\beta$ and the stop mixing, in the relevant region of parameters that reproduces the measured value of the Higgs mass. For definiteness we took a degenerate spectrum of superpartners, we checked that the size of the uncertainties remains of the same order when this assumption is relaxed. The dominant source of error comes from higher order corrections in the matching and running of the SM couplings. SUSY thresholds are only important for low SUSY scale and large stop mixing, while power corrections are negligible throughout the parameter space unless some of the sparticles are very close to the EW scale.

It is fair to say that, for most part of the relevant parameter space, the Higgs mass in the MSSM has reached the same level of accuracy as the determination of the Higgs potential in the SM. Further improvements from the theory side can be achieved by extending the SM calculations at higher orders. The size of

[1] More specifically, we multiply the one loop contributions from the scalars $\Delta\lambda_\phi^{1\ell}$ and the fermions $\Delta\lambda_\chi^{1\ell}$ by the factors v^2/m_0^2 and $m_Z^2/m_{1/2}^2$ respectively, where the mass scale of the scalars m_0 and fermions $m_{1/2}$ are taken as the average stop mass and the minimum between the higgsino and wino masses $\min(|\mu|, |M_2|)$. Then the total estimate is considered as the linear sum of the absolute value of the three partial estimates from the tree-level, one loop scalar and one loop fermion contributions.

the uncertainties remains practically unchanged in the split scenario, where the fermions are parametrically lighter than the scalar superpartners.

The total theoretical uncertainty (computed here conservatively as the linear sum of the three sources discussed above) is of order 1 GeV or below for most of the relevant parameter space (i.e. the parameter space that reproduces m_h =125 GeV, see fig. 3.2). It is thus below the error induced by the experimental uncertainty in the value of the top mass. Indeed, the latter produces a shift in the Higgs mass of order 1.5÷2.5 GeV depending on $m_{\rm SUSY}$, when the top mass value is changed by 2σ=1.5 GeV. The error increases with $m_{\rm SUSY}$ due to RGE effects.

As usual, estimates of theoretical errors provide only for the order of magnitude of the expected corrections and must be taken with a grain of salt. However since for most of the parameter space the error is dominated by the SM uncertainties, where we have been rather conservative, the estimate of fig. 3.2 should represent a fair assessment, at least away from the lower end.

3.1.3 Comparison with existing computations

Our EFT computation agrees within the uncertainties with all the others which use the same technique. As already noticed in [94], however, the EFT computation seems to give a smaller Higgs mass with respect to other approaches, such as those based on full diagrammatic and effective potential computations such as [95, 99, 101, 102]. In some cases the disagreement amounts to up to ∼10 GeV, well beyond the expected quoted uncertainties, even in regions of parameter space where both approaches are expected to hold.

A comparison between the EFT computation and some of the available computer codes is shown in fig. 3.4. In order to compare with FeynHiggs, we converted the masses and the stop mixing from the $\overline{\rm DR}$ to the on-shell renormalization scheme employed in that code, using the results from [79]. The disagreement is around 3 GeV for $m_{\rm SUSY} >$ TeV at large tanβ and zero stop mixing and increases up to 9 GeV for maximal mixing and $m_{\rm SUSY}$ = 2 TeV. Moreover, it can not be explained in terms of the claimed uncertainties.

Effect of the electroweak gauge couplings in the resummation

The FeynHiggs code performs the resummation of logarithmic corrections of the top-stop sector, while those controlled by the electroweak gauge couplings are included at fixed order. In order to determine their effect in the resummation, we compare the solution of the coupled $(\lambda, y_t, g_3, g_2, g_1)$ two-loop RGE of the

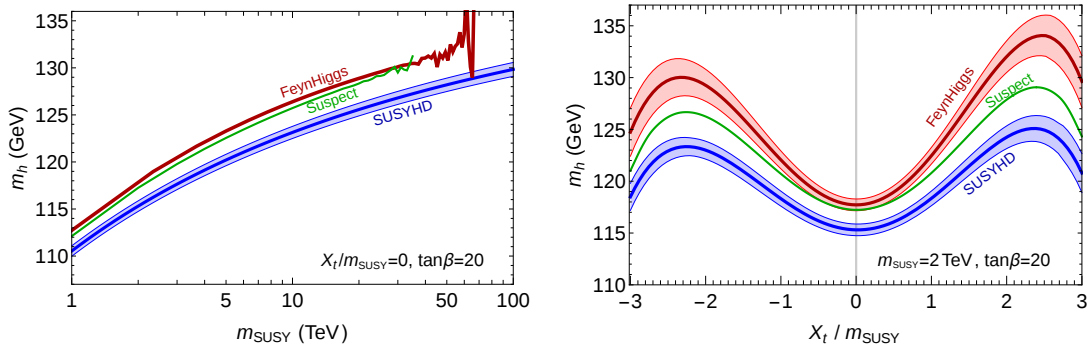

Figure 3.4: *Comparison between the EFT computation (lower blue band) and two existing codes: FeynHiggs [96] and Suspect [101]. We used a degenerate SUSY spectrum with mass $m_{\rm SUSY}$ in the $\overline{\rm DR}$-scheme with $\tan\beta = 20$. The plot on the left is m_h vs $m_{\rm SUSY}$ for vanishing stop mixing. The plot on the right is m_h vs $X_t/m_{\rm SUSY}$ for $m_{\rm SUSY} = 2$ TeV. Since the FeynHiggs code works in the OS scheme, we converted the $\overline{\rm DR}$ parameters to OS-scheme using the 1-loop formulas in [79] as input for the FeynHiggs code. On the left plot the instability of the non-EFT codes at large $m_{\rm SUSY}$ is visible.*

Standard Model with the solution of the coupled (λ, y_t, g_3) RGE plus the logarithmic contributions controlled by g_1 and g_2 taken at fixed order up to two-loops, obtained by iterative solution of the RGEs[1].

One can use the RGE to obtain the logarithmic higher-oder contributions, as already discussed in section 2.3.2. The Higgs quartic coupling at the top mass can be written as

$$\lambda(m_t) = \sum_{n=0}^{\infty} \kappa^n \sum_{p=0}^{n} L^p C_{n.p}, \text{ with } \kappa = \frac{1}{16\pi^2}, \quad L = \ln \frac{m_{\rm SUSY}}{m_t}. \tag{3.8}$$

The term $C_{0,0}$ contains the tree-level contribution, $C_{1,1}$ the one-loop LL, $C_{1,0}$ the one-loop thresholds, $C_{2,2}$ the two-loop LL, $C_{2,1}$ the two-loop NLL, $C_{2,0}$ the two-loop thresholds and so on.

We solved iteratively the SM two-loop RGE, denoted generically as

$$\frac{dX}{dt} = \kappa \beta_X^{(1)} + \kappa^2 \beta_X^{(2)}, \qquad t = \ln(Q/Q_0) \tag{3.9}$$

where $X = \lambda, y_t, g_3, g, g'$. We obtain

$$C_{1,1} = -\beta_\lambda^{(1)} \tag{3.10}$$

[1] In FeynHiggs the tree level contribution to the quartic coupling does not appear as a boundary condition at the SUSY scale; instead it appears at fixed order. We follow the same procedure to facilitate the analysis.

$m_{\rm SUSY}$ (GeV)	10^4	10^5	10^8
Δm_h (GeV): full$-g, g'$ at 2 loops	0.5	1.7	6.2
Δm_h (GeV): full$-g, g'$ at 1 loop	0.9	2.6	10.2

Table 3.1: Deviation from the the Higgs mass calculation with a full RG resummation due to considering the logarithms controlled by g and g' at fixed order.

$$C_{2,2} = \frac{1}{2}\sum_X \beta_X^{(1)} \frac{\partial \beta_\lambda^{(1)}}{\partial X} = \frac{1}{2}\left[\beta_\lambda^{(1)} \frac{\partial \beta_\lambda^{(1)}}{\partial \lambda} - \beta_{y_t}^{(1)} \frac{\partial \beta_\lambda^{(1)}}{\partial y_t} - \beta_{g'}^{(1)} \frac{\partial \beta_\lambda^{(1)}}{\partial g'} - \beta_g^{(1)} \frac{\partial \beta_\lambda^{(1)}}{\partial g}\right] \tag{3.11}$$

$$C_{2,1} = -\beta_\lambda^{(2)} - \frac{\partial \beta_\lambda^{(1)}}{\lambda} C_{1,0}, \tag{3.12}$$

where all the couplings in the β functions are evaluated at the top mass except the quartic coupling λ which is evaluated at $m_{\rm SUSY}$. The difference in sign in eq. (3.11) is because we are running from a higher scale to the top mass, and y_t, g_3, g and g' are evaluated at the top mass. The logarithmic contributions to λ controlled by g, g' denoted by $C_{n,p}^{g,g'}$ are obtained by subtracting the g, g'-independent contributions from the full one: $C_{n,p}^{g,g'} = C_{n,p}(g, g') - C_{n,p}(g, g' = 0)$. We also found iteratively the RG contribution to $g(m_{\rm SUSY})$ and $g'(m_{\rm SUSY})$ up to two loops needed to evaluate $\lambda(m_{\rm SUSY})$.

The effect of the electroweak gauge couplings in the resummation is illustrated in Fig. 3.5. It is not very sensitive to the stop mixing X_t, because the X_t-dependent contributions are controlled by y_t and g_3. We consider $\tan\beta = 20$ and $X_t = 0$ for definiteness. We plot the shift in the Higgs mass Δm_h, with respect to the result with full resummation in all couplings, induced by considering the logarithms proportional to g and g' at fixed order. To facilitate the analysis we have also presented the results in the table 3.1.

We see in fig. 3.5 and table 3.1 that despite the deviation in the Higgs mass induced by considering the loop corrections controlled by g, g' at fixed order (as FeynHiggs does) become very important for $m_{\rm SUSY} \gtrsim 10^5$ GeV, for $m_{\rm SUSY} = 10^4$ GeV this deviation is less than 1 GeV. Moreover including all the LL and NLL corrections controlled by g and g' increases the Higgs mass, i.e. it shifts the Higgs mass in the direction such that the fixed-order result in fig. 3.4 deviates more from the EFT one. Therefore, the logarithmic corrections controlled by the electroweak gauge couplings can not explain the discrepancies.

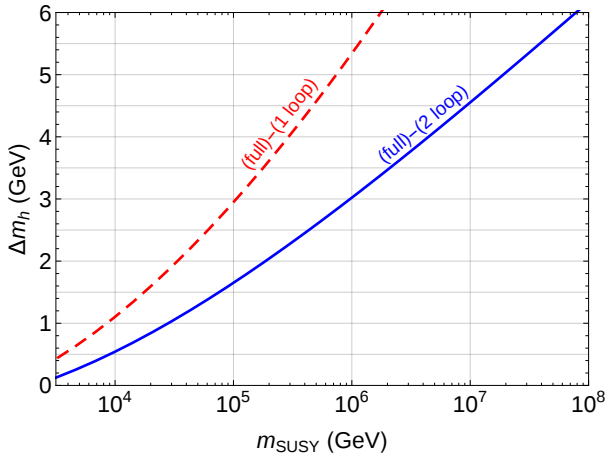

Figure 3.5: Effect of the electroweak gauge couplings in the resummation. The curves show the difference between the Higgs mass computed with NLL resummation in all the couplings and NLL resummation in λ, y_t, g_3 but including the logarithms proportional to g and g' at fixed order, up to one-loop (red dashed) or two loops (blue solid). We assume a degenerate spectrum of superparticles and $\tan\beta = 20$.

Sensitivity to the top Yukawa

The large disagreement with the FeynHiggs 2.10.1 code can mostly be understood as follows. The computation in [96] included full 1-loop plus the leading 2-loop SUSY corrections of the Higgs mass at fixed order combined with partial 2-loop RGE resummation of the logarithms of the top-stop sector. Consistently with this however, they only include the 1-loop corrections proportional to g_3 and y_t to the matching of the $\overline{\rm MS}$ top Yukawa coupling. Instead, including the 1-loop electroweak, the complete 2-loop and the 3-loop strong corrections to the relation between the $\overline{\rm MS}$ and the OS mass of the top quark accounts for a shift in the $\overline{\rm MS}$ top mass of roughly 4 GeV. Hence, the bulk of the disagreement is due to these missing corrections in the $\overline{\rm MS}$ top mass and Yukawa coupling[1].

Note that, as discussed in the previous section, the uncertainty in the EFT approach is dominated by the 3-loop top matching conditions, the 2-loop ones are thus mandatory in any precision computation of the Higgs mass[2]. We checked

[1] It was brought to our attention that a similar observation was also made in [118].

[2] The four loop $\mathcal{O}(\alpha_s^4)$ correction to the relation between the top mass defined in the on-shell and the $\overline{\rm MS}$ schemes was recently computed [119]. It confirms the slow convergence of the QCD perturbative expansion.

that after their inclusion, the FeynHiggs code would perfectly agree with the EFT computation at zero squark mixing. At maximal mixing the disagreement would be reduced to 4 GeV, which should be within the expected theoretical uncertainties of the diagrammatic computation.

For comparison, in fig. 3.4 we also show the results obtained with a different code (Suspect [101]) which uses a diagrammatic approach. Unlike FeynHiggs, Suspect includes the $\mathcal{O}(\alpha_s^2)$ threshold corrections to the top Yukawa matching condition but does not perform RGE improvement and its applicability becomes questionable for m_{SUSY} in the multi TeV region.

3.2 Results

After having seen that the EFT computation is reliable for most of the relevant parameter space we present here some of the implications for the supersymmetric spectrum. Given the generic agreement with previous computations using the same approach, we tried to be as complementary as possible in the presentation of our results, putting emphasis on the improvements of our computation and novel analysis in the EFT approach.

3.2.1 Where is SUSY?

Fig. 3.6 represents the parameter space compatible with the experimental value of the Higgs mass in the plane of $(m_{1/2}, m_0)$ for zero (blue) and increasing values (red) of the stop mixing. For simplicity we took degenerate scalar masses m_0 as well as degenerate fermion masses $m_{1/2} = M_{1,2,3} = \mu$. All SUSY parameters of this plot are in the $\overline{\text{DR}}$ scheme[1]. The figure highlights a number of features:

- The main effect at small fermion masses is given by the scale of the scalars (in particular the stops). The lower part of the allowed region corresponds to large values of $\tan\beta \gtrsim 10$. Lowering $\tan\beta$ allows to access larger scalar masses (see also fig. 3.8 below).

- The dependence on the fermion masses can be understood as follows. For $m_{1/2} \lesssim m_0$ the biggest contribution comes from the higgsino-wino loop in the running of the Higgs quartic. It makes the quartic coupling run larger in the IR thus making the Higgs heavier. This correction is only there when both wino and higgsino become light. There is also a smaller 1-loop correction from the individual EWinos, which affects the running of the

[1] All $\overline{\text{DR}}$ parameters are computed at the scale $Q = \sqrt{m_{\tilde{t}_L} m_{\tilde{t}_R}}$ unless specified otherwise.

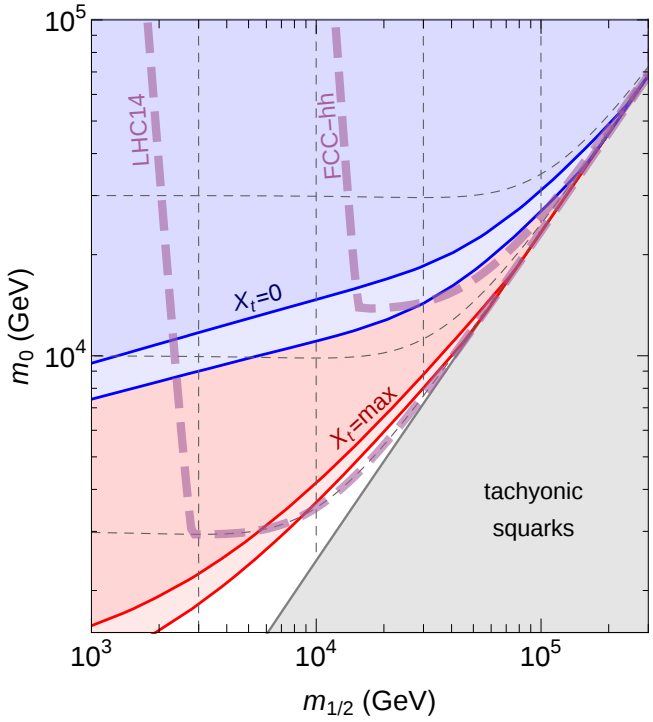

Figure 3.6: *Higgs mass constraint on the value of scalar (m_0) and fermionic ($m_{1/2}$) superpartners (taken degenerate). The upper blue region refer to zero mixing, the lower red to increasing values of the stop mixing. The lighter bands corresponds to the uncertainty from the top mass. The gray shaded region corresponds to tachyonic on-shell masses for the squarks. The non-vertical thin dashed lines correspond to on-shell values for the squark masses: when $m_{1/2}$ grows the $\overline{\text{DR}}$ mass m_0 must be increased to keep the on-shell mass constant. The thick dashed burgundy lines correspond roughly to the expected reach of LHC14 and of an hypothetical 100 TeV machine.*

EW gauge couplings. They make the gauge coupling run bigger in the UV increasing the tree-level contribution to the Higgs quartic (3.3) and thus its pole mass. Lowering the gluino mass decreases the Higgs mass but the effect is two-loop suppressed and only non-negligible at large stop mixings. The region $m_{1/2} \gtrsim 2m_0$ should be treated with care. In the $\overline{\text{DR}}$ scheme there are negative quadratic corrections to the squark masses proportional to the gaugino masses [69]

$$m_{\tilde{q}}^{2,\text{OS}} = m_{\tilde{q}}^{2,\overline{\text{DR}}}(m_{\tilde{q}}^2) - \frac{4\alpha_s}{3\pi} M_3^2 \left[\log\left(\frac{M_3^2}{m_{\tilde{q}}^2}\right) - 1\right] + \dots \tag{3.13}$$

In particular when M_3 becomes larger than roughly a factor of four with

respect to the squark masses the corresponding on-shell masses become tachyonic. Just before this happens the on-shell masses (the dashed lines in the figure) start becoming smaller and smaller with respect to the $\overline{\text{DR}}$ parameters, in this tuned region large corrections make the $\overline{\text{DR}}$ computation unstable. This explains the strong apparent dependence on $m_{1/2}$ on the right-hand part of the plot, which would disappear if plotted in terms of the on-shell masses. We decided to keep the plot in terms of the $\overline{\text{DR}}$ parameters to highlight the tuning required to explore such region.

- Current LHC searches already probed squark and gluino masses up to 1.5 TeV circa [120]. This corresponds to the very lowest part of the allowed parameter space, where the stop mixing is maximal, $\tan\beta$ is large and fermions must be lighter than scalars. This, of course, with the caveat that the strongest experimental bounds apply to first generation squarks and gluino while the Higgs mass mostly depend on the stops and (somewhat weaklier) on EWino. With the same caveat LHC14 should eventually be able to more confidently explore the same region (extending the squark-gluino reach to 3 TeV, see e.g. [121]), while the small stop mixing region could only be reached directly with a 100 TeV machine (capable of probing colored sparticles of roughly 15 TeV masses, see e.g. [121]). Of course (mini-)Split scenarios where the heavy scalars are responsible for the Higgs mass and the light fermions are within reach at lower energies remain a valid possibility.

3.2.2 The EFT gets on-shell

Previous computations using the EFT approach have used the $\overline{\text{DR}}$ scheme for the SUSY and the soft parameters. This scheme has the advantage of being the natural framework for the computations of the soft parameters in theories of SUSY breaking. In some cases, however, it results inadequate for the computation of the Higgs mass.

First of all, physical on-shell masses are needed to compare theoretical computation with experiments. While the difference in the schemes is one-loop suppressed, there are non-decoupling effects which require care. For example the difference between the on-shell and the $\overline{\text{DR}}$ squared mass of the squarks receives an additive one-loop correction proportional to the gluino mass squared, see eq. (3.13). Such correction is negative and big—it is enough for the gluino mass to be a factor of four above the squark masses to drive the corresponding on-shell mass tachyonic.

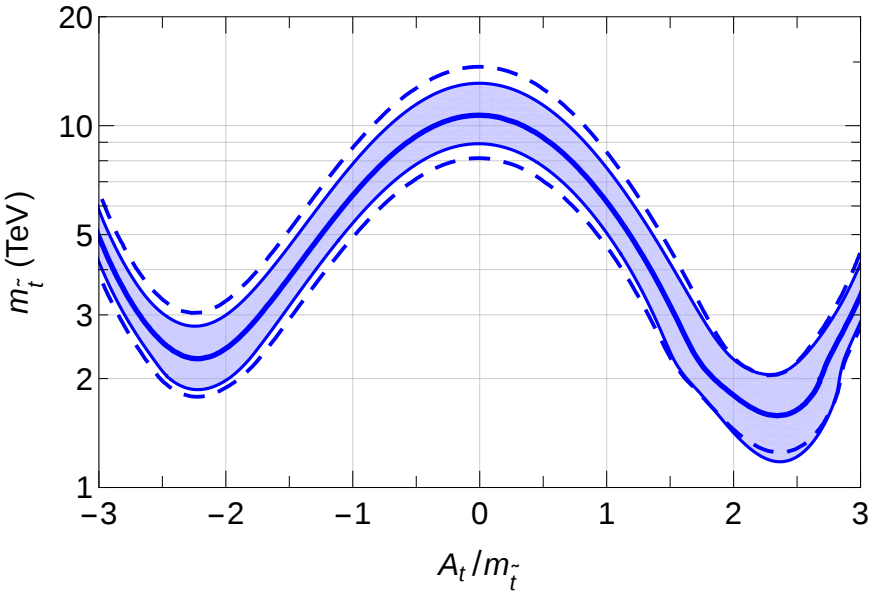

Figure 3.7: *Allowed values of the OS stop mass reproducing $m_h = 125$ GeV as a function of the stop mixing, with $\tan\beta = 20$, $\mu = 300$ GeV and all the other sparticles at 2 TeV. The band reproduce the theoretical uncertainties while the dashed line the 2σ experimental uncertainty from the top mass. The wiggle around the positive maximal mixing point is due to the physical threshold when $m_{\tilde{t}}$ crosses $M_3 + m_t$.*

For similar reasons in the $\overline{\text{DR}}$ scheme the gluino contribution to the Higgs mass does not decouple [81]. Another consequence is the instability of the Higgs mass with respect to the renormalization scale—even if the on-shell squark masses are positive, the $\overline{\text{DR}}$ stop mass becomes highly sensitive to the renormalization scale when the gluino is more than a factor of $2 \div 3$ above it, which results in an instability of the estimate of the Higgs mass. What is happening is that the physical on-shell squark masses becomes tuned and highly sensitive to the soft parameters. The situation is similar to trying to compute the Higgs mass in terms of the soft parameter $m^2_{H_u}$ instead of the on-shell (tuned) EW vev v.

All these problems disappear in the OS scheme, the gluino decouples up to a physical log correction [81], there are no tachyons since the physical OS masses are given as input and larger hierarchies can be introduced safely within the SUSY spectrum (with the usual caveat that large logarithms may require resummation). Besides, the input masses are directly the physical quantities to be compared with experiments.

For these reasons we also performed our computation in the OS scheme. Fig. 3.7 shows an application of such calculation. It corresponds to the region

of allowed OS stop masses (taken degenerate in this case) which reproduces the observed Higgs mass for different A_t-terms. Our definition of A_t in the on-shell scheme, eq. (A.24), is different from the usual one, this explains why the point of maximal mixing is not at $X_t/m_{\tilde{t}} \simeq 2$. In the spirit of *natural* SUSY [122–124] we kept the higgsino light at 300 GeV while the gauginos and first generation squarks safely above collider bounds at 2 TeV. The lightest stop masses allowed in this case (for maximal stop mixing) are about 1.7±0.4 TeV, in the region where the EFT approach should be reliable.

Had we drawn the same plot in terms of the $\overline{\text{DR}}$ masses we would not be able to draw the same conclusion—the error would blow up in the region where the stops are sufficiently lighter than the gluino.

3.2.3 Large-$\tan\beta$ High-Scale SUSY strikes back?

While for most values of $\tan\beta$ the contributions from the bottom and tau sector can be neglected, at very large $\tan\beta$ the corresponding superpotential couplings become large and their effects to the SUSY threshold can eventually dominate over the others. In particular the one loop sbottom threshold to the Higgs quartic coupling at leading order in $\tan\beta$ and degenerate sbottoms ($m_{\tilde{b}}$) reads

$$\Delta\lambda_{\tilde{b}}^{(1)} = -\frac{\hat{y}_b^4}{32\pi^2}\frac{\mu^4}{m_{\tilde{b}}^4}\,, \tag{3.14}$$

and analogously for the tau. At tree-level the superpotential Yukawa coupling $\hat{y}_b$ is related to the SM Yukawa y_b by $\hat{y}_b = y_b/\cos\beta$. At large $\tan\beta$, $\hat{y}_b$ may become larger than one. In this situation the negative threshold correction (3.14) may cancel or even overcome the tree-level contribution, especially at high SUSY scale where the SM EW gauge couplings are smaller. This effect may allow to maintain $m_h = 125$ GeV and large $\tan\beta$ with arbitrary heavy scalar fields, reopening the High Scale SUSY window above 10^{10} GeV, which was thought to be excluded by the Higgs mass within the MSSM. As an example, we show in fig. 3.8 how the m_{SUSY}-vs-$\tan\beta$ plot would look like at large $\tan\beta$ after including the leading bottom (and tau) contributions. For the plot we chose degenerate spectrum with mass m_{SUSY}, negative $\mu = -m_{\text{SUSY}}$ and $A_t = m_{\text{SUSY}}/2$. The SUSY parameters are given in the OS scheme. The behavior at small and moderately large $\tan\beta$ ($\tan\beta \lesssim 40$) is well-known [36, 47, 94]. However further increasing $\tan\beta$, the bottom coupling $\hat{\alpha}_b = \hat{y}_b^2/(4\pi)$ grows, decreasing the Higgs mass [66]. For very large $\tan\beta$ the tree-level contribution to the bottom mass is so suppressed that loop corrections cannot be neglected [125, 126]. In fact the bottom mass receives

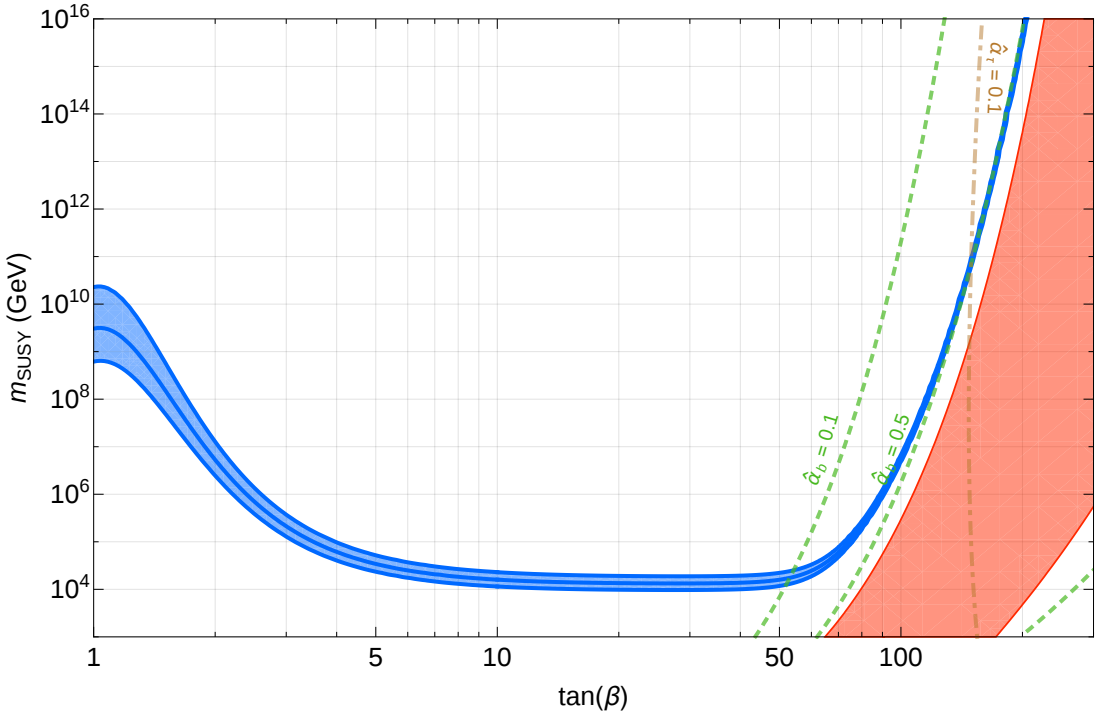

Figure 3.8: *Effects of the sbottom threshold at large* $\tan\beta$*. The blue band corresponds to the* $m_h = 125$ *GeV constraint (the width is given by the estimated theoretical uncertainties) for different values of* $\tan\beta$ *and the degenerate SUSY mass* $m_{\rm SUSY}$*. We fixed* $\mu = -m_{\rm SUSY}$ *and* $A_t = m_{\rm SUSY}/2$*. Dashed and dot dashed lines correspond to different values of the bottom and tau couplings respectively. The red region correspond to tachyonic Higgs and/or non-perturbative bottom Yukawa coupling.*

corrections from SUSY breaking proportional to $v_u = v\sin\beta$, *i.e.* not $\tan\beta$ suppressed

$$y_b = \hat{y}_b\cos\beta + \hat{y}_b\sin\beta\left[\frac{8}{3}\frac{\alpha_s}{4\pi}\frac{\mu M_3}{m^2_{\tilde{b}}}F\left(\frac{M_3^2}{m^2_{\tilde{b}}}\right) + \frac{\alpha_t}{4\pi}\frac{1}{\sin^2\beta}\frac{\mu X_t}{m^2_{\tilde{b}}}F\left(\frac{\mu^2}{m^2_{\tilde{b}}}\right)\right] + \dots \quad (3.15)$$

where $F(x) = (1 - x + x\log x)/(1-x)^2$ and we considered $m_{Q_3} = m_{U_3} = m_{D_3} \equiv m_{\tilde{b}}$. The loop corrections are proportional to μ and a combination of gauginos and A-terms. If the latter are small or have opposite sign with respect to μ (like in fig. 3.8), $\hat{y}_b$ will become strong at large $\tan\beta$ in order to reproduce the observed bottom Yukawa (the red region in the plot). Before that, $\hat{y}_b$ is large enough to make the threshold (3.14) win over the tree-level contribution and allow $m_{\rm SUSY} > 10^{10}$ GeV at large $\tan\beta$. For example the observed Higgs mass can be reproduced for GUT scale SUSY with $\tan\beta \sim 200$. In this case the bottom

coupling $\hat{\alpha}_b \sim 0.5$, which is still perturbative but with a very close Landau pole $\Lambda_{LP} \approx 10 m_{\rm SUSY}$. The perturbativity of $\hat{\alpha}_b$ could be improved by choosing larger μ terms, however this may become in tension with bounds from tunneling into charge/color breaking vacua [57, 58]. We do not know what are the corresponding bounds on the μ term in this regime, this require a dedicated study which is beyond the scope of this work.

We thus find that the upper bound of 10^{10} GeV on the SUSY scale from the observed Higgs mass may not apply for arbitrary values of $\tan\beta$ but only for small to moderately large $\tan\beta$. High scale SUSY at larger $\tan\beta$, however, requires large μ terms, gauginos may be lighter but not too much since they receive loop corrections. Therefore high scale Split SUSY does not seem possible in this way.

If gaugino masses and/or A-terms are large and with the same sign as μ, the loop corrections may saturate the full contribution to the physical fermion mass. If this happens, arbitrary large values of $\tan\beta$ can be reached without ever running into strong coupling effects.

Finally for smaller μ (not shown in the plot) the bottom-tau sector remains decoupled from the low energy Higgs, the threshold (3.14) is never important and $m_{\rm SUSY}$ at large $\tan\beta$ stays constant. The bottom and tau Yukawa couplings still become strongly coupled at large $\tan\beta$ but the effect on the Higgs mass remain small. Of course the effect from the new physics present at the strong coupling scale is model dependent and may be important.

3.2.4 Split vs High-Scale SUSY computation

As mentioned before, in (mini)split-SUSY scenarios, where gauginos and possibly the higgsinos are sensibly lighter than the scalar sector, a new mass scale is present and large logarithms may require resummation. In this case the correct procedure would be: 1) to interrupt the SM running at the split scale, where the light fermion superpartners are, 2) to match to the split-SUSY effective theory, which includes SM particles and the fermion superpartners, 3) to perform a second running within the new EFT and eventually 4) to match to the full SUSY theory at the scalar mass scale. This procedure, which has been employed since the birth of split SUSY, and became more popular recently after the Higgs discovery, is more involved than the high-scale SUSY computation. Besides, the thresholds and the RGE of the split EFT are only known at a lower order in perturbation theory.

Note however the following. The leading effect of resumming the logarithms generated from splitting the fermion superpartners is to change the running of the Higgs quartic and EW gauge couplings. Numerically the change in the running of the Higgs quartic coupling is the leading contribution but it is only present

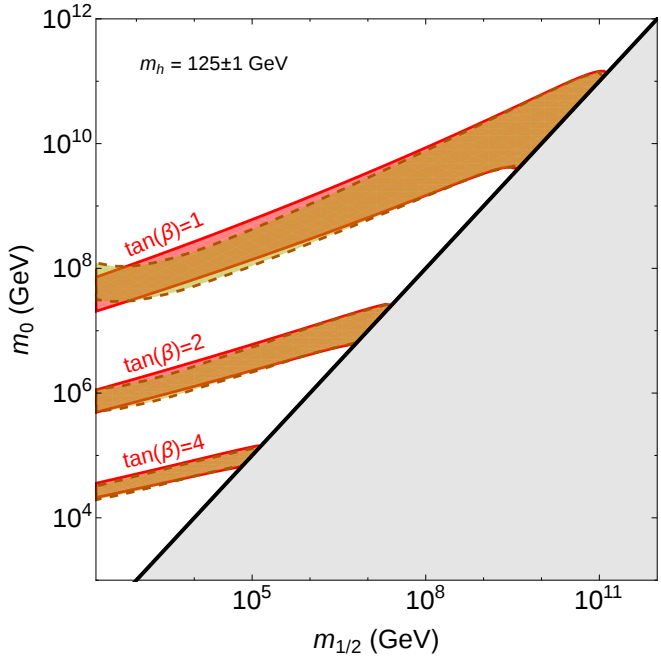

Figure 3.9: *Constraints in the* $(m_0, m_{1/2})$ *plane from* $m_h = 125 \pm 1$ *GeV for different values on* $\tan\beta$ *using the proper split-SUSY computation (dark yellow, dashed line) or the approximate high-scale computation (red, continuous line) which does not resum the logs induced by the splitting of* $m_{1/2}$ *from* m_0*. The agreement is remarkable in the whole relevant parameter space.*

when both higgsino and gauginos are light. The effect from the change in the RGE of the EW gauge couplings is instead smaller and it is further suppressed at small $\tan\beta$, exactly when the logarithms are the largest. Finally the effects from gluinos are negligible. Since they affect the running of the strong coupling at one-loop and of the top Yukawa at two-loops, their effect is confined to scales much higher than their mass. On the other hand the Higgs quartic coupling is mostly determined by the value of the SM couplings at low energies, which are fixed by the experimental values.

The observed value of the Higgs mass is not very large and its value limits the SUSY scale to roughly 10^{10} GeV. This scale gets further reduced to $10^{7\div 8}$ GeV if the SUSY fermions are split, as an effect of the extra contribution to the running of the Higgs quartic. This translates into an upper bound on how large the logarithmic thresholds from splitting the fermions can grow.

It turns out that in the whole parameter space relevant for the observed value of the Higgs mass, the effect of resumming the logs of the splitting between fermion and scalar superpartners is negligible and the results obtained with the

single-scale SUSY theory are reliable. This is shown in fig. 3.9 where we compare the computation made resumming the logs of the split threshold, using an intermediate Split-SUSY EFT, with the one that does not resum the logs, which uses one scale only and just the SM RGE up to the scalar masses. The agreement between the two procedures is impressive. In the worst case ($\tan\beta = 1$, fermions at 200 GeV and scalars at 10^8 GeV) the mismatch is less than 1 GeV, well within the estimated uncertainties. It can also be seen that the two procedures start deviating exactly at that point. Indeed, had the SUSY scale and the splitting between fermions and scalars been bigger, the two computations would start deviating sensibly, fortunately that region is not relevant for $m_h = 125$ GeV.

We conclude that for all the relevant parameter space the computation of the Higgs mass can reliably be made using only the SM as EFT up to the scalar masses, independently of the scale of the fermions[1], whose main effect is well approximated by the one-loop thresholds at the SUSY scale.

3.3 The SusyHD code

The computation described in the previous sections has been implemented into a simple Mathematica [129] package, SusyHD (SUperSYmmetric Higgs mass Determination), which we made public [111]. The package provides two main functions that compute the Higgs mass and its theoretical uncertainties[2] from the input soft parameters, and an auxiliary function to change the SM parameters (m_t and α_s).

The most time consuming part of the EFT calculation is the integration of the RGE. The code avoids such step by using an interpolating formula for the solution of the RGE, which is only function of the amount of running $\log(Q/m_t)$ and the value of the Higgs quartic coupling at the high scale $\lambda(Q)$, set by the SUSY threshold corrections, eq. (3.3). The interpolating formula only depends on the SM parameters, so the RGE integration needs to be run only once, when the package is first called or if the SM parameters are changed. The result is a very fast code which allows to effectively use the observed value of the Higgs mass as a constraint for the SUSY parameter space. All plots of this chapter have been generated with SusyHD.

[1] The usual caveat from $v/m_{\rm SUSY}$ corrections applies when the fermions are very close to the EW scale. In this case the full contributions from the SM+fermion states [127, 128] should be used in the matching at the low scale.

[2] The latest version of SusyHD also estimates the experimental uncertainty by considering the uncertainty in the value of the top mass, which is the dominant source.

The input SUSY parameters can be given in either $\overline{\text{DR}}$ or OS schemes and thanks to the EFT approach they can be arbitrary heavy. The code also accepts simplified input where not all the SUSY parameters needs to be specified. There are also extra options which allow: 1) to switch off independently some of the higher order corrections, 2) to change the matching scale Q, 3) to use the full numerical code, which integrates the RGE numerically and 4) to use the Split SUSY code which integrates the RGE in two steps: SM up to the fermion scale and Split-SUSY up to the scalars. The function that computes the theoretical uncertainties accepts also the option to compute the individual uncertainties coming from the SM corrections, the SUSY thresholds, and the EFT approximation.

All the necessary documentation can be downloaded with the code from [111].

3.4 Recent improvements

We present recent progress in the EFT calculation of the Higgs mass, which allows to further reduce the theoretical uncertainty and clarifies the regime of validity of the EFT computation.

3.4.1 NNNLO SM strong corrections

For most of the relevant parameter space, particularly for stops above ~ 1 TeV, the uncertainty in the EFT Higgs mass calculation is dominated by the SM part. It is associated to higher order corrections in the matching of the SM couplings at the EW scale and their RG evolution. Due to the high sensitivity of m_h to the top Yukawa coupling y_t, QCD corrections to the determination of the value of y_t in the $\overline{\text{MS}}$ scheme at the EW scale from the pole mass have a sizable effect.

The perturbative QCD expansion of the relation between the top quark mass defined in the on-shell and $\overline{\text{MS}}$ schemes converges slowly [119]

$$m_t^{\overline{\text{MS}}} = (173.34 - 8.00 - 1.90 - 0.59 - 0.21)\ \text{GeV}, \tag{3.16}$$

where the first term correspond to the tree level and the next terms are the subsequent loop corrections. In fact, the 3-loop contribution is around one third of the 2-loop one and shift the top mass by ~ 0.6 GeV. This implies a variation in the Higgs mass of around half a GeV. Since the VEV of the Higgs field does not receive pure strong corrections we do not need to distinguish between different renormalization schemes for its input. As a consequence, the strong contributions to the matching of y_t have the same form as those of $m_t^{\overline{\text{MS}}}$ and loop corrections in the perturbative expansion are not so suppressed.

One may wonder whether other strong corrections to the matching at the weak scale and the running from the high SUSY scale have similar effects to those due to the determination of y_t. We address this query by including the SM NNNLO corrections in the strong coupling. This task requires three loop thresholds and the four loop RGE of the quartic, the top Yukawa and the strong gauge couplings. This is collected in table 3.2, together with the corresponding references.

The four loop contribution, leading in the strong coupling, to the beta functions of the strong coupling $\beta_{g_s}^{(\alpha_s^4)}$ is known since some time ago [115, 116]. The corrections proportional to the top Yukawa and Higgs quartic have also been computed recently [130, 131]; although they are subleading with respect to $\beta_{g_s}^{(\alpha_s^4)}$, especially those terms involving the quartic coupling. The (numerical) expression for the pure QCD corrections is given by [115, 116] (see also eg. [93])

$$\frac{dg_3^2}{d\ln Q^2} \supset \frac{g_3^{10}}{(4\pi)^8}\,(-2472.28)\,. \tag{3.17}$$

While the leading QCD correction to the running of the top Yukawa $\beta_{y_t}^{(\alpha_t\alpha_s^3)}$ can be read form the running of the top mass, since the β-function of the vev does not receive strong corrections at leading order. Analytical formulas are available in [132, 133], also in eqs. (6) and (7) of ref. [134], or for a recent work see [135]. Numerically, they lead to

$$\frac{dy_t^2}{d\ln Q^2} \supset \frac{1}{(4\pi)^8} y_t^2 g_3^8(-13078.)\,. \tag{3.18}$$

Recently, the four loop correction to the running of the quartic coupling was obtained as an application of the four-loop effective potential in eq. (5.1) of [136] (see also [135])

$$\frac{d\lambda}{d\ln Q^2} \supset \frac{1}{(4\pi)^8} y_t^4 g_3^6(33232.). \tag{3.19}$$

The top Yukawa and the quartic couplings are extracted from the on-shell masses of the top quark and Higgs boson respectively. Therefore we need these matching relations. A different situation takes place for the running strong coupling constant, which is directly measured in experiments.

The $\mathcal{O}(\alpha_s^3)$ correction to the relation between the $\overline{\text{MS}}$ and OS top mass were computed in [114, 137, 138]. They have been already used in Buttazzo et. al. [93] for their numerical formula and applied to the vacuum stability of the SM. Recently also the $\mathcal{O}(\alpha_s^4)$ was computed [119], which is of order of Λ_{QCD}, i.e. of the same order of the expected non-perturbative effects.

Extracting the Higgs quartic coupling from the pole mass requires the self-energy evaluated at external momentum equal to the mass. However a three

Coupling	λ	y_t	g_s
RGE	$\mathcal{O}(\alpha_t\alpha_s^3)$ [136]	$\mathcal{O}(\alpha_t\alpha_s^3)$ [132, 133]	$\mathcal{O}(\alpha_s^4)$ [115, 116]
Thresholds	$\mathcal{O}(\alpha_t\alpha_s^2)$ [93]	$\mathcal{O}(\alpha_t\alpha_s^2)$ [114, 137, 138]	

Table 3.2: Four-loop RGE and three-loop threshold corrections in the Standard Model, leading in the strong coupling, needed for EFT calculation of the Higgs mass at NNNLO.

loop computation of the two point function at non-zero external momentum is a very hard task. The three-loop SM effective potential at leading order in strong and top Yukawa coupling was calculated in [139], which allows to obtain the contribution to λ at zero external momentum. In a later work they also obtained the 4-loop corrections leading in the strong coupling [136].

We want to write λ in terms of OS masses (as in [93])

$$\lambda = \frac{G_\mu}{\sqrt{2}} m_h^2 + \Delta\lambda^{(1)} + \Delta\lambda^{(2)} + \Delta\lambda^{(3)}_{\alpha_t\alpha_s^2}\,, \tag{3.20}$$

different from the approach in ref. [140] where it was expressed in terms of $\overline{\text{MS}}$ couplings. The term $\Delta\lambda^{(3)}_{\alpha_t\alpha_s^2}$ gets corrections from the effective potential and from the renormalization of the top mass in the 1-loop and 2-loop corrections

$$\Delta\lambda^{(3)}_{\alpha_t\alpha_s^2} = \frac{1}{2}\frac{\partial^4 V^{\alpha_t\alpha_s^2}}{\partial^2 H^\dagger \partial^2 H} + \Delta\lambda^{(3,\text{shift})}_{\alpha_t\alpha_s^2}. \tag{3.21}$$

We find for the 3-loop pure QCD correction in the approximation $m_h \ll m_t$

$$\begin{aligned}\Delta\lambda^{(3)}_{\alpha_t\alpha_s^2} = &-\frac{16 g_3^4 G_F^2 M_t}{135(4\pi)^6}\Bigg[-2415 + 720\pi^2 + 176\pi^4 + 1440\pi^2\ln 2 + 960\pi^2\ln^2 2 \\ &- 960\ln^4 2 - 23040\text{Li}_4\left(\frac{1}{2}\right) + 8640\zeta(3) + 22680\ln^3\frac{M_t^2}{Q^2} - 50220\ln^2\frac{M_t^2}{Q^2} \\ &+ 90\left(1327 + 16\pi^2 + 16\pi^2\ln 4 - 48\zeta(3)\right)\ln\frac{M_t^2}{Q^2}\Bigg],\end{aligned} \tag{3.22}$$

where $\text{Li}_4(x)$ is the polylogarithm function. A similar expression was obtained in ref. [93] for $Q = M_t$.

We updated our estimate of the theoretical uncertainty of the MSSM Higgs mass calculation in fig. 3.10. We tried to estimate the uncertainty by varying the renormalization scale but there is an accidental cancellation between the matching

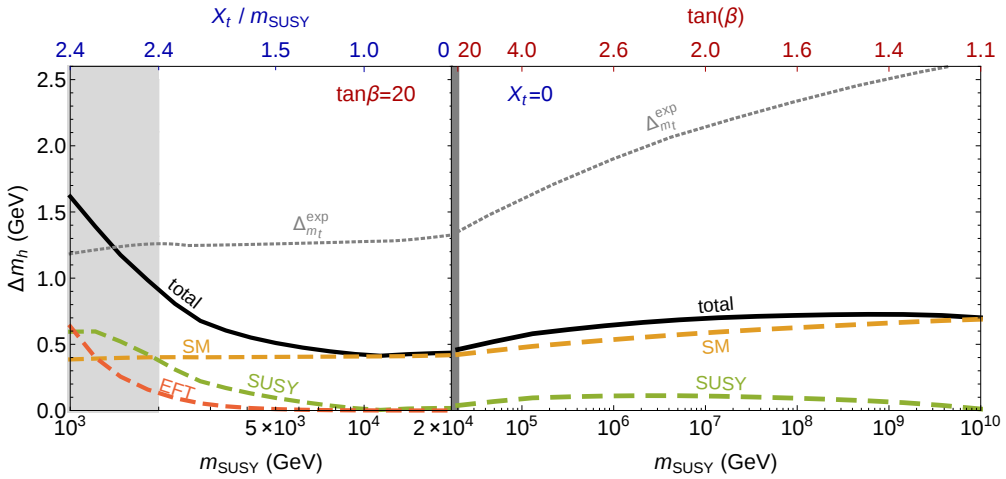

Figure 3.10: Reduction of the uncertainties of the Higgs mass calculation after the NNNLO SM corrections leading in the strong coupling are included. The meaning of the curves is the same as in fig. 3.2.

effects on y_t and λ, leading to a too optimistic estimate. For this reason, we used a similar estimate as before. We assign a theoretical uncertainty of 0.3 GeV to y_t and combine it with the uncertainty in the matching of the quartic coupling. Note that the SM uncertainty in m_h has been reduced to the range $0.3 \div 0.6$ GeV for $m_{\rm SUSY}$ between 10^3 GeV and 10^{10} GeV. The EFT calculation works remarkably well for heavy SUSY spectrum $\gtrsim 10$ TeV, where other sources of uncertainty are negligible. Although the effect of the added corrections in the value of the Higgs mass is tiny, we have now better control of our estimate of the SM uncertainty.

Implications for the SM vacuum stability

The condition of absolute stability of the SM vacuum up to the Planck scale is obtained by studying the RG improved full effective potential . The critical value of the Higgs field above which the potential becomes smaller than its value at the EW vacuum is known as the instability scale Λ_I. But Λ_I is not a physical quantity as it is gauge dependent. The SM absolute stability is highly disfavored [48, 93].

It is a very good approximation to trade the stability condition by the requirement $\lambda(\Lambda) \geq 0$ for any value Λ up to the Planck scale (see eg. [48]). For this reason, the evolution of the Higgs quartic coupling with the renormalization scale (fig. 3.11) gives an indication of the effect of including the leading QCD corrections to the 3-loop matching of λ and the 4-loop RGE on the vacuum stability

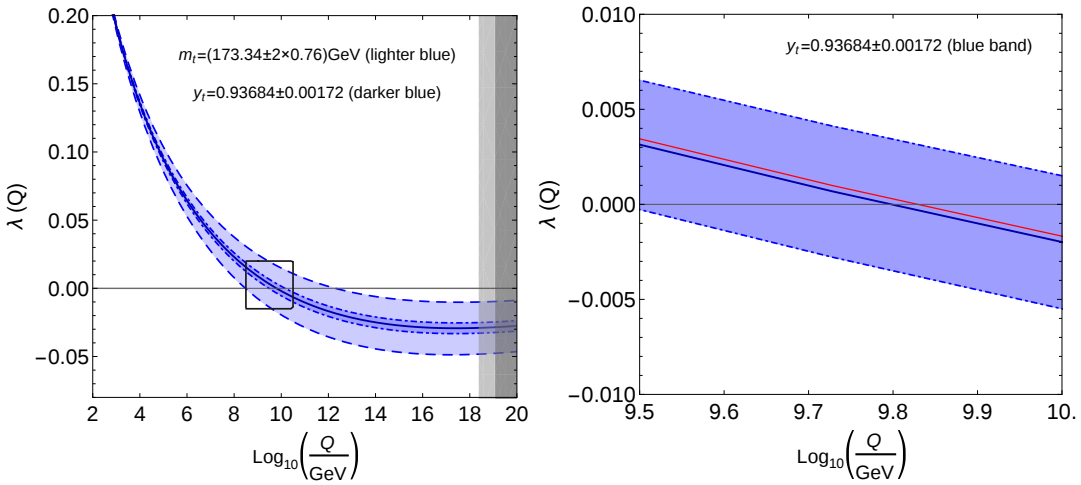

Figure 3.11: Evolution of the Higgs quartic coupling λ with the renormalization scale Q. The dark and light blue regions enclosed by the dashed and dot-dashed curves are obtained by varying the top mass by the 2σ experimental uncertainty or by considering the theoretical uncertainty in the top Yukawa respectively. The right plot zooms in the region where λ becomes negative and highlights the effect of including the leading QCD corrections in the matching of λ at three loops and in the 4-loop RGE (red line). Grey bands correspond to values of Q above the Planck mass $M_{\mathrm{Pl}} \approx 1.2 \times 10^{19}$ GeV and the reduced Planck mass $\overline{M}_{\mathrm{Pl}} = M_{\mathrm{Pl}}/\sqrt{8\pi}$.

condition. The right panel of fig. 3.11 shows the theoretical uncertainty around the region where λ becomes negative. The blue band represent the estimated theoretical uncertainty in the matching of the top Yukawa, while the red curve contains the (tiny) contributions of the newly included corrections in addition to those already contained by the blue curve.

We see that the theoretical uncertainty is clearly dominated by the matching of the top Yukawa[1]. Although the added leading NNNLO corrections have a tiny effect, we are now more confident of the uncertainty estimate. However, the experimental uncertainty in the top mass is the main limitation by far.

[1]For the theoretical uncertainty in the matching of the top Yukawa, we use a more conservative estimate than ref. [93]. That is because we tried to account for non-perturbative (unknown) QCD effects, but also because the four-loop QCD contributions are non small due to the slow convergence of the perturbative expansion.

3.4.2 Two-loop Yukawa corrections

We include the two-loop SUSY threshold corrections to the Higgs quartic coupling controlled by the third generation Yukawa couplings. More specifically, we obtain the $\mathcal{O}(\alpha_t^2)$ corrections for a generic SUSY spectrum, the $\mathcal{O}(\alpha_s\alpha_b, \alpha_b^2)$ and the mixed $\mathcal{O}(\alpha_t\alpha_b)$ terms important for large $\tan\beta$ and sizable μ term, and those from the sbottom sector $\mathcal{O}(\alpha_\tau^2, \alpha_b\alpha_\tau)$ for completeness (although they are subleading with respect to the sbottom contributions). The computation is quite long but straightforward. The analogous fixed-order corrections for the Higgs mass, obtained with the effective potential method, were discussed in [71, 79, 82–84, 105].

The two-loop SUSY thresholds are calculated by taking the fourth derivative of the corresponding two-loop MSSM effective potential V_{2l} as

$$\Delta\lambda_{2l} = \frac{1}{2}\frac{\partial^4 V_{2l}}{\partial^2 H^\dagger \partial^2 H}\bigg|_{H=0} + \Delta\lambda_{2l}^{(\text{shift})} + \Delta\lambda_{2l}^{(\text{WFR})}, \tag{3.23}$$

where $\Delta\lambda_{2l}^{(\text{shift})}$ is the shift contribution induced by writing the MSSM Yukawa couplings in the one-loop contributions to λ in terms of the corresponding SM coupling and $\Delta\lambda_{2l}^{(\text{WFR})}$ arises from the wave function renormalization of the Higgs field. A similar procedure for the $\mathcal{O}(\alpha_s\alpha_t)$ threshold corrections was explained in detail in [94]. It is convenient to trade the derivatives with respect to the Higgs field by the derivatives with respect to the Higgs-field-dependent quark masses m_q (with $q = t, b, \tau$).

It is important to notice that $\Delta\lambda_{2l}^{(\text{shift})}$ generically contains two contributions. One arises from expressing the MSSM Yukawa coupling in the one-loop SM contribution to λ from the quark box diagram in terms of the corresponding coupling of the low-energy theory. This two-loop expression contains terms proportional to $\ln(m_q^2/Q^2)$, which diverges in the limit of vanishing quark masses or equivalently $H \to 0$. In fact, this shift is essential to cancel the logarithmic dependence of the quark masses contained in the derivatives of V_{2l}, first term in eq. (3.23), which allows to have a meaningful $H \to 0$ limit. The other possible contribution to $\Delta\lambda_{2l}^{(\text{shift})}$ is due to expressing the MSSM Yukawa coupling in the one-loop contribution to λ from integrating out the sparticles in terms of the corresponding SM coupling. But, since it does not contain logarithmically-divergent terms, the definition of the coupling entering the sparticle contributions is a matter of choice.

As expected, the general result of the $\mathcal{O}(\alpha_t^2)$ correction to λ agrees with the approximate expression for the simplified case of degenerate scalars obtained from the corresponding correction to the Higgs mass in section 3.1.1. In fig. 3.12,

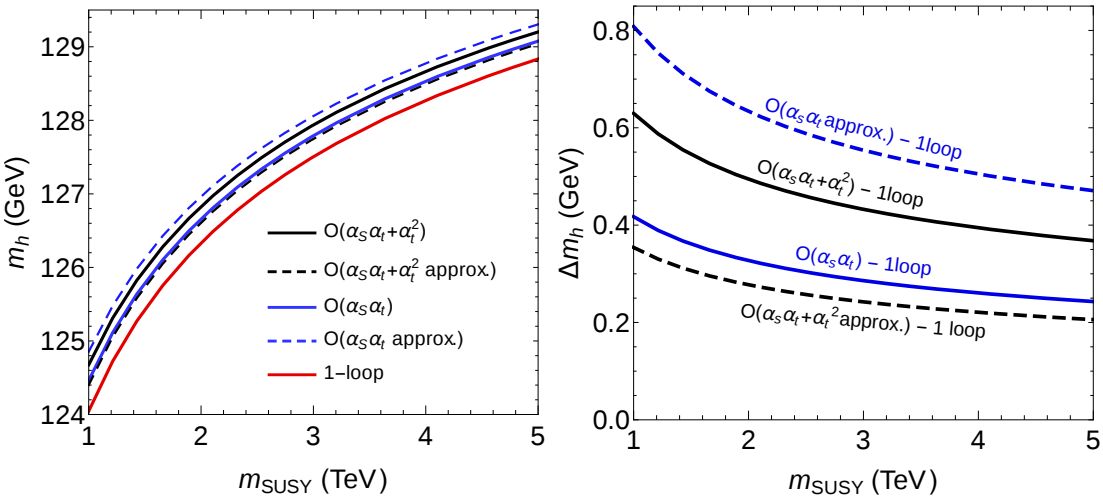

Figure 3.12: Effect of the general two-loop top Yukawa corrections, compared with the approximate expressions for degenerate scalars. We consider all masses degenerate equal to $m_{\rm SUSY} = 1$ TeV, except $m_{Q_3} = 3m_{\rm SUSY}$, maximal stop mixing $X_t = (6m_{Q_3}m_{U_3})^{1/2}$, $\tan\beta = 20$, $A_b = A_t$, $\mu = 4m_{\rm SUSY}$. For the the approximate $\mathcal{O}(\alpha_s\alpha_t)$ and $\mathcal{O}(\alpha_t^2)$ corrections we take scalar masses degenerate and equal to the average $(m_{Q_3}m_{U_3})^{1/2}$. The right plot shows the shift in m_h with respect to the 1-loop result to improve readability.

we compare the general $\mathcal{O}(\alpha_t^2)$ and $\mathcal{O}(\alpha_s\alpha_t)$ results with the approximate ones, for which we take the scalar masses equal to the (geometric) average stop mass $\sqrt{m_{Q_3}m_{U_3}}$. We used the following values of the parameters for the plot: all masses degenerate equal to $m_{\rm SUSY} = 1$ TeV, except $m_{Q_3} = 3m_{\rm SUSY}$, maximal stop mixing $X_t = (6m_{Q_3}m_{U_3})^{1/2}$, $\tan\beta = 20$, $A_b = A_t$, and $\mu = 4m_{\rm SUSY}$. The difference between solid and dashed lines of the same color is the error in using the approximate expression with degenerate scalars. The approximate $\mathcal{O}(\alpha_s\alpha_t)$ expression gives roughly twice the value of the exact one for $m_{Q_3} = 3m_{U_3}$, and even more for larger splitting. The simplified $\mathcal{O}(\alpha_t^2)$ formula deviates for large values of the μ parameter, for $\mu = 4m_{\rm SUSY}$ it has opposite sign with respect to the exact result and their difference is about 0.3 GeV. The different between the solid black and blue curves is the effect of including the $\mathcal{O}(\alpha_t^2)$ terms.

It is well-known that the bottom (and tau) Yukawa couplings of the MSSM can receive large SUSY threshold corrections at large values of $\tan\beta$ and μ. In fig. 3.13, it is shown the MSSM bottom Yukawa coupling as a function of μ for $\tan\beta = 40$ and maximal mixing, and as a function of $\tan\beta$ for $\mu = -1$ TeV. The other parameters are fixed as $m_{Q_3} = m_{D_3} = M_3 = m_{\rm SUSY} = 1$ TeV and

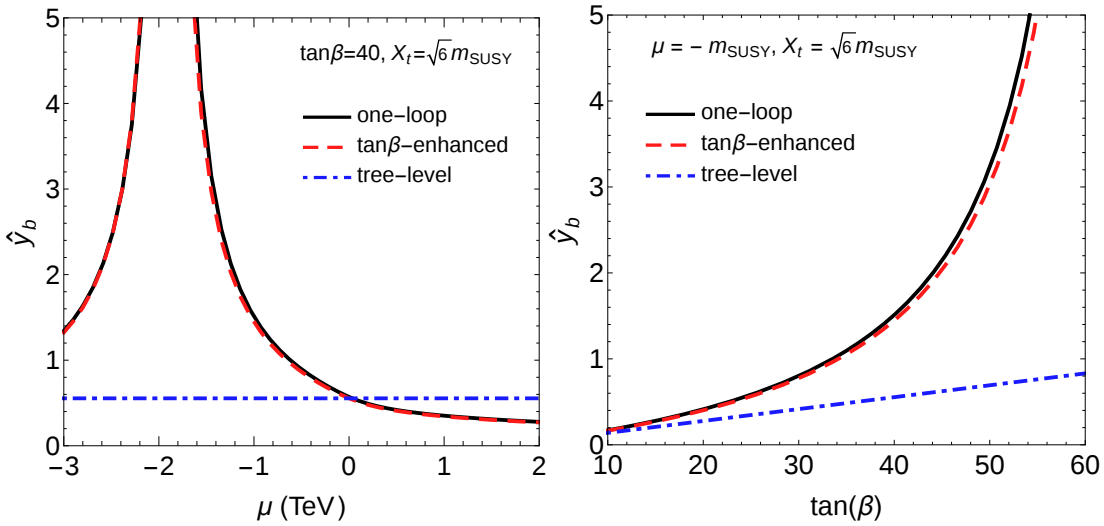

Figure 3.13: SUSY threshold corrections to the MSSM bottom Yukawa coupling $\hat{y}_b$. It shows the dependence on μ for $\tan\beta = 40$ and maximal mixing (left) and the dependence on $\tan\beta$ for $\mu = -1$ TeV (right). We also set $m_{Q_3} = m_{D_3} = M_3 = m_{\text{SUSY}} = 1$ TeV and $A_b = A_t$.

$A_b = A_t$. The curves represent the results including the full one-loop SUSY thresholds (black), only the $\tan\beta$-enhanced thresholds (red dashed) and the tree-level expression (blue dot-dashed). We see that the $\tan\beta$-enhanced corrections are clearly the dominant ones and can considerably increase $\hat{y}_b$. When the one-loop SUSY thresholds to λ from the sbottom sector is expressed in terms of the MSSM bottom Yukawa couplings the potentially large $\tan\beta$-enhanced corrections $\mathcal{O}(\alpha_b\alpha_s^n \tan^n\beta + \alpha_b\alpha_t^n \tan^n\beta)$ are automatically resummed.

When including the two-loop corrections from the sbottom and stau sectors one has to be careful of not re-introducing unphysically large $\tan\beta$-enhanced thresholds associated to the matching of the corresponding Yukawa couplings. While the pure $\mathcal{O}(\alpha_b^2)$ and $\mathcal{O}(\alpha_\tau^2)$ corrections can be obtained from the $\mathcal{O}(\alpha_t^2)$ expression by doing the appropriate replacements [84], the mixed $\mathcal{O}(\alpha_t\alpha_b)$ and $\mathcal{O}(\alpha_b\alpha_\tau)$ terms require a computation. The relevant formulas for the $\mathcal{O}(\alpha_t\alpha_b)$ and $\mathcal{O}(\alpha_b\alpha_\tau)$ terms of the effective potential are given in appendix D[1] of ref. [79] and appendix B of ref. [105] respectively.

In fig. 3.14 we plot the Higgs mass as a function on $\tan\beta$ to illustrate the effect of the two-loop SUSY thresholds controlled by the bottom Yukawa coupling. We

[1]The expression for the two-loop top and bottom Yukawa potential in eq. (D.6) of the arxiv version of ref. [79] has a typo: the penultimate line should have an overall minus sign.

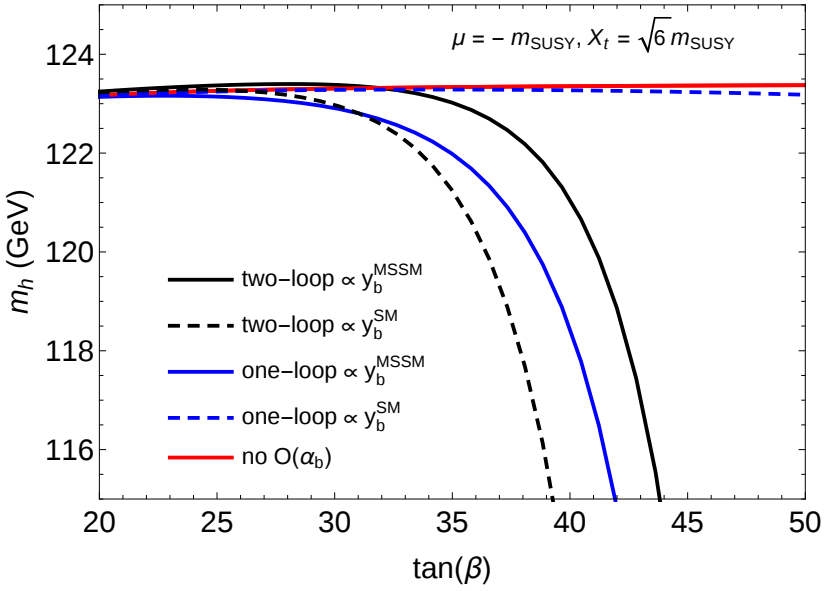

Figure 3.14: Impact of SUSY threshold corrections proportional to the bottom Yukawa coupling at large $\tan\beta$. We used a degenerate spectrum with masses $m_{\rm SUSY} = 1$ TeV, negative sign of μ, maximal stop mixing $X_t = \sqrt{6} m_{\rm SUSY}$ and $A_b = A_t$. We consider two different choices for writing the bottom Yukawa coupling entering the corrections from the sbottom sector as: the SM coupling (dashed lines) and the MSSM coupling (solid lines).

use the freedom in the definition of the bottom Yukawa coupling entering in the threshold corrections from the sbottom sector, showing two choices: the MSSM (solid lines) and the SM (dashed lines) bottom Yukawa couplings. The red line represents the Higgs mass result neglecting all the bottom Yukawa corrections, while the blue and black curves include one-loop $\mathcal{O}(\alpha_b)$ and additionally the two-loop $\mathcal{O}(\alpha_b\alpha_s + \alpha_b\alpha_t + \alpha_b^2)$ respectively. When written in term of the SM Yukawa, we see that the two-loop corrections are anomalously large. On the other hand, using the MSSM Yukawa for the sbottom corrections is a very convienent choice.

The EFT calculation of m_h now incorporates the complete two-loop Yukawa thresholds at the SUSY scale. The effect of the tau Yukawa is not shown in fig. 3.14 because it is subleading. Since in the gaugeless limit there are no $\tan\beta$-enhanced terms in the matching of $\hat{y}_\tau$, we do not have to worry about the definition of the tau Yukawa coupling in the two-loop corrections at this order. Finally, note that unlike the case when the two-loop corrections are expressed in terms of the SM bottom Yukawa coupling, when using the MSSM coupling there are mixed two-loop corrections to the quartic coupling proportional to $\hat{g}_b^4 g_\tau^2$ arising

from Higgs WFR which are not canceled by shift contributions.

3.4.3 Effect of higher dimensional operators

In this section we consider the leading contributions to m_h induced by the dimension-six operators of the SM EFT[1]. The most sizable corrections are expected to come from the stop sector because of the maximal mixing enhancement. In first approximation, we focus on the corrections proportional to g_3 and y_t that can be potentially enhanced by the stop mixing, neglecting those proportional to λ and the electroweak gauge couplings (gaugeless limit). However, the EW gauge couplings appear at tree-level in the matching of λ at the SUSY scale. As a consequence, the effect of dimension-six operators in the matching of the g_1 and g_2 at the EW scale may be comparable, thus we also estimate it. For simplicity we assume degenerate soft masses $m_{\tilde{t}}$. Still our discussion can be easily extended for generic masses and to include other corrections.

Using the Standard Model as a renormalizable effective field theory, one neglects corrections suppressed by the ratio of the electroweak scale over the new physics (SUSY) scale, of $\mathcal{O}(m_t^2/m_{\rm SUSY}^2)$. The effect of these corrections on the Higgs mass calculation for a light SUSY spectrum (for stops around the TeV scale) might or might not be negligible, and has aroused debate in the community. We include the dimension-six operators of the SM EFT important for the Higgs mass calculation, generated by matching with the SUSY theory. This computation should clarify the regime of validity of the EFT approach. Moreover these operators can contribute to other observables, which may represent additional constraints on the model.

The Lagrangian of the SM EFT is given by

$$\mathcal{L}_{\text{SM-EFT}} = \mathcal{L}_{\text{SM}} + \sum_i c_i \mathcal{O}_i \,, \tag{3.24}$$

where $\mathcal{L}_{\text{SM}}$ is the renormalizable SM Lagrangian, $\mathcal{O}_i$ are the dimension-six operators and, c_i their associated Wilson coefficients.

The use of the EFT framework to study phenomenological consequences of BSM models at low energy is carried out in three steps. The first one consists of matching the BSM model onto the SM EFT at high scale, set by the mass of the heavy particles being integrated out. Then, the Wilson coefficient are evolved down to the weak scale using the RGE of the SM EFT. Finally, the effective Lagrangian at low energy is used to compute physical observables, which will depend on the Wilson coefficients. For a comprehensive review see ref. [141].

[1]This is a work in progress in collaboration with Emanuele Bagnaschi and Pietro Slavich.

$\mathcal{O}_{GG}$	$=$	$g_s^2\lvert H\rvert^2 G^a_{\mu\nu}G^{a,\mu\nu}$	$\mathcal{O}_H$	$=$	$\frac{1}{2}\big(\partial_\mu\lvert H\rvert^2\big)^2$
$\mathcal{O}_{WW}$	$=$	$g^2\lvert H\rvert^2 W^a_{\mu\nu}W^{a,\mu\nu}$	$\mathcal{O}_T$	$=$	$\frac{1}{2}\big(H^\dagger \overleftrightarrow{D^\mu} H\big)^2$
$\mathcal{O}_{BB}$	$=$	$g'^2\lvert H\rvert^2 B_{\mu\nu}B^{\mu\nu}$	$\mathcal{O}_R$	$=$	$\lvert H\rvert^2\lvert D_\mu H\rvert^2$
$\mathcal{O}_{WB}$	$=$	$2gg' H^\dagger t^a H W^a_{\mu\nu}B^{\mu\nu}$	$\mathcal{O}_D$	$=$	$\lvert D^2 H\rvert^2$
$\mathcal{O}_W$	$=$	$ig\big(H^\dagger t^a \overleftrightarrow{D^\mu} H\big)D^\nu W^a_{\mu\nu}$	$\mathcal{O}_6$	$=$	$\lvert H\rvert^6$
$\mathcal{O}_B$	$=$	$ig'Y_H\big(H^\dagger \overleftrightarrow{D^\mu} H\big)\partial^\nu B_{\mu\nu}$	$\mathcal{O}_{2G}$	$=$	$-\frac{1}{2}\big(D^\mu G^a_{\mu\nu}\big)^2$
$\mathcal{O}_{3G}$	$=$	$\frac{1}{3!}g_s f^{abc}G^{a\mu}_\rho G^{b\nu}_\mu G^{c\rho}_\nu$	$\mathcal{O}_{2W}$	$=$	$-\frac{1}{2}\big(D^\mu W^a_{\mu\nu}\big)^2$
$\mathcal{O}_{3W}$	$=$	$\frac{1}{3!}g\varepsilon^{abc}W^{a\mu}_\rho W^{b\nu}_\mu W^{c\rho}_\nu$	$\mathcal{O}_{2B}$	$=$	$-\frac{1}{2}\big(\partial^\mu B_{\mu\nu}\big)^2$
			$\mathcal{O}_t$	$=$	$y_t\lvert H\rvert^2\,\overline{q}_L H t_R$

Table 3.3: Dimension-six CP-even bosonic operators and the operator $\mathcal{O}_t$ which contributes to the top Yukawa matching. They are potentially relevant for the Higgs mass calculation.

In order to match the SUSY theory onto the SM EFT it is convenient to use the so-called covariant derivative expansion (CDE) [142, 143]. The CDE is a method for computing the one-loop effective action in a manifestly gauge-invariant way. Using this technique, ref. [144] obtained the one-loop contribution from integrating out the stops with degenerate soft masses to the Wilson coefficients of the CP-conserving dimension-six bosonic operators in table 3.3. The general expressions in the non-degenerate case for the subset of operators involving the Higgs field are given in [145, 146].

Since the RGE evolution of the Wilson coefficients [147–153] from the UV scale to the low scale introduces an additional loop factor, we can safely neglect this effect in our analysis at leading order. The logarithmic factor is never large enough to compensate the loop factor because the heavy particles decouple power-like with their masses, i.e. as v^2/m^2_{SUSY}. Typically, the RGE running is only important when some of the c_i are generated at tree level [141]. We are interested in the leading effect on the Higgs mass calculation induced by the SM dimension-six operators. Therefore, for our purposes it is enough to consider the Wilson coefficients at one-loop order.

Precision observables at the EW scale constraint the Wilson coefficients. Higgs production through gluon fusion represent the strongest constraint on operators

of the Higgs sector (see eg. [144]). Higgs decay into two photons, as well as electroweak precision observables such as the S and T parameters are also important (see [141] and references therein). Here we focus on the contribution of the Wilson coefficients to the Higgs mass.

The Wilson coefficient c_6 have been computed in several references [144–146, 154]. By deriving the effective potential we also obtained the following expression arising from integrating out the stops

$$c_6 = -\frac{y_t^6}{32\pi^2}\frac{1}{m_{\tilde{t}}^2}\left(2 - 3\hat{X}_t^2 + \hat{X}_t^4 - \frac{1}{10}\hat{X}_t^6\right) + \dots\,, \tag{3.25}$$

where the ellipsis represents the one-loop EW and higher order terms. One also requires the coefficient c_t, which receives stop-gluino and stop-higgsino one-loop contributions. We notice that c_t can be obtained from the top quark self-energy

$$c_t = \frac{g_3^2 y_t^2}{144\pi^2}\frac{1}{m_{\tilde{t}}^2}\left(-6 - 6\hat{X}_t + 3\hat{X}_t^2 + 2\hat{X}_t^3\right) + \frac{y_t^4}{384\pi^2}\frac{1}{\sin^2\beta}\frac{1}{m_{\tilde{t}}^2}\left(-5 + 3\hat{X}_t^2\right) + \dots\,, \tag{3.26}$$

where we assumed $M_3 = \mu = m_{Q_3} = m_{U_3} = m_{\tilde{t}}$. The expressions for the other Wilson coefficients can be found in [144–146].

We now consider the impact of the Wilson coefficients on the physical Higgs mass. Note that the Higgs potential contains the operator $\mathcal{O}_6$. Therefore this operator produces corrections to the Higgs tadpole and self-energy. Additionally, we also need the contribution of the Wilson coefficients to the self-energy of the top quark, the Z-boson and the W-boson which modify the matching of the top Yukawa, the electroweak gauge couplings and the relation between the VEV and the Fermi constant.

Including the dimension-six operators the potential of the Higgs doublet H is given by

$$V = -m^2|H|^2 + \frac{\lambda}{2}|H|^4 - c_6|H|^6. \tag{3.27}$$

The vacuum minimization condition imply

$$m^2 = \frac{\lambda v^2}{2} - \frac{3}{4}\,c_6\,v^4, \tag{3.28}$$

where v is the minimum of the potential in eq. (3.27). The condition (3.28) guarantees the absence of a linear term of the physical Higgs field h. As in refs. [48, 93], we identify the renormalized vacuum with the minimum of the radiatively corrected potential, including in addition the dimension-six operators.

The relation between the Higgs pole mass and the quartic coupling at one-loop order can be written as [48, 93, 155]

$$m_h^2 = \lambda v_{\rm OS}^2 + \Delta m_h^{2,(\lambda)}\,, \tag{3.29}$$

$$\Delta m_h^{2,(\lambda)} = \mathrm{Re}\,\Pi_{hh}(m_h^2) + \frac{T}{v_{\rm OS}} + m_h^2\,\Delta r_0. \tag{3.30}$$

Here we have used a similar notation as in [93]: $v_{\rm OS} = (\sqrt{2}G_\mu)^{-1/2}$ with G_μ being the Fermi constant, $\Pi_{hh}(p^2)$ is the Higgs self-energy, iT represents the sum of the tadpole diagrams, and Δr_0 relates the bare VEV v_0 and the Fermi constant as $v_0^2 = v_{\rm OS}^2(1+\Delta r_0)$. At leading order, in eq. (3.30) there are no tadpole contributions from the dimension-six operators, while the last term is generically suppressed by the Higgs mass (or the quartic coupling). The contributions of dimension-six operators to the self-energies, including $\Pi_{hh}(p^2)$, are given in appendix A.3.

On the other hand, the top Yukawa coupling and the electroweak gauge couplings are extracted from the on-shell masses of the top quark and the gauge bosons respectively. We need to obtain the corrections to these relations. The terms of the SM effective Lagrangian involving both the Higgs field and the top quark are

$$\mathcal{L}_{\rm SM-EFT} \supset -y_t \bar{q}_L H t_R + c_t\, y_t |H|^2 \bar{q}_L H t_R. \tag{3.31}$$

The second term in eq. (3.31) affects the top quark self-energy (see appendix A.3) and in consequence the top Yukawa matching, which at one-loop reads

$$y_t = \frac{\sqrt{2}\,m_t}{v_{\rm OS}} + \delta y_t\,, \tag{3.32}$$

$$\delta y_t = \frac{\sqrt{2}\,m_t}{v_{\rm OS}}\left(-\frac{\Sigma_t(m_t)}{m_t} + \frac{\Delta r_0}{2}\right). \tag{3.33}$$

Since the value of the top Yukawa coupling is not measured experimentally but extracted from the top mass, the dimension-six operators affect the input value of y_t we use throughout all the EFT calculation. We refer to the corrections to the Higgs mass produced indirectly by the effect of c_i in the matching of the top Yukawa at low energy as *indirect corrections* and are denoted as $\Delta m_h^{2,(y_t)}$, to distinguish them from the (direct) corrections to the matching of m_h and λ in eq. (3.30) arising from diagrams involving one c_i vertex. Although the indirect corrections to m_h from the matching of the top Yukawa appear formally at two-loop order through the one-loop $\mathcal{O}(y_t^4)$ corrections to m_h^2, they are numerically of leading order because they are enhanced by the parameters of the stop sector. In fact, the loop counting of the corrections to the Higgs mass might lead to confusion

since the one-loop contributions from the stop sector at maximal mixing are larger than the tree-level one.

We can approximate this indirect corrections by

$$\Delta m_h^{2,(y_t)} = \frac{\delta y_t}{y_t}\left(4\, m_h^{2,(\alpha_t)}\right), \tag{3.34}$$

where $m_h^{2,(\alpha_t)}$ are the one-loop $\mathcal{O}(y_t^4)$ terms

$$m_h^{2,(\alpha_t)} = \frac{6y_t^4 v^2}{(4\pi)^2}\left(\hat{X}_t^2 - \frac{\hat{X}_t^4}{12} + \ln\frac{m_{\tilde{t}}^2}{m_t^2}\right). \tag{3.35}$$

From eqs. (3.34) and (3.35) we see that at maximal mixing $\Delta m_h^{2,(y_t)} \sim (\delta y_t/y_t) v_{\rm OS}^2$, i.e. $\Delta m_h^{2,(y_t)}$ is numerically of leading order. For example, we compared the indirect corrections from $\mathcal{O}_t$ with the one-loop contribution involving one c_t vertex to the matching of m_h in eq. (3.30), and the latter is generically one order of magnitude smaller at maximal mixing.

Analogously for the gauge couplings

$$\begin{aligned} g' &= \frac{2\sqrt{m_Z^2 - m_W^2}}{v_{\rm OS}} + \delta g', \;\; \delta g' = \frac{2\sqrt{m_Z^2 - m_W^2}}{v_{\rm OS}}\left(-\frac{\Pi_{ZZ}(m_Z^2) - \Pi_{WW}(m_W^2)}{m_Z^2 - m_W^2} + \Delta r_0\right), \\ g &= \frac{2m_W}{v_{\rm OS}} + \delta g, \qquad \delta g = \frac{2m_W}{v_{\rm OS}}\left(-\frac{\Pi_{WW}(m_Z^2)}{m_W^2} + \Delta r_0\right), \end{aligned} \tag{3.36}$$

with terms proportional to the Wilson coefficients contained in δg and $\delta g'$, influencing the matching of the EW gauge couplings. From the tree-level term in $\lambda(m_{\rm SUSY})$, the operators entering the matching of g and g' will induce (indirect) corrections to the Higgs mass $\Delta m_h^{2,(g,g')}$. We can approximate $\Delta m_h^{2,(g,g')}$ by the expression

$$\Delta m_h^{2,(g,g')} = m_Z^2\left(2g\delta g + 2g'\delta g'\right). \tag{3.37}$$

Finally, the total contribution to the Higgs mass from the dimension-six operators is the sum of the corrections to the matching of the Higgs mass, as well as the induced effects from the matching of the gauge and top Yukawa couplings

$$\Delta m_h^2 = \Delta m_h^{2,(\lambda)} + \Delta m_h^{2,(g_1,g_2)} + \Delta m_h^{2,(y_t)}. \tag{3.38}$$

In fig. 3.15 we show the shift in the Higgs induced by the operators $\mathcal{O}_6$ and $\mathcal{O}_t$ at leading order for maximal stop mixing. For the plot we considered only the corrections to c_6 and c_t proportional to g_3 and y_t. We see that there is an accidental cancellation between the effects of $\mathcal{O}_6$ and $\mathcal{O}_t$, making the combined

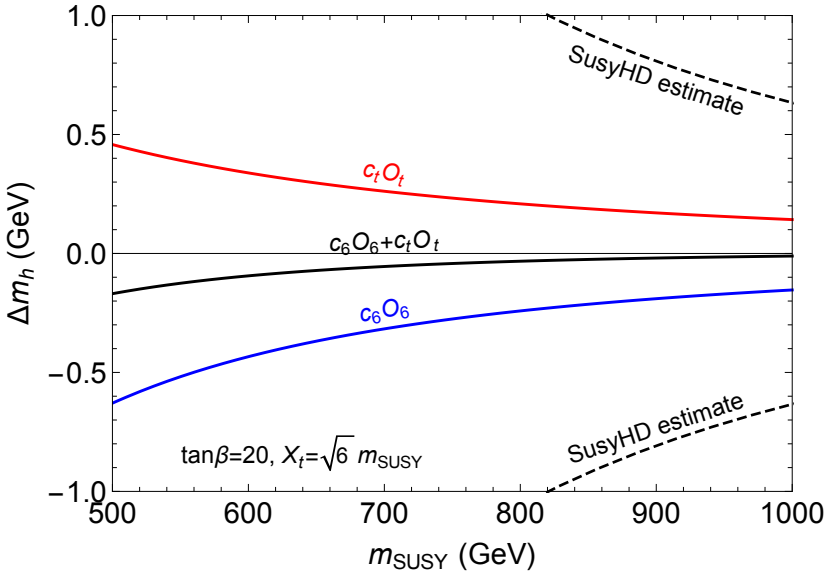

Figure 3.15: Shift in the Higgs mass induced by the operators $\mathcal{O}_6$ and $\mathcal{O}_t$ of the SM EFT at leading order in the couplings g_3 and y_t. The black-dashed line represents the estimate of the EFT theoretical uncertainty of SusyHD. We considered degenerate soft masses $m_{\rm SUSY}$, $\tan\beta = 20$ and maximal stop mixing.

effect very small (black-solid line). We also see that the uncertainty estimate of SusyHD is a fair assessment.

We also evaluate the effect in the Higgs mass of the one-loop EW corrections to the matching of c_6 and c_t, as well as the impact of other dimension-six operators. These contributions to the Higgs mass are proportional to g, g' or λ and are generically smaller than the ones induced by $\mathcal{O}_6$ or $\mathcal{O}_t$ at leading order in g_3 and y_t. In general, we expect the total $\mathcal{O}(v^2/m^2_{\rm SUSY})$ contribution to the Higgs mass behave roughly as

$$\Delta m_h \sim \text{few } 0.1 \text{ GeV} \left(\frac{\text{TeV}}{m_{\tilde{t}}}\right)^2 , \tag{3.39}$$

which guarantees very precise EFT results for stops around the TeV scale.

3.5 Phenomenological Applications

3.5.1 Predicting the spectrum of Minimal Gauge Mediation

Gauge mediated supersymmetry breaking (GMSB) [39, 156–162] is among the simplest and most elegant calculable mechanisms for generating the MSSM soft terms. A very special property is the absence of dangerous FCNC, a very rare property in extensions of the SM Higgs sector, supersymmetric and non.

However, using GMSB to implement a natural solution of the hierarchy problem has always been hard. The main obstruction being the μ problem, *viz.* why the supersymmetric higgsino mass happens to be at the same scale of the SUSY-breaking soft terms. Solutions of the μ problem generically produce a μ/B_μ problem [38]: both μ and B_μ are generated radiatively at the same order in perturbation theory, which produces an unwanted hierarchy, $B_\mu \gg \mu^2$. Solutions to the μ/B_μ problem exist (see e.g. [38–40] and references therein) but at the cost of an excessive model building.

All these problems arise when we try to obtain a natural SUSY spectrum—it is like we are forcing the theory to do something it was not meant to. In line with what discussed in the introduction, we are then going to relax this requirement and try to use experiments instead of naturalness to infer the properties of new physics.

The apparent gap between the EW and the new physics scale motivates us to revisit the simplest and more elegant GMSB model, minimal gauge mediation (MGM)[1], without the unnecessary baroque model building associated to the Higgs sector. Indeed, ignoring the naturalness problem allows us to also ignore the μ-problem, as the two are closely related. When μ is much larger than the soft masses EWSB is not possible, when μ is much smaller, the EW scale v would be of order the soft masses. Therefore if the SUSY scale is above v, μ must automatically be close to the SUSY scale in order for EWSB to be tuned to its experimental value.

In MGM all soft masses are generated with the same order of magnitude by the gauge mediated contribution, one gauge loop below the scale $\Lambda = F/M$ (the ratio between the effective scale of SUSY breaking F and the mass of the messengers). Besides Λ, the spectrum also depends, in a milder way, on the actual mass of the messengers M, which determines the amount of running of the soft parameters,

[1]Here by MGM we really mean the most minimal realization, where the Higgs sector only receives the standard gauge mediated contribution, μ is a free parameter and B_μ is generated radiatively in the IR.

and the number of messengers N (typically $N = 1$ or 3 for a vector like messenger in the **5** or **10** of SU(5) respectively).

As mentioned before, the μ-term, being supersymmetric, would be an independent parameter, but its value is fixed by requiring (tuning) the correct EWSB. Finally the A-terms and B_μ are generated radiatively from RGE effects. This fact has very interesting consequences [41, 42]. First, being A and B_μ terms generated at the quantum level from gaugino masses and μ-term implies that the corresponding CP phases vanish, avoiding potentially dangerous bounds from EDMs. Second, small suppressed A-terms imply that the stop mixing will never be large, while small B_μ implies large values of $\tan\beta$. These two predictions combined with the measured value of the Higgs mass allows to fix also the overall scale Λ, which must then lie at around the PeV scale to produce the $\mathcal{O}(10)$ TeV SUSY scale required by the Higgs mass. The only remaining free parameters are the messenger mass scale M and their number N, which affect the properties of the spectrum in a milder way.

Using our computation for the Higgs mass we can thus *predict* the spectrum of MGM in terms of N and M, the result is shown in fig. 3.16. Four different spectra are reported, changing independently N (1 or 3) and the messenger scale M from $M = 10^7$ GeV (to allow the use of leading $\mathcal{O}(F/M)$ formulas) to $M = 10^{14}$ GeV (to avoid dangerous FCNC contributions from gravity mediated contributions). For each choice of N and M the spectrum is not completely determined because of the uncertainty in the Higgs mass computation. Indeed the effect of varying N and M is actually subleading with respect to the Higgs mass uncertainty. In the relevant region of parameters ($m_{\rm SUSY} \sim 10^4$ TeV and small stop mixing) the Higgs mass determination is at its best (see fig. 3.2). Theoretical uncertainties are completely dominated by the SM ones, which are subleading with respect to the experimental uncertainties in the top mass. In fact, what limits the prediction of the MGM spectrum is not the Higgs mass, or its determination in SUSY, but our poor knowledge of the top mass! Improvements in this quantity are required to further improve the predictions of fig. 3.16. The lowest (upper) bounds correspond to values of the top mass 2σ above (below) its measured central value. The overall scale Λ results to be at the PeV scale, in particular it varies roughly from 0.5 to 2.6 PeV for different choices of the top mass, N and M. The values of $\tan\beta$ are typically around 45 but they can vary up to 60 and down to 30 in the corners of the parameter space, the corresponding values for the supersymmetric bottom and tau Yukawa couplings are largish (typically around 0.5-0.7) but remain always below the one of the top Yukawa. Similarly the stop mixing parameter is always small $\hat{X}_t < 1$.

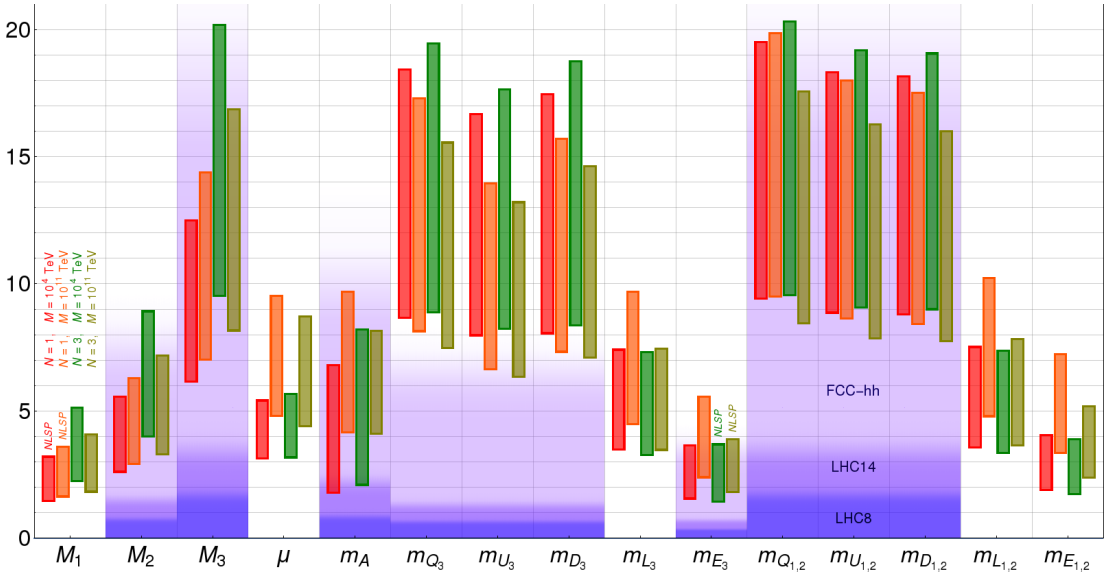

Figure 3.16: *Prediction for the spectrum of MGM after imposing the constraint from the Higgs mass (or better from the top mass). For each superpartner we plot the allowed range of masses (in TeV) for four different combinations of $N = 1(3)$ and $M = 10^4(10^{11})$ TeV. For each mass the lowest (highest) value corresponds to increasing (decreasing) the value of the top mass by 2σ with respect to its experimental central value. The values of $\tan\beta$ at the bottom (top) side of each of the four bands, from left to right, are 58 (42), 49 (45), 56 (29) and 44 (46) respectively. The three differently shaded areas represent "pictorially" the existing LHC8 bounds and the expected reach at LHC14 and at a future 100 TeV collider, respectively from the bottom.*

Except for the overall scale Λ, which is one order of magnitude larger than the one usually considered in the literature, the rest of the spectrum has the typical GMSB form, with bino or right-handed stau being the NLSP depending if $N = 1$ or 3 respectively.

On the experimental side, besides the simplified model and the generic SUSY searches, ATLAS and CMS also performed a number of dedicated GMSB searches [163–170], which exploits some of the most peculiar properties of its spectrum, such as photon and taus in the final states. Of particular relevance for this scenario is the direct search for the pseudoscalar Higgs boson A^0, which, for the large values of $\tan\beta$ predicted here, bounds $m_A \gtrsim 950$ GeV [55, 56]. This channel appears to be the most powerful for MGM, with a slightly better reach than the standard GMSB candles.

While a dedicated study is required, in fig. 3.16 we also show "pictorially" the existing experimental bounds and the expected reach at LHC14 and at an

hypothetical 100 TeV machine. The latter are obtained by rescaling the pdf on the existing bounds [61, 171] and should serve only to guide the eye. However, given the expected scale of the spectrum we can confidently say that this model is mostly out of the reach of existing collider machines[1], but could be seriously (if not completely) explored by a 100 TeV hadron collider. In fact, MGM may well represent one of the strongest motivations for such machine.

We checked that, while the values of $\tan\beta$ in this model are large, bounds from the rare decays $B_{d,s} \to \mu\mu$ [50] are not strong enough to be sensitive to the spectrum in fig. 3.16 yet. An improvement on the experimental bounds by a factor $3\div5$ could be enough to start probing the bottom part of the spectrum.

In conclusion, MGM represents probably the simplest and most predictive implementation of SUSY. The whole spectrum is almost completely determined just by experimental data. In particular, the upper bound on the scale of the superpartners exists independently from any naturalness consideration, in fact the value of the Higgs mass predicts a SUSY scale not too far beyond our current reach. The model also makes other successful *predictions* such as: gauge coupling unification, the absence of SUSY particles at current hadron colliders, no EDMs and no deviation from any flavor observables. Gravitino may be dark matter although this possibility is more model dependent.

3.5.2 Lopsided gauge mediation

As discussed in section 1.4.2, in lopsided gauge mediation models EWSB is problematic. In the original reference [43], new degrees of freedom are added to avoid this issue. Here we examine the simplest versions of Lopsided gauge mediation and analyze whether the correct EWSB can be achieved without introducing additional particles.

The very minimal choice is to generate the soft parameters of the Higgs sector with the same spurion and messenger fields used to generate the scalar and gaugino masses. The soft masses $m^2_{H_u}$ and $m^2_{H_d}$ receive two contributions at the messenger scale M

$$m^2_{H_{u,d}}(M) = m^{2\,(l)}_{H_{u,d}} + m^{2\,(g)}_{H_{u,d}}, \tag{3.40}$$

where $m^{2\,(g)}_{H_{u,d}}$ comes from gauge mediation and $m^{2\,(l)}_{H_{u,d}}$ arises from the superpotential coupling between the Higgs doublets and the messenger fields as explained in section 1.4.2. Their evolution to low scales is governed by the MSSM RGE presented in section 1.3.3.

[1] We would like to point out that in some corners of the allowed parameter space A^0 may be light enough to be within the reach of LHC14.

The simplest possibility of overcoming the problematic relation of lopsided in eq. (1.90) is to have a sizable gauge mediation contribution $m_{H_u}^{2\,(g)} \gtrsim m_{H_u}^{2\,(l)}$. Unfortunately, it does not work because of the usual issue of gauge mediation: $m_{H_u}^2$ receives large negative radiative corrections dominated by the stops.

On the other hand, it is technically natural to expect that the effective scale of SUSY breaking of the doublet and the triplet messenger fields, Λ_D and Λ_T, have slightly different values ($\Lambda_D \neq \Lambda_T$). Although they should have similar values such that gauge coupling unification is not spoiled. For instance, it can be achieved with $M_D \neq M_T$ and $F_D = F_T$. The expressions for the soft masses are modified as

$$M_a^{(g)} = n_G \Lambda_a \frac{\alpha_a}{4\pi}, \quad \tilde{m}_I^{2\,(g)} = 2 n_G \sum_{a=1}^{3} C_a^{(I)} \left(\frac{\alpha_a}{4\pi}\right)^2 \Lambda_a^2, \tag{3.41}$$

$$\Lambda_3 = \Lambda_T, \quad \Lambda_2 = \Lambda_D, \quad \Lambda_1 = \frac{2}{5}\Lambda_T + \frac{3}{5}\Lambda_D. \tag{3.42}$$

Under this consideration, one can compensate the negative radiative corrections to $m_{H_u}^2$, and one easily gets EWSB with a doublet-triplet splitting close to unity (but greater)

$$n_{DT} \equiv \frac{\Lambda_D}{\Lambda_T} \gtrsim 1. \tag{3.43}$$

This very-minimal model of lopsided gauge mediation has a phenomenological drawback: it is very difficult to test. Since B_μ is generated at one loop, the EWSB condition implies that, in general, one-loop in $\lambda_{u,d}$ is numerically equivalent to two loops in the gauge couplings. Therefore, higgsinos will be very light, one electroweak loop lighter than the scalars and gauginos, i.e. approximately two orders of magnitude.

We show the spectrum of superparticles in fig. 3.17 for $M = 10\Lambda_D$ and one set messenger fields $n_G = 1$. The model is characterized by three independent parameters: μ, n_{DT}, and $\tan\beta$. The last two are fixed by requiring the correct EWSB and $m_h \approx 125$ GeV. The doublet triplet splitting $n_{DT} \gtrsim 1$ slightly increases the mass of the doublets relative to the colored particles, leading to a spectrum slightly different from the one usually presented in gauge mediation. Since there is no large amount of running from the messenger scale to $m_{\rm SUSY}$ and the top Yukawa coupling runs to smaller values at high energies, the scalar masses of the three generations are similar.

In the model above we used the same spurion and messenger fields to generate the scalar and gaugino masses, and the Higgs soft parameters. In the original proposal of the model [43], they started by considering two sets of spurions and messengers. One was responsible for the scalar and gaugino masses while the

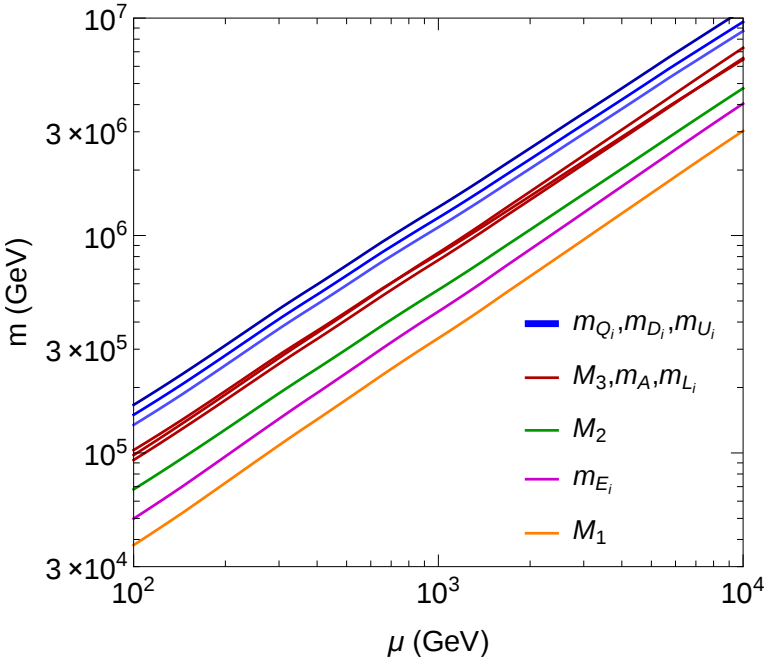

Figure 3.17: Spectrum of superparticles as a function of the μ parameter. The soft masses are evaluated at the SUSY scale $m_{\rm SUSY} = \sqrt{m_{Q_3} m_{U_3}}$. We used $M = 10\Lambda_D$ and number of messenger $n_G = 1$. By requiring the correct EWSB and the experimental value of the Higgs mass, we fixed the doublet triplet messenger splitting $n_{DT} \approx 1.2 \div 1.3$ and $\tan\beta \approx 2.1 \div 3.5$ from right to left.

other one for the parameters of the Higgs sector. Is it possible to have not-so-light higgsinos $\mu \lesssim m_{\rm SUSY}$ in this way?

Consider two spurions and messenger pairs: (X^A, Φ^A, $\bar{\Phi}^A$) which generates the scalars and gaugino masses, and (X^B, Φ^B, $\bar{\Phi}^B$) which generates the soft parameters of the Higgs sector. To motivate the existence of the singlets S and $\bar{S}$, we can suppose that the messengers $\Phi^B + \bar{\Phi}^B$ transform in the $10 \oplus \overline{10}$ of $SU(5)$ group.

We analyze the implications of the EWSB condition for the μ term. We assume the contributions to $m_{H_u}^2$ and $m_{H_d}^2$ are dominated by gauge mediation. In this way we relax the relation between the Higgs soft masses and the other parameter of the Higgs sector (μ and B_μ). Then the value of μ behaves approximately like

$$\mu \sim \sqrt{\frac{\alpha_\lambda}{16\pi^2}} B_\mu, \tag{3.44}$$

with $\alpha_\lambda \equiv \lambda_u \lambda_d/(4\pi)$. The EWSB condition requires that B_μ has to be of the

order of the Higgs soft masses $|B_\mu|^2 \approx m_{H_u}^2 m_{H_d}^2$. Depending on the ratio of the effective scales of SUSY breaking in the visible sector $\Lambda_D^A/\Lambda_D^B \gtrsim 1$ we can have μ in the range

$$\frac{\alpha_2}{4\pi} m_A \lesssim \mu \lesssim \sqrt{\frac{\alpha_\lambda}{4\pi}} m_A. \tag{3.45}$$

But now we can expect (the square root of) the loop factor in α_λ to be not so small, while still in the perturbative regime.

3.5.3 Anomaly Mediation

Minimal anomaly mediated supersymmetry breaking (AMSB) models [44, 172] probably provide for the simplest implementation of Mini Split supersymmetry. Scalars get their mass from gravity mediation of order the gravitino mass, while fermions, protected by R-symmetry, get one-loop suppressed soft masses from anomalies. The generation of the μ and B_μ parameters require also the breaking of the Peccei-Quinn (PQ) symmetry so that the higgsino mass is practically a free parameter—it can be of order the gravitino mass or naturally smaller if the PQ breaking is not efficient. The theory is thus defined by three main parameters: the gravitino mass $m_{3/2}$ setting the scale of scalars and gauginos, the higgsino mass μ and $\tan\beta$ which is determined by the details of the scalar masses and B_μ.

Unlike in MGM the details of the scalar spectrum are model dependent, however, given the large scales involved in this scenario, threshold corrections at the SUSY scale are almost irrelevant, for definiteness we fix all the scalars degenerate, $m_0 = m_{3/2}$. The actual value of the Higgs mass gives a further constraint on these parameters. It can be used, for example, to fix $\tan\beta$ in terms of the other two parameters. It is trivial to impose such constraint using SusyHD, the result is shown in fig 3.18. Values of $\tan\beta$ larger than $3 \div 4$ are already excluded, for they would require too low SUSY scale and the wino would lie below the LHC bounds [173]. Also a wino with mass ~ 3 TeV, which would provide for a good thermal dark matter candidate, corresponds to $\tan\beta \sim 2 \div 3$. Bounds on such parameters from direct detection experiment can be found for instance in [61].

Since a LSP wino above ~ 3 TeV would overclose the universe in the minimal AMSB scenario, the allowed parameter space reduces to the "narrow" strip below the red line in fig. 3.18, and the one with $|\mu| \lesssim 1$ TeV $\lesssim M_3$ where the higgsino is the LSP. Most of this parameter space could in principle be probed at a larger hadron collider and future dark matter experiments [61, 174–178]. In this interesting region, $\tan\beta$ is constrained between 2 and 3; scalars are clearly out of reach, between 10^2 and 10^3 TeV, but not heavy enough to guarantee the

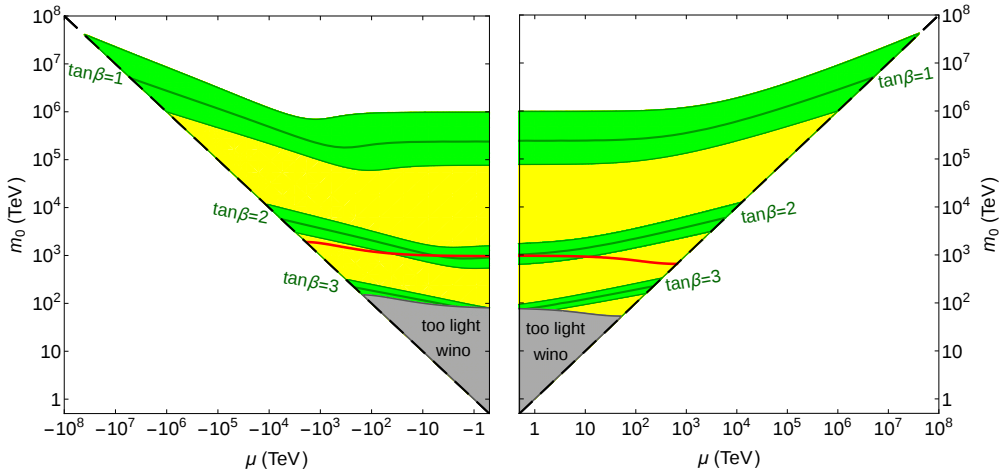

Figure 3.18: *Allowed parameter space of minimal anomaly mediation in the plane* $(m_0,\ \mu)$ *for different values of* $\tan\beta$*, after imposing the constraint from the Higgs mass. According to AMSB gauginos are one-loop lighter than the scalars, here taken with a common mass* m_0*. The wiggle for negative* μ *at small* $\tan\beta$ *is due to a cancellation in the one loop threshold correction from EWinos when* μ *crosses the gaugino masses. Values of* $\tan\beta \gtrsim 3$ *are excluded by LHC bounds on Winos. The horizontal red line corresponds to* $M_2 \simeq 3$ *TeV.*

absence of FCNC [46]. Gauge coupling unification further prefers values of μ below $\mathcal{O}(10)$ TeV [36].

Part II

QCD axion properties

Introduction

Quantum chromodynamics allows the presence of a CP-violating θ-term, which combined with the common phase of the quark mass matrix form the physical quantity $\overline{\theta} = \theta + \arg\det M_q$. Experimental limits on the neutron electric dipole moment [30, 31] imply $|\overline{\theta}| \lesssim 10^{-10}$. While values $\theta = \mathcal{O}(1)$ would completely change nuclear physics, its effects rapidly decouple for smaller values, already becoming irrelevant for $|\overline{\theta}| \lesssim 10^{-1} \div 10^{-2}$. As a consequence, this extremely small vale of $\overline{\theta}$ does not seem necessary to explain any known large-distance physics. Since other phases in the Yukawa matrices are $\mathcal{O}(1)$ and CP-violating new physics at high scales can contribute to $\overline{\theta}$, its tiny value seems to require a high degree of cancellation between θ and $\arg\det M_q$, two apparently unrelated parameters. This puzzle of why $\overline{\theta}$ is so small is known as the strong CP-problem.

Perhaps the simplest solution is the Peccei-Quinn mechanism [179]. It predicts the existence of the QCD axion [180–185], the pseudo-Goldstone boson of an additional $U(1)$ PQ symmetry. The axion only couples non-derivatively to the QCD topological charge and the coupling is determined by the scale f_a. Such a coupling allows to rotate away $\overline{\theta}$ through a shift of the axion field, whose VEV is then guaranteed to vanish [186]. Extra model dependent derivative couplings may be present but they do not affect the solution to the strong CP-problem. All the physical properties of the axion are controlled by a single scale f_a.

Presently astrophysical constraints bound f_a between few 10^8 GeV (see for e.g. [187]) and few 10^{17} GeV [188–190]. It has been known for a long time [191–193] that in most of the available parameter space the axion may explain the observed dark matter of the universe. Indeed, non-thermal production from the misalignment mechanism can easily generate a suitable abundance of cold axions for values of f_a large enough, compatible with those allowed by current bounds. Such a feature is quite model independent and, if confirmed, may give non-trivial constraints on early cosmology.

After the recently discovered Higgs boson, another scalar that may exist in nature is the QCD axion, one of the best motivated beyond the standard model particles. The axion provides an elegant solution to the strong CP problem

and represents an excellent dark matter candidate. Moreover axion-like particles naturally arise in string theory.

The field of experimental searches for axions is very active. Due to the extremely small couplings allowed by astrophysical bounds, in order to enhance the signal some experiments use resonance effects and the fact that, if the axion is dark matter, the line width of the resonance is suppressed by $v^2 \sim 10^{-6}$ (v being the virial velocity in our galaxy) [194, 195]. The Axion Dark Matter eXperiment (ADMX) [196] is expected to become sensitive to a new region of parameter space unconstrained by indirect searches soon. Other experiments are also being planned and several new ideas have recently been proposed to directly probe the QCD axion [197–200]. In the case of a successful discovery of the axion by such experiments, its mass would be known with a comparably high precision of $\mathcal{O}(10^{-6})$ and some axion couplings may also be determined depending on the experiment.

In this part we try to explore how such high precision experimental measurements in the axion mass and maybe couplings could be combined with accurate theoretical predictions to gain information about the axion physics, in particular to infer its UV completion and its cosmology. We will show that high theoretical precision is possible despite most of the axion properties, such as its mass, couplings to matter and relic abundance are dominated by non perturbative QCD dynamics. Since the axion mass is extremely light, QCD chiral Lagrangians [201–203] can be used reliably. Performing a NLO computation we were able to extract the full axion potential, its mass, self-coupling and the tension of domain walls. The coupling to photon can be extracted with similar precision. We also describe a new strategy to extract the coupling to nucleons directly from first principle QCD.

We also study the finite temperature dependence of the axion potential for its important role in cosmology since it controls the axion relic abundance. At temperatures below the QCD crossover chiral Lagrangians allow to compute the temperature dependence of the axion potential and consequently of its mass. Around the critical temperature non-perturbative methods such as lattice QCD [204, 205] are required. At higher temperatures, when QCD becomes perturbative, we point out however that the instanton gas approximation is completely unreliable for temperatures below 10^6 GeV. At the end we consider the effect of the uncertainty of the temperature dependence of the axion potential and mass in the axion relic abundance, providing updated plots for the allowed axion parameter space.

This part, about the physics of the QCD axion, contains two chapters. In chapter 4 we study the basic aspects of the QCD axion and its physical properties.

In chapter 5, we present our original results about precision corrections to the properties of the QCD axion and their temperature dependence in connection with the axion relic abundance.

Chapter 4

Basics of the QCD axion

In this chapter we review some basic aspects of the QCD axion. In section 4.1, we introduce the strong CP problem and consider a possible solution through the Peccei-Quinn mechanism. This type of solutions predicts the existence of the QCD axion, the pseudo Nambu-Goldstone boson associated to the spontaneous breaking of the PQ symmetry.

The most common axion models are briefly mentioned in section 4.2. In section 4.3, we review some basic elements of chiral perturbation theory, which are relevant for section 4.4 where we present the physical properties of the axion at leading order. Finally, in section 4.5 we describe the current experimental limits on the axion parameter space.

4.1 The strong CP problem

In the SM one can write the following term in the Lagrangian

$$\mathcal{L}_\theta = -\theta \frac{g_s^2}{32\pi^2} G^{a,\mu\nu} \widetilde{G}^a_{\mu\nu}, \tag{4.1}$$

where g_s is the QCD coupling constant, $G^a_{\mu\nu}$ is the field strength tensor of the strong interactions and θ is a parameter with values $-\pi \leq \theta \leq \pi$ as physical observables are periodic in θ with period 2π. The dual field strength tensor $\widetilde{G}^a_{\mu\nu}$ is defined as

$$\widetilde{G}^a_{\mu\nu} = \frac{1}{2} \epsilon_{\mu\nu\rho\sigma} G^{a,\rho\sigma}, \tag{4.2}$$

with the convention for the antisymmetric tensor such that $\epsilon^{0123} = 1$. This term $\mathcal{L}_\theta$ respects all the SM symmetries. It violates $\mathcal{CP}$ which is anyway badly broken by the quark sector. Then one would naively expect $\theta = \mathcal{O}(1)$.

The pseudoscalar combination $G\widetilde{G}$ is a total derivative, so it does not affect the equations of motion. However there are non-trivial gauge configurations with finite action known as instantons [24, 206] and with

$$G_{\mu\nu} = \pm\widetilde{G}_{\mu\nu}. \tag{4.3}$$

Their contribution to the action can be written as a surface integral characterized by the integer index n, the winding number [207]

$$\frac{1}{4}\int d^4x G^{a,\mu\nu}G^a_{\mu\nu} = \pm\frac{1}{4}\int d^4x G^{a,\mu\nu}\widetilde{G}^a_{\mu\nu} = \pm 8\pi^2 n. \tag{4.4}$$

From this equation we see the periodicity in the θ angle.

Instantons have a characteristic scale (their size), which is the integration constant arising from solving eq. (4.3). This scale breaks the scale invariance of the classical QCD action. Then there are instantons with any size. All of them should be taken into account in the path integral. The instanton contribution to the QCD action is dominated by large instantons which are controlled by larger values of the strong coupling. They are intrinsically non-perturbative.

Under chiral transformations of the quark fields

$$q_f \to e^{i\alpha\gamma_5/2}q_f, \tag{4.5}$$

QCD is apparently invariant in the massless quark limit. But actually quantum effects explicitly break this symmetry due to the chiral anomaly [208–211]. That is, the massless QCD Lagrangian is invariant while the path integral transforms non-trivially. This leads to the shift in the action

$$\delta S = \alpha\frac{g_s^2 N_f}{32\pi^2}\int d^4x G^{a,\mu\nu}\widetilde{G}^a_{\mu\nu}, \tag{4.6}$$

where N_f is the number of quark flavors contributing to the anomaly. From here we see that chiral transformations change the value of the θ angle

$$\theta \to \theta + \alpha. \tag{4.7}$$

But the SM Lagrangian also contains a mass term for the quarks

$$\mathcal{L}_{SM} = \overline{q}_{iL}M_{ij}q_{Rj} + h.c. + \ldots \tag{4.8}$$

Chiral transformations, which transforms differently left and right components of the quark fields, induces a phase in the quark mass matrix

$$\arg M \to \arg M + \alpha. \tag{4.9}$$

The parameters θ and $\arg M$ separately are not physical quantities because they change under the field redefinition in eq. (4.5). But there is a physical combination given by

$$\overline{\theta} = \theta - \arg(\det M). \tag{4.10}$$

The strongest experimental limit on $\overline{\theta}$ is based on the bounds on the neutron electric dipole moment (EDM) [30, 31]. Since the $\overline{\theta}$-term breaks $\mathcal{CP}$ it will induce a contribution to the neutron EDM. Although estimate of this contribution have large uncertainties associated to nuclear physics. The most sensitive experimental result set $d_n < 2.9 \times 10^{-26} e\,\text{cm}$ [212]. This implies the upper bound

$$|\overline{\theta}| \lesssim 10^{-10}. \tag{4.11}$$

Why should $\overline{\theta}$ have such extremely small value is known as the strong-$\mathcal{CP}$ problem. Generically one would expect order one values for θ and $\arg(\det M)$. After all, the off-diagonal Cabibbo-Kobayashi-Maskawa (CKM) phases are order one. One would need a high degree of cancellation between the two parameters of unrelated origin.

4.1.1 Possible solutions: the axion

Possible solutions to the strong $\mathcal{CP}$ problem can be divided into two groups depending on their underlying mechanism: spontaneously broken $\mathcal{CP}$ or an additional chiral symmetry called Peccei-Quinn (PQ) symmetry [179, 213]. In the first class of models [214–217], $\mathcal{CP}$ is a symmetry of the fundamental theory in the UV. Then θ and $\arg(\det M)$ are zero at tree-level. When $\mathcal{CP}$ is broken in order to produce the CKM phase a special choice of the particle content and the couplings of the theory guarantees the absence of tree-level contributions to $\overline{\theta}$ and the sufficient suppression of loop corrections. They also require some model-building to avoid FCNC and other problems. Perhaps the biggest drawback of these type of solutions is that experimental data perfectly agree with the Yukawa sector of the SM where $\mathcal{CP}$ is explicitly broken, so how they get $\mathcal{O}(1)$ CKM phases may seem a bit artificial.

The second group of solutions is based on an additional chiral symmetry. It is very elegant since these transformations induce a shift of the action due to the anomaly which can be used to rotate the θ term away. That is, the θ term becomes non physical. If the up quark were massless there would be an additional chiral symmetry one could use. But this possibility is strongly disfavored by the current value $m_u(2\text{ GeV}) = 2.15(15)$ MeV [51] extracted from lattice simulations. Hence in the SM there are no chiral symmetries available.

The most compelling option is to introduce a global chiral symmetry $U(1)_{PQ}$ as in [179]. It is spontaneously broken and the axion is the corresponding Goldstone boson [180, 181]. Under $U(1)_{PQ}$ transformations the axion shift as

$$a(x) \to a(x) + \alpha f_a, \tag{4.12}$$

where f_a is the order parameter corresponding to the $U(1)_{PQ}$ breaking. This implies the axion should only have derivative couplings.

We need to add extra terms to the SM Lagrangian involving the axion

$$\mathcal{L} = -\theta \frac{g_s^2}{32\pi^2} G^{a,\mu\nu} \widetilde{G}^a_{\mu\nu} + \frac{1}{2}\partial^\mu a \partial_\mu a + \frac{a}{f_a} \frac{g_s^2}{32\pi^2} G^{a,\mu\nu} \widetilde{G}^a_{\mu\nu} + \dots, \tag{4.13}$$

where the last term, which explicitly breaks $U(1)_{PQ}$, is due to the anomaly. The $U(1)_{PQ}$ symmetry is used to absorb the θ term. That is, the QCD anomaly generates a potential for the axion, such that the total contribution cancel in the vacuum $\overline{\theta} = 0$ [186] and there is no $\mathcal{CP}$ violating term in the strong sector.

Since the last term in eq. (4.13) contains a dimension-five operator the theory is non renormalizable. At very high energy the theory becomes strongly coupled. There are renormalizable models which UV complete this theory with a weakly coupled theory at high energy. In fact, this is the historical way the axion was introduced.

4.2 Models of axions

The axion decay constant f_a is associated with the PQ breaking scale but in general it is a free parameter of UV models. The originally proposed model of axions tried to relate f_a to the electroweak scale v. It was introduced by Peccei, Quinn [179, 213], and Weinberg and Wilczek [180, 181]. In the SM the Higgs boson can not account for the axion field because the would be Goldstone bosons are eaten by the gauge fields. One needs to introduce two Higgs fields, H_u and H_d, with vacuum expectation values $\langle H_u \rangle = v_u$ and $\langle H_d \rangle = v_d$, such that $v_u^2 + v_d^2 = v^2 \sim (246 \text{ GeV})^2$. Similar to the MSSM, H_u generates the masses of the up-type quarks and H_d generates the masses of down-type quark and leptons. In this model, the axion decay constant is fixed by the relation

$$f_a = v[N_f(\tan\beta + \cot\beta)]^{-1}, \tag{4.14}$$

where N_f is the number of generations and $\tan\beta = v_u/v_d$. This imply that $f_a \lesssim 41$ GeV, severely excluded by experimental bounds.

To be consistent with the allowed range of values of f_a ($f_a \gg v$), other models introduce an electroweak singlet scalar field Φ whose vacuum expectation value (VEV) $\langle\Phi\rangle = v_{PQ}/\sqrt{2}$ is not related to the weak scale. These models are called invisible axion models because they predict a very light and very weakly coupled axion.

The first invisible axion proposal is the KSVZ model, which is an acronym of the authors Kim [182], and Shifman, Vainshtein and Zakharov [183]. The scalar field Φ breaks $U(1)_{PQ}$ spontaneously. One can introduce N extra quarks in the fundamental representation of $SU(3)_C$. Then, the value of f_a is fixed by v_{PQ} and the color anomaly N as

$$f_a = v_{PQ}/N. \tag{4.15}$$

In this model the axion does not couple directly to the SM fermions. Axion interactions at low energy arise only from the axion-gluon coupling, which is generic of the PQ solution of the strong $\mathcal{CP}$ problem.

Dine, Fischler and Srednicki [185], and Zhitnitskii [184] introduced another UV completion known as the DFSZ model. It combines ingredients of both PQWW and KSVZ models. The model contains two electroweak doublet H_u and H_d with the same role as above and a scalar field Φ. All of them get a vev, the PQ breaking scale is mostly determined by the vev of Φ, although there is a small contribution from the Higgs doublets. The axion decay constant is given by $f_a = v_{PQ}/N_f$. The axion couples directly to the SM fermions which now carry PQ charges, their relative strength depends on the angle β defined by the ratio of the Higgs vevs.

4.3 Chiral Lagrangians

For a theory with a global symmetry group G, spontaneously broken to a subgroup H, there is a general formalism to construct the effective Lagrangian at low energy proposed by Callan, Coleman, Wess and Zumino [218, 219]. The vacuum has the structure of the coset space G/H. The effective Lagrangian is written in terms of the relevant coordinates at low energy, associated to a set of broken generators.

In the massless quark limit, the QCD Lagrangian with N_f flavors has a global $SU(N_f)_L \times SU(N_f)_R$ chiral symmetry, which transforms independently the left and right components of the quark fields

$$q_L(x) \to L\, q_L(x), \quad q_R(x) \to R\, q_R(x). \tag{4.16}$$

This symmetry is spontaneously broken by the chiral condensate to the diagonal combination

$$SU(N_f)_L \times SU(N_f)_R \longrightarrow SU(N_f)_V. \tag{4.17}$$

At low energy, it is convenient to use the following field

$$U = e^{i\,\Pi/f_\pi}, \tag{4.18}$$

where f_π is the pion decay constant, and Π the mass matrix of pions, the Goldstone bosons associated to the broken generators. In the case of three flavors, it is given by

$$\Pi = \pi^a T^a = \frac{1}{\sqrt{2}} \begin{bmatrix} \frac{1}{\sqrt{2}}\pi^0 + \frac{1}{\sqrt{6}}\eta & \pi^+ & K^+ \\ \pi^- & -\frac{1}{\sqrt{2}}\pi^0 + \frac{1}{\sqrt{6}}\eta & K^0 \\ K^- & \overline{K}^0 & -\frac{2}{\sqrt{6}}\eta \end{bmatrix}, \tag{4.19}$$

where T^a are the generators of $SU(3)$.

Under chiral transformation the field U transforms as

$$U \to LUR^\dagger. \tag{4.20}$$

Since the quark masses explicitly break the chiral symmetry, it is convenient to treat the mass matrix as an external spurion field transforming also as

$$M \to LMR^\dagger. \tag{4.21}$$

We can absorb the θ term into the quark mass matrix with a chiral rotation, such that

$$M = e^{-i\frac{\theta}{2}Q_a} M_0 e^{-i\frac{\theta}{2}Q_a}, \text{ with } \mathrm{tr}\, Q_a = 1. \tag{4.22}$$

Here $M_0 = \mathrm{diag}(m_u, m_d, m_s)$ is the diagonal mass matrix.

We construct the most general effective Lagrangian consistent with Lorentz symmetry and invariant under chiral transformations [201–203]. At lowest order in momenta, it reads

$$\mathcal{L} = \frac{f_\pi^2}{4}\mathrm{tr}\left(\partial_\mu U \partial^\mu U^\dagger\right) + 2B_0\frac{f_\pi^2}{4}\mathrm{tr}\left(M^\dagger U + M U^\dagger\right), \tag{4.23}$$

where the parameters B_0 and the pion decay constant f_π are not fixed by symmetry arguments. Higher order terms in the chiral expansion will involve more derivative or more insertions of M. Since the field U is a non-linear representation of the pions, by expanding one obtains the pion mass term and interactions.

By expanding U at the quadratic level one finds the relation between the meson masses and the quark masses

$$\begin{aligned} M^2_{\pi^\pm} &= B_0(m_u + m_d)\,, & M^2_{\pi^0} &= B_0(m_u + m_d) - \varepsilon + \mathcal{O}(\varepsilon^2)\,, \\ M^2_{K^\pm} &= B_0(m_u + m_s)\,, & M^2_{K^0} &= B_0(m_d + m_s)\,, \\ M^2_{\eta_8} &= \frac{1}{3}B_0(m_u + m_d + 4m_s) + \varepsilon + \mathcal{O}(\varepsilon^2)\,, \end{aligned} \tag{4.24}$$

with

$$\varepsilon = \frac{B_0}{4}\frac{(m_u - m_d)^2}{(m_s - \hat{m})}\,. \tag{4.25}$$

Chiral Lagrangians does not allow to obtain the quark masses from experiments, but only the product of B_0 and the quark masses or their ratio. Using the values of the quark masses extracted from Lattice simulations we can find the value of B_0. While the pion decay constant f_π can be fitted from pion-pion scattering or the pion decay and it is around $f_\pi \approx 92$ MeV.

At low energy, the momenta on-shell are of the same order of the meson masses. In order to have a consistent low energy expansion for non-zero quark masses one have to treat the meson masses as a term of the same order as the derivatives, and expand in powers of the momenta at fixed m_π^2/p^2 [202]. As consequence, we count the external field M as a quantity of order p^2.

To see how dimensional analysis works we consider the $\pi - \pi$ scattering amplitude at order p^4 (for a review on chiral perturbation theory and power counting see [220, 221]). The power counting of the one-loop contribution gives

$$I \sim \frac{p^2}{f_\pi^2}\,\frac{p^2}{f_\pi^2}\int \frac{d^4k}{(4\pi)^2}\;\;\frac{1}{k^2}\frac{1}{k^2}, \tag{4.26}$$

where the factors of the external momentum p^2/f_π^2 come from the two four-pion interaction vertices and the two pion internal propagators are of order $1/k^2$, where k is the loop momentum. The result of this integral is log-divergent and goes like

$$I \sim \frac{1}{16\pi^2}\frac{p^4}{f_\pi^4}\log\frac{p}{\mu}, \tag{4.27}$$

where μ is the renormalization scale. The scale dependence of the total four-pion amplitude is canceled by a four-derivative operator of order p^4

$$a\ \mathrm{tr}\left(\partial^\mu U \partial_\mu U^\dagger \partial^\nu U \partial_\mu U^\dagger\right). \tag{4.28}$$

From eqs. (4.27) and (4.28) we see that loop corrections in chiral perturbation theory will be suppressed by $1/(4\pi)^2\ p^2/f_\pi^2$. This means that the cut-off of the effective theory is at most

$$\Lambda_\chi \sim 4\pi f_\pi \sim 1\ \mathrm{GeV}, \tag{4.29}$$

and the expansion parameter is p^2/Λ_χ^2. As long as the energy is smaller than Λ_χ the loop expansion converges and the theory is perturbative. That is the case for processes involving pions and to a lesser extent kaons.

We are now interested in the effective Lagrangian for axions. Above the weak scale the interactions of the axion consist of gauge invariant derivative couplings to matter and anomalous couplings to gauge bosons. While the strength of the couplings to matter are arbitrary the anomalous couplings are fixed by the anomaly. Below the chiral symmetry breaking scale, the effective Lagrangian will describe the interactions of the axion with photons, leptons, mesons and baryons.

Just above the weak scale, we assume that under PQ transformations all fields are invariant except the axion field, which is shifted by an additive constant

$$a \to a + \theta f_a. \tag{4.30}$$

The most general effective Lagrangian at first order in the axion field is given by

$$\mathcal{L}_a = \frac{1}{2}\partial^\mu a \partial_\mu a + \frac{\partial_\mu a}{f_a} j_a^\mu + \left(\frac{a}{f_a} - \theta\right) \frac{g_s^2}{32\pi^2} G^{\mu\nu}\widetilde{G}_{\mu\nu} + \frac{1}{4} g^0_{a\gamma\gamma} a F^{\mu\nu}\widetilde{F}_{\mu\nu}. \tag{4.31}$$

Here j_a^μ is the axial current containing the SM matter fields $j^\mu_{a,0} = c_f^0 \overline{f}\gamma^\mu\gamma_5 f$, where the coefficients c_f^0 depend on the specific UV model. Color indices are implicitly contracted and the mass parameter f_a is defined in terms of the axion coupling to gluons. This definition is convenient because f_a is the parameter relevant for the axion mass and coupling to hadrons. The coupling to the photon field strength $F_{\mu\nu}$ is

$$g^0_{a\gamma\gamma} = \frac{\alpha_{em}}{2\pi f_a}\frac{E}{N}\,, \tag{4.32}$$

where E/N is the ratio of the Electromagnetic (EM) and the color anomaly, equals to 8/3 for complete SU(5) representations.

By shifting the axion field according to eq. (4.30) we can remove the θ-angle in eq. (4.31). The only non-derivative coupling to QCD can be conveniently moved away into the quark mass matrix by a field redefinition of the quark fields. Performing a change of field variables on the up and down quarks

$$q = \begin{pmatrix} u \\ d \end{pmatrix} \to e^{i\gamma_5 \frac{a}{2f_a} Q_a} \begin{pmatrix} u \\ d \end{pmatrix}, \qquad \mathrm{tr}\, Q_a = 1\,, \tag{4.33}$$

the axion Lagrangian (4.31) becomes

$$\mathcal{L}_a = \frac{1}{2}(\partial_\mu a)^2 + \frac{1}{4}\, a\, g_{a\gamma\gamma} F_{\mu\nu}\tilde{F}^{\mu\nu} + \frac{\partial_\mu a}{2f_a}\, j_a^\mu - \bar{q}_L M_a q_R + h.c.\,, \tag{4.34}$$

where

$$g_{a\gamma\gamma} = \frac{\alpha_{em}}{2\pi f_a}\left[\frac{E}{N} - 6\,\mathrm{tr}\left(Q_a Q^2\right)\right], \qquad j_a^\mu = j_{a,0}^\mu - \bar{q}\gamma^\mu\gamma_5 Q_a q\,, \tag{4.35}$$

$$M_a = e^{i\frac{a}{2f_a}Q_a} M_q\, e^{i\frac{a}{2f_a}Q_a}\,, \qquad M_q = \begin{pmatrix} m_u & 0 \\ 0 & m_d \end{pmatrix}, \qquad Q = \begin{pmatrix} \frac{2}{3} & 0 \\ 0 & -\frac{1}{3} \end{pmatrix}.$$

This basis of axion couplings has two advantages. The axion coupling to the axial current only renormalizes multiplicatively unlike the coupling to the gluon operator, which mixes with the axial current divergence at one-loop. Secondly the non-derivative couplings only arise from the quark mass terms.

For the values of f_a we are interested in, axion couplings are very small. As a consequence, we can work at leading order in this parameter. Virtual axion contributions are suppressed by this quantity and the axion can be treated as an external source. The non-derivative couplings are contained in the phase dependence of the matrix field of the quark masses M_a, while in the derivative couplings the axion appears as an external axial current.

The choice of field redefinition (4.33) allowed us to move the non-derivative couplings entirely into the lightest two quarks. In this way we can integrate out all the other quarks and directly work in the 2-flavor effective theory, with M_a capturing the whole axion dependence, at least for observables that do not depend on the derivative couplings. The Lagrangian at leading order in the chiral expansion has the form

$$\mathcal{L}_{p^2} = \frac{f_\pi^2}{4}\left[\mathrm{tr}\left(D^\mu U D_\mu U^\dagger\right) + 2B_0 \mathrm{tr}\left(U M_a^\dagger + M_a U^\dagger\right)\right], \tag{4.36}$$

where

$$U = e^{i\Pi/f_\pi}\,, \quad \Pi = \begin{pmatrix} \pi^0 & \sqrt{2}\pi^+ \\ \sqrt{2}\pi^- & -\pi^0 \end{pmatrix}, \tag{4.37}$$

tr represents the trace over flavor indices, D_μ is the covariant derivative containing the axial gauge field, the pion decay constant is normalized such that $f_\pi \simeq 92$ MeV, and B_0 is related to the chiral condensate and determined by the pion mass in term of the quark masses. Using this Lagrangian we can compute any process involving the axion and pions through a perturbative expansion.

4.4 Physical properties

The axion potential contains all the relevant information about the mass, the self-coupling, and the tension of its domain wall solutions. At leading order, it is

enough to consider the neutral pion sector. Taking Q_a in the dressed pion mass matrix proportional to the identity we find

$$\begin{aligned} V(a,\pi^0) &= -B_0 f_\pi^2 \left[m_u \cos\left(\frac{\pi^0}{f_\pi} - \frac{a}{2f_a}\right) + m_d \cos\left(\frac{\pi^0}{f_\pi} + \frac{a}{2f_a}\right)\right] \\ &= -m_\pi^2 f_\pi^2 \sqrt{1 - \frac{4m_u m_d}{(m_u+m_d)^2}\sin^2\left(\frac{a}{2f_a}\right)}\ \cos\left(\frac{\pi^0}{f_\pi} - \phi_a\right) \end{aligned} \tag{4.38}$$

where

$$\tan\phi_a \equiv \frac{m_u - m_d}{m_d + m_u}\tan\left(\frac{a}{2f_a}\right)\,. \tag{4.39}$$

The neutral pion π^0 gets a VEV $\langle\pi^0\rangle = f_\pi\phi_a$ to minimize the potential, which corresponds to the cosine in eq. (4.38) equals to unity. Then π^0 can be trivially integrated out leaving the axion effective potential

$$V(a) = -m_\pi^2 f_\pi^2 \sqrt{1 - \frac{4m_u m_d}{(m_u+m_d)^2}\sin^2\left(\frac{a}{2f_a}\right)}\,. \tag{4.40}$$

As expected the minimum is at $\langle a\rangle = 0$, thus solving the strong CP problem. Deriving twice the potential we obtain the well-known [181] expression for the axion mass

$$m_a^2 = \frac{m_u m_d}{(m_u+m_d)^2}\frac{m_\pi^2 f_\pi^2}{f_a^2}\,. \tag{4.41}$$

Although the expression for the potential (4.40) was derived long ago [222], we would like to stress some points often under-emphasized in the literature.

The axion potential (4.40) is nowhere close to the single cosine suggested by the instanton calculation (see fig. 4.1). This is not surprising given that the latter relies on a semiclassical approximation, which is not under control in this regime. Indeed the shape of the potential is $\mathcal{O}(1)$ different from that of a single cosine, and its dependence on the quark masses is non-analytic, as a consequence of the presence of light Goldstone modes. The axion self coupling, which is extracted from the fourth derivative of the potential

$$\lambda_a \equiv \left.\frac{\partial^4 V(a)}{\partial a^4}\right|_{a=0} = -\frac{m_u^2 - m_u m_d + m_d^2}{(m_u+m_d)^2}\,\frac{m_a^2}{f_a^2}\,, \tag{4.42}$$

is roughly a factor of 3 smaller than $\lambda_a^{(inst)} = -m_a^2/f_a^2$, the one extracted from the single cosine potential $V^{inst}(a) = -m_a^2 f_a^2\cos(a/f_a)$. The six-axion couplings differ in sign as well.

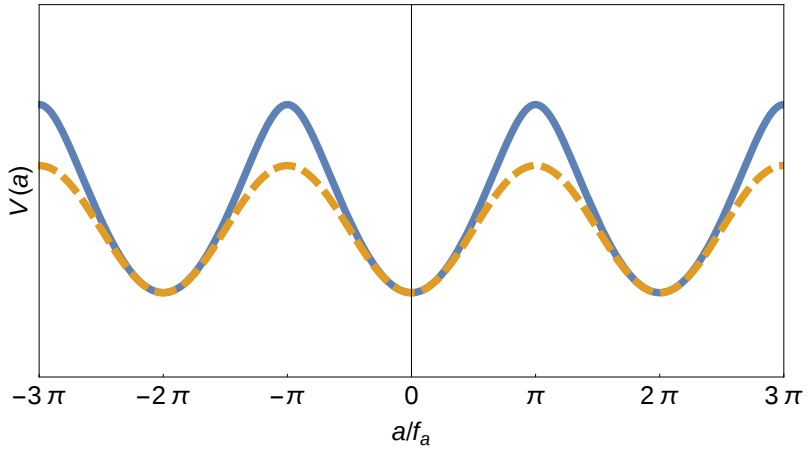

Figure 4.1: Comparison between the axion potential predicted by chiral Lagrangians, eq. (4.40) (continuous line) and the single cosine instanton one, $V^{inst}(a) = -m_a^2 f_a^2 \cos(a/f_a)$ (dashed line).

The non-trivial potential (4.40) allows for domain wall solutions [223]. These have width $\mathcal{O}(m_a^{-1})$ and their tension is computed from the definition

$$\sigma = 2 f_a \int_0^\pi d\theta \, \sqrt{2[V(\theta) - V(0)]} \,, \tag{4.43}$$

which gives

$$\sigma = 8 m_a f_a^2 \, \mathcal{E}\left[\frac{4 m_u m_d}{(m_u + m_d)^2}\right] , \qquad \mathcal{E}[q] \equiv \int_0^1 \frac{dy}{[2(1-y)(1+\sqrt{1-qy})]^{1/2}} \,. \tag{4.44}$$

The function $\mathcal{E}[q]$ can be written in terms of elliptic functions but the integral form is more compact. Note that changing the quark masses over the whole possible range, $q \in [0,1]$, only varies $\mathcal{E}[q]$ between $\mathcal{E}[0] = 1$ (cosine-like potential limit) and $\mathcal{E}[1] = 4 - 2\sqrt{2} \simeq 1.17$ (for degenerate quarks). For physical quark masses $\mathcal{E}[q_{phys}] \simeq 1.12$, only 12% off the cosine potential prediction, and $\sigma \simeq 9 m_a f_a^2$.

In a non vanishing axion field background, such as inside the domain wall or to a much lesser extent in the axion dark matter halo, QCD properties are different than in the vacuum. This can easily be seen expanding eq. (4.38) at the quadratic order in the pion field. For $\langle a \rangle = \theta f_a \neq 0$ the pion mass becomes

$$m_\pi^2(\theta) = m_\pi^2 \sqrt{1 - \frac{4 m_u m_d}{(m_u + m_d)^2} \sin^2\left(\frac{\theta}{2}\right)} \,, \tag{4.45}$$

and for $\theta = \pi$ the pion mass is reduced by a factor $\sqrt{(m_d + m_u)/(m_d - m_u)} \simeq \sqrt{3}$. Even more drastic effects are expected to occur in nuclear physics (see e.g. [224]).

Expanding at the quadratic order the potential of the axion and the neutral pion in eq. (4.38) we see the existence of π^0-a mass mixing controlled by isospin breaking effects. In fact, it was pointed out in ref. [225] that the leading order chiral Lagrangian contains (4.36) the mixing term

$$\mathcal{L}_{p^2} \supset 2B_0 \frac{f_\pi}{4f_a} a \,\mathrm{tr}\left(\Pi\{Q_a, M_q\}\right). \tag{4.46}$$

The mixing can be avoided by choosing the matrix Q_a as

$$Q_a = \frac{M_q^{-1}}{\mathrm{tr}(M_q^{-1})}. \tag{4.47}$$

Loop level corrections reintroduce the mixing. But since they are small they can be treated as a perturbation.

Finite temperature effects modify the axion properties. In particular, the behavior of the mass at high temperature (above the QCD scale Λ_{QCD}) has been widely studied for its role in the axion relic abundance. Well above the QCD crossover, the plasma of thermal fluctuations screen all color electric fields and quarks are deconfined. Functional dependence of the axion mass at high temperature has been estimated in the dilute instanton gas approximation. It can be written as [191–193, 226]

$$m_a(T) \sim 2 \times 10^{-2} \frac{(\Lambda_{\mathrm{QCD}} m_u m_d m_s)^{1/2}}{f_a} \left(9 \ln \frac{\pi T}{\Lambda_{\mathrm{QCD}}}\right) \left(\frac{\Lambda_{\mathrm{QCD}}}{\pi T}\right)^4, \tag{4.48}$$

where m_u, m_d, and m_s are the light quark masses. It approaches asymptotically to zero as $T \to \infty$. However the instanton computation suffer from large uncertainties, commented in section 5.2.1 of the next chapter.

The axion photon interaction, defined in eq. (4.34), can be obtained in chiral perturbation theory. From eqs. (4.35) and (4.47) one finds

$$g_{a\gamma\gamma} = \frac{\alpha_{em}}{2\pi f_a} \left[\frac{E}{N} - \frac{2}{3} \frac{4m_d + m_u}{m_d + m_u}\right], \tag{4.49}$$

where E/N is the model dependent EM anomaly of the PQ symmetry, while the second term is model independent and arises from the minimal coupling to QCD at the non-perturbative level. For the most common grand unified models we have $E/N = 8/3$ (DFSZ) and $E/N = 0$ (KSVZ). One may use a different basis for Q_a, but then the pion-photon coupling will induce a contribution through the a-π^0 mixing.

Other axion couplings to matter are either more model dependent (as the derivative couplings) or theoretically more challenging to study (as the coupling to EDM operators), or both. The derivative interaction with leptons, in particular to electrons, appears through the pseudoscalar current containing the SM fermions as

$$\mathcal{L}_{aff} = \frac{c_f^0}{2f_a}\overline{f}\gamma^\mu\gamma_5 f\partial_\mu a, \tag{4.50}$$

where f is the fermion field and c_f^0 a model dependent coefficient. The tree-level coefficient of the coupling to electrons in the DFSZ model reads

$$c_e = \frac{\sin^2\beta}{3}, \tag{4.51}$$

with β defined in section 4.2. In the KSVZ model C_e vanishes at tree level but it appears at one loop through the axion coupling to photons.

Usually, the axion-nucleon couplings has been extracted by combining experimental data from neutron beta decay, deep inelastic scattering and semi-leptonic hyperon decays. In section 5.1.4, we present a new strategy using experimental data and lattice QCD simulations and we explain its advantages. Unlike previous studies our analysis is based only on first principle QCD computations. While the precision is not as good as for the coupling to photons, the uncertainties are already below 10% and may improve as more lattice simulations are performed. Interactions with pions can be reliably obtained using chiral Lagrangians.

Results with the 3-flavor chiral Lagrangian are often found in the literature. In the 2-flavor Lagrangian the extra contributions from the strange quark are contained inside the low-energy couplings. Within the 2-flavor effective theory the difference between using 2 or 3 flavor formulas, is a higher order effect. Indeed the difference is $\mathcal{O}(m_u/m_s)$ which corresponds to the expansion parameter of the 2-flavor Lagrangian. As we will see in the next chapter these effects can only be consistently taken into account after including the full NLO correction.

4.5 Experimental limits

Constraints from astrophysical sources suggest that f_a should lie between few 10^8 GeV (see for eg. [187]) and few 10^{17} GeV [188–190, 211]. Axions are produced in hot astrophysical plasmas and can extract energy from stars. The couplings to matter and radiation are bounded by observations of stellar lifetimes or energy-loss rates. Current limits are based on measurements of the duration of the neutrino signal of the supernova SN 1987A, the white dwarfs luminosity

function (WDLF), the number counts of stars in the horizontal branch of globular clusters, red giant branch of the color-magnitude diagram of globular clusters, and helioscopes searches of axion fluxes potentially emitted from the sun. The absence of gamma-ray signals form the supernova SN 1987A also sets a constraint. The upper limit on f_a is associated to stellar black hole spin measurements that would be affected by the phenomenon of superrandiance in the presence of axions. These limits are reviewed in [51].

In most of the allowed parameter space the axion represents an excellent dark matter candidate and it could account for the whole dark matter density of the universe [191–193]. They can be produced through the misalignment mechanism and play the role of cold dark matter for sufficiently low masses. The details of the production mechanism depend on whether PQ symmetry is broken or not after inflation. However light axions have extremely small couplings, making them very hard to detect.

Searches for the QCD axion as dark matter use some resonance effects and the fact that the line width of the resonance is suppressed by the virial velocity in our galaxy $v^2 \sim 10^{-6}$ [194, 195] in order to enhance the tiny signal. Soon, the ADMX experiment is expected to probe a new region of parameter space unconstrained by indirect searches. Other experiments to directly search for the QCD axion are being planned [197–199]. If the axion is discovered by such experiments, we will know its mass with a high precision and possibly also the couplings depending on the experiment.

There are also laboratory experiments searching for axions and axion-like particles which do not rely on cosmological or astrophysical sources [200]. As light bosons would mediate long range forces, they are constrained by "fifth force" experiments, but at present these limits are far from realistic values expected for axions.

Chapter 5

Precision physics of the QCD axion

The experimental program searching for axions is very active and promising. If the axion were discovered, its mass would be determined with high precision. Similarly other axion couplings may also be extracted depending on the experiment. What can we learn from such measurements? Will we be able to infer the UV completion of the axion and its cosmology? In this chapter we try to make a small step towards answering these questions.

Since most of the axion properties, like the mass, couplings to matter and relic abundance are controlled by non-perturbative dynamics, high precision in QCD axion physics seems unachievable at first sight. However we will show that high precision is within reach. Given its extremely light mass, QCD chiral Lagrangians [201–203] can be used reliably. Performing a NLO computation we are able to extract the axion mass, self coupling and its full potential at the percent level. The coupling to photons can be extracted with similar precision, as well as the tension of domain walls. As a spin-off we provide estimates of the topological susceptibility and the quartic moment with similar precision and new estimates of some low energy constants.

We also describe a new strategy to extract the couplings to nucleons directly from first principle QCD. At the moment the precision is not yet at the percent level, but there is room for improvement as more lattice QCD results become available.

Finite temperature effects to the axion potential are also considered. At temperatures below $T_c \sim 170$ MeV chiral Lagrangians allow to precisely compute the temperature dependent axion potential. Around the crossover region one needs to rely on non-perturbative methods as lattice QCD simulations [204, 205].

At sufficiently higher temperature one may expect the dilute instanton gas approximation to work. However the bad convergence of the perturbative QCD expansion at finite temperature makes this computation unreliable for temperatures below 10^6 GeV, in accordance with the large discrepancy observed in recent lattice QCD simulations [227–229]. Finally, we evaluate the impact of such uncertainty in the computation of the axion relic abundance, providing updated plots for the allowed axion parameter space.

The chapter is organized as follows. In section 5.1 we present our new computations of the axion properties, most of them obtained based on NLO chiral Lagrangians, and their numerical estimates at zero temperature. In section 5.2 we discuss the temperature dependence of the axion mass and potential and the implications for the axion dark matter abundance. Some details about the input parameters used and extra formulas can be found in appendix B.

5.1 Properties at zero temperature

In this section we address the question of how good are the estimates obtained so far using leading order chiral Lagrangians. NLO corrections are typically about 20-30% in 3-flavor chiral perturbation theory. The 2-flavor theory enjoys a much better perturbative expansion given the larger hierarchy between pions and the other mass thresholds. To have a quantitative answer one must perform a complete NLO calculation. As the 2-flavor expansion enjoys a better convergence we perform all our computation in this theory.

When working with 2-flavor chiral Lagrangian a reduced number of physical observables are available to fit the higher order couplings. This difficulty is overcome by using 3-flavor theory to extract the values of the 2-flavor couplings when needed. This will produce intrinsic uncertainties $\mathcal{O}(30\%)$ in the extraction of the 2-flavor couplings. Such uncertainties however will only have a small impact on the final results whose dependence on the higher order 2-flavor couplings is suppressed by the light quark masses.

5.1.1 The mass

Because of the smallness of the relevant values of the axion decay constant the axion can be treated as an external source. Therefore its mass is related to the topological susceptibility χ_{top} through the relation

$$m_a^2 = \frac{\delta^2}{\delta a^2} \log \mathcal{Z}\big(\tfrac{a}{f_a}\big)\Big|_{a=0} = \frac{1}{f_a^2}\frac{d^2}{d\theta^2} \log \mathcal{Z}(\theta)\Big|_{\theta=0} = \frac{\chi_{top}}{f_a^2}\,, \tag{5.1}$$

where $\mathcal{Z}(\theta)$ is the QCD generating functional in the presence of a theta term.

A partial computation of the axion mass at one loop was first attempted in [230], followed by a recent computation of the full NLO corrections to the topological susceptibility in ref. [231]. The latter results are presented in terms of unphysical masses and couplings in the chiral limit. Here we recompute this quantity independently. We present the result for the axion mass in terms of observable renormalized quantities and the quark masses.

It is convenient to work in a basis with no tree-level mass mixing between the axion and the neutral pion. Then, since there are no cubic vertices with one axion and two pion fields, only diagrams with one single vertex contributes. In terms of Lagrangian parameters we find

$$m_a^2 = \frac{B_0 m_u m_d}{m_u + m_d} \frac{(f_\pi)^2}{f_a^2} \left\{ 1 + \frac{2B_0(m_u + m_d)}{f_\pi^2} \left[-\frac{3}{64\pi^2} \ln \frac{m_\pi^2}{\mu^2} + h_1^r - h_3^r + l_3^r \right.\right. \\ \left.\left. -4 \frac{m_u m_d}{(m_u + m_d)^2} l_7^r \right] \right\}, \tag{5.2}$$

where μ is the renormalization scale, h_1^r, h_3^r, l_4^r and l_7^r are the renormalized NLO couplings of [202], and both the couping B_0 and the pion decay constant f_π are in the chiral limit. Rewritten in terms of the physical observables it has the form

$$m_a^2 = \frac{m_u m_d}{(m_u + m_d)^2} \frac{m_\pi^2 f_\pi^2}{f_a^2} \left[1 + 2 \frac{m_\pi^2}{f_\pi^2} \left(h_1^r - h_3^r - l_4^r + \frac{m_u^2 - 6 m_u m_d + m_d^2}{(m_u + m_d)^2} l_7^r \right) \right], \tag{5.3}$$

where m_π and f_π are the physical (neutral) pion mass and decay constant (which include NLO corrections). After having reabsorbed one loop corrections of the tree-level factor $m_\pi^2 f_\pi^2$, there is no remaining contribution from loop diagrams at this order. In particular l_7^r and the combination $h_1^r - h_3^r - l_4^r$ are separately renormalization scale invariant.

We reproduce the result for the axion mass in the 3-flavor effective theory by matching with the computation of the 2-flavor effective theory in appendix B.2. Similar properties are also exhibited in the 3-flavor computation. After expressing the axion mass in terms of physical quantities, potentially large corrections of $\mathcal{O}(m_K^2)$ are absent, as noticed already in [230].

Based on the Appelquist-Carrazone decoupling theorem [232] one can understand the absence of power corrections proportional to the heavy meson masses as we checked explicitly in our calculation. The reason is that the dependence on large particle masses is absorbed by the low-energy parameters of the effective field theory describing the physics at scales much smaller than the large particle masses. In this way the dependence on the physics at large scales disappear from

the physics at low scales in the effective field theory, remaining only the (physical) logarithmic dependence related to processes that contribute at all scales.

When we performed the computation using two flavor ChPT, the heavy mesons have been integrated out, so the explicit dependence on their masses disappear from the effective theory. On the other hand, using three flavor ChPT the axion mass do contains power corrections proportional to the heavy meson masses when written in terms of the Lagrangian (unrenormalized) parameters. However, after writing the axion mass in terms of physical parameters this dependence gets absorbed by the physical parameters.

For the numerical evaluation of the axion mass and the size of the corrections in eq. (5.3) we need the values of the NLO low energy constants. The values of l_7^r and the difference $h_1^r - h_3^r$ are not available in the literature. Despite h_1^r and h_3^r separately are non physical, their difference is indeed physical, as they appear in eq. (5.3). In principle l_7^r could be extracted from the QCD contribution to the π^+-π^0 mass splitting. While lattice simulations have started to become sensitive to EM and isospin breaking effects, at the moment there are no reliable estimates of this quantity from first principle QCD. Even less is known about $h_1^r - h_3^r$, which does not appear in other measured observables. The only hope would be to use lattice QCD computation to extract such coupling by studying the quark mass dependence of observables such as the topological susceptibility.

Fortunately the values of the low energy constants of 2-flavor ChPT can be obtained in terms of the 3-flavor ones using the relations in [203]. We find

$$\begin{aligned} l_7^r &= \frac{m_u + m_d}{m_s}\frac{f_\pi^2}{8m_\pi^2} - 36L_7 - 12L_8^r + \frac{\log(m_\eta^2/\mu^2)+1}{64\pi^2} + \frac{3\log(m_K^2/\mu^2)}{128\pi^2} = 7(4)\cdot 10^{-3}, \\ h_1^r - h_3^r - l_4^r &= -8L_8^r + \frac{\log(m_\eta^2/\mu^2)}{96\pi^2} + \frac{\log(m_K^2/\mu^2)+1}{64\pi^2} = (4.8 \pm 1.4)\cdot 10^{-3}. \end{aligned} \quad (5.4)$$

The first term in l_7^r is due to the tree-level contribution to the π^+-π^0 mass splitting due to the π^0-η mixing from isospin breaking effects. The rest of the contribution, formally NLO, includes the effect of the η-η' mixing and numerically is as important as the tree-level piece [203]. We thus only need the values of the 3-flavor couplings L_7 and L_8^r, which can be extracted from chiral fits [233] and lattice QCD [234], we refer to appendix B.1 for more details on the values used. An important point is that by using 3-flavor couplings the precision of the estimates of the 2-flavor ones will be limited to the convergence of the 3-flavor Lagrangian. However, given the small size of such corrections even an $\mathcal{O}(1)$ uncertainty will still translate into a small overall error.

We also need the numerical value of the ratio of the light quark masses. As this quantity appears at tree level we need a precise estimate. Because of the Kaplan-Manohar (KM) ambiguity [235], it cannot be extracted within the meson Lagrangian. One may wonder whether the KM ambiguity also affects our computation of the axion mass. In 3-flavor ChPT the KM term has the form

$$\mathcal{L} \supset \frac{B_0 f_\pi^2}{2}\left[\mathrm{tr}\,(MU) + \frac{\delta}{m_s}\det(M)\mathrm{tr}\left(M^{-1}U^\dagger\right) + h.c.\right]. \tag{5.5}$$

Using matrix identities it can be written as

$$\det(M)\mathrm{tr}\left(M^{-1}U^\dagger\right) = \frac{1}{2}\left\{\left[\mathrm{tr}(U^\dagger M)\right]^2 - \mathrm{tr}\left[(U^\dagger M)^2\right]\right\}. \tag{5.6}$$

This shows that at NLO it is absorbed by the higher-order operators of the $\mathcal{O}(p^4)$ Lagrangian. In 2-flavor ChPT the KM term is of order p^2. However using the vector form it is clear that there is no ambiguity because one can form only one invariant at leading order ($\mathcal{M}^T\mathcal{U}$, with $\mathcal{M}$ and $\mathcal{U}$ being the analogous of M and U in the vector representation). In fact, we have

$$\mathrm{tr}[\det(M)M^{-1}U]^\dagger + h.c. = 4\mathcal{M}^T\mathcal{U}. \tag{5.7}$$

Therefore, the KM coupling is absorbed into the definition of B_0. Our expression for the axion mass is not affected by the KM ambiguity and we can safely use the quark masses at high energy.

Recent lattice QCD simulations have seriously improved our knowledge of the ratio of the up and down quark masses

$$z \equiv \frac{m_u^{\overline{\mathrm{MS}}}(2\ \mathrm{GeV})}{m_d^{\overline{\mathrm{MS}}}(2\ \mathrm{GeV})} = 0.48(3)\,, \tag{5.8}$$

where we have conservatively taken a larger error than the one associated with just averaging the latest results in [236–238] (see the appendix B.1 for more details). Note that z is scale independent up to α_{em} and Yukawa suppressed corrections. Another important observation is that since lattice QCD simulations allow us to relate physical observables directly to the high-energy $\overline{\mathrm{MS}}$ Yukawa couplings, in principle[1], they do not suffer from the KM ambiguity, which is a feature of chiral Lagrangians. It is reasonable to expect that the precision on the ratio z will increase further in the near future.

[1]Modulo well-known effects present when chiral non-preserving fermions are used.

Evaluating the axion mass in eq. (5.3) we obtain

$$m_a = 5.70(6)(4)\ \mu\text{eV}\left(\frac{10^{12}\text{GeV}}{f_a}\right) = 5.70(7)\ \mu\text{eV}\left(\frac{10^{12}\text{GeV}}{f_a}\right), \tag{5.9}$$

where the first error comes from the uncertainties in the light quark mass ratio (5.8) and the second is associated to the uncertainties in the low energy constants (5.4). The total error of $\sim$1% is much smaller than the relative errors in the quark mass ratio ($\sim$6%) and in the NLO couplings ($\sim$30$\div$60%) because of the weaker dependence of the axion mass on these quantities

$$\begin{aligned} m_a = \Bigg[& 5.70 + 0.06\,\frac{z-0.48}{0.03} - 0.04\,\frac{10^3 l_7^r - 7}{4} \\ & + 0.017\,\frac{10^3(h_1^r - h_3^r - l_4^r) - 4.8}{1.4}\Bigg]\mu\text{eV}\,\frac{10^{12}\,\text{GeV}}{f_a}\,. \end{aligned} \tag{5.10}$$

Note that the full NLO correction is numerically smaller than the quark mass error and its uncertainty is dominated by l_7^r. The error on the latter is particularly large because of a partial cancellation between L_7^r and L_8^r in eq. (5.4). As the contribution of l_7^r dominates over the others, extracting its value from Lattice QCD simulations would represent a considerable improvement.

We used the value of the pion decay constant $f_\pi = 92.21(14)$ MeV [51], extracted from π^+ decays and including the leading Quantum Electrodynamics (QED) corrections. Other electromagnetic corrections to m_a are expected to be sub-percent, but further reduction of the error on the axion mass may require a dedicated study of this source of uncertainty as well.

As a by-product we also provide a comparably high precision estimate of the topological susceptibility itself

$$\chi_{top}^{1/4} = \sqrt{m_a f_a} = 75.5(5)\,\text{MeV}\,, \tag{5.11}$$

against which lattice simulations can be calibrated.

5.1.2 The potential and derived quantities

The potential can be computed at NLO using the 2-flavor chiral Lagrangian, similar to the mass. It receives three corrections: the pure Coleman-Weinberg 1-loop potential from pion loops, the tree-level contribution from the NLO Lagrangian, and the corrections from the renormalization of the tree-level result,

when rewritten in terms of physical quantities (m_π and f_π). The complete result has the form

$$\begin{aligned} V(a)^{\text{NLO}} = -m_\pi^2\left(\tfrac{a}{f_a}\right) f_\pi^2 \Bigg\{ 1 - 2\frac{m_\pi^2}{f_\pi^2}\left[l_3^r + l_4^r - \frac{(m_d-m_u)^2}{(m_d+m_u)^2} l_7^r - \frac{3}{64\pi^2}\log\left(\frac{m_\pi^2}{\mu^2}\right)\right] \\ + \frac{m_\pi^2\left(\frac{a}{f_a}\right)}{f_\pi^2}\left[h_1^r - h_3^r + l_3^r + \frac{4m_u^2 m_d^2}{(m_u+m_d)^4}\frac{m_\pi^8 \sin^2\left(\frac{a}{f_a}\right)}{m_\pi^8\left(\frac{a}{f_a}\right)} l_7^r \right. \\ \left. - \frac{3}{64\pi^2}\left(\log\left(\frac{m_\pi^2\left(\frac{a}{f_a}\right)}{\mu^2}\right) - \frac{1}{2}\right)\right]\Bigg\}\,, \end{aligned} \tag{5.12}$$

where $m_\pi^2(\theta)$ is the function defined in eq. (4.45), and all quantities have been rewritten in terms of the physical NLO quantities[1]. In fact, the first line contains those terms arising from the NLO corrections to m_π and f_π in the tree-level potential.

The dependence on the axion is highly non-trivial, however the NLO corrections account for only up to few percent change in the shape of the potential (for example the difference in vacuum energy between the minimum and the maximum of the potential changes by 3.5% when NLO corrections are included). The numerical values for the additional low-energy constants $l_{3,4}^r$ are reported in appendix B.1. We thus know the full QCD axion potential at the percent level!

The quartic self-coupling of the axion at NLO can be obtained straightforwardly by expanding the effective potential (5.12) around the origin

$$V(a) = V_0 + \frac{1}{2}m_a^2 a^2 + \frac{\lambda_a}{4!}a^4 + \dots \tag{5.13}$$

It is written as

$$\begin{aligned} \lambda_a = &-\frac{m_a^2}{f_a^2}\Bigg\{\frac{m_u^2 - m_u m_d + m_d^2}{(m_u+m_d)^2} \\ &+6\frac{m_\pi^2}{f_\pi^2}\frac{m_u m_d}{(m_u+m_d)^2}\left[h_1^r - h_3^r - l_4^r + \frac{4\bar{l}_4 - \bar{l}_3 - 3}{64\pi^2} - 4\frac{m_u^2 - m_u m_d + m_d^2}{(m_u+m_d)^2} l_7^r\right]\Bigg\}\,, \end{aligned} \tag{5.14}$$

in terms of the physical one-loop corrected axion mass m_a of eq. (5.3). Numerical evaluation leads to

$$\lambda_a = -0.346(22)\cdot\frac{m_a^2}{f_a^2}\,, \tag{5.15}$$

with the uncertainty dominated by l_7^r and representing about the 6%.

[1] See also [239] for a related result computed in terms of the LO quantities.

Finally the NLO result for the domain wall tensions can be simply extracted from the definition, eq. (4.43), and numerically it gives

$$\sigma = 8.97(5)\, m_a f_a^2 \,, \tag{5.16}$$

where the uncertainty is below percent and it receives comparable contributions from the errors on l_7^r and the quark masses.

As a by-product we also provide a precision estimate of the topological quartic moment of the topological charge Q_{top}

$$b_2 \equiv -\frac{\langle Q_{top}^4\rangle - 3\langle Q_{top}^2\rangle^2}{12\langle Q_{top}^2\rangle} = \frac{f_a^2 V''''(0)}{12V''(0)} = \frac{\lambda_a f_a^2}{12 m_a^2} = -0.029(2)\,, \tag{5.17}$$

to be compared to the cosine-like potential $b_2^{inst} = -1/12 \simeq -0.083$.

5.1.3 Axion-photon coupling

Like the axion potential, the coupling to photons (4.49) also gets QCD corrections at NLO, which are completely model independent. Indeed derivative couplings only produce m_a suppressed corrections which are negligible, thus the only model dependence lies in the anomaly coefficient E/N.

For physical quark masses the QCD contribution (the second term in eq. (4.49)) is accidentally close to -2. This implies that models with $E/N = 2$ can have anomalously small coupling to photons, relaxing astrophysical bounds. The degree of this cancellation is very sensitive to the uncertainties from the quark mass and the higher order corrections, which we compute here for the first time.

NLO corrections to the coupling to photons arise from Feynman diagrams with one anomalous vertex, i.e. one vertex containing the antisymmetric tensor, as shown in fig. 5.1. These anomalous vertices come from the Wess-Zumino-Witten (WZW) Lagrangian or the anomalous $\mathcal{O}(p^6)$ Lagrangian. To study anomalous processes involving the axion field in chiral perturbation theory, both single vector (v_μ) and axial (a_μ) currents need to be included. In that case, the $\mathcal{O}(p^4)$ chiral Lagrangian of ref. [202] is generalized to include extra operators with new low energy constants $l_8, \ldots, l_{12}$ and $h_4, \ldots, h_7$ as discussed in [240]. Fortunately, the contributions from these extra operators to the axion mass and the coupling $g_{a\gamma\gamma}$ are further suppressed by the ratio f_a/f_π because they contain derivatives on the axion field; thus they do not induce axion-pion mixing. There are also electromagnetic corrections which were estimated in [241], but they can be safely neglected at the level of precision we are currently able to achieve.

Higher-dimensional operators of $\mathcal{O}(p^6)$ correcting the WZW Lagrangian in the presence of a single vector current were classified in [242], which is the basis we

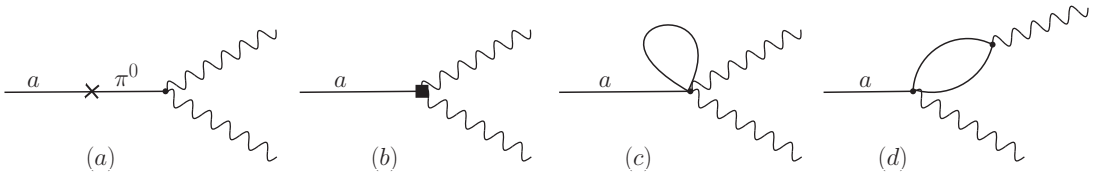

Figure 5.1: Corrections to the axion-photon coupling from: (a) the axion-pion mass mixing, (b) the anomalous $\mathcal{O}(p^6)$ Lagrangian, (c) the WZW Lagrangian, (d) the WZW Lagrangian and the $\mathcal{O}(p^2)$ pion photon vertex.

use. For the WZW term a significantly simple expression in 2-flavor ChPT was derived in [240]

$$\mathcal{L}_{\text{WZW}} = -\frac{N_c}{32\pi^2}\,\epsilon^{\mu\nu\rho\sigma}\big\{\langle U^\dagger \hat{r}_\mu U \hat{l}_\nu - \hat{r}_\mu \hat{l}_\nu + i\Sigma_\mu (U^\dagger \hat{r}_\nu U + \hat{l}_\nu)\rangle \langle v_{\rho\sigma}\rangle + \frac{2}{3}\langle \Sigma_\mu \Sigma_\nu \Sigma_\rho\rangle \langle v_\sigma\rangle \big\}\,, \tag{5.18}$$

where we use the notation

$$\hat{r}_\mu = \hat{v}_\mu + \hat{a}_\mu\,, \qquad \hat{l}_\mu = \hat{v}_\mu - \hat{a}_\mu\,, \qquad \Sigma_\mu = U^\dagger \partial_\mu U\,, \tag{5.19}$$

$$\hat{X} = X - \frac{1}{2}\langle X\rangle\,, \quad \text{for any matrix } X. \tag{5.20}$$

The corrections to the axion-photon couping can be decomposed as

$$g_{a\gamma\gamma} = \frac{\alpha}{2\pi}\frac{1}{f_a}\left(\frac{E}{N} - \frac{2}{3}\frac{4m_d + m_u}{m_d + m_u}\right) + \Delta g^{(a)}_{a\gamma\gamma} + \Delta g^{(b)}_{a\gamma\gamma} + \Delta g^{(c)}_{a\gamma\gamma} + \Delta g^{(d)}_{a\gamma\gamma}, \tag{5.21}$$

where the $\Delta g_{a\gamma\gamma}$'s are the contributions from the diagrams in fig. 5.1. From the $a - \pi^0$ mixing diagram and the tree-level diagrams with insertions of the NLO WZW operators we obtain

$$\Delta g^{(a)}_{a\gamma\gamma} = \frac{\alpha}{2\pi f_a}\left[-\frac{8B_0 m_u m_d (m_d - m_u)}{f_\pi^2 (m_u + m_d)^2} l_7^r\right], \tag{5.22}$$

$$\Delta g^{(b)}_{a\gamma\gamma} = \frac{\alpha}{2\pi f_a}\left[\frac{1024 B_0 \pi^2 m_u m_d (5c_3^W + c_7^W + 2c_8^W)}{9(m_u + m_d)}\right]. \tag{5.23}$$

While one-loop diagrams involve the following vertices contained in the $\mathcal{O}(p^2)$ and the WZW Lagrangians

$$\mathcal{L}_{p^2} \supset -ieA^\mu\left(\pi^+\partial_\mu\pi^- - \pi^-\partial_\mu\pi^+\right)\,, \tag{5.24}$$

$$\mathcal{L}_{\text{WZW}} \supset \frac{1}{8\pi^2 f_\pi^2 f_a}\frac{m_d - m_u}{m_u + m_d}\epsilon^{\mu\nu\rho\sigma} a\left[-e^2\pi^+\pi^-\partial_\mu A_\nu \partial_\rho A_\sigma + ie\partial_\mu\pi^+\partial_\nu\pi^-\partial_\rho A_\sigma\right].$$

One loop diagrams exactly cancel similarly to what happens for $\pi \to \gamma\gamma$ and $\eta \to \gamma\gamma$ processes [243]

$$\Delta g^{(c)}_{a\gamma\gamma} + \Delta g^{(d)}_{a\gamma\gamma} = \frac{\alpha}{2\pi f_a}(4-4)\left[\left(\frac{m_d - m_u}{m_u + m_d}\right) m_\pi^2 \left(1 - \ln\frac{m_\pi^2}{\mu^2}\right)\right], \tag{5.25}$$

where the first and second factors in eq. (5.25) corresponds to the contributions of $\pi^+\pi^-$ loops in figs. 5.1(a) and 5.1(b) respectively. The final result reads

$$\begin{aligned} g_{a\gamma\gamma} = \frac{\alpha_{em}}{2\pi f_a}\Bigg\{ & \frac{E}{N} - \frac{2}{3}\frac{4m_d + m_u}{m_d + m_u} \\ & + \frac{m_\pi^2}{f_\pi^2}\frac{8 m_u m_d}{(m_u + m_d)^2}\left[\frac{8}{9}\left(5\tilde{c}_3^W + \tilde{c}_7^W + 2\tilde{c}_8^W\right) - \frac{m_d - m_u}{m_d + m_u} l_7^r\right]\Bigg\}, \end{aligned} \tag{5.26}$$

where the couplings c_i^W of [242] have been rescaled into $\tilde{c}_i^W \equiv c_i^W (4\pi f_\pi)^2$ for simplicity. Notice that the l_7^r term includes the m_u/m_s contributions which one obtains from the 3-flavor tree-level computation.

Unlike the NLO couplings entering the axion mass and potential little is known about the couplings $\tilde{c}_i^W$, so we describe the way to extract them here.

We can attempt to use the available observables within 2-flavor ChPT, the $\pi^0 \to \gamma\gamma$ width and the vector form factor F_V^π, in order to extract the anomalous couplings c_i^W. Calling δ_i the relative correction at NLO to the amplitude for the i process, i.e.

$$\Gamma_i^{\rm NLO} \equiv \Gamma_i^{\rm tree}(1 + \delta_i)^2\,, \tag{5.27}$$

the expressions for $\Gamma^{\rm tree}_{\pi\gamma\gamma}$ and $\delta_{\pi\gamma\gamma}$ read

$$\begin{aligned} \Gamma^{\rm tree}_{\pi\gamma\gamma} &= \frac{\alpha_{em}^2}{(4\pi)^3}\frac{m_\pi^3}{f_\pi^2}\,, \\ \delta_{\pi\gamma\gamma} &= \frac{16}{9}\frac{m_\pi^2}{f_\pi^2}\left[\frac{m_d - m_u}{m_d + m_u}\left(5\tilde{c}_3^W + \tilde{c}_7^W + 2\tilde{c}_8^W\right) - 3\left(\tilde{c}_3^W + \tilde{c}_7^W + \frac{\tilde{c}_{11}^W}{4}\right)\right]. \end{aligned} \tag{5.28}$$

Once again the loop corrections are reabsorbed by the renormalization of the tree-level parameters and the only contributions come from the NLO WZW terms. While the isospin breaking correction involves exactly the same combination of couplings entering the axion width, the isospin preserving one does not. This means that we cannot extract the required NLO couplings from the pion width alone. However in the absence of large cancellations between the isospin breaking and the isospin preserving contributions we can use the experimental value for the pion decay rate to estimate the order of magnitude of the corresponding corrections to the axion case. Given the small difference between the experimental

and the tree-level prediction for $\Gamma_{\pi\to\gamma\gamma}$ the NLO axion correction is expected of order few percent.

Analogously we can consider the vector form factor[1]

$$F_V^\pi = F_V^{\pi,\text{tree}}\,(1+\delta_F)\,, \tag{5.29}$$

with

$$F_V^{\pi,\text{tree}} = \frac{m_{\pi^+}}{4\sqrt{2}\pi^2 f_\pi} \tag{5.30}$$

$$\delta_F = \frac{8}{3}m_\pi^2(4\tilde{c}_3^W + 4\tilde{c}_7^W + \tilde{c}_{11}^W) + 32m_\pi^2\frac{m_d}{m_u+m_d}\tilde{c}_5^W + \frac{16}{3}(k^2)\tilde{c}_{13}^W. \tag{5.31}$$

For on-shell photons $k^2=0$, thus the form factor does not depend on $\tilde{c}_{13}^W$. However it depends additionally on the coupling $\tilde{c}_{11}^W$ and cannot be used in combination with the $\pi^0\to\gamma\gamma$ width to fit the anomalous coefficients.

To obtain numerical values for the unknown couplings we can try to use the 3-flavor theory, in analogy with the axion mass computation. In fact at NLO in the 3-flavor theory the decay rates $\pi\to\gamma\gamma$ and $\eta\to\gamma\gamma$ only depend on two low-energy couplings that can thus be determined. Matching these couplings to the 2-flavor theory ones we are able to extract the required combination entering in the axion coupling. Because the $\tilde{c}_i^W$ couplings enter eq. (5.26) only at NLO in the light quark mass expansion we only need to determine them at LO in the $m_{u,d}$ expansion.

The $\eta\to\gamma\gamma$ decay rate at NLO is

$$\Gamma_{\eta\to\gamma\gamma}^{\text{tree}} = \frac{\alpha_{em}^2}{3(4\pi)^3}\frac{m_\eta^3}{f_\eta^2},\ \delta_{\eta\gamma\gamma}^{(3)} = \frac{32}{9}\frac{m_\pi^2}{f_\pi^2}\left[\frac{2m_s-4m_u-m_d}{m_u+m_d}\tilde{C}_7^W + 6\,\frac{2m_s-m_u-m_d}{m_u+m_d}\tilde{C}_8^W\right]$$
$$\simeq \frac{64}{9}\frac{m_K^2}{f_\pi^2}\left(\tilde{C}_7^W + 6\,\tilde{C}_8^W\right)\,, \tag{5.32}$$

where in the last step we consistently neglected higher order corrections $\mathcal{O}(m_{u,d}/m_s)$. The 3-flavor couplings $\tilde{C}_i^W \equiv (4\pi f_\pi)^2 C_i^W$ are defined in [242].

The expression for the correction to the $\pi\to\gamma\gamma$ amplitude with three flavors also receives important corrections from the π-η mixing ϵ_2,

$$\delta_{\pi\gamma\gamma}^{(3)} = \frac{32}{9}\frac{m_\pi^2}{f_\pi^2}\left[\frac{m_d-4m_u}{m_u+m_d}\tilde{C}_7^W + 6\,\frac{m_d-m_u}{m_u+m_d}\tilde{C}_8^W\right] + \frac{f_\pi}{f_\eta}\frac{\epsilon_2}{\sqrt{3}}(1+\delta_{\eta\gamma\gamma}^{(3)})\,, \tag{5.33}$$

[1]Contributions from chiral loops were computed and shown to vanish in [244].

where the π-η mixing derived in [203] can be conveniently rewritten as

$$\frac{\epsilon_2}{\sqrt{3}} \simeq \frac{m_d - m_u}{6 m_s} \left[1 + \frac{4 m_K^2}{f_\pi^2}\left(l_7^r - \frac{1}{64\pi^2}\right)\right], \tag{5.34}$$

at leading order in $m_{u,d}$. In both decay rates the loop corrections are reabsorbed in the renormalization of the tree-level amplitude[1].

By comparing the light quark mass dependence in eqs. (5.28) and (5.33) we can match the 2 and 3 flavor couplings as follows

$$\begin{aligned} &\tilde{c}_3^W + \tilde{c}_7^W + \frac{\tilde{c}_{11}^W}{4} = \tilde{C}_7^W\,, \\ &5\tilde{c}_3^W + \tilde{c}_7^W + 2\tilde{c}_8^W = 5\tilde{C}_7^W + 12\tilde{C}_8^W + \frac{3}{32}\frac{f_\pi^2}{m_K^2}\left[1 + 4\frac{m_K^2}{f_\pi f_\eta}\left(l_7^r - \frac{1}{64\pi^2}\right)\right](1+\delta_{\eta\gamma\gamma})\,. \end{aligned} \tag{5.35}$$

Notice that the second combination of couplings is exactly the one needed for the axion-photon coupling. By using the experimental results for the decay rates (reported in appendix B.1), we can extract $C_{7,8}^W$. The result is shown in fig. 5.2, the precision is low for two reasons: 1) $\tilde{C}_{7,8}^W$ are 3 flavor couplings so they suffer from an intrinsic $\mathcal{O}(30\%)$ uncertainty from higher order corrections[2], 2) for $\pi \to \gamma\gamma$ the experimental uncertainty is not smaller than the NLO corrections we want to fit.

For the combination we are interested in, $5\tilde{c}_3^W + \tilde{c}_7^W + 2\tilde{c}_8^W$, the final result reads

$$\begin{aligned} 5\tilde{c}_3^W + \tilde{c}_7^W + 2\tilde{c}_8^W = \frac{3 f_\pi^2}{64 m_K^2}\frac{m_u + m_d}{m_u}\Bigg\{&\left[1 + 4\frac{m_K^2}{f_\pi^2}\left(l_7^r - \frac{1}{64\pi^2}\right)\right]\frac{f_\pi}{f_\eta}(1+\delta_{\eta\gamma\gamma}) \\ &+3\delta_{\eta\gamma\gamma} - 6\frac{m_K^2}{m_\pi^2}\delta_{\pi\gamma\gamma}\Bigg\} \\ 5\tilde{c}_3^W + \tilde{c}_7^W + 2\tilde{c}_8^W = 0.033(6)\,. \end{aligned} \tag{5.36}$$

When combined with eq. (5.26) we finally get

$$g_{a\gamma\gamma} = \frac{\alpha_{em}}{2\pi f_a}\left[\frac{E}{N} - 1.92(4)\right] = \left[0.203(3)\frac{E}{N} - 0.39(1)\right]\frac{m_a}{\text{GeV}^2}\,. \tag{5.37}$$

[1] NLO corrections to π and η decay rates to photons including isospin breaking effects were also computed in [241]. For the $\eta \to \gamma\gamma$ rate we disagree in the expression of the terms $\mathcal{O}(m_{u,d}/m_s)$, which are however subleading. For the $\pi \to \gamma\gamma$ rate we also included the mixed term coming from the product of the NLO corrections to ϵ_2 and to $\Gamma_{\eta\gamma\gamma}$. Formally this term is NNLO but given that the NLO corrections to both ϵ_2 and $\Gamma_{\eta\gamma\gamma}$ are of the same size as the corresponding LO contributions such terms cannot be neglected.

[2] We implement these uncertainties by adding a 30% error on the experimental input values of $\delta_{\pi\gamma\gamma}$ and $\delta_{\eta\gamma\gamma}$.

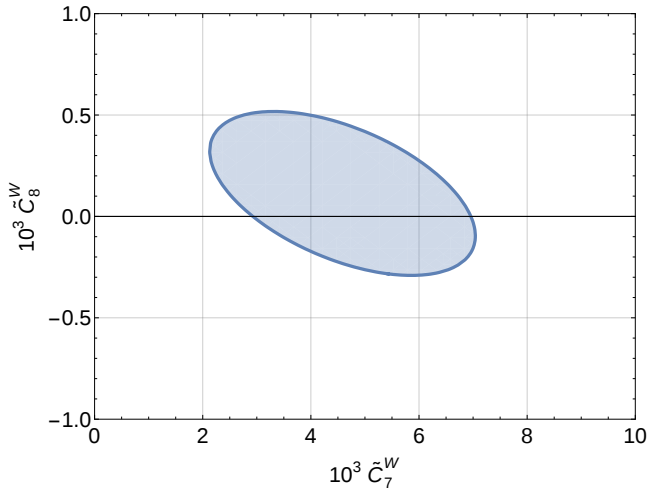

Figure 5.2: Result of the fit of the 3-flavor couplings $\tilde{C}^W_{7,8}$ from the decay width of $\pi \to \gamma\gamma$ and $\eta \to \gamma\gamma$, which include the experimental uncertainties and a 30% systematic uncertainty from higher order corrections.

Note that despite the rather large uncertainties of the NLO couplings we are able to extract the model independent contribution to $a \to \gamma\gamma$ at the percent level. This is due to the fact that, analogously to the computation of the axion mass, the NLO corrections are suppressed by the light quark mass values. Modulo experimental uncertainties, eq. (5.37) would allow the parameter E/N to be extracted from a measurement of $g_{a\gamma\gamma}$ at the percent level.

For the three reference models with respectively $E/N = 0$ (such as hadronic or KSVZ-like models [182, 183] with electrically neutral heavy fermions), $E/N = 8/3$ (as in DFSZ models [184, 185] or KSVZ models with heavy fermions in complete SU(5) representations) and $E/N = 2$ (as in some KSVZ "unificaxion" models [245]) the coupling reads

$$g_{a\gamma\gamma} = \begin{cases} -2.227(44) \cdot 10^{-3}/f_a & E/N = 0 \\ 0.870(44) \cdot 10^{-3}/f_a & E/N = 8/3 \\ 0.095(44) \cdot 10^{-3}/f_a & E/N = 2 \end{cases} . \tag{5.38}$$

Even after the inclusion of NLO corrections the coupling to photons in $E/N = 2$ models is still suppressed. The current uncertainties are not yet small enough to completely rule out a higher degree of cancellation, but a suppression bigger than $\mathcal{O}(20)$ with respect to $E/N = 0$ models is highly disfavored. Therefore the result for $g_{a\gamma\gamma}^{E/N=2}$ of eq. (5.38) can now be taken as a lower bound to the axion coupling to photons, below which tuning is required. The result is shown in fig. 5.3.

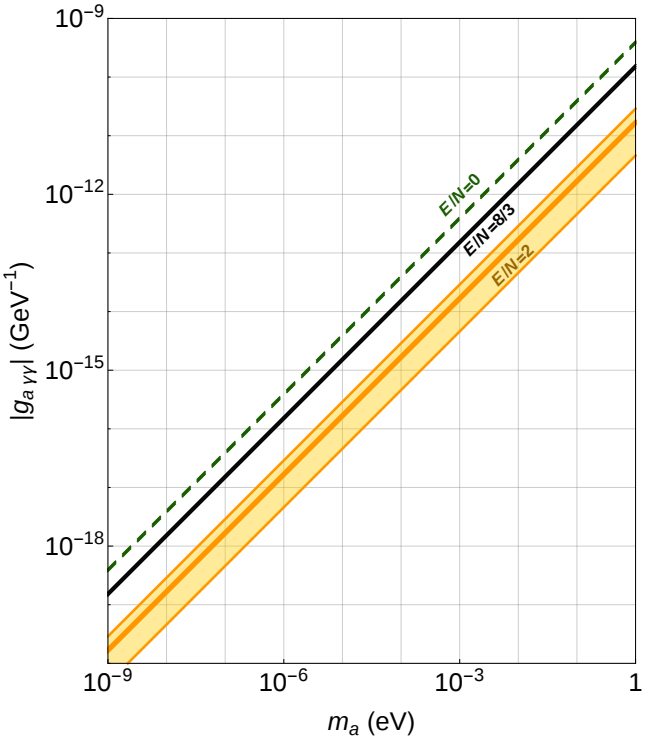

Figure 5.3: The relation between the axion mass and its coupling to photons for the three reference models with $E/N = 0$, $8/3$ and 2. Notice the larger relative uncertainty in the latter model due to the cancellation between the UV and IR contributions to the anomaly (the band corresponds to 2σ errors.). Values below the lower band require a higher degree of cancellation.

5.1.4 Coupling to matter

Axion couplings to matter are more model dependent as they involve all the UV couplings defining the effective axial current in eq. (4.50). Of course, there is also a model independent contribution from the axion coupling to gluons and to a less extent to the other gauge bosons.

Derivative interactions with leptons are simple since they can be read off directly from the UV Lagrangian up to one loop effects coming from the coupling to the EW gauge bosons. The latter are particularly important for hadronic axions, where axions do not couple to quarks and leptons at tree-level, as they generate higher-order axion-lepton couplings [246].

Interactions with hadrons are more delicate because they involve matching hadronic to elementary quark physics. Phenomenologically the most interesting ones are the axion couplings to nucleons, which could in principle be tested from

long range force experiments, or from dark-matter direct-detection like experiments. They also affect stellar energy-loss rate from nucleon bremsstrahlung.

In principle we could attempt to follow a similar procedure to the one used in the previous section, namely to employ chiral Lagrangians with baryons and use known experimental data to extract the necessary low energy couplings. Unfortunately effective Lagrangians involving baryons are on much less solid ground—there are no parametrically large energy gaps in the hadronic spectrum to justify the use of low energy expansions.

A much safer thing to do is to use an effective theory valid at energies much lower than the QCD mass gaps $\Delta \sim \mathcal{O}(100\text{ MeV})$. In this regime nucleons are non-relativistic, their number is conserved and they can be treated as external fermionic currents. For exchanged momenta q parametrically smaller than Δ, heavier modes are not excited and the effective field theory is under control. The axion, as well as the electro-weak gauge bosons, enters as classical sources in the effective Lagrangian, which would otherwise be a free non-relativistic Lagrangian at leading order. At energies much smaller than the QCD mass gap the only active flavor symmetry we can use is isospin, which is explicitly broken only by the small quark masses (and QED effects). The leading order effective Lagrangian for the 1-nucleon sector reads

$$\mathcal{L}_N = \bar{N} v^\mu D_\mu N + 2 g_A \, A^i_\mu \, \bar{N} S^\mu \sigma^i N + 2 g_0^q \, \hat{A}^q_\mu \, \bar{N} S^\mu N + \sigma \langle M_a \rangle \bar{N} N + b \bar{N} M_a N + \dots \tag{5.39}$$

where $N = (p, n)$ is the isospin doublet nucleon field, v^μ is the four-velocity of the non-relativistic nucleons, $D_\mu = \partial_\mu - V_\mu$, V_μ is the vector external current, σ^i are the Pauli matrices, the index $q = (\frac{u+d}{2}, s, c, b, t)$ runs over isoscalar quark combinations, $2\bar{N} S^\mu N = \bar{N} \gamma^\mu \gamma_5 N$ is the nucleon axial current, the matrix field $M_a = \cos(Q_a a / f_a) \mathrm{diag}(m_u, m_d)$, and A^i_μ and $\hat{A}^q_\mu$ are the axial isovector and isoscalar external currents respectively. Neglecting SM gauge bosons, the external currents only depend on the axion field as follows

$$\hat{A}^q_\mu = c_q \frac{\partial_\mu a}{2 f_a} \,, \qquad A^3_\mu = c_{(u-d)/2} \, \frac{\partial_\mu a}{2 f_a} \,, \qquad A^{1,2}_\mu = V_\mu = 0 \,, \tag{5.40}$$

where we used the short-hand notation $c_{(u \pm d)/2} \equiv \frac{c_u \pm c_d}{2}$. The couplings $c_q = c_q(Q)$ computed at the scale Q will in general differ from the high scale ones because of the running of the anomalous axial current [247]. In particular under RG evolution the couplings $c_q(Q)$ mix, so that in general they will all be different from zero at low energy. We explain the details of this effect in appendix B.3.

Note that the linear axion couplings to nucleons are all contained in the derivative interactions through A_μ while there are no linear interactions[1] coming from the non derivative terms contained in M_a. In Eq. (5.39) dots stand for higher order terms involving higher powers of the external sources V_μ, A_μ, and M_a. Among these the leading effects to the axion-nucleon coupling will come from isospin breaking terms $\mathcal{O}(M_a A_\mu)$.[2] These corrections are small $\mathcal{O}(\frac{m_d - m_u}{\Delta})$, below the uncertainties associated to our determination of the effective coupling g_0^q, which are extracted from lattice simulations performed in the isospin limit.

The effective field theory of eq. (5.39) should not be confused with the usual heavy baryon chiral Lagrangian [248] because here pions have been integrated out. The advantage of using this Lagrangian is clear: for axion physics the relevant scale is of order m_a, so higher order terms are negligibly small $\mathcal{O}(m_a/\Delta)$. The price to pay is that the couplings g_A and g_0^q can only be extracted from very low-energy experiments or lattice QCD simulations. Fortunately the combination of the two will be enough for our purposes.

Actually at the leading order in the isospin breaking expansion, g_A and g_0^q can simply be extracted by matching single nucleon matrix elements computed with the axion UV Lagrangian (4.34) and with the effective axion-nucleon theory (5.39). The result is given by

$$g_A = \Delta u - \Delta d\,, \quad g_0^q = (\Delta u + \Delta d, \Delta s, \Delta c, \Delta b, \Delta t)\,, \quad s^\mu \Delta q \equiv \langle p|\bar{q}\gamma^\mu\gamma_5 q|p\rangle\,, \tag{5.41}$$

where $|p\rangle$ is a proton state at rest, s^μ its spin and we used isospin symmetry to relate proton and neutron matrix elements. Note that the isoscalar matrix elements Δq inside g_0^q depend on the matching scale Q, such dependence is however canceled once the couplings $g_0^q(Q)$ are multiplied by the corresponding UV couplings $c_q(Q)$ inside the isoscalar currents $\hat{A}_\mu^q$. Non-singlet combinations such as g_A are instead protected by non-anomalous Ward identities, as long as we use renormalization schemes which preserve them. For future convenience we set the matching scale $Q = 2$ GeV.

Writing the EFT Lagrangian (5.39) directly in terms of the UV couplings leads to

$$\mathcal{L}_N = \bar{N} v^\mu D_\mu N + \frac{\partial_\mu a}{f_a}\Big\{\frac{c_u - c_d}{2}(\Delta u - \Delta d)\bar{N} S^\mu \sigma^3 N$$

[1] This is no longer true in the presence of extra CP violating operators such as those coming from the CKM phase or new physics. The former are known to be very small, while the latter are more model dependent and we will not discuss them in the current work.

[2] Axion couplings to EDM operators also appear at this order.

$$+\left[\frac{c_u+c_d}{2}(\Delta u+\Delta d)+\sum_{q=s,c,b,t} c_q\Delta q\right]\bar{N}S^\mu N\Big\}\,. \quad (5.42)$$

It just remains to determine the matrix elements Δq.

The isovector combination can be accurately determined from neutron beta decay [51]

$$\Delta u-\Delta d=g_A=1.2723(23)\,, \quad (5.43)$$

which is renormalization-scale independent. The tiny neutron-proton mass splitting $m_n-m_p=1.3$ MeV guarantees that we are within the regime of our effective theory. The uncertainty quoted is experimental and does not include possible isospin-breaking corrections.

Unfortunately we do not have other low energy experimental inputs to determine the remaining matrix elements. Until now such information has been extracted from a combination of deep-inelastic-scattering data and semi-leptonic hyperon decays: the former suffer from uncertainties coming from the integration over the low-x kinematic region, which is known to give large contributions to the observable of interest; the latter are not really within the EFT regime, which does not allow a reliable estimate of the accuracy.

Opportunely lattice simulations have recently started producing direct reliable results for these matrix elements. From [249–254] (see also [255, 256]) we extract the following inputs computed at $Q=2$ GeV in $\overline{\text{MS}}$

$$g_0^{ud}=\Delta u+\Delta d=0.521(53)\,,\qquad \Delta s=-0.026(4)\,,\qquad \Delta c=\pm 0.004\,. \quad (5.44)$$

Details of the derivation are contained in appendix B.1. Notice that the charm spin content is so small that its value has not been determined yet, only an upper bound exists. Similarly we can neglect the analogous contributions from bottom and top quarks which are expected to be even smaller. As mentioned before, lattice simulations do not include isospin breaking effects, these are however expected to be smaller than the current uncertainties. Combining eqs. (5.43) and (5.44) we obtain the individual matrix elements with good precision

$$\Delta u=0.897(27)\,,\qquad \Delta d=-0.376(27)\,,\qquad \Delta s=-0.026(4)\,, \quad (5.45)$$

evaluated at the renormalization scale $Q=2$ GeV.

Using the values in eq. (5.45) we can obtain the axion-nucleon couplings:

$$\begin{aligned} c_p &= -0.47(3)+0.88(3)c_u^0-0.39(2)c_d^0-0.038(5)c_s^0 \\ &\quad -0.012(5)c_c^0-0.009(2)c_b^0-0.0035(4)c_t^0\,, \\ c_n &= -0.02(3)+0.88(3)c_d^0-0.39(2)c_u^0-0.038(5)c_s^0 \end{aligned}$$

$$- 0.012(5)c_c^0 - 0.009(2)c_b^0 - 0.0035(4)c_t^0\,, \tag{5.46}$$

which are defined in analogy to the couplings to quarks as

$$\mathcal{L}_{aNN} = \frac{\partial_\mu a}{2f_a} c_N \bar{N}\gamma^\mu\gamma_5 N\,, \tag{5.47}$$

and are scale invariant (as they are defined in the effective theory below the QCD mass gap). The errors in eq. (5.46) include the uncertainties from the lattice data and those from higher order corrections in the perturbative RG evolution of the axial current (the latter is only important for the coefficients of $c^0_{s,c,b,t}$). The couplings c_q^0 are those appearing in eq. (4.31) computed at the high scale $f_a = 10^{12}$ GeV. The effect of varying the matching scale to a different value of f_a within the experimentally allowed range is smaller than the theoretical uncertainties.

We make some observations about the result (5.46). The theoretical errors quoted here are dominated by the lattice results, which for these matrix elements are still in an early phase and the systematic uncertainties are not fully explored yet. Still the error on the final result is already good (below ten percent), and there is room for a large improvement which is expected in the near future. Note that when the uncertainties decrease sufficiently for results to become sensitive to isospin breaking effects, new couplings will appear in eq. (5.39). These could in principle be extracted from lattice simulations by studying the explicit quark mass dependence of the matrix element. In this regime the experimental value of the isovector coupling g_A cannot be used anymore because of different isospin breaking corrections to charged versus neutral currents.

The numerical values of the couplings we get are not too far off those already in the literature (see e.g. [51]). However, because of the caveats in the relation of the deep inelastic scattering and hyperon data to the relevant matrix elements the uncertainties in those approaches are not under control. On the other hand the lattice uncertainties are expected to be reduced in the near future, which would further improve the precision of the estimate performed with the technique presented here.

The numerical coefficients in eq. (5.46) include the effect of running from the high scale f_a (here fixed to 10^{12} GeV) to the matching scale $Q = 2$ GeV, which we performed at the NLLO order (more details in appendix B.3). The running effects are evident from the fact that the couplings to nucleons depend on all quark couplings including charm, bottom and top, even though we took the corresponding spin content to vanish. This effect has been neglected in previous analysis.

Finally it is interesting to notice that there is a cancellation in the model independent part of the axion coupling to the neutron in KSVZ-like models, where $c_q^0 = 0$,

$$c_p^{\text{KSVZ}} = -0.47(3)\,, \qquad c_n^{\text{KSVZ}} = -0.02(3)\,, \tag{5.48}$$

the coupling to neutrons is suppressed with respect to the coupling to protons by a factor $\mathcal{O}(10)$ at least, in fact this coupling still is compatible with zero. The cancellation can be understood from the fact that, neglecting running and sea quark contributions

$$c_n \sim \left\langle Q_a \cdot \begin{pmatrix} \Delta d & 0 \\ 0 & \Delta u \end{pmatrix} \right\rangle \propto m_d \Delta d + m_u \Delta u\,, \tag{5.49}$$

and the down-quark spin content of the neutron Δu is approximately $\Delta u \approx -2\Delta d$, *i.e.* the ratio m_u/m_d is accidentally close to the ratio between the number of up over down valence quarks in the neutron. This cancellation may have important implications on axion detection and astrophysical bounds.

In models with $c_q^0 \neq 0$ both the couplings to proton and neutron can be large, for example for the DFSZ axion models, where $c_{u,c,t}^0 = \frac{1}{3}\sin^2\beta = \frac{1}{3} - c_{d,s,b}^0$ at the scale $Q \simeq f_a$, we get

$$c_p^{\text{DFSZ}} = -0.617 + 0.435\sin^2\beta \pm 0.025\,, \qquad c_n^{\text{DFSZ}} = 0.254 - 0.414\sin^2\beta \pm 0.025\,. \tag{5.50}$$

A cancellation in the coupling to neutrons is still possible for special values of $\tan\beta$.

5.2 Properties at finite temperature

Axions can be produced thermally in the early universe from its coupling to the SM particles in the thermal bath, in particular from the coupling to gluons, for sufficiently small values of f_a. This population of hot axions would be subdominant for the allowed values of f_a [257–260], but it gives a small contribution to the total relativistic energy fraction, usually parametrized by the effective number of neutrinos. Other mechanisms of axion production do not rely on its interactions with SM particles. The misalignment mechanism [191–193] is the most model independent and is almost completely determined by the shape of the axion potential at finite temperature and its zero temperature mass. Hence the importance of the temperature dependence of this quantities as they control the relic abundance of axions today (for a review see e.g. [261]). Radiation from topological defects (strings and domain walls), which can be present if the PQ symmetry is restored after inflation, can be the dominant source of dark matter

[262–268]. Their contribution also depends on the finite temperature behavior of the axion potential; although large uncertainties, associated to the dynamical evolution of these topological defects (for a recent numerical study see e.g. [269]), may change the predicted abundance by two orders of magnitude.

At low temperature we perform a high precision computation based on chiral Lagrangians, whose convergence degrades as the temperature approaches the critical value $T_c \simeq$160-170 MeV where QCD starts deconfining. At T_c the chiral approach is already out of control. Fortunately around the QCD cross-over region lattice computations are possible. The current precision is not yet competitive with our low temperature results but they are expected to improve soon. One expects the dilute instanton gas approximation to provide a reliable estimate for $T \gg T_c$, where a perturbative computation is well behaved. However finite temperature QCD converges fast only for very high temperatures, above $\mathcal{O}(10^6)$ GeV (see e.g. [270]). The instanton computation is especially problematic due to an exponential sensitivity to quantum thermal loop effects. In fact, the resulting uncertainty on the axion mass and potential can easily be one order of magnitude or more!

5.2.1 Behavior of the potential

Below the critical temperature axion properties can be reliably computed using finite temperature chiral Lagrangians [271, 272]. In this region finite temperature effects are exponentially suppressed thanks to the QCD mass gap. Temperature dependence can be computed by simply evaluating the loop corrections using the corresponding sum-integrals (see eg. [273]). It can only arise from (non-local) loop corrections that can feel the finite temperature.

The leading temperature dependence of the potential, contained in vacuum graphs with virtual pions, is given by

$$\frac{V(a;T)}{V(a)} = 1 + \frac{3}{2}\frac{T^4}{f_\pi^2 m_\pi^2\left(\frac{a}{f_a}\right)}\, J_0\left[\frac{m_\pi^2\left(\frac{a}{f_a}\right)}{T^2}\right] , \tag{5.51}$$

with loop integrals J_n defined as

$$J_0[\xi] \equiv -\frac{1}{\pi^2}\int_0^\infty dq\, q^2 \log\left(1 - e^{-\sqrt{q^2+\xi}}\right) , \quad J_n[\xi] = \frac{1}{(n-1)!}\left(-\frac{\partial}{\partial\xi}\right)^n J_0[\xi]. \tag{5.52}$$

By taking the second derivative of the potential we easily get the temperature dependent axion mass

$$\frac{m_a^2(T)}{m_a^2} = \frac{\chi_{top}(T)}{\chi_{top}} \overset{\text{NLO}}{=} \frac{m_\pi^2(T) f_\pi^2(T)}{m_\pi^2 f_\pi^2} = \frac{\langle\bar{q}q\rangle_T}{\langle\bar{q}q\rangle} = 1 - \frac{3}{2}\frac{T^2}{f_\pi^2}\, J_1\left[\frac{m_\pi^2}{T^2}\right] , \tag{5.53}$$

where we have used a recursive relation of the J_n functions. At one loop the axion mass only receives contributions from the local NLO couplings once rewritten in terms of the physical m_π and f_π [274]. Therefore the leading temperature dependence is completely determined by the temperature dependence of m_π and f_π, and in particular is the same as that of the chiral condensate [271, 272, 274]. The function $J_1(\xi)$ approaches asymptotically to $\xi^{1/4}e^{-\sqrt{\xi}}/(2\pi)^{3/2}$ at large ξ and to $1/12$ at small ξ. Note that in the ratio $m_a^2(T)/m_a^2$ the dependence on the quark masses and the NLO couplings cancel out. This means that, at $T \ll T_c$, this ratio is known at a even better precision than the axion mass at zero temperature itself. The temperature dependence of the quartic self-coupling is also extracted from the potential

$$\frac{\lambda_a(T)}{\lambda_a} = 1 - \frac{3}{2}\frac{T^2}{f_\pi^2} J_1\left[\frac{m_\pi^2}{T^2}\right] + \frac{9}{2}\frac{m_\pi^2}{f_\pi^2}\frac{m_u m_d}{m_u^2 - m_u m_d + m_d^2} J_2\left[\frac{m_\pi^2}{T^2}\right] . \tag{5.54}$$

Higher order corrections are small for all values of T below T_c. There are also contributions from the heavier states that are not captured by the low energy Lagrangian. In principle these are exponentially suppressed by $e^{-m/T}$, where m is the mass of the heavy state. However, because the ratio m/T_c is not very large and a large number of states appear above T_c there is a large effect at around T_c, where the chiral expansion ceases to reliably describe QCD physics. An in depth discussion of such effects appears in [275] for the similar case of the chiral condensate.

In summary, eqs. (5.51), (5.53) and (5.54) work very well for $T \lesssim T_c$, while at some temperature close to T_c they no longer apply and full non-perturbative QCD computations are needed.

Around the crossover the theory is clearly non-perturbative and information is obtained by means of lattice QCD simulations. For sufficiently high temperature perturbation theory is expected to work, such that the potential can be computed under the dilute instanton gas approximation [226]. Contrary to the zero temperature case, where large gauge configurations dominate because of the larger gauge coupling, at high temperature these are exponentially suppressed due to Debye screening. This justifies the instanton computation.

The axion effective potential is calculated in terms of the single instanton contribution to the partition function and has the form

$$V^{inst}(a;T) = -f_a^2 m_a^2(T)\cos(a/f_a)\,, \tag{5.55}$$

where

$$f_a^2 m_a^2(T) \simeq 2\int d\rho\, n(\rho,0) e^{-\frac{2\pi^2}{g_s^2} m_{D1}^2 \rho^2 + \dots} . \tag{5.56}$$

Here the integral is over the instanton size ρ, $n(\rho,0) \propto \Pi_q \det(\not{D} + m_q) e^{-8\pi^2/g_s^2}$ is the zero temperature instanton density proportional to the quark determinant, $m_{D1}^2 = g_s^2 T^2 (1+n_f/6)$ is the Debye mass squared at LO, n_f is the number of flavor degrees of freedom active at the temperature T, and the dots stand for smaller corrections (see [226] for more details[1]). The functional dependence of eq. (5.56) on temperature is approximately a power law $T^{-\alpha}$ where $\alpha \approx 7 + n_f/3 + \ldots$ is fixed by the QCD beta function.

Nevertheless the dilute instanton gas approximation suffers from a serious problem. It relies on finite temperature perturbative QCD, which is valid at very high temperatures $T \gtrsim 10^6$ GeV due to IR divergences of the thermal bath [279]. Moreover, the temperature dependent axion mass, being exponentially sensitive to quantum corrections, converges even worse than other observables. Indeed lattice simulations [280, 281] and NLO perturbative computations [282–284] suggest an order one deviation from the LO perturbative estimate of the Debye mass, for temperatures around few GeV. As the axion mass depends exponentially on the Debye mass, higher order effects can easily shift its value at a given temperature by an order of magnitude or more. Even the shape of the potential in eqs. (5.55), (5.56) and the functional dependence on the temperature may be questioned. Thus non-perturbative methods as lattice QCD are highly appreciated.

There are lattice simulations [204, 228] for temperatures around T_c and above, which however do not correspond to real QCD. Although they provide useful insights, numerical results should be treated with care. They use light-quark masses which are heavier than the physical ones (corresponding to larger pion masses) and rather coarse lattice spacing. It is essential for future lattice computations to use the right quark masses and to perform a reliable extrapolation to the continuum limit.

Very recently, in refs. [229, 285, 286] the temperature dependence of the topological susceptibility above T_c have been studied with physical quark masses and performing the continuum limit. The simulations use different techniques and approximations to overcome the difficulties of this type of computations. The results however do not agree and further studies are requiered to get a reliable estimate only based on first principle QCD. These large uncertainties in the temperature dependence above the crossover are transfered to the calculation of the axion relic density.

[1]The instanton density was first computed by 't Hooft [276] at one-loop for number of colors $N_c = 2$, it was generalized by Bernard [277] to arbitrary N_c and computed at finite temperature in ref. [226]. The ultraviolet divergent part of the two-loop correction to the vacuum energy in the presence of an instanton background field was calculated in [278], resulting in a two-loop renormalization group invariant size distribution.

5.2.2 Dark matter abundance

The axion relic density and the features of the production mechanisms in the early universe depend sensibly on whether PQ symmetry is broken or not after inflation. First we consider the case where PQ symmetry is broken before inflation ($H_I \lesssim f_a$) and the universe is not reheated beyond the PQ scale ($T_{\max} \lesssim f_a$). At some moment of the cosmic evolution the temperature of the universe falls below the PQ scale, then the scalar field Φ, which contains the axions as a phase, develops a VEV spontaneously breaking the PQ symmetry. While still at $T \gg \Lambda_{\rm QCD}$, the axion potential is negligible and the exponential expansion during inflation renders the axion field homogeneously constant over the observable universe, with initial value $a(x) = \theta_0 f_a$, $(0 \leq \theta_0 \leq 2\pi)$.

Between the PQ phase transition and the QCD crossover, the evolution of the axion field, in particular of its zero mode, is determined by the equation

$$\ddot{a} + 3H\dot{a} + m_a^2(T)\, f_a \sin\left(\frac{a}{f_a}\right) = 0\,. \tag{5.57}$$

where we assumed that the shape of the axion potential is well described by the dilute instanton gas approximation, eq. (5.55). As the Universe cools, the Hubble parameter decreases while the axion potential grow. When the pull from the latter becomes comparable to the Hubble friction, i.e. $m_a(T) \sim 3H$, the axion field starts oscillating with frequency m_a. This typically happens at temperatures above T_c, around the GeV scale, depending on the value of f_a and the temperature dependence of the axion mass. Soon after that the comoving number density $n_a = \langle m_a a^2 \rangle$ becomes an adiabatic invariant and the axion behaves as cold dark matter.

The other possibility is that PQ symmetry is broken after inflation. At temperatures around the PQ breaking scale v_{PQ}, the axion field is randomly distributed over the interval $[0, 2\pi f_a]$ in different regions of space, which in this case remain causally connected. Such field configurations imply the formation of topological defects, like strings and domain walls. These decay into axions, whose abundance is affected by large uncertainties associated with the evolution and decay of the topological defects. Independently of this evolution there is a misalignment contribution to the dark matter relic density from axion modes with very close to zero momentum. The calculation of this is the same as for the case where inflation happens after PQ breaking, except that the relic density must be averaged over all possible values of θ_0. While the misalignment contribution gives only a part of the full abundance, it can still be used to give an upper bound to f_a in this scenario.

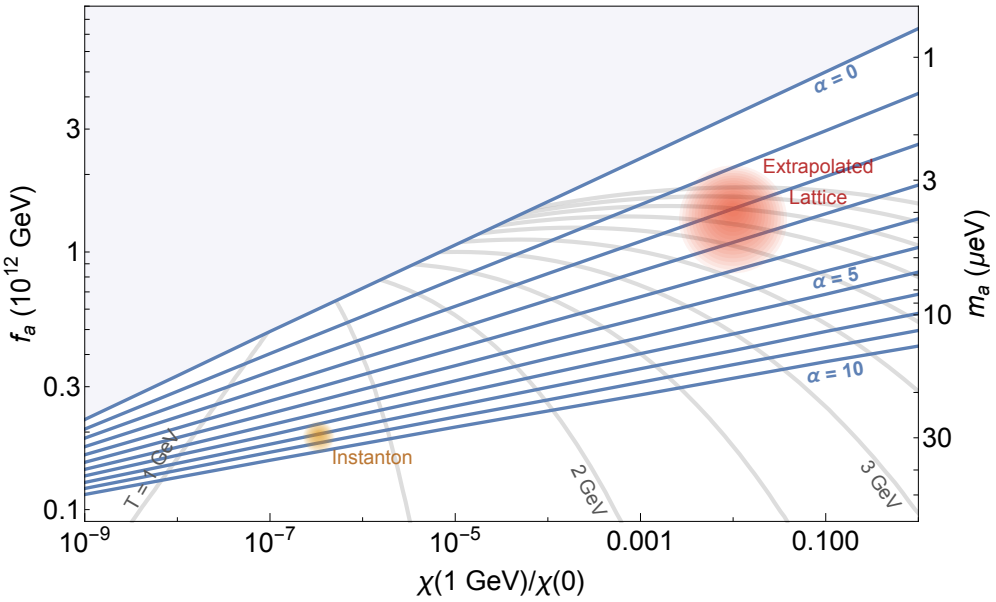

Figure 5.4: Values of f_a such that the misalignment contribution to the axion abundance matches the observed dark matter one for different choices of the parameters of the axion mass dependence on temperature. For definiteness the plot refers to the case where the PQ phase is restored after the end of inflation (corresponding approximately to the choice $\theta_0 = 2.15$). The temperatures where the axion starts oscillating, i.e. satisfying the relation $m_a(T) = 3H(T)$, are also shown. The two points corresponding to the dilute instanton gas prediction and the recent preliminary lattice data are shown for reference.

The current axion abundance from misalignment, assuming standard cosmological evolution, is given by

$$\Omega_a = \frac{86}{33}\frac{\Omega_\gamma}{T_\gamma}\frac{n_a^\star}{s^\star}m_a\,, \tag{5.58}$$

where Ω_γ and T_γ are the current photon abundance and temperature respectively and $s^\star$ and $n_a^\star$ are the entropy density and the average axion number density computed at any moment in time $t_\star$ sufficiently after the axion starts oscillating such that $n_a^\star/s^\star$ is constant. The latter quantity can be obtained by solving eq. (5.57) and depends on 1) the QCD energy and entropy density around T_c, 2) the initial condition for the axion field θ_0, and 3) the temperature dependence of the axion mass and potential. The first is reasonably well known from perturbative methods and lattice simulations (see e.g. [287, 288]). The initial value θ_0

is a free parameter in the first scenario, where the PQ transition happen before inflation—since in this case θ_0 can be chosen in the whole interval $[0, 2\pi]$ only an upper bound to Ω_a can be obtained in this case. In the scenario where the PQ phase is instead restored after inflation $n_a^\star$ is obtained by averaging over all θ_0, which numerically corresponds to choosing[1] $\theta_0 \simeq 2.1$. Since θ_0 is fixed, Ω_a is completely determined as a function of f_a in this case. At the moment the biggest uncertainty on the misalignment contribution to Ω_a comes from our knowledge of $m_a(T)$. Assuming that $m_a(T)$ can be approximated by the power law

$$m_a^2(T) = m_a^2(1\text{ GeV})\left(\frac{\text{GeV}}{T}\right)^\alpha = m_a^2\,\frac{\chi(1\text{ GeV})}{\chi(0)}\left(\frac{\text{GeV}}{T}\right)^\alpha ,$$

around the temperatures where the axion starts oscillating, eq. (5.57) can easily be integrated numerically. In fig. 5.4 we plot the values of f_a that would reproduce the correct dark matter abundance for different choices of $\chi(T)/\chi(0)$ and α in the scenario where θ_0 is integrated over. We also show two representative points with parameters ($\alpha \approx 8$, $\chi(1\text{ GeV})/\chi(0) \approx$ few 10^{-7}) and ($\alpha \approx 2$, $\chi(1\text{ GeV})/\chi(0) \approx 10^{-2}$) corresponding respectively to the expected behavior from instanton computations and to the suggested one from the preliminary lattice data in [205]. The figure also shows the corresponding temperature at which the axion starts oscillating, here defined by the condition $m_a(T) = 3H(T)$.

It is important to mention that for large values of α, as predicted by instanton computations, the sensitivity to the overall size of the axion mass at fixed temperature ($\chi(1\text{ GeV})/\chi(0)$) is weak. However if the slope of the axion mass with the temperature is much smaller, as suggested by the results in [205], then the corresponding value of f_a required to give the correct relic abundance can even be larger by an order of magnitude (note also that in this case the temperature at which the axion starts oscillating would be higher, around $4 \div 5$ GeV). The difference between the two cases could be taken as an estimate of the current uncertainty on this type of computation. More accurate lattice results would be very welcome to assess the actual temperature dependence of the axion mass and potential.

To show the impact of this uncertainty on the viable axion parameter space and the experiments probing it, in fig. 5.5 we plot the various constraints as a function of the Hubble scale during inflation and the axion decay constant. Limits that depend on the temperature dependence of the axion mass are shown for the instanton and lattice inspired forms (solid and dashed lines respectively), corresponding to the labeled points in fig. 5.4. On the right side of the plot we

[1] The effective θ_0 corresponding to the average is somewhat bigger than $\langle\theta^2\rangle = \pi^2/3$ because of anharmonicities of the axion potential.

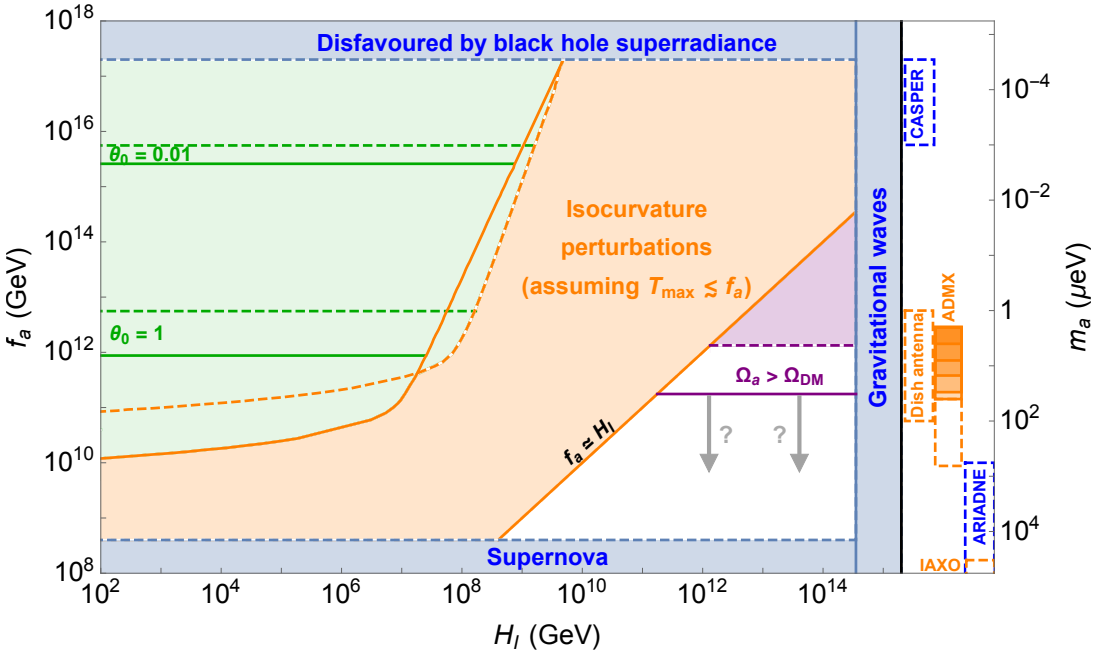

Figure 5.5: The axion parameter space as a function of the axion decay constant and the Hubble parameter during inflation. The bounds are shown for the two choices for the axion mass parametrization suggested by instanton computations (continuous lines) and by preliminary lattice results (dashed lines), corresponding to the labeled points in fig. 5.4. In the green shaded region the misalignment axion relic density can make up the entire dark matter abundance, and the isocurvature limits are obtained assuming that this is the case. In the white region the axion misalignment population can only be a sub-dominant component of dark matter. The region where PQ symmetry is restored after inflation does not include the contributions from topological defects, the lines thus only represent conservative upper bounds to the value of f_a. Ongoing (solid) and proposed (dashed empty) experiments testing the available axion parameter space are represented on the right side.

also show the values of f_a that will be probed by ongoing experiments (solid) and those that could be probed by proposed experiments (dashed empty). Orange colors are used for experiments using the axion coupling to photons, blue for the others. Experiments in the last column (IAXO and ARIADNE) do not rely on the axion being dark matter. The boundary of the allowed axion parameter space is constrained by the CMB limits on tensor modes [289], supernova SN1985 and other astrophysical bounds including black-hole superradiance.

When the PQ preserving phase is not restored after inflation (i.e. when both the Hubble parameter during inflation H_I and the maximum temperature after inflation T_{max} are smaller than the PQ scale) the axion abundance can match the observed dark matter one for a large range of values of f_a and H_I by varying the initial axion value θ_0. In this case isocurvature bounds [290] (see e.g. [291] for a recent discussion) constrain H_I from above. At small f_a obtaining the correct relic abundance requires θ_0 to be close to π, where the potential is flat, so the the axion begins oscillating at relatively late times. In the limit $\theta_0 \to \pi$ the axion energy density diverges. Given the sensitivity of Ω_a to θ_0 in this regime, isocurvatures are enhanced by $1/(\pi - \theta_0)$ and the bound on H_I is thus strengthened by a factor $\pi - \theta_0$.[1] Meanwhile, the axion decay constant is bounded from above by black-hole superradiance. For smaller values of f_a axion misalignment can only explain part of the dark matter abundance. In fig. 5.5 we show the value of f_a required to explain Ω_{DM} when $\theta_0 = 1$ and $\theta_0 = 0.01$ for the two reference values of the axion mass temperature parameters.

If the PQ phase is instead restored after inflation, e.g. for high scale inflation models, θ_0 is not a free parameter anymore. In this case only one value of f_a will reproduce the correct dark matter abundance. Given our ignorance about the contributions from topological defect we can use the misalignment computation to give an upper bound on f_a. This is shown on the bottom-right side of the plot, again for the two reference models, as before. Contributions from higher-modes and topological defects are likely to make such bound stronger by shifting the forbidden region downwards. Note that while the instanton behavior for the temperature dependence of the axion mass would point to axion masses outside the range which will be probed by ADMX (at least in the current version of the experiment), if the lattice behavior will be confirmed the mass window which will be probed would look much more promising.

[1] This constraint guarantees that we are consistently working in a regime where quantum fluctuations during inflation are much smaller than the distance of the average value of θ_0 from the top of the potential.

Chapter 6

Conclusions

We computed the mass of the MSSM Higgs boson and several QCD axion properties with high precision. For this task, effective field theory methods proved to be very powerful.

The Higgs mass calculation improves previous computations by including extra two-loop SUSY threshold corrections, the contributions from the sbottom/stau sectors relevant at large tan β and the implementation of the OS scheme, the relevant formulas can be found in the appendix A.2 and in [111].

We also performed a study of the theoretical uncertainties, showing that for most of the relevant parameter space the error is sub-GeV and dominated by higher order SM corrections. The result is summarized in fig. 3.10. The recent inclusion of the SM NNNLO corrections leading in the strong coupling and the effect of the dimension six operators allow to have more control on our estimate of the theoretical uncertainty.

The computation has been arranged into an efficient computer package which we made publicly available [111]. The code exploits the power of the EFT approach, allowing to compute the Higgs mass for arbitrary heavy sparticles, even when a large hierarchy between fermions and scalars is present. Analytic formulas for the solution of the RGE make the code very fast, which allows to efficiently use the Higgs mass as a constraint on the spectrum.

We then performed several studies on the implication of the Higgs mass constraint on SUSY:

- In agreement with previous EFT computation we find that the SUSY spectrum needs to be a little heavier than expected, in particular stops below 2 TeV are disfavored (see fig. 3.7).

- The upper bound on the SUSY spectrum, which is $\mathcal{O}(10^{10})$ GeV ($\mathcal{O}(10^4)$ GeV at large $\tan\beta$), can actually be relaxed without adding new degrees of freedom. At very large $\tan\beta$, if μ is not suppressed with respect to the scalar masses, sbottom/stau contributions may reduce the Higgs mass, allowing larger values for the SUSY scale (see fig. 3.8).

- In mini-split SUSY, in the region of parameter space relevant for the Higgs mass, the effect of the thresholds from splitting the fermions from the scalars is completely captured by the leading fixed order one loop corrections (see fig. 3.9). This allows to use the SM as an effective field theory all the way up to the scalar mass scale, avoiding the need of using an intermediate split SUSY effective theory.

- We point out that the value of the Higgs mass may be used to predict the spectrum of minimal gauge mediation, the simplest calculable SUSY model, almost completely. The spectrum of SUSY in this case can thus be bounded just by experimental data alone without the need of arguments based on naturalness. Interestingly enough the spectrum lies just above the expected reach of LHC14 (see fig. 3.16), making it an ideal target for a future 100 TeV hadron machine.

- Finally we discuss about the analogous implications for lopsided gauge mediation and anomaly mediation models, constraining the allowed values of $\tan\beta$ and the parameter space (see figs. 3.17 and 3.18).

For most of the allowed parameter space the Higgs mass computation is dominated by the experimental uncertainty in the top mass. The theoretical uncertainties instead are mostly dominated by the SM higher order corrections. Only for maximal stop mixing and at the lightest possible stop masses uncertainties from SUSY corrections and from higher-order terms in the EFT expansion may become important. Improvements in this region can be achieved by including subleading two-loop SUSY threshold corrections neglected in this work, such as $\mathcal{O}(\alpha\alpha_{s,t})$ or $\mathcal{O}(\alpha_t\alpha_s^2)$.

Regarding the physics of the QCD axion, we explain how several properties can be computed with high accuracy, despite of being controlled by non perturbative dynamics. More specifically, we calculated higher order corrections to the axion potential and its derived quantities (mass, self-coupling, domain-wall tension), as well as the coupling to photons, providing numerical estimates for these quantities with percent accuracy. We also showed how lattice data can be used to extract the axion-nucleon couplings reliably, estimating their values with better than 10% precision. These results are important both experimentally, to assess the actual

axion parameter space probed and to design new experiments, and theoretically, since in the case of a discovery they would help determining the underlying theory behind the PQ breaking scale.

We also considered the temperature dependence of the axion mass and potential, which are relevant to determine the axion relic density. At low temperature, we computed accurately this dependence using chiral Lagrangians. However, we comment that close to the crossover region and above, perturbative methods like the instanton gas approximation, are unreliable due to serious convergence problems of the QCD perturbative expansion at finite temperature. We analyze the effect of this uncertainty on the calculation of the axion relic abundance and the bounds on the axion parameter space. As a consequence, more dedicated non-perturbative computations such as lattice QCD are needed to reliably determine the axion relic abundance today.

Appendix A

Details of the Higgs mass calculation

A.1 Interpolating functions and coefficients

When the gluino mass is of the order of the degenerate stop mass, we obtain an approximate expression by expanding up to the quadratic order in power of $(m_{\tilde{g}} - m_{\tilde{t}})/m_{\tilde{t}}$, given by

$$\begin{aligned}
\Delta m_h^{2,(\alpha_t\alpha_s)} = \frac{\alpha_s m_t^4}{\pi^3 v^2}\Bigg\{ & -3\ln^2\frac{m_{\tilde{t}}^2}{m_t^2} - 6\ln\frac{m_{\tilde{t}}^2}{m_t^2} + 6\frac{X_t}{m_{\tilde{t}}} - 3\frac{X_t^2}{m_{\tilde{t}}^2} - \frac{3}{4}\frac{X_t^4}{m_{\tilde{t}}^4} \\
& + \left(\frac{m_{\tilde{g}} - m_{\tilde{t}}}{m_{\tilde{t}}}\right)\left[-\frac{28}{9} + \frac{86}{9}\frac{X_t}{m_{\tilde{t}}} - 4\frac{X_t}{m_{\tilde{t}}}\ln\frac{m_{\tilde{t}}^2}{m_t^2} + 8\frac{X_t^2}{m_{\tilde{t}}^2} - 4\frac{X_t^2}{m_{\tilde{t}}^2}\ln\frac{m_{\tilde{t}}^2}{m_t^2}\right. \\
& \qquad \left. - \frac{32}{9}\frac{X_t^3}{m_{\tilde{t}}^3} + \frac{2}{3}\frac{X_t^3}{m_{\tilde{t}}^3}\ln\frac{m_{\tilde{t}}^2}{m_t^2} - \frac{26}{9}\frac{X_t^4}{m_{\tilde{t}}^4} + \frac{2}{3}\frac{X_t^4}{m_{\tilde{t}}^4}\ln\frac{m_{\tilde{t}}^2}{m_t^2}\right] \\
& + \left(\frac{m_{\tilde{g}} - m_{\tilde{t}}}{m_{\tilde{t}}}\right)^2\left[\frac{\pi m_{\tilde{t}}}{m_t}\left(-\frac{X_t}{m_{\tilde{t}}} - \frac{3}{2}\frac{X_t^2}{m_{\tilde{t}}^2} - \frac{1}{24}\frac{X_t^3}{m_{\tilde{t}}^3} + \frac{3}{16}\frac{X_t^4}{m_{\tilde{t}}^4}\right) - \frac{8}{3}\right. \\
& \qquad + 2\ln\frac{m_{\tilde{t}}^2}{m_t^2} - 3\frac{X_t}{m_{\tilde{t}}}\ln\frac{m_{\tilde{t}}^2}{m_t^2} + 3\frac{X_t^2}{m_{\tilde{t}}^2} - 3\frac{X_t^2}{m_{\tilde{t}}^2}\ln\frac{m_{\tilde{t}}^2}{m_t^2} - \frac{4}{3}\frac{X_t^3}{m_{\tilde{t}}^3} \\
& \qquad \left. + 8\frac{X_t^3}{m_{\tilde{t}}^3}\ln\frac{m_{\tilde{t}}^2}{m_t^2} - \frac{3}{2}\frac{X_t^4}{m_{\tilde{t}}^1} + \frac{1}{2}\frac{X_t^4}{m_{\tilde{t}}^4}\ln\frac{m_{\tilde{t}}^2}{m_t^2}\right]\Bigg\}. \qquad \text{(A.1)}
\end{aligned}$$

The interpolating functions used to capture the dependence of the Higgs mass

on the gluino mass (for arbitrary values) are defined as

$$F_1(m_{\tilde{g}}) = \begin{cases} 3/2\left(1 - m_{\tilde{g}}/m_{\tilde{t}}^-\right)\theta(m_{\tilde{t}}^- - m_{\tilde{g}}); & m_{\tilde{g}} \leq m_{\tilde{t}} \\ c_1\left(1 - m_{\tilde{t}}/m_{\tilde{g}}\right); & m_{\tilde{g}} > m_{\tilde{t}} \end{cases} \tag{A.2}$$

$$F_2(m_{\tilde{g}}) = \begin{cases} m_{\tilde{g}}/m_{\tilde{t}}^-; & m_{\tilde{g}} < m_{\tilde{t}}^- \\ 1; & m_{\tilde{t}}^- \leq m_{\tilde{g}} \leq m_{\tilde{t}} \\ c_2 + (1-c_2)m_{\tilde{t}}^2/m_{\tilde{g}}^2; & m_{\tilde{g}} > m_{\tilde{t}} \end{cases} \tag{A.3}$$

$$F_3(m_{\tilde{g}}) = \begin{cases} m_{\tilde{g}}/m_{\tilde{t}}^-; & m_{\tilde{g}} < m_{\tilde{t}}^- \\ 1; & m_{\tilde{t}}^- \leq m_{\tilde{g}} \leq m_{\tilde{t}} \\ 1/3 + 2/3\,(m_{\tilde{t}}/m_{\tilde{g}}); & m_{\tilde{g}} > m_{\tilde{t}} \end{cases} \tag{A.4}$$

$$F_4(m_{\tilde{g}}) = \theta(m_{\tilde{t}}^- - m_{\tilde{g}})(1 - m_{\tilde{g}}/m_{\tilde{t}}^-), \tag{A.5}$$

$$F_5(m_{\tilde{g}}) = 1 - m_{\tilde{t}}/m_{\tilde{g}}. \tag{A.6}$$

One may choose different functions $F_1, \ldots, F_5$ to improve the behavior of the expression of the approximate expression of m_h as a function of $m_{\tilde{g}}$, but these formulas (A.3)–(A.6) are appropriate enough.

The numerical coefficients of the interpolating polynomials used to approximate the solution of the SM RGE in section 2.3.2 have the values

$$\begin{aligned}
C_{0,0}^{(\lambda)} &= 0.003355 + 0.003856(m_t/\text{GeV} - 173.34), \\
C_{0,1}^{(\lambda)} &= 0.05064 + 0.2342(m_t/\text{GeV} - 173.34), \\
C_{0,2}^{(\lambda)} &= -0.005348 - 0.02380(m_t/\text{GeV} - 173.34), \\
C_{0,3}^{(\lambda)} &= [0.0003460 + 0.001533(m_t/\text{GeV} - 173.34)] \cdot 10^{-4}, \\
C_{0,4}^{(\lambda)} &= -[1.202 + 0.533(m_t/\text{GeV} - 173.34)] \cdot 10^{-5}, \\
C_{0,5}^{(\lambda)} &= [1.676 + 0.749(m_t/\text{GeV} - 173.34)] \cdot 10^{-7}, \\
C_{1,0}^{(\lambda)} &= 0.9986 + 0.02490(m_t/\text{GeV} - 173.34), \\
C_{1,1}^{(\lambda)} &= -0.04026 - 0.1638(m_t/\text{GeV} - 173.34), \\
C_{1,2}^{(\lambda)} &= 0.001021 + 0.002849(m_t/\text{GeV} - 173.34), \\
C_{2,0}^{(\lambda)} &= -0.1087 - 0.2808(m_t/\text{GeV} - 173.34), \\
C_{2,1}^{(\lambda)} &= -0.02403 + 0.1386(m_t/\text{GeV} - 173.34), \\
C_{0}^{(y_t)} &= 0.92663 + 1.00678(m_t/\text{GeV} - 173.34), \\
C_{1}^{(y_t)} &= -0.037365 - 0.002349(m_t/\text{GeV} - 173.34),
\end{aligned}$$

$$
\begin{aligned}
C_2^{(y_t)} &= [1.2622 + 0.1657(m_t/\text{GeV} - 173.34)] \cdot 10^{-2}, \\
C_3^{(y_t)} &= -[1.8251 - 0.4791(m_t/\text{GeV} - 173.34)] \cdot 10^{-5}, \\
C_1^{(g_Y)} &= 9.8 \cdot 10^{-6}, \quad C_2^{(g_Y)} = 5.0 \cdot 10^{-7}, \\
C_1^{(g_2)} &= 2.0 \cdot 10^{-4}, \quad C_2^{(g_2)} = -5.1 \cdot 10^{-6}.
\end{aligned} \tag{A.7}
$$

A.2 SUSY thresholds

This appendix is dedicated to some analytical expressions of the threshold corrections from integrating out supersymmetric particles that were not written in the body for the sake of readability. We start summarizing our conventions. For the numerical part we used the values $m_t = 173.34$ GeV [113], $\alpha_s(m_Z) = 0.1185$ [51], $y_b(m_t) = 0.0156$ and $y_\tau(m_t) = 0.0100$ [104]. The MSSM Lagrangian is written with all the parameters in the $\overline{\text{DR}}$ scheme (or the "OS" scheme described below), and is matched with the SM Lagrangian with all couplings and masses in the $\overline{\text{MS}}$ scheme. For $\tan\beta$ we used the definition of [94]. As in the rest of the paper, unless specified otherwise, all the formulae are written in terms of the SM couplings ($g_{1,2,3}$, $y_{t,b,\tau}$ and λ, or $\alpha_i \equiv g_i^2/(4\pi)$ and $\alpha_{t,b,\tau} \equiv y_{t,b,\tau}^2/(4\pi)$) in the $\overline{\text{MS}}$ scheme and the soft parameters (masses and trilinear couplings) in the $\overline{\text{DR}}$ or OS schemes.

The SUSY-breaking masses for the scalars of the i-th generation are denoted by m_{Q_i}, m_{U_i}, m_{D_i}, m_{L_i} and m_{E_i}, the soft SUSY-breaking Higgs-squarks cubic couplings are written in terms of the superpotential Yukawas $\hat{y}_{t,b,\tau}$ as $a_t \equiv \hat{y}_t A_t$, $a_b \equiv \hat{y}_b A_b$, $a_b \equiv \hat{y}_b A_b$ for the stops, sbottoms and staus respectively, while the relative signs of the μ parameter, gaugino masses and A-terms are the same as in [14], so that the scalar mass mixings depend on $X_t = A_t - \mu\cot\beta$, $X_b = A_b - \mu\tan\beta$ and $X_\tau = A_\tau - \mu\tan\beta$.

In this work, we extended the one-loop threshold in eq. (10) of [94] to include also the $\tan\beta-$enhanced contributions from integrating out sbottoms and staus:

$$
\begin{aligned}
(4\pi)^2\Delta\lambda^{1\ell,\phi} = {} & 3y_t^2\left[y_t^2+\frac{1}{2}\left(g_2^2-\frac{g_1^2}{5}\right)\cos 2\beta\right]\ln\frac{m_{Q_3^2}}{\tilde{m}^2}+3y_t^2\left[y_t^2+\frac{2}{5}g_1^2\cos 2\beta\right]\ln\frac{m_{U_3}^2}{\tilde{m}^2} \\
& + \frac{\cos^2 2\beta}{300}\sum_{i=1}^{3}\left[3\left(g_1^4+25g_2^4\right)\ln\frac{m_{Q_i}^2}{\tilde{m}^2}+24g_1^4\ln\frac{m_{U_i}^2}{\tilde{m}^2}+6g_1^4\ln\frac{m_{D_i}^2}{\tilde{m}^2}\right. \\
& \qquad \left. + \left(9g_1^4+25g_2^4\right)\ln\frac{m_{L_i}^2}{\tilde{m}^2}+18g_1^4\ln\frac{m_{E_i}^2}{\tilde{m}^2}\right] \\
& + \frac{1}{4800}\left[261g_1^4+630g_1^2g_2^2+1325g_2^4-4\cos 4\beta\left(9g_1^4+90g_1^2g_2^2+175g_2^4\right)\right.
\end{aligned}
$$

$$
\begin{aligned}
&- 9\cos 8\beta \left(3g_1^2 + 5g_2^2\right)^2 \Bigg] \ln\frac{m_A^2}{\tilde{m}^2} - \frac{3}{16}\left(\frac{3}{5}g_1^2 + g_2^2\right)^2 \sin^2 4\beta \\
&+ \sum_{\phi=t,b,\tau} \Bigg\{ 2N_c^\phi y_\phi^4 r_\phi^4 \widetilde{X}_\phi \left[\widetilde{F}_1(x_\phi) - \frac{\widetilde{X}_\phi}{12}\widetilde{F}_2(x_\phi)\right] \\
&+ \frac{N_c^\phi}{4} y_\phi^2 r_\phi^2 \widetilde{X}_\phi \cos 2\beta \left[\frac{9}{10}g_1^2 Q_\phi \widetilde{F}_3(x_\phi) + \left(2g_2^2 T_{\phi_L}^3 + \frac{3}{5}g_1^2\left(2T_{\phi_L}^3 - \frac{3}{2}Q_\phi\right)\right)\widetilde{F}_4(x_\phi)\right] \\
&- \frac{N_C^\phi}{12} y_\phi^2 r_\phi^2 \widetilde{X}_\phi \left(\frac{3}{5}g_1^2 + g_2^2\right)\cos^2 2\beta\, \widetilde{F}_5(x_\phi) \Bigg\} .
\end{aligned} \tag{A.8}
$$

In the last three lines of the equation above we sum over the contributions of the stops, sbottoms and staus, where $T_{\phi_L}^3$ is the third component of weak isospin of the left-handed chiral multiplet to which the sfermions belongs, Q_ϕ is the electric charge, $\widetilde{X}_\phi \equiv \{X_t^2/(m_{Q_3}m_{U_3}),\ X_b^2/(m_{Q_3}m_{D_3}),\ X_\tau^2/(m_{L_3}m_{E_3})\}$, $N_c^\phi \equiv \{3,3,1\}$ is the color factor, $x_\phi \equiv \{m_{Q_3}/m_{U_3}, m_{Q_3}/m_{D_3}, m_{L_3}/m_{E_3}\}$, and $r_\phi \equiv \{1,\ \hat{y}_b\cos\beta/y_b,\ \hat{y}_\tau\cos\beta/y_\tau\}$. The latter coefficients take into account the $\tan\beta$ enhanced corrections discussed in sec. 3.2.3 which require resummation, the explicit expressions can be found e.g. in [104, 111]. The loop functions $\widetilde{F}_n$ are defined in appendix A of [94]. Because of the smallness of the bottom Yukawa coupling, the one-loop $\mathcal{O}(\alpha_b)$ SUSY threshold corrections are only sizable for large $\tan\beta$ and $|\mu| \gtrsim \sqrt{m_{Q_3}m_{D_3}}$.

We obtained the two-loop $\mathcal{O}(\alpha_t^2)$ SUSY threshold corrections to the quartic coupling of the Higgs from the corresponding correction to the Higgs mass, under the simplifying assumption of degenerate scalars ($m_{Q_3} = m_{U_3} = m_A = m_{\tilde{t}}$) while the μ parameter and the renormalization scale are kept independent. The two-loop $\mathcal{O}(\alpha_t^2)$ correction to the Higgs mass from the matching between the MSSM and the SM in the EFT approach can be written as the sum of various contributions:

$$
m_h^{2\,(\alpha_t^2)} = m_h^{2\,(\alpha_t^2,\,\mathrm{EP})} + m_h^{2\,(\alpha_t^2,\,\mathrm{shift})} + m_h^{2\,(\alpha_t^2,\,\mathrm{WFR})} - m_h^{2\,(\alpha_t^2,\,\mathrm{top\ EP})}. \tag{A.9}
$$

The meaning of the various terms in this equation is explained below. The term $m_h^{2\,(\alpha_t^2,\,\mathrm{EP})}$ is the contribution from the effective potential in the $\overline{\mathrm{DR}}$ scheme, which was calculated by Espinosa and Zhang [79]:

$$
\begin{aligned}
m_h^{2\,(\alpha_t^2,\,\mathrm{EP})} = \frac{3y_t^6 v^2}{(4\pi)^4 s_\beta^2} \Bigg\{ &9\ln^2\frac{m_{\tilde{t}}^2}{Q^2} - 6\ln\frac{m_t^2}{Q^2}\ln\frac{m_{\tilde{t}}^2}{Q^2} - 3\ln^2\frac{m_t^2}{Q^2} \\
&+2\left[3f_2(\hat{\mu}) - 3f_1(\hat{\mu}) - 8\right]\ln\frac{m_{\tilde{t}}^2}{m_t^2} + 6\hat{\mu}^2\left(1 - \ln\frac{m_{\tilde{t}}^2}{Q^2}\right) - 2(4+\hat{\mu}^2)f_1(\hat{\mu}) + 4f_3(\hat{\mu}) - \frac{\pi^2}{3}
\end{aligned}
$$

$$
\begin{aligned}
&+\left[(33+6\hat{\mu}^2)\ln\frac{m_{\tilde{t}}^2}{Q^2}-10-6\hat{\mu}^2-4f_2(\hat{\mu})+(4-6\hat{\mu}^2)f_1(\hat{\mu})\right]\hat{X}_t^2\\
&+\left[-4(7+\hat{\mu}^2)\ln\frac{m_{\tilde{t}}^2}{Q^2}+23+4\hat{\mu}^2+2f_2(\hat{\mu})-2(1-2\hat{\mu}^2)f_1(\hat{\mu})\right]\frac{\hat{X}_t^4}{4}\\
&+\frac{1}{2}s_\beta^2\hat{X}_t^6\left(\ln\frac{m_{\tilde{t}}^2}{Q^2}-1\right)+c_\beta^2\Bigg[3\ln^2\frac{m_{\tilde{t}}^2}{m_t^2}+7\ln\frac{m_{\tilde{t}}^2}{Q^2}-4\ln\frac{m_t^2}{Q^2}-3+60K+\frac{4\pi^2}{3}\\
&+\left(12-24K-18\ln\frac{m_{\tilde{t}}^2}{Q^2}\right)\hat{X}_t^2-\left(3+16K-3\ln\frac{m_{\tilde{t}}^2}{Q^2}\right)(4\hat{X}_t\hat{Y}_t+\hat{Y}_t^2)\\
&+\left(-6+\frac{11}{2}\ln\frac{m_{\tilde{t}}^2}{Q^2}\right)\hat{X}_t^4+\left(4+16K-2\ln\frac{m_{\tilde{t}}^2}{Q^2}\right)\hat{X}_t^3\hat{Y}_t\\
&+\left(\frac{14}{3}+24K-3\ln\frac{m_{\tilde{t}}^2}{Q^2}\right)\hat{X}_t^2\hat{Y}_t^2-\left(\frac{19}{12}+8K-\frac{1}{2}\ln\frac{m_{\tilde{t}}^2}{Q^2}\right)\hat{X}_t^4\hat{Y}_t^2\Bigg]\Bigg\}. \qquad \text{(A.10)}
\end{aligned}
$$

where $X_t = A_t - \mu\cot\beta$, $Y_t = A_t + \mu\cot\beta$, $c_\beta \equiv \cos\beta$, $s_\beta \equiv \sin\beta$, we use the notation $\hat{z} \equiv z/m_{\tilde{t}}$ where z stands for any of the parameters μ, X_t or Y_t, and the definitions

$$f_1(\hat{\mu}) = \frac{\hat{\mu}^2}{1-\hat{\mu}^2}\ln\hat{\mu}^2, \qquad \text{(A.11)}$$

$$f_2(\hat{\mu}) = \frac{1}{1-\hat{\mu}^2}\left[1+\frac{\hat{\mu}^2}{1-\hat{\mu}^2}\ln\hat{\mu}^2\right], \qquad \text{(A.12)}$$

$$f_3(\hat{\mu}) = \frac{(-1+2\hat{\mu}^2+2\hat{\mu}^4)}{(1-\hat{\mu}^2)^2}\left[\ln\hat{\mu}^2\ln(1-\hat{\mu}^2)+Li_2(\hat{\mu}^2)-\frac{\pi^2}{6}-\hat{\mu}^2\ln\hat{\mu}^2\right], \qquad \text{(A.13)}$$

$$K = -\frac{1}{\sqrt{3}}\int_0^{\pi/6} dx\ \ln(2\cos x) \simeq -0.1953256. \qquad \text{(A.14)}$$

Here $Li_2(x)$ is the dilogarithm function. Below the SUSY scale we use the SM as an effective field theory in the $\overline{\text{MS}}$ scheme. Then we need to write the MSSM top mass and the EW vev (in the $\overline{\text{DR}}$ scheme) in terms of the SM ones in the $\overline{\text{MS}}$ scheme in the one-loop $\mathcal{O}(\alpha_t)$ correction to the Higgs mass. Doing so will produce an additional (shift) contribution at two loops

$$
\begin{aligned}
m_h^{2\,(\alpha_t^2,\ \text{shift})} &= \frac{3y_t^6v^2}{(4\pi)^4s_\beta^2}\Bigg\{\left(-\frac{3}{2}+3\ln\frac{m_{\tilde{t}}^2}{Q^2}-6\ln\frac{m_{\tilde{t}}^2}{m_t^2}\ln\frac{m_{\tilde{t}}^2}{Q^2}+3\ln\frac{m_{\tilde{t}}^2}{m_t^2}\right)(1+c_\beta^2)\\
&+3\hat{\mu}^2f_2(\hat{\mu})-6\hat{\mu}^2f_2(\hat{\mu})\ln\frac{m_{\tilde{t}}^2}{m_t^2}+\hat{X}_t^2\left[\left(3-6\ln\frac{m_{\tilde{t}}^2}{Q^2}\right)(1+c_\beta^2)+s_\beta^2\ln\frac{m_{\tilde{t}}^2}{m_t^2}-6\hat{\mu}^2f_2(\hat{\mu})\right]\\
&+\hat{X}_t^4\left[\frac{3}{4}-\frac{5}{4}c_\beta^2+\frac{1}{2}\hat{\mu}^2f_2(\hat{\mu})+\frac{1}{2}(1+c_\beta^2)\ln\frac{m_{\tilde{t}}^2}{Q^2}\right]-\frac{\hat{X}_t^6}{12}s_\beta^2\Bigg\}. \qquad \text{(A.15)}
\end{aligned}
$$

Unlike the two-loop $\mathcal{O}(\alpha_t\alpha_s)$ correction to the Higgs mass, the $\mathcal{O}(\alpha_t^2)$ one receives a wave-function renormalization contribution. It arises as a combination of the one-loop $\mathcal{O}(\alpha_t)$ contribution of the stops to the wave-function renormalization of the Higgs field and the one-loop correction to the Higgs mass from the matching at the SUSY scale. It reads:

$$m_h^{2\,(\alpha_t^2,\,\mathrm{WFR})} = -\frac{3\,y_t^6 v^2}{(4\pi)^4}\hat{X}_t^2\left(\ln\frac{m_{\tilde{t}}^2}{m_t^2} + \hat{X}_t^2 - \frac{1}{12}\hat{X}_t^4\right). \tag{A.16}$$

Finally, we need to subtract the $\mathcal{O}(\alpha_t^2)$ corrections to the Higgs mass associated with the contribution of the top-quark loops to the effective potential because it is already present in the matching at the EW scale. The two-loop $\mathcal{O}(\alpha_t^2)$ correction to the Higgs mass in the SM from the matching at the top mass, which receives EP and WFR contributions, is given in eq. (20) of [48]. We extract the EP piece which is given by

$$m_h^{2\,(\alpha_t^2,\,\mathrm{top\ EP})} = -\frac{3\,y_t^6 v^2}{(4\pi)^4}\left(2 + \frac{\pi^2}{3} - 7\ln\frac{m_t^2}{Q^2} + 3\ln^2\frac{m_t^2}{Q^2}\right). \tag{A.17}$$

Evaluating eq. (A.9) we obtain for the Higgs quartic coupling

$$\begin{aligned}
\Delta\lambda^{(2)}_{\alpha_t^2} = \frac{3\,y_t^6}{(4\pi)^4 s_\beta^2}\Bigg\{ & \left(-4\ln\frac{m_{\tilde{t}}^2}{Q^2} + 3\ln^2\frac{m_{\tilde{t}}^2}{Q^2}\right)s_\beta^2 - 6\hat{\mu}^2\ln\frac{m_{\tilde{t}}^2}{Q^2} + \frac{1}{2} + 6\hat{\mu}^2 \\
& - (8+2\hat{\mu}^2)f_1(\hat{\mu}) + 3\hat{\mu}^2 f_2(\hat{\mu}) + 4f_3(\hat{\mu}) + \hat{X}_t^6 s_\beta^2\left(-\frac{1}{2} + \frac{1}{2}\ln\frac{m_{\tilde{t}}^2}{Q^2}\right) \\
& + \hat{X}_t^2\left(-7 - 6\hat{\mu}^2 + 4f_1(\hat{\mu}) - 6\hat{\mu}^2 f_1(\hat{\mu}) - 4f_2(\hat{\mu}) - 6\hat{\mu}^2 f_2(\hat{\mu}) + 27\ln\frac{m_{\tilde{t}}^2}{Q^2} + 6\hat{\mu}^2\ln\frac{m_{\tilde{t}}^2}{Q^2}\right) \\
& + \frac{\hat{X}_t^4}{2}\left(11 + 2\hat{\mu}^2 - f_1(\hat{\mu}) + 2\hat{\mu}^2 f_1(\hat{\mu}) + f_2(\hat{\mu}) + \hat{\mu}^2 f_2(\hat{\mu}) - 13\ln\frac{m_{\tilde{t}}^2}{Q^2} - 2\hat{\mu}^2\ln\frac{m_{\tilde{t}}^2}{Q^2}\right) \\
& + c_\beta^2\Bigg[-\frac{13}{2} + 60K + \pi^2 + 9\ln\frac{m_{\tilde{t}}^2}{Q^2} + \hat{X}_t^2\left(15 - 24K - 24\ln\frac{m_{\tilde{t}}^2}{Q^2}\right) - \hat{X}_t^4\left(\frac{25}{4} - 6\ln\frac{m_{\tilde{t}}^2}{Q^2}\right) \\
& - \hat{X}_t\hat{Y}_t\left(12 + 64K - 12\ln\frac{m_{\tilde{t}}^2}{Q^2}\right) + \hat{X}_t^3\hat{Y}_t\left(4 + 16K - 2\ln\frac{m_{\tilde{t}}^2}{Q^2}\right) - \hat{Y}_t^2\left(3 + 16K - 3\ln\frac{m_{\tilde{t}}^2}{Q^2}\right) \\
& + \hat{X}_t^2\hat{Y}_t^2\left(\frac{14}{3} + 24K - 3\ln\frac{m_{\tilde{t}}^2}{Q^2}\right) + \hat{X}_t^4\hat{Y}_t^2\left(-\frac{19}{12} - 8K + \frac{1}{2}\ln\frac{m_{\tilde{t}}^2}{Q^2}\right)\Bigg]\Bigg\}.
\end{aligned} \tag{A.18}$$

After taking into account all the contributions in eq. (A.9), we checked that the logarithmic dependence on the top mass of the SM quartic coupling is canceled,

as it is shown in eq. (A.18). We also verified analytically that the inclusion of the two-loop $\mathcal{O}(\alpha_t^2)$ correction in eq. (A.18) makes the result of the pole Higgs mass independent of the renormalization scale at this order.

The two-loop $\mathcal{O}(\alpha_t\alpha_s)$ correction was also re-computed in this work. The explicit expressions for the SUSY thresholds are too long to be reported here and can be found in the SusyHD package [111].

On-shell scheme

A change in the renormalization of the parameters entering in the one-loop SUSY thresholds to λ will produce a two-loop (shift) contribution. We present the relation between the MSSM parameters in the $\overline{\text{DR}}$ and OS schemes. In particular, we need the relations for the stop masses and mixing at $\mathcal{O}(\alpha_s)$ and $\mathcal{O}(\alpha_t)$, the latter for degenerate stops. This will determine the shift contributions to the two-loop $\mathcal{O}(\alpha_t\alpha_s)$ and $\mathcal{O}(\alpha_t^2)$ SUSY corrections in the OS scheme.

In the OS renormalization scheme the masses are defined as the poles of the propagators. The relation between the $\overline{\text{DR}}$ and OS masses for a scalar particle with squared mass m^2 is given by

$$m^{2\,(\text{OS})} = m^{2\,(\overline{\text{DR}})}(Q) - \delta m^2(Q) \tag{A.19}$$

$$\delta m^2(Q) \equiv \text{Re}\,\hat{\Pi}(m^2, Q), \tag{A.20}$$

where $m^{2\,(\overline{\text{DR}})}(Q)$ is the tree-level $\overline{\text{DR}}$ mass evaluated at the renormalization scale Q, and $\hat{\Pi}(m^2, Q)$ is the $\overline{\text{DR}}$ renormalized one-loop self-energy.

On the other hand, the OS renormalization for the mixing angle is more subtle. At tree-level, the mixing angle of the stops is

$$\sin 2\theta_{\tilde{t}} = \frac{2m_t X_t}{m^2_{\tilde{t}_1} - m^2_{\tilde{t}_2}}. \tag{A.21}$$

We use the symmmetric renormalization for the stop mixing angle (for a discussion on possible renormalizations see [292] and references therein):

$$\delta\theta_{\tilde{t}} = \frac{1}{2}\frac{\hat{\Pi}_{12}(m^2_{\tilde{t}_1}) + \hat{\Pi}_{12}(m^2_{\tilde{t}_2})}{m^2_{\tilde{t}_1} - m^2_{\tilde{t}_2}}, \tag{A.22}$$

where $\hat{\Pi}_{12}(p^2)$ is the off-diagonal self-energy of the stops. We define the OS combination $(m_t X_t)^{OS}$ from eqs. (A.21) and (A.22), which implies

$$\frac{\delta(m_t X_t)}{m_t X_t} = \left(\frac{\delta m^2_{\tilde{t}_1} - \delta m^2_{\tilde{t}_2}}{m^2_{\tilde{t}_1} - m^2_{\tilde{t}_2}} + \frac{\delta \sin 2\theta_{\tilde{t}}}{\sin 2\theta_{\tilde{t}}}\right). \tag{A.23}$$

In the usual definition for the stop mixing on-shell, $X_t^{\rm OS} = (m_t X_t)^{\rm OS}/m_t^{\rm OS}$, terms proportional to $\log(m_{\tilde{t}}/m_t)$ appear in the two loop thresholds. In the EFT approach these logs are big and need resummation. Therefore we use a different definition for X_t which does not produce such terms and is more suitable for the EFT computation:

$$X_t(Q) \equiv \frac{(m_t X_t)^{OS}}{m_t^{\overline{\rm MS}}(Q)}\,, \tag{A.24}$$

where the numerator is computed from eq. (A.23) and we stress again that $m_t^{\overline{\rm MS}}(Q)$ is the top mass in the SM as any other $\overline{\rm MS}$ quantities in this paper. An analogous definition applies for the sbottom and stau mixings. The decoupling of heavy particles like the gluino is ensured in our on-shell renormalization scheme.

For the squarks, the $\mathcal{O}(\alpha_s)$ shift (neglecting the quark masses) reads [69]:

$$\frac{\delta m_{\tilde{q}}^2}{m_{\tilde{q}}^2} = -\frac{g_3^2}{6\pi^2}\left[1 + 3x + (x-1)^2 \ln|x-1| - x^2 \ln x + 2x \ln\frac{Q^2}{m_{\tilde{q}}^2}\right], \tag{A.25}$$

with $x = M_3^2/m_{\tilde{q}}^2$. For the product $(m_t X_t)$ we obtain

$$\begin{aligned}\delta(m_t X_t) = \frac{8}{3}\frac{g_3^2}{(4\pi^2)} m_t \Bigg[&4M_3 - (2M_3 - X_t)\log\frac{M_3^2}{Q^2} + M_3 \widetilde{F}_{10}\left(\frac{m_{Q_3}}{M_3}\right) \\ &+ M_3 \widetilde{F}_{10}\left(\frac{m_{U_3}}{M_3}\right) + X_t \widetilde{F}_{11}\left(\frac{m_{Q_3}}{M_3}, \frac{m_{U_3}}{M_3}\right)\Bigg]\end{aligned} \tag{A.26}$$

and for the shift between the $\overline{\rm DR}$ top mass in the MSSM and the $\overline{\rm MS}$ top mass in the SM (which is also given in [94])

$$\frac{\delta m_t}{m_t} = -\frac{4}{3}\frac{g_3^2}{(4\pi)^2}\left[1 + \log\frac{M_3^2}{Q^2} + \widetilde{F}_6\left(\frac{m_{Q_3}}{M_3}\right) + \widetilde{F}_6\left(\frac{m_{U_3}}{M_3}\right) - \frac{X_t}{M_3}\widetilde{F}_9\left(\frac{m_{Q_3}}{M_3}, \frac{m_{U_3}}{M_3}\right)\right]. \tag{A.27}$$

The functions $\widetilde{F}_{10}$ and $\widetilde{F}_{11}$ in eq. (A.26) are defined as:

$$\widetilde{F}_{10}(x) = \frac{1-x^2}{x^2}\ln|1-x^2| \tag{A.28}$$

$$\begin{aligned}\widetilde{F}_{11}(x_1, x_2) = &-2 + \frac{2(x_1^2 \ln x_1^2 - x_2^2 \ln x_2^2)}{x_1^2 - x_2^2} \\ &+ \frac{x_1^2(1-x_2^2)^2 \ln|1-x_2^2| - x_2^2(1-x_1^2)^2 \ln|1-x_1^2|}{x_1^2 x_2^2 (x_1^2 - x_2^2)}.\end{aligned} \tag{A.29}$$

Analogously for the $\mathcal{O}(\alpha_t^2)$ corrections for degenerate scalars [79]

$$\frac{\delta m_{\tilde{t}}^2}{m_{\tilde{t}}^2} = \frac{3y_t^2}{32\pi^2 s_\beta^2}\left[(\hat{X}_t^2 s_\beta^2 + \hat{Y}_t^2 c_\beta^2)\left(2 - \ln\frac{m_{\tilde{t}}^2}{Q^2}\right) + c_\beta^2\left(1 - \frac{\pi}{\sqrt{3}}\hat{Y}_t^2 - \ln\frac{m_{\tilde{t}}^2}{Q^2}\right)\right.$$

$$+\hat{\mu}^4\ln\hat{\mu}^2+(1-\hat{\mu}^2)\left(3-2\ln\frac{m_{\tilde{t}}^2}{Q^2}\right)-(1-\hat{\mu}^2)^2\ln(1-\hat{\mu}^2)\Big], \tag{A.30}$$

$$\delta(m_tX_t)=\frac{3y_t^2}{(4\pi)^2s_\beta^2}m_t\Bigg\{(X_ts_\beta^2+Y_tc_\beta^2)\left(2-\ln\frac{m_{\tilde{t}}^2}{Q^2}\right)-\frac{\pi}{\sqrt{3}}Y_tc_\beta^2+X_t\left(1-\frac{3}{2}\ln\frac{m_{\tilde{t}}^2}{Q^2}\right)$$
$$-\frac{1}{2}\big[1-\hat{\mu}^2+\hat{\mu}^4\ln\hat{\mu}^2+(1-\hat{\mu}^4)\ln(1-\hat{\mu}^2)\big]X_t\Bigg\}, \tag{A.31}$$

and the top mass shift is

$$\frac{\delta m_t}{m_t}=\frac{3}{4}\frac{y_t^2}{(4\pi)^2s_\beta^2}\left[\left(1+c_\beta^2\right)\left(\frac{1}{2}-\ln\frac{m_{\tilde{t}}^2}{Q^2}\right)-\hat{\mu}^2f_2(\hat{\mu})\right]. \tag{A.32}$$

As it was discussed in section 3.2.2, in the $\overline{\rm DR}$ scheme there are power-like corrections from the gluino-stop loops to the Higgs quartic coupling which do not decouple in the limit of heavy gluino. We illustrate this effect for the simplified case of degenerate stops

$$\Delta\lambda_{\alpha_t\alpha_s}^{(2,\overline{\rm DR})}=\frac{y_t^4g_3^2}{96\pi^4}\left[12\frac{M_3^2}{m_{\tilde{t}}^2}\left(1-\ln\frac{M_3^2}{Q^2}\right)-15+4\pi^2+12\ln\frac{M_3^2}{Q^2}-18\ln^2\frac{m_{\tilde{t}}^2}{Q^2}\right.$$
$$\left.-42\ln\frac{M_3^2}{m_{\tilde{t}}^2}+12\ln^2\frac{M_3^2}{m_{\tilde{t}}^2}+\mathcal{O}(M_3^{-1})\right]. \tag{A.33}$$

While our on-shell result, obtained from the $\overline{\rm DR}$ one by shifting the parameters in the one-loop $\mathcal{O}(\alpha_t)$ correction, guarantees the decoupling of heavy gluino

$$\Delta\lambda_{\alpha_t\alpha_s}^{(2,\rm OS)}=\frac{y_t^4g_3^2}{96\pi^4}\left[-30+4\pi^2+12\ln\frac{M_3^2}{Q^2}-18\ln^2\frac{m_{\tilde{t}}^2}{Q^2}-48\ln\frac{M_3^2}{m_{\tilde{t}}^2}+12\ln^2\frac{M_3^2}{m_{\tilde{t}}^2}+\mathcal{O}(M_3^{-1})\right]. \tag{A.34}$$

We also see that eq. (A.34) does not contain large logarithms $\ln m_{\tilde{t}}/m_t$. At last, the two-loop $\mathcal{O}(\alpha_t^2)$ SUSY threshold in our on-shell scheme is given by

$$\Delta\lambda_{\alpha_t^2}^{(2)}=\frac{3\,y_t^6}{(4\pi)^4s_\beta^2}\Bigg\{\left(-10\ln\frac{m_{\tilde{t}}^2}{Q^2}+3\ln^2\frac{m_{\tilde{t}}^2}{Q^2}\right)s_\beta^2+\frac{19}{2}-3\hat{\mu}^2-(8+2\hat{\mu}^2)f_1(\hat{\mu})+3\hat{\mu}^2f_2(\hat{\mu})$$
$$+4f_3(\hat{\mu})+3\hat{\mu}^4\ln\hat{\mu}^4-(3-6\hat{\mu}^2+3\hat{\mu}^4)\ln(1-\hat{\mu}^2)+\frac{\hat{X}_t^6}{2}s_\beta^2+\hat{X}_t^2\left[\frac{37}{2}+3\ln\frac{m_{\tilde{t}}^2}{Q^2}+9\hat{\mu}^2\right.$$
$$\left.+(4-6\hat{\mu}^2)f_1(\hat{\mu})-4f_2(\hat{\mu})-3\hat{\mu}^2f_2(\hat{\mu})-9\hat{\mu}^4\ln\hat{\mu}^2-(3+6\hat{\mu}^2-9\hat{\mu}^4)\ln(1-\hat{\mu}^4)\right]$$
$$-\hat{X}_t^4\left[\frac{15}{4}+\frac{3}{2}\hat{\mu}^2+\left(\frac{1}{2}-\hat{\mu}^2\right)f_1(\hat{\mu})-\frac{1}{2}f_2(\hat{\mu})-\frac{3}{2}\hat{\mu}^4\ln\hat{\mu}^2-\left(\frac{1}{2}+\hat{\mu}^2-\frac{3}{2}\hat{\mu}^4\right)\ln(1-\hat{\mu}^2)\right]$$

$$+c_\beta^2\Bigg[-\frac{7}{2}+60K+\pi^2-\hat{X}_t^2\left(\frac{39}{2}+24K+3\ln\frac{m_{\tilde{t}}^2}{Q^2}\right)+\hat{X}_t^4\frac{9}{2}$$
$$+\hat{X}_t\hat{Y}_t\left(12-64K-4\sqrt{3}\pi\right)+\hat{Y}_t^2\left(3-16K-\sqrt{3}\pi\right)-\hat{X}_t^2\hat{Y}_t^2\left(\frac{4}{3}-24K-\sqrt{3}\pi\right)$$
$$+\hat{X}_t^3\hat{Y}_t\left(16K+\frac{2\pi}{\sqrt{3}}\right)-\hat{X}_t^4\hat{Y}_t^2\left(\frac{7}{12}+8K+\frac{\pi}{2\sqrt{3}}\right)\Bigg]\Bigg\}. \tag{A.35}$$

A.3 Contribution of dimension-six operators to self-energies

We calculate the contribution of higher dimensional operators to the self-energies of the Higgs Π_{hh}, the W-boson Π_{WW}, the Z-bosom Π_{ZZ} and the top quark Σ_t. We focus on the terms proportional to the Wilson coefficients. To that end, we expand the Lagrangian around the vacuum and write it in terms of the physical Higgs field h. The relevant terms of the Lagrangian are

$$\begin{aligned}
\mathcal{L}_{hh} &= -\frac{1}{2}h(\partial^2)h-\frac{1}{2}(\lambda V_M^2)h^2+\frac{c_D}{2}h\left(\partial^4\right)h-\frac{1}{4}(c_R+2c_H)V_M^2h(\partial^2)h+\frac{3}{2}c_6V_M^4h^2,\\
\mathcal{L}_{WW} &= -\frac{1}{2}W^{+\mu\nu}W^-_{\mu\nu}+m_W^2W^{+\mu}W^-_\mu-c_{2W}(\partial^\mu W^+_{\mu\nu})(\partial_\rho W^{-\rho\nu})\\
&\quad+c_Dm_W^2\partial^\mu W^+_\mu\partial^\nu W^-_\nu+4c_{WW}m_W^2W^{+\mu\nu}W^-_{\mu\nu}+c_Wm_W^2(W^{+\mu}\partial^\nu W^-_{\mu\nu}\\
&\quad+W^{-\mu}\partial^\nu W^+_{\mu\nu})+\frac{1}{2}c_Rm_W^2v^2c_RW^{+\mu}W^-_\mu,\\
\mathcal{L}_{WW} &= W^+_\mu(\partial^2g^{\mu\nu}-\partial^\mu\partial^\nu)W^-_\nu+m_W^2W^{+\mu}W^-_\mu-c_{2W}W^+_\mu(\partial^4g^{\mu\nu}-\partial^2\partial^\mu\partial^\nu)W^-_\nu\\
&\quad+2(4c_{WW}+c_W)m_W^2W^+_\mu(-\partial^2g^{\mu\nu}+\partial^\mu\partial^\nu)W^-_\nu-c_Dm_W^2W^+_\mu(\partial^\mu\partial^\nu)W^-_\nu\\
&\quad+\frac{1}{2}c_Rm_W^2v^2W^+_\mu(g^{\mu\nu})W^-_\nu,\\
\mathcal{L}_{ZZ} &= -\frac{1}{4}Z^{\mu\nu}Z_{\mu\nu}+\frac{1}{2}m_Z^2Z^\mu Z_\mu-\frac{1}{2}(s_Z^2c_{2B}+c_Z^2c_{2W})(\partial^\mu Z_{\mu\nu})^2+\frac{1}{2}c_Dm_Z^2(\partial^\mu Z_\mu)^2\\
&\quad+\frac{1}{2}m_Z^2(s_Z^2c_B+4s_Z^4c_{BB}+c_Z^2c_W+4c_Z^2s_Z^2c_{WB}+4c_Z^4c_{WW})Z^{\mu\nu}Z_{\mu\nu}\\
&\quad+\frac{1}{4}(c_R-2c_T)m_Z^2v^2Z^\mu Z_\mu,\\
\mathcal{L}_{ZZ} &= \frac{1}{2}Z_\mu(\partial^2g^{\mu\nu}-\partial^\mu\partial^\nu)Z_\nu+\frac{m_Z^2}{2}Z^\mu Z_\mu-\frac{(s_Z^2c_{2B}+c_Z^2c_{2W})}{2}Z_\mu(\partial^4g^{\mu\nu}-\partial^2\partial^\mu\partial^\nu)Z_\nu\\
&\quad+m_Z^2\left[4(s_Z^4c_{BB}+c_Z^2s_Z^2c_{WB}+c_Z^4c_{WW})+s_Z^2c_B+c_Z^2c_W\right]Z_\mu(-\partial^2g^{\mu\nu}+\partial^\mu\partial^\nu)Z_\nu,\\
&\quad-\frac{1}{2}c_Dm_Z^2Z_\mu(\partial^\mu\partial^\nu)Z_\nu+\frac{1}{4}(c_R-2c_T)m_Z^2v^2Z_\mu(g^{\mu\nu})Z_\nu.
\end{aligned} \tag{A.36}$$

For the self-energies of the gauge bosons we extract the transverse part, given by

$$i\Pi^{\mu\nu}_{VV}(p^2) = i\left(g^{\mu\nu} - \frac{p^\mu p^\nu}{p^2}\right)\Pi_{VV}(p^2) + \frac{ip^\mu p^\nu}{p^2}\Pi^L_{VV}(p^2). \tag{A.37}$$

Then, the vacuum polarization functions read

$$\Pi_{hh}(p^2) = -p^4 c_D - p^2\frac{v^2}{2}(c_R + 2c_H) - 3v^4 c_6, \tag{A.38}$$

$$\Pi_{WW}(p^2) = -p^4 c_{2W} + 2p^2 m_W^2(4c_{WW} + c_W) + \frac{1}{2}m_W^2 v^2 c_R, \tag{A.39}$$

$$\begin{aligned}\Pi_{ZZ}(p^2) = {} & -p^4(c_Z^2 c_{2W} + s_Z^2 c_{2B}) + p^2(2m_Z^2)\big[4(c_Z^4 c_{WW} + c_Z^2 s_Z^2 c_{WB} + s_Z^4 c_{BB}) \\ & + (c_Z^2 c_W + s_Z^2 c_B)\big] + \frac{m_Z^2 v^2}{2}(c_R - 2c_T)\end{aligned} \tag{A.40}$$

$$\Sigma_t(p) = -m_t c_t\frac{v^2}{2} \tag{A.41}$$

The expressions for the self-energies derived in this appendix A.3 agree with those given in [141], except for the last term in $\Pi_{hh}(p^2)$ in eq. (A.38) which does not appear in [141].

A. DETAILS OF THE HIGGS MASS CALCULATION

Appendix B

Numerical values and formulas relevant for axion physics

B.1 Input parameters and conventions

For convenience in table B.1 we report the values of the parameters used in this work. When uncertainties are not quoted it means that their effect was negligible and they have not been used.

In the following we discuss in more in details the origin of some of these values.

Quark masses

The value of $z = m_u/m_d$ has been extracted from the following lattice estimates:

$$z = \begin{cases} 0.52(2) & [238] \\ 0.50(2)(3) & [236] \\ 0.451(4)(8)(12) & [237] \end{cases} \tag{B.1}$$

which use different techniques, fermion formulations, etc. In [293] the extra preliminary result $z = 0.49(1)(1)$ is also quoted, which agrees with the results above. Some results are still preliminary and the study of systematics may not be complete. Indeed the spread from the central values is somewhat bigger than the quoted uncertainties. Averaging the results above we get $z = 0.48(1)$. Waiting for more complete results and a more systematic study of all uncertainties we used a more conservative error, $z = 0.48(3)$, which better captures the spread between the different computations.

Axion properties have a much weaker dependence on the strange quark mass which only enter at higher orders. For definiteness we used the value of the ratio

z	0.48(3)	l_3	3(1)
r	27.4(1)	l_4	4.0(3)
m_π	134.98	l_7	0.007(4)
m_K	498	L_7^r	$-0.0003(1)$
m_η	548	L_8^r	0.00055(17)
f_π	92.2	g_A	1.2723(23)
f_η/f_π	1.3(1)	$\Delta u + \Delta d$	0.52(5)
$\Gamma_{\pi\gamma\gamma}$	$5.16(18)\,10^{-4}$	Δs	$-0.026(4)$
$\Gamma_{\eta\gamma\gamma}$	$7.63(16)\,10^{-6}$	Δc	0.000(4)

Table B.1: Numerical input values used in the computations. Dimensionful quantities are given in MeV. The values of scale dependent low-energy constants are given at the scale $\bar{\mu} = 770$ MeV, while the scale dependent proton spin content Δq are given at $Q = 2$ GeV.

$$r \equiv \frac{2m_s}{m_u + m_d} = 27.4(1)\,, \tag{B.2}$$

from [293].

ChPT low energy constants

For the value of the pion decay constant we used the PDG [51] value:

$$f_\pi = 92.21(14)\ \text{MeV}\,, \tag{B.3}$$

which is free from the leading EM corrections present in the leptonic decays used for the estimates.

Following [203] the ratio f_η/f_π can be related to f_K/f_π, whose value is very well known, up to higher order corrections. Assuming the usual 30% uncertainty on the $SU(3)$ chiral estimates we get $f_\eta/f_\pi = 1.3(1)$.

For the NLO low energy couplings we used the usual conventions of [202, 203]. As described in the main text we used the matching of the 3 and 2 flavor Lagrangians to estimate the SU(2) couplings from the SU(3) ones. In particular we only need the values of $L_{7,8}^r$, which we took as

$$L_7^r \equiv L_7^r(\bar{\mu}) = -0.3(1)\cdot 10^{-3}\,, \qquad L_8^r \equiv L_8^r(\bar{\mu}) = 0.55(17)\cdot 10^{-3}\,, \tag{B.4}$$

computed at the scale $\bar{\mu} = 770$ MeV. The first number has been extracted from the fit in [233] using the constraints for L_4^r in [234]. The second from [234]. A 30% intrinsic uncertainty from higher order 3-flavor corrections has been added.

This intrinsic uncertainty is not present for the 2-flavor constants where higher order corrections are much smaller.

In the main text we used the values

$$\bar{l}_3 = 3(1)\,, \qquad l_3^r(\bar{\mu}) = -\frac{1}{64\pi^2}\left(\bar{l}_3 + \log\left(\frac{m_\pi^2}{\bar{\mu}^2}\right)\right)\,,$$
$$\bar{l}_4 = 4.0(3)\,, \qquad l_4^r(\bar{\mu}) = \frac{1}{16\pi^2}\left(\bar{l}_4 + \log\left(\frac{m_\pi^2}{\bar{\mu}^2}\right)\right)\,,$$

extracted from 3-flavor simulations in [234].

From the values above and using the matching in [203] between the 2 and the 3 flavor theories we can also extract:

$$l_7 = 7(4)\,10^{-3}\,, \qquad h_1^r - h_3^r - l_4^r = -0.0048(14)\,. \tag{B.5}$$

Preliminary results using estimates from lattice QCD simulations [294] give $\bar{l}_3 = 2.97(19)(14)$, $\bar{l}_4 = 3.90(8)(14)$, $l_7 = 0.0066(54)$ and $L_8^r = 0.51(4)(12)\,10^{-3}$. The new results in [295] using partially quenched simulations give $\bar{l}_3 = 2.81(19)(45)$, $\bar{l}_4 = 4.02(8)(24)$ and $l_7 = 0.0065(38)(2)$. All these results are in agreement with the numbers used here.

Proton spin content

While the axial charge, which is equivalent to the isovector spin content of the proton, is very well known (see discussion around eq. (5.43)) the isosinglet components are less known.

To estimate $g^{ud} = \Delta u + \Delta d$ we use the results in [249–254]. In particular we used [253], whose value for $g_A = 1.242(57)$ is compatible with the experimental one, to estimate the connected contribution to g^{ud}. For the disconnected contribution, which is much more difficult to simulate, we averaged the results in [251, 252, 254] increasing the error to accommodate the spread in central values, which may be due to different systematics. Combining the results we get

$$g^{ud}_{conn.} + g^{ud}_{disc.} = 0.611(48) - 0.090(20) = 0.52(5)\,. \tag{B.6}$$

All the results provided here are in the $\overline{\text{MS}}$ scheme at the reference scale $Q = 2$ GeV.

The strange spin contribution only have the disconnected contribution, which we extract averaging the results in [249–252, 254]

$$g^s = \Delta s = -0.026(4)\,. \tag{B.7}$$

All the results mostly agree with each others but they are still preliminary or use heavy quark masses or coarse lattice spacing or only two dynamical quarks. For this reason the estimate of the systematic uncertainties is not yet complete and further studies are required.

Finally [251] also explored the charm spin contribution. They could not see a signal and thus their results can only be used to put an upper bound which we extracted as in table B.1.

B.2 Matching between 2- and 3-flavor theories

The matching between the theory containing kaons, the η-meson, and pions (three flavors) and the theory with only pions (two flavors) is done at an intermediate scale of order of the masses m_K and m_η. The low-energy effective field theory with two flavors is valid for:

$$p^2 \ll M_K^2, \quad m_u, m_d \ll m_s. \tag{B.8}$$

Order by order in perturbation theory and at a given order in the momentum expansion both theories are matched, i.e. they are required to reproduce the same physics at the boundary. In ref. [203] the matching is done at $\mathcal{O}(p^4)$, by comparing the generating functional (or the Green functions) of the two theories up to one-loop oder. That is, first the two theories are matched at tree level at $\mathcal{O}(p^4)$ and then one proceeds with the matching at one-loop. It is also given the relation between the low-energy constants of the two chiral Lagrangians.

We illustrate the procedure for the axion mass, similarly it can be applied to other observables like the coupling to photons. Integrating out the η- and K- mesons does not require introducing an explicit axion mass because it is not a parameter of the low-energy theory. The parameters of the low-energy theory (with two-flavors) are f_π and B_0 present in the LO Lagrangian and the parameters of the $\mathcal{O}(p^4)$-Lagrangian $(l_1, \ldots, l_7, h_1, h_2, h_3)$. Unlike the theory obtained after integrating out all the mesons (i.e. everything except the axion, where no chiral symmetry remains) in which an explicit axion mass appears in the Lagrangian, in the low-energy theory with two-flavors the chiral symmetry fixes the way in which the axion field appears in the Lagrangian (i.e. through $e^{-iaQ_A/f} M e^{-iaQ_A/f}$). After the matching, the dependence on the parameters of the high-energy theory with three flavors is absorbed by the low energy parameters.

The expressions for the conversion of the parameters of the two theories are in eqs. (11.2)-(11.6) of [203]. We recover the expression for the axion mass with three flavors from the expressions obtained in the two-flavor case. We start from

the expression for the axion mass with two flavors in terms of the tree-level parameters (B_0 and f_π):

$$m_a^2 = \frac{B_0 m_u m_d}{m_u + m_d}\frac{f_\pi^2}{f_a^2}\left\{1 + \frac{2B_0(m_u+m_d)}{f_\pi^2}\left[-\frac{3}{64\pi^2}\ln\frac{m_\pi^2}{\mu^2} + h_1^r - h_3^r + l_3^r \right.\right. \\ \left.\left. -4\frac{m_u m_d}{(m_u+m_d)^2} l_7^r\right]\right\}. \quad \text{(B.9)}$$

Substituting the expression of the low-energy parameters in terms of the parameters of the 3-flavor theory we obtain:

$$\begin{aligned} m_a^2 =& \frac{B_0 f_\pi^2 m(-w+z+1)}{f_a^2(z+1)^2} - \frac{32B_0^2m^2\left(z+z^2+w\left(1+z+z^2\right)\right)}{f_a^2 wz(z+1)^2}L_6^r + \frac{288B_0^2m^2}{f_a^2(z+1)^2}L_7^r \\ &+ \frac{96B_0^2m^2}{f_a^2(z+1)^2}L_8^r - \frac{B_0^2m^2\left(1+38z+z^2\right)}{288f_a^2z(z+1)^2} - \frac{B_0^2m^2(2w+z+1)\log\left(\frac{B_0m}{\mu^2w}\right)}{16\pi^2f_a^2w(z+1)^2} \\ &\frac{B_0^2m^2\left(w\left(5z^2-22z+5\right)-4z(z+1)\right)\log\left(\frac{4B_0m}{3\mu^2w}\right)}{288\pi^2f_a^2wz(z+1)^2} - \frac{3B_0^2m^2\log\left(\frac{B_0m(z+1)}{\mu^2z}\right)}{32\pi^2f_a^2z}, \end{aligned} \quad \text{(B.10)}$$

where $z = m_u/m_d$, $w = m_u/m_s$ and $m = m_u + m_d/2$. Here there are some things to notice. The low energy constant l_r^7 contains a tree level piece proportional to $1/m_s$ that contributes to the tree-level axion mass. Despite the term proportional to l_7^r in eq. (B.9) is formally one loop in the 2-flavor theory, since there is a tree-level piece in l_7^r it will produce additional one-loop contributions to the axion mass when substituting B_0 and f_π by its one-loop expression. Also, the conversion from two to three flavors only reproduce the leading dependence on w (that is, $\mathcal{O}(w)$ in the tree-level piece and $\mathcal{O}(w^0)$ in the one-loop piece) because higher powers of w is equivalent to higher powers of the cutoff and corresponds to higher order in the momentum expansion. We have checked explicitly that eq. (B.10) perfectly agree with the corresponding expression obtained using the 3-flavor effective theory.

B.3 Renormalization of axial couplings

While anomalous dimensions of conserved currents vanish it is not true for anomalous currents. This means that the axion coupling to the singlet component of the axial current is scale dependent:

$$\frac{\partial_\mu a}{2f_a}\sum_q c_q j_q^\mu = \frac{\partial_\mu a}{2f_a}\left[\sum_q\left(c_q - \frac{\sum_{q'}c_{q'}}{n_f}\right)j_q^\mu + \frac{\sum_{q'}c_{q'}}{n_f}j_{\Sigma q}^\mu\right] \quad \text{(B.11)}$$

$$\to \quad \frac{\partial_\mu a}{2f_a}\left[\sum_q\left(c_q - \frac{\sum_{q'} c_{q'}}{n_f}\right) j_q^\mu + Z_0(Q)\frac{\sum_{q'} c_{q'}}{n_f} j_{\Sigma q}^\mu\right] \tag{B.12}$$

where $Z_0(Q)$ is the renormalization of the singlet axial current $j^\mu_{\Sigma q}$. It is important to note that $j^\mu_{\Sigma q}$ only renormalizes multiplicatively, this is not true for the coupling to the gluon operator ($G\tilde{G}$) which mixes at one-loop with $\partial_\mu j^\mu_{\Sigma q}$ after renormalization (see e.g. [296]).

The anomalous dimension of $j^\mu_{\Sigma q}$ starts only at 2-loops and is known up to 3-loops in QCD [247, 297]

$$\frac{\partial \log Z_0(Q)}{\partial \log Q^2} = \gamma_A = \frac{n_f}{2}\left(\frac{\alpha_s}{\pi}\right)^2 + n_f\frac{177-2n_f}{72}\left(\frac{\alpha_s}{\pi}\right)^3 + \dots\,. \tag{B.13}$$

The evolution of the couplings $c_q(Q)$ can thus be written as

$$c_q(Q) = c_q(Q_0) + \left(\frac{Z_0(Q)}{Z_0(Q_0)} - 1\right)\frac{\langle c_q\rangle_{n_f}}{n_f}\,, \tag{B.14}$$

where we used the short hand notation $\langle\cdot\rangle_{n_f}$ for the sum of q over n_f flavors. Iterating the running between the high scale f_a and the low scale $Q = 2$ GeV across the bottom and top mass thresholds we can finally write the relation between the low energy couplings $c_q(Q)$ and the high energy ones $c_q = c_q(f_a)$:

$$\begin{aligned}
c_t(m_t) &= c_t + \left(\frac{Z_0(m_t)}{Z_0(f_a)} - 1\right)\frac{\langle c_q\rangle_6}{6}\,,\\
c_b(m_b) &= c_b + \left(\frac{Z_0(m_b)}{Z_0(m_t)} - 1\right)\frac{\langle c_q\rangle_5}{5} + \frac{Z_0(m_b)}{Z_0(m_t)}\left(\frac{Z_0(m_t)}{Z_0(f_a)} - 1\right)\frac{\langle c_q\rangle_6}{6}\,,\\
c_{q=u,d,s,c}(Q) &= c_q + \left(\frac{Z_0(Q)}{Z_0(m_b)} - 1\right)\frac{\langle c_q\rangle_4}{4} + \frac{Z_0(Q)}{Z_0(m_b)}\left(\frac{Z_0(m_b)}{Z_0(m_t)} - 1\right)\frac{\langle c_q\rangle_5}{5}\\
&\quad + \frac{Z_0(Q)}{Z_0(m_t)}\left(\frac{Z_0(m_t)}{Z_0(f_a)} - 1\right)\frac{\langle c_q\rangle_6}{6}\,,
\end{aligned} \tag{B.15}$$

where at each mass threshold we matched the couplings at LO. In eq. (B.15) we can recognize the contributions from the running from f_a to m_t with 6 flavors, from m_t to m_b with 5 flavors and the one down to Q with 4 flavors.

The value for $Z_0(Q)$ can be computed from eq. (B.13), at LLO the solution is simply

$$Z_0(Q) = Z_0(Q_0)\; e^{-\frac{6n_f}{33-2n_f}\frac{\alpha_s(Q)-\alpha_s(Q_0)}{\pi}}\,. \tag{B.16}$$

At NLLO the numerical values at the relevant mass scales are

$$Z_0(10^{12}\,\text{GeV}) = 0.984\,, \quad Z_0(m_t) = 0.939(3)\,, \quad Z_0(m_b) = 0.888(15)\,, \quad Z_0(2\,\text{GeV}) = 0.863(24)\,, \tag{B.17}$$

where the error is estimated by the difference with the LLO which should capture the order of magnitude of the 1-loop thresholds not included in the computation. For the computation above we used the $\overline{\text{MS}}$ values of the quark masses, i.e. $m_t(m_t) = 164$ GeV and $m_b(m_b) = 4.2$ GeV. The dependence of $Z_0(f_a)$ on the actual value of f_a is very mild, shifting $Z_0(f_a)$ by less than $\pm 0.5\%$ for $f_a = 10^{12\pm 3}$ GeV.

Note that DFSZ models at high energy can be written so that the axion couples only through the quark mass matrix. In this case no running effect should be present above the first SM mass threshold (at the top mass). Indeed in this models, $\langle c_q \rangle_6 = \langle c_q^0 \rangle_6 - \operatorname{tr} Q_a = 0$ and the renormalization effects from f_a to m_t cancel out.

B. NUMERICAL VALUES AND FORMULAS RELEVANT FOR AXION PHYSICS

References

[1] J. P. Vega and G. Villadoro, "SusyHD: Higgs mass Determination in Supersymmetry," *JHEP* **07** (2015) 159, arXiv:1504.05200 [hep-ph]. iii, 46, 47, 63, 64

[2] G. Grilli di Cortona, E. Hardy, J. Pardo Vega, and G. Villadoro, "The QCD axion, precisely," *JHEP* **01** (2016) 034, arXiv:1511.02867 [hep-ph]. iii

[3] **ATLAS** Collaboration, G. Aad *et al.*, "Observation of a new particle in the search for the Standard Model Higgs boson with the ATLAS detector at the LHC," *Phys.Lett.* **B716** (2012) 1–29, arXiv:1207.7214 [hep-ex]. 3

[4] **CMS** Collaboration, S. Chatrchyan *et al.*, "Observation of a new boson at a mass of 125 GeV with the CMS experiment at the LHC," *Phys.Lett.* **B716** (2012) 30–61, arXiv:1207.7235 [hep-ex]. 3

[5] ATLAS and CMS searches of SUSY, "https://twiki.cern.ch/twiki/bin/view/AtlasPublic/SupersymmetryPublicResults, https://twiki.cern.ch/twiki/bin/view/CMSPublic/PhysicsResultsSUS and references therein,". 3, 34, 35, 36

[6] N. Craig, "The State of Supersymmetry after Run I of the LHC," arXiv:1309.0528 [hep-ph]. 3, 35

[7] G. F. Giudice, "Naturalness after LHC8," *PoS* **EPS-HEP2013** (2013) 163, arXiv:1307.7879 [hep-ph]. 3

[8] A. Arvanitaki, M. Baryakhtar, X. Huang, K. van Tilburg, and G. Villadoro, "The Last Vestiges of Naturalness," *JHEP* **1403** (2014) 022, arXiv:1309.3568 [hep-ph]. 3

[9] N. Arkani-Hamed and S. Dimopoulos, "Supersymmetric unification without low energy supersymmetry and signatures for fine-tuning at the LHC," *JHEP* **0506** (2005) 073, arXiv:hep-th/0405159 [hep-th]. 3, 32, 62, 64

[10] G. Giudice and A. Romanino, "Split supersymmetry," *Nucl.Phys.* **B699** (2004) 65–89, arXiv:hep-ph/0406088 [hep-ph]. 3, 32, 62, 64, 66

[11] **ATLAS, CMS** Collaboration, G. Aad *et al.*, "Combined Measurement of the Higgs Boson Mass in pp Collisions at $\sqrt{s} = 7$ and 8 TeV with the ATLAS and CMS Experiments," arXiv:1503.07589 [hep-ex]. 4, 7, 61

[12] M. Sohnius, "Introducing Supersymmetry," *Phys.Rept.* **128** (1985) 39–204. 5, 9

[13] S. Weinberg, "The quantum theory of fields. Vol. 3: Supersymmetry,". 5, 9

[14] S. P. Martin, "A Supersymmetry primer," *Adv.Ser.Direct.High Energy Phys.* **21** (2010) 1–153, arXiv:hep-ph/9709356 [hep-ph]. 5, 6, 9, 16, 17, 19, 24, 165

[15] P. Ramond, "Dual Theory for Free Fermions," *Phys. Rev.* **D3** (1971) 2415–2418. 7

[16] G. 't Hooft, "Naturalness, chiral symmetry, and spontaneous chiral symmetry breaking," *NATO Sci.Ser.B* **59** (1980) 135. 7

[17] G. F. Giudice, "Naturally Speaking: The Naturalness Criterion and Physics at the LHC," arXiv:0801.2562 [hep-ph]. 7

[18] S. R. Coleman and J. Mandula, "All Possible Symmetries of the S Matrix," *Phys.Rev.* **159** (1967) 1251–1256. 8

[19] R. Haag, J. T. Lopuszanski, and M. Sohnius, "All Possible Generators of Supersymmetries of the s Matrix," *Nucl.Phys.* **B88** (1975) 257. 8

[20] M. Bertolini, "Lectures on Supersymmetry," *SISSA* (2015) . 9

[21] R. Barbier, C. Berat, M. Besancon, M. Chemtob, A. Deandrea, *et al.*, "R-parity violating supersymmetry," *Phys.Rept.* **420** (2005) 1–202, arXiv:hep-ph/0406039 [hep-ph]. 14

[22] **Super-Kamiokande** Collaboration, H. Nishino *et al.*, "Search for Nucleon Decay into Charged Anti-lepton plus Meson in Super-Kamiokande I and II," *Phys.Rev.* **D85** (2012) 112001, arXiv:1203.4030 [hep-ex]. 14, 36

[23] **Super-Kamiokande** Collaboration, K. Abe *et al.*, "Search for proton decay via $p \to \nu ? K^+$ using 260??kilotonyear data of Super-Kamiokande," *Phys.Rev.* **D90** no. 7, (2014) 072005, arXiv:1408.1195 [hep-ex]. 14, 36

[24] G. 't Hooft, "Symmetry Breaking Through Bell-Jackiw Anomalies," *Phys.Rev.Lett.* **37** (1976) 8–11. 14, 116

[25] P. Fayet, "Spontaneously Broken Supersymmetric Theories of Weak, Electromagnetic and Strong Interactions," *Phys.Lett.* **B69** (1977) 489. 14

[26] S. Dimopoulos and H. Georgi, "Softly Broken Supersymmetry and SU(5)," *Nucl.Phys.* **B193** (1981) 150. 14

[27] **MEG** Collaboration, J. Adam *et al.*, "New constraint on the existence of the $\mu^+ \to e^+\gamma$ decay," *Phys. Rev. Lett.* **110** (2013) 201801, arXiv:1303.0754 [hep-ex]. 16, 36

[28] **BaBar** Collaboration, B. Aubert *et al.*, "Searches for Lepton Flavor Violation in the Decays tau+- —¿ e+- gamma and tau+- —¿ mu+- gamma," *Phys. Rev. Lett.* **104** (2010) 021802, arXiv:0908.2381 [hep-ex]. 16

[29] M. Ciuchini *et al.*, "Delta M(K) and epsilon(K) in SUSY at the next-to-leading order," *JHEP* **10** (1998) 008, arXiv:hep-ph/9808328 [hep-ph]. 16, 36

[30] R. J. Crewther, P. Di Vecchia, G. Veneziano, and E. Witten, "Chiral Estimate of the Electric Dipole Moment of the Neutron in Quantum Chromodynamics," *Phys. Lett.* **B88** (1979) 123. [Erratum: Phys. Lett.B91,487(1980)]. 16, 111, 117

[31] J. M. Pendlebury *et al.*, "Revised experimental upper limit on the electric dipole moment of the neutron," *Phys. Rev.* **D92** no. 9, (2015) 092003, arXiv:1509.04411 [hep-ex]. 16, 36, 111, 117

[32] **ACME** Collaboration, J. Baron *et al.*, "Order of Magnitude Smaller Limit on the Electric Dipole Moment of the Electron," *Science* **343** (2014) 269–272, arXiv:1310.7534 [physics.atom-ph]. 16, 36

[33] W. Siegel, "Supersymmetric Dimensional Regularization via Dimensional Reduction," *Phys.Lett.* **B84** (1979) 193. 17

[34] A. Salam and J. Strathdee, "On Superfields and Fermi-Bose Symmetry," *Phys.Rev.* **D11** (1975) 1521–1535. 17

[35] M. T. Grisaru, W. Siegel, and M. Rocek, "Improved Methods for Supergraphs," *Nucl.Phys.* **B159** (1979) 429. 17

[36] A. Arvanitaki, N. Craig, S. Dimopoulos, and G. Villadoro, "Mini-Split," *JHEP* **1302** (2013) 126, arXiv:1210.0555 [hep-ph]. 20, 32, 33, 64, 81, 108

[37] G. Giudice and A. Masiero, "A Natural Solution to the mu Problem in Supergravity Theories," *Phys.Lett.* **B206** (1988) 480–484. 20, 32

[38] G. Dvali, G. Giudice, and A. Pomarol, "The Mu problem in theories with gauge mediated supersymmetry breaking," *Nucl.Phys.* **B478** (1996) 31–45, arXiv:hep-ph/9603238 [hep-ph]. 29, 101

[39] G. Giudice and R. Rattazzi, "Theories with gauge mediated supersymmetry breaking," *Phys.Rept.* **322** (1999) 419–499, arXiv:hep-ph/9801271 [hep-ph]. 101

[40] G. F. Giudice, H. D. Kim, and R. Rattazzi, "Natural mu and B mu in gauge mediation," *Phys.Lett.* **B660** (2008) 545–549, arXiv:0711.4448 [hep-ph]. 29, 101

[41] M. Dine, Y. Nir, and Y. Shirman, "Variations on minimal gauge mediated supersymmetry breaking," *Phys.Rev.* **D55** (1997) 1501–1508, arXiv:hep-ph/9607397 [hep-ph]. 30, 102

[42] R. Rattazzi and U. Sarid, "Large tan Beta in gauge mediated SUSY breaking models," *Nucl.Phys.* **B501** (1997) 297–331, arXiv:hep-ph/9612464 [hep-ph]. 30, 102

[43] A. De Simone, R. Franceschini, G. F. Giudice, D. Pappadopulo, and R. Rattazzi, "Lopsided Gauge Mediation," *JHEP* **1105** (2011) 112, arXiv:1103.6033 [hep-ph]. 30, 31, 104, 105

[44] G. F. Giudice, M. A. Luty, H. Murayama, and R. Rattazzi, "Gaugino mass without singlets," *JHEP* **9812** (1998) 027, arXiv:hep-ph/9810442 [hep-ph]. 31, 107

[45] L. Randall and R. Sundrum, "Out of this world supersymmetry breaking," *Nucl.Phys.* **B557** (1999) 79–118, arXiv:hep-th/9810155 [hep-th]. 31

[46] F. Gabbiani, E. Gabrielli, A. Masiero, and L. Silvestrini, "A Complete analysis of FCNC and CP constraints in general SUSY extensions of the standard model," *Nucl.Phys.* **B477** (1996) 321–352, arXiv:hep-ph/9604387 [hep-ph]. 32, 108

[47] G. F. Giudice and A. Strumia, "Probing High-Scale and Split Supersymmetry with Higgs Mass Measurements," *Nucl.Phys.* **B858** (2012) 63–83, arXiv:1108.6077 [hep-ph]. 33, 60, 61, 62, 66, 81

[48] G. Degrassi, S. Di Vita, J. Elias-Miro, J. R. Espinosa, G. F. Giudice, *et al.*, "Higgs mass and vacuum stability in the Standard Model at NNLO," *JHEP* **1208** (2012) 098, arXiv:1205.6497 [hep-ph]. 33, 60, 61, 62, 64, 89, 97, 98, 168

[49] **BaBar** Collaboration, J. P. Lees *et al.*, "Measurement of B($B \to X_s\gamma$), the $B \to X_s\gamma$ photon energy spectrum, and the direct CP asymmetry in $B \to X_{s+d}\gamma$ decays," *Phys. Rev.* **D86** (2012) 112008, arXiv:1207.5772 [hep-ex]. 36

[50] **CMS, LHCb** Collaboration, V. Khachatryan *et al.*, "Observation of the rare $B_s^0 \to \mu^+\mu^-$ decay from the combined analysis of CMS and LHCb data," arXiv:1411.4413 [hep-ex]. 36, 104

[51] **Particle Data Group** Collaboration, K. A. Olive *et al.*, "Review of Particle Physics," *Chin. Phys.* **C38** (2014) 090001. 36, 37, 117, 128, 134, 145, 146, 165, 176

[52] P. H. Chankowski and S. Pokorski, "Chargino mass and R(b) anomaly," *Nucl. Phys.* **B475** (1996) 3–26, arXiv:hep-ph/9603310 [hep-ph]. 36

[53] T. Moroi, "The Muon anomalous magnetic dipole moment in the minimal supersymmetric standard model," *Phys. Rev.* **D53** (1996) 6565–6575, arXiv:hep-ph/9512396 [hep-ph]. [Erratum: Phys. Rev.D56,4424(1997)]. 36

[54] W. Altmannshofer, M. Carena, N. R. Shah, and F. Yu, "Indirect Probes of the MSSM after the Higgs Discovery," *JHEP* **1301** (2013) 160, arXiv:1211.1976 [hep-ph]. 37, 38

[55] **CMS** Collaboration, C. Collaboration, "Search for a neutral MSSM Higgs boson decaying into $\tau\tau$ at 13 TeV,". 37, 103

[56] **ATLAS** Collaboration, M. Aaboud *et al.*, "Search for Minimal Supersymmetric Standard Model Higgs bosons H/A and for a Z' boson in the $\tau\tau$ final state produced in pp collisions at $\sqrt{s} = 13$ TeV with the ATLAS Detector," `arXiv:1608.00890 [hep-ex]`. 37, 103

[57] J. Casas, A. Lleyda, and C. Munoz, "Strong constraints on the parameter space of the MSSM from charge and color breaking minima," *Nucl.Phys.* **B471** (1996) 3–58, `arXiv:hep-ph/9507294 [hep-ph]`. 37, 83

[58] A. Kusenko, P. Langacker, and G. Segre, "Phase transitions and vacuum tunneling into charge and color breaking minima in the MSSM," *Phys.Rev.* **D54** (1996) 5824–5834, `arXiv:hep-ph/9602414 [hep-ph]`. 37, 83

[59] D. Chowdhury, R. M. Godbole, K. A. Mohan, and S. K. Vempati, "Charge and Color Breaking Constraints in MSSM after the Higgs Discovery at LHC," *JHEP* **1402** (2014) 110, `arXiv:1310.1932 [hep-ph]`. 37

[60] **Planck** Collaboration, P. Ade *et al.*, "Planck 2013 results. XVI. Cosmological parameters," *Astron.Astrophys.* **571** (2014) A16, `arXiv:1303.5076 [astro-ph.CO]`. 37

[61] G. Grilli di Cortona, "Hunting electroweakinos at future hadron colliders and direct detection experiments," `arXiv:1412.5952 [hep-ph]`. 38, 104, 107

[62] **XENON100** Collaboration, E. Aprile *et al.*, "Dark Matter Results from 225 Live Days of XENON100 Data," *Phys.Rev.Lett.* **109** (2012) 181301, `arXiv:1207.5988 [astro-ph.CO]`. 38

[63] **LUX** Collaboration, D. Akerib *et al.*, "First results from the LUX dark matter experiment at the Sanford Underground Research Facility," *Phys.Rev.Lett.* **112** (2014) 091303, `arXiv:1310.8214 [astro-ph.CO]`. 38

[64] H. Georgi, "Effective field theory," *Ann.Rev.Nucl.Part.Sci.* **43** (1993) 209–252. 43

[65] C. P. Burgess, "Introduction to Effective Field Theory," *Ann. Rev. Nucl. Part. Sci.* **57** (2007) 329–362, `arXiv:hep-th/0701053 [hep-th]`. 43

[66] G. Degrassi, S. Heinemeyer, W. Hollik, P. Slavich, and G. Weiglein, "Towards high precision predictions for the MSSM Higgs sector," *Eur.Phys.J.* **C28** (2003) 133–143, arXiv:hep-ph/0212020 [hep-ph]. 44, 81

[67] T. Hahn, S. Heinemeyer, W. Hollik, H. Rzehak, and G. Weiglein, "Prediction of the light CP-even Higgs-Boson Mass of the MSSM: Towards the ILC Precision," arXiv:1404.0186 [hep-ph].

[68] P. Draper and H. Rzehak, "A Review of Higgs Mass Calculations in Supersymmetric Models," *Phys. Rept.* **619** (2016) 1–24, arXiv:1601.01890 [hep-ph]. 44

[69] D. M. Pierce, J. A. Bagger, K. T. Matchev, and R.-j. Zhang, "Precision corrections in the minimal supersymmetric standard model," *Nucl.Phys.* **B491** (1997) 3–67, arXiv:hep-ph/9606211 [hep-ph]. 44, 78, 170

[70] A. Dabelstein, "The One loop renormalization of the MSSM Higgs sector and its application to the neutral scalar Higgs masses," *Z.Phys.* **C67** (1995) 495–512, arXiv:hep-ph/9409375 [hep-ph]. 44

[71] R. Hempfling and A. H. Hoang, "Two loop radiative corrections to the upper limit of the lightest Higgs boson mass in the minimal supersymmetric model," *Phys.Lett.* **B331** (1994) 99–106, arXiv:hep-ph/9401219 [hep-ph]. 45, 61, 91

[72] S. Heinemeyer, W. Hollik, and G. Weiglein, "QCD corrections to the masses of the neutral CP - even Higgs bosons in the MSSM," *Phys.Rev.* **D58** (1998) 091701, arXiv:hep-ph/9803277 [hep-ph]. 61

[73] S. Heinemeyer, W. Hollik, and G. Weiglein, "Precise prediction for the mass of the lightest Higgs boson in the MSSM," *Phys. Lett.* **B440** (1998) 296–304, arXiv:hep-ph/9807423 [hep-ph].

[74] S. Heinemeyer, W. Hollik, and G. Weiglein, "The Masses of the neutral CP - even Higgs bosons in the MSSM: Accurate analysis at the two loop level," *Eur.Phys.J.* **C9** (1999) 343–366, arXiv:hep-ph/9812472 [hep-ph]. 61

[75] S. Heinemeyer, W. Hollik, and G. Weiglein, "The Mass of the lightest MSSM Higgs boson: A Compact analytical expression at the two loop level," *Phys.Lett.* **B455** (1999) 179–191, arXiv:hep-ph/9903404 [hep-ph]. 48

[76] S. Heinemeyer, W. Hollik, H. Rzehak, and G. Weiglein, "High-precision predictions for the MSSM Higgs sector at O(alpha(b) alpha(s))," *Eur.Phys.J.* **C39** (2005) 465–481, arXiv:hep-ph/0411114 [hep-ph]. 61

[77] R.-J. Zhang, "Two loop effective potential calculation of the lightest CP even Higgs boson mass in the MSSM," *Phys.Lett.* **B447** (1999) 89–97, arXiv:hep-ph/9808299 [hep-ph]. 66

[78] J. R. Espinosa and R.-J. Zhang, "MSSM lightest CP even Higgs boson mass to O(alpha(s) alpha(t)): The Effective potential approach," *JHEP* **0003** (2000) 026, arXiv:hep-ph/9912236 [hep-ph]. 48, 61

[79] J. R. Espinosa and R.-J. Zhang, "Complete two loop dominant corrections to the mass of the lightest CP even Higgs boson in the minimal supersymmetric standard model," *Nucl.Phys.* **B586** (2000) 3–38, arXiv:hep-ph/0003246 [hep-ph]. 48, 49, 52, 55, 61, 67, 73, 74, 91, 93, 166, 170

[80] M. S. Carena, H. Haber, S. Heinemeyer, W. Hollik, C. Wagner, *et al.*, "Reconciling the two loop diagrammatic and effective field theory computations of the mass of the lightest CP - even Higgs boson in the MSSM," *Nucl.Phys.* **B580** (2000) 29–57, arXiv:hep-ph/0001002 [hep-ph]. 48

[81] G. Degrassi, P. Slavich, and F. Zwirner, "On the neutral Higgs boson masses in the MSSM for arbitrary stop mixing," *Nucl.Phys.* **B611** (2001) 403–422, arXiv:hep-ph/0105096 [hep-ph]. 50, 51, 52, 53, 54, 55, 61, 80

[82] A. Brignole, G. Degrassi, P. Slavich, and F. Zwirner, "On the O(alpha(t)**2) two loop corrections to the neutral Higgs boson masses in the MSSM," *Nucl.Phys.* **B631** (2002) 195–218, arXiv:hep-ph/0112177 [hep-ph]. 91

[83] A. Brignole, G. Degrassi, P. Slavich, and F. Zwirner, "On the two loop sbottom corrections to the neutral Higgs boson masses in the MSSM," *Nucl.Phys.* **B643** (2002) 79–92, arXiv:hep-ph/0206101 [hep-ph].

[84] A. Dedes, G. Degrassi, and P. Slavich, "On the two loop Yukawa corrections to the MSSM Higgs boson masses at large tan beta," *Nucl.Phys.* **B672** (2003) 144–162, arXiv:hep-ph/0305127 [hep-ph]. 45, 61, 91, 93

[85] M. S. Carena, D. Garcia, U. Nierste, and C. E. Wagner, "Effective Lagrangian for the $\bar{t}bH^+$ interaction in the MSSM and charged Higgs phenomenology," *Nucl.Phys.* **B577** (2000) 88–120, arXiv:hep-ph/9912516 [hep-ph]. 45

[86] S. P. Martin, "Complete two loop effective potential approximation to the lightest Higgs scalar boson mass in supersymmetry," *Phys.Rev.* **D67** (2003) 095012, arXiv:hep-ph/0211366 [hep-ph]. 45, 61

[87] S. P. Martin, "Strong and Yukawa two-loop contributions to Higgs scalar boson self-energies and pole masses in supersymmetry," *Phys. Rev.* **D71** (2005) 016012, arXiv:hep-ph/0405022 [hep-ph]. 45

[88] S. Borowka, T. Hahn, S. Heinemeyer, G. Heinrich, and W. Hollik, "Momentum-dependent two-loop QCD corrections to the neutral Higgs-boson masses in the MSSM," arXiv:1404.7074 [hep-ph]. 45

[89] G. Degrassi, S. Di Vita, and P. Slavich, "Two-loop QCD corrections to the MSSM Higgs masses beyond the effective-potential approximation," *Eur.Phys.J.* **C75** no. 2, (2015) 61, arXiv:1410.3432 [hep-ph]. 45

[90] S. Borowka, T. Hahn, S. Heinemeyer, G. Heinrich, and W. Hollik, "Renormalization scheme dependence of the two-loop QCD corrections to the neutral Higgs-boson masses in the MSSM," *Eur. Phys. J.* **C75** no. 9, (2015) 424, arXiv:1505.03133 [hep-ph]. 45

[91] R. V. Harlander, P. Kant, L. Mihaila, and M. Steinhauser, "Higgs boson mass in supersymmetry to three loops," *Phys. Rev. Lett.* **100** (2008) 191602, arXiv:0803.0672 [hep-ph]. [Phys. Rev. Lett.101,039901(2008)]. 45

[92] P. Kant, R. Harlander, L. Mihaila, and M. Steinhauser, "Light MSSM Higgs boson mass to three-loop accuracy," *JHEP* **1008** (2010) 104, arXiv:1005.5709 [hep-ph]. 45, 47, 61

[93] D. Buttazzo, G. Degrassi, P. P. Giardino, G. F. Giudice, F. Sala, A. Salvio, and A. Strumia, "Investigating the near-criticality of the Higgs boson," *JHEP* **12** (2013) 089, arXiv:1307.3536 [hep-ph]. 45, 58, 59, 65, 69, 87, 88, 89, 90, 97, 98

[94] E. Bagnaschi, G. F. Giudice, P. Slavich, and A. Strumia, "Higgs Mass and Unnatural Supersymmetry," arXiv:1407.4081 [hep-ph]. 45, 46, 47, 57, 60, 61, 62, 64, 65, 66, 73, 81, 91, 165, 166, 170

[95] S. Heinemeyer, W. Hollik, and G. Weiglein, "FeynHiggs: A Program for the calculation of the masses of the neutral CP even Higgs bosons in the MSSM," *Comput.Phys.Commun.* **124** (2000) 76–89, arXiv:hep-ph/9812320 [hep-ph]. 45, 46, 47, 73

[96] T. Hahn, S. Heinemeyer, W. Hollik, H. Rzehak, and G. Weiglein, "High-Precision Predictions for the Light CP -Even Higgs Boson Mass of the Minimal Supersymmetric Standard Model," *Phys.Rev.Lett.* **112** no. 14, (2014) 141801, arXiv:1312.4937 [hep-ph]. 45, 46, 47, 74, 76

[97] S. Heinemeyer, S. Kraml, W. Porod, and G. Weiglein, "Physics impact of a precise determination of the top quark mass at an e^+e^- linear collider," *JHEP* **0309** (2003) 075, arXiv:hep-ph/0306181 [hep-ph]. 46

[98] S. Heinemeyer, W. Hollik, and G. Weiglein, "Electroweak precision observables in the minimal supersymmetric standard model," *Phys.Rept.* **425** (2006) 265–368, arXiv:hep-ph/0412214 [hep-ph]. 46

[99] B. Allanach, "SOFTSUSY: a program for calculating supersymmetric spectra," *Comput.Phys.Commun.* **143** (2002) 305–331, arXiv:hep-ph/0104145 [hep-ph]. 46, 47, 73

[100] B. Allanach, A. Bednyakov, and R. Ruiz de Austri, "Higher Order Corrections and Unification in the Minimal Supersymmetric Standard Model: SOFTSUSY3.5.0," arXiv:1407.6130 [hep-ph]. 46

[101] A. Djouadi, J.-L. Kneur, and G. Moultaka, "SuSpect: A Fortran code for the supersymmetric and Higgs particle spectrum in the MSSM," *Comput.Phys.Commun.* **176** (2007) 426–455, arXiv:hep-ph/0211331 [hep-ph]. 46, 47, 73, 74, 77

[102] W. Porod, "SPheno, a program for calculating supersymmetric spectra, SUSY particle decays and SUSY particle production at e+ e- colliders," *Comput.Phys.Commun.* **153** (2003) 275–315, arXiv:hep-ph/0301101 [hep-ph]. 46, 47, 73

[103] W. Porod and F. Staub, "SPheno 3.1: Extensions including flavour, CP-phases and models beyond the MSSM," *Comput.Phys.Commun.* **183** (2012) 2458–2469, arXiv:1104.1573 [hep-ph]. 46, 47

[104] P. Draper, G. Lee, and C. E. M. Wagner, "Precise Estimates of the Higgs Mass in Heavy SUSY," *Phys.Rev.* **D89** (2014) 055023, arXiv:1312.5743 [hep-ph]. 46, 47, 57, 61, 62, 64, 165, 166

[105] B. Allanach, A. Djouadi, J. Kneur, W. Porod, and P. Slavich, "Precise determination of the neutral Higgs boson masses in the MSSM," *JHEP* **0409** (2004) 044, arXiv:hep-ph/0406166 [hep-ph]. 47, 91, 93

[106] J. S. Lee, M. Carena, J. Ellis, A. Pilaftsis, and C. E. M. Wagner, "CPsuperH2.3: an Updated Tool for Phenomenology in the MSSM with Explicit CP Violation," *Comput. Phys. Commun.* **184** (2013) 1220–1233, arXiv:1208.2212 [hep-ph]. 47

[107] M. S. Carena, J. Espinosa, M. Quiros, and C. Wagner, "Analytical expressions for radiatively corrected Higgs masses and couplings in the MSSM," *Phys.Lett.* **B355** (1995) 209–221, arXiv:hep-ph/9504316 [hep-ph]. 47

[108] S. P. Martin, "Three-loop corrections to the lightest Higgs scalar boson mass in supersymmetry," *Phys.Rev.* **D75** (2007) 055005, arXiv:hep-ph/0701051 [hep-ph]. 48, 57

[109] G. Degrassi and A. Sirlin, "Gauge invariant selfenergies and vertex parts of the Standard Model in the pinch technique framework," *Phys.Rev.* **D46** (1992) 3104–3116. 52

[110] J. Espinosa and M. Quiros, "Two loop radiative corrections to the mass of the lightest Higgs boson in supersymmetric standard models," *Phys.Lett.* **B266** (1991) 389–396. 61, 62, 64

[111] J. Pardo Vega and G. Villladoro, "http://www.ictp.it/∼susyhd,". 63, 66, 85, 86, 159, 166, 169

[112] N. Arkani-Hamed, A. Gupta, D. E. Kaplan, N. Weiner, and T. Zorawski, "Simply Unnatural Supersymmetry," arXiv:1212.6971 [hep-ph]. 64

[113] **ATLAS Collaboration, CDF Collaboration, CMS Collaboration, D0 Collaboration** Collaboration, "First combination of Tevatron and LHC measurements of the top-quark mass," arXiv:1403.4427 [hep-ex]. 65, 165

[114] K. Melnikov and T. v. Ritbergen, "The Three loop relation between the MS-bar and the pole quark masses," *Phys.Lett.* **B482** (2000) 99–108, arXiv:hep-ph/9912391 [hep-ph]. 65, 87, 88

[115] T. van Ritbergen, J. Vermaseren, and S. Larin, "The Four loop beta function in quantum chromodynamics," *Phys.Lett.* **B400** (1997) 379–384, arXiv:hep-ph/9701390 [hep-ph]. 65, 87, 88

[116] M. Czakon, "The Four-loop QCD beta-function and anomalous dimensions," *Nucl.Phys.* **B710** (2005) 485–498, arXiv:hep-ph/0411261 [hep-ph]. 65, 87, 88

[117] T. A. collaboration, "Constraints on New Phenomena via Higgs Coupling Measurements with the ATLAS Detector,". 71

[118] P. Slavich, "Presentation at *The 9th Workshop of the LHC Higgs Cross Section Working Group*, 22-24 January 2015 - CERN,". 76

[119] P. Marquard, A. V. Smirnov, V. A. Smirnov, and M. Steinhauser, "Quark Mass Relations to Four-Loop Order in Perturbative QCD," *Phys.Rev.Lett.* **114** no. 14, (2015) 142002, arXiv:1502.01030 [hep-ph]. 76, 86, 87

[120] **ATLAS** Collaboration, G. Aad *et al.*, "Search for squarks and gluinos with the ATLAS detector in final states with jets and missing transverse momentum using $\sqrt{s} = 8$ TeV proton–proton collision data," *JHEP* **1409** (2014) 176, arXiv:1405.7875 [hep-ex]. 79

[121] T. Cohen, T. Golling, M. Hance, A. Henrichs, K. Howe, *et al.*, "SUSY Simplified Models at 14, 33, and 100 TeV Proton Colliders," *JHEP* **1404** (2014) 117, arXiv:1311.6480 [hep-ph]. 79

[122] S. Dimopoulos and G. Giudice, "Naturalness constraints in supersymmetric theories with nonuniversal soft terms," *Phys.Lett.* **B357** (1995) 573–578, arXiv:hep-ph/9507282 [hep-ph]. 81

[123] A. G. Cohen, D. Kaplan, and A. Nelson, "The More minimal supersymmetric standard model," *Phys.Lett.* **B388** (1996) 588–598, arXiv:hep-ph/9607394 [hep-ph].

[124] A. Pomarol and D. Tommasini, "Horizontal symmetries for the supersymmetric flavor problem," *Nucl.Phys.* **B466** (1996) 3–24, arXiv:hep-ph/9507462 [hep-ph]. 81

[125] T. Banks, "Supersymmetry and the Quark Mass Matrix," *Nucl.Phys.* **B303** (1988) 172. 81

[126] L. J. Hall, R. Rattazzi, and U. Sarid, "The Top quark mass in supersymmetric SO(10) unification," *Phys.Rev.* **D50** (1994) 7048–7065, arXiv:hep-ph/9306309 [hep-ph]. 81

[127] M. Binger, "Higgs boson mass in split supersymmetry at two-loops," *Phys.Rev.* **D73** (2006) 095001, arXiv:hep-ph/0408240 [hep-ph]. 85

[128] N. Bernal, A. Djouadi, and P. Slavich, "The MSSM with heavy scalars," *JHEP* **0707** (2007) 016, arXiv:0705.1496 [hep-ph]. 85

[129] "Wolfram Research, Inc., Mathematica, Version 10.1, Champaign, IL (2015),". 85

[130] A. V. Bednyakov and A. F. Pikelner, "Four-loop strong coupling beta-function in the Standard Model," arXiv:1508.02680 [hep-ph]. 87

[131] M. F. Zoller, "Top-Yukawa effects on the β-function of the strong coupling in the SM at four-loop level," *JHEP* **02** (2016) 095, arXiv:1508.03624 [hep-ph]. 87

[132] K. G. Chetyrkin, "Quark mass anomalous dimension to O (alpha-s**4)," *Phys. Lett.* **B404** (1997) 161–165, arXiv:hep-ph/9703278 [hep-ph]. 87, 88

[133] J. A. M. Vermaseren, S. A. Larin, and T. van Ritbergen, "The four loop quark mass anomalous dimension and the invariant quark mass," *Phys. Lett.* **B405** (1997) 327–333, arXiv:hep-ph/9703284 [hep-ph]. 87, 88

[134] K. G. Chetyrkin, J. H. Kuhn, and M. Steinhauser, "RunDec: A Mathematica package for running and decoupling of the strong coupling and quark masses," *Comput. Phys. Commun.* **133** (2000) 43–65, arXiv:hep-ph/0004189 [hep-ph]. 87

[135] K. G. Chetyrkin and M. F. Zoller, "Leading QCD-induced four-loop contributions to the β-function of the Higgs self-coupling in the SM and vacuum stability," arXiv:1604.00853 [hep-ph]. 87

[136] S. P. Martin, "Four-loop Standard Model effective potential at leading order in QCD," *Phys. Rev.* **D92** no. 5, (2015) 054029, arXiv:1508.00912 [hep-ph]. 87, 88

[137] K. Chetyrkin and M. Steinhauser, "Short distance mass of a heavy quark at order α_s^3," *Phys.Rev.Lett.* **83** (1999) 4001–4004, arXiv:hep-ph/9907509 [hep-ph]. 87, 88

[138] K. Chetyrkin and M. Steinhauser, "The Relation between the MS-bar and the on-shell quark mass at order alpha(s)**3," *Nucl.Phys.* **B573** (2000) 617–651, arXiv:hep-ph/9911434 [hep-ph]. 87, 88

[139] S. P. Martin, "Three-loop Standard Model effective potential at leading order in strong and top Yukawa couplings," *Phys.Rev.* **D89** no. 1, (2014) 013003, arXiv:1310.7553 [hep-ph]. 88

[140] S. P. Martin and D. G. Robertson, "Higgs boson mass in the Standard Model at two-loop order and beyond," *Phys. Rev.* **D90** no. 7, (2014) 073010, arXiv:1407.4336 [hep-ph]. 88

[141] B. Henning, X. Lu, and H. Murayama, "How to use the Standard Model effective field theory," *JHEP* **01** (2016) 023, arXiv:1412.1837 [hep-ph]. 95, 96, 97, 173

[142] M. K. Gaillard, "The Effective One Loop Lagrangian With Derivative Couplings," *Nucl. Phys.* **B268** (1986) 669–692. 96

[143] O. Cheyette, "Effective Action for the Standard Model With Large Higgs Mass," *Nucl. Phys.* **B297** (1988) 183–204. 96

[144] B. Henning, X. Lu, and H. Murayama, "What do precision Higgs measurements buy us?," arXiv:1404.1058 [hep-ph]. 96, 97

[145] R. Huo, "Effective Field Theory of Integrating out Sfermions in the MSSM: Complete One-Loop Analysis," arXiv:1509.05942 [hep-ph]. 96

[146] A. Drozd, J. Ellis, J. Quevillon, and T. You, "The Universal One-Loop Effective Action," arXiv:1512.03003 [hep-ph]. 96, 97

[147] C. Grojean, E. E. Jenkins, A. V. Manohar, and M. Trott, "Renormalization Group Scaling of Higgs Operators and $\Gamma(h- > \gamma\gamma)$," *JHEP* **04** (2013) 016, arXiv:1301.2588 [hep-ph]. 96

[148] J. Elias-Mir, J. R. Espinosa, E. Masso, and A. Pomarol, "Renormalization of dimension-six operators relevant for the Higgs decays $h \to \gamma\gamma, \gamma Z$," *JHEP* **08** (2013) 033, arXiv:1302.5661 [hep-ph].

[149] E. E. Jenkins, A. V. Manohar, and M. Trott, "Renormalization Group Evolution of the Standard Model Dimension Six Operators I: Formalism and lambda Dependence," *JHEP* **10** (2013) 087, arXiv:1308.2627 [hep-ph].

[150] E. E. Jenkins, A. V. Manohar, and M. Trott, "Renormalization Group Evolution of the Standard Model Dimension Six Operators II: Yukawa Dependence," *JHEP* **01** (2014) 035, arXiv:1310.4838 [hep-ph].

[151] R. Alonso, E. E. Jenkins, A. V. Manohar, and M. Trott, "Renormalization Group Evolution of the Standard Model Dimension Six Operators III: Gauge Coupling Dependence and Phenomenology," *JHEP* **04** (2014) 159, arXiv:1312.2014 [hep-ph].

[152] J. Elias-Miro, J. R. Espinosa, E. Masso, and A. Pomarol, "Higgs windows to new physics through d=6 operators: constraints and one-loop anomalous dimensions," *JHEP* **11** (2013) 066, arXiv:1308.1879 [hep-ph].

[153] J. Elias-Mir, C. Grojean, R. S. Gupta, and D. Marzocca, "Scaling and tuning of EW and Higgs observables," *JHEP* **05** (2014) 019, arXiv:1312.2928 [hep-ph]. 96

[154] J. A. Casas, J. R. Espinosa, M. Quiros, and A. Riotto, "The Lightest Higgs boson mass in the minimal supersymmetric standard model," *Nucl. Phys.* **B436** (1995) 3–29, arXiv:hep-ph/9407389 [hep-ph]. [Erratum: Nucl. Phys.B439,466(1995)]. 97

[155] A. Sirlin and R. Zucchini, "Dependence of the Quartic Coupling H(m) on M(H) and the Possible Onset of New Physics in the Higgs Sector of the Standard Model," *Nucl. Phys.* **B266** (1986) 389–409. 98

[156] M. Dine, W. Fischler, and M. Srednicki, "Supersymmetric Technicolor," *Nucl.Phys.* **B189** (1981) 575–593. 101

[157] S. Dimopoulos and S. Raby, "Supercolor," *Nucl.Phys.* **B192** (1981) 353.

[158] L. Alvarez-Gaume, M. Claudson, and M. B. Wise, "Low-Energy Supersymmetry," *Nucl.Phys.* **B207** (1982) 96.

[159] C. R. Nappi and B. A. Ovrut, "Supersymmetric Extension of the SU(3) x SU(2) x U(1) Model," *Phys.Lett.* **B113** (1982) 175.

[160] M. Dine and A. E. Nelson, "Dynamical supersymmetry breaking at low-energies," *Phys.Rev.* **D48** (1993) 1277–1287, arXiv:hep-ph/9303230 [hep-ph].

[161] M. Dine, A. E. Nelson, and Y. Shirman, "Low-energy dynamical supersymmetry breaking simplified," *Phys.Rev.* **D51** (1995) 1362–1370, arXiv:hep-ph/9408384 [hep-ph].

[162] M. Dine, A. E. Nelson, Y. Nir, and Y. Shirman, "New tools for low-energy dynamical supersymmetry breaking," *Phys.Rev.* **D53** (1996) 2658–2669, arXiv:hep-ph/9507378 [hep-ph]. 101

[163] **ATLAS** Collaboration, T. A. collaboration, "Search for Diphoton Events with Large Missing Transverse Momentum in 8 TeV pp Collision Data with the ATLAS Detector,". 103

[164] **CMS** Collaboration, C. Collaboration, "Search for supersymmetry in events with one photon, jets and missing transverse energy at sqrt(s) = 8 TeV,".

[165] **ATLAS** Collaboration, G. Aad *et al.*, "Search for nonpointing and delayed photons in the diphoton and missing transverse momentum final state in 8 TeV *pp* collisions at the LHC using the ATLAS detector," *Phys.Rev.* **D90** no. 11, (2014) 112005, arXiv:1409.5542 [hep-ex].

[166] **ATLAS** Collaboration, G. Aad *et al.*, "Search for supersymmetry in events with large missing transverse momentum, jets, and at least one tau lepton in 20 fb^{-1} of $\sqrt{s} = 8$ TeV proton-proton collision data with the ATLAS detector," *JHEP* **1409** (2014) 103, arXiv:1407.0603 [hep-ex].

[167] **ATLAS** Collaboration, G. Aad *et al.*, "Searches for heavy long-lived charged particles with the ATLAS detector in proton-proton collisions at $\sqrt{s} = 8$ TeV," *JHEP* **1501** (2015) 068, arXiv:1411.6795 [hep-ex].

[168] **CMS** Collaboration, S. Chatrchyan *et al.*, "Searches for long-lived charged particles in pp collisions at $\sqrt{s}$=7 and 8 TeV," *JHEP* **1307** (2013) 122, arXiv:1305.0491 [hep-ex].

[169] **ATLAS** Collaboration, G. Aad *et al.*, "Search for direct top squark pair production in events with a Z boson, b-jets and missing transverse momentum in sqrt(s)=8 TeV pp collisions with the ATLAS detector," *Eur.Phys.J.* **C74** no. 6, (2014) 2883, arXiv:1403.5222 [hep-ex].

[170] **CMS** Collaboration, V. Khachatryan *et al.*, "Search for neutral MSSM Higgs bosons decaying to a pair of tau leptons in pp collisions," *JHEP* **1410** (2014) 160, arXiv:1408.3316 [hep-ex]. 103

[171] " G. Salam and A. Weiler, Collider Reach (β) – http://collider-reach.web.cern.ch/,". 104

[172] J. D. Wells, "Implications of supersymmetry breaking with a little hierarchy between gauginos and scalars," arXiv:hep-ph/0306127 [hep-ph]. 107

[173] **ATLAS** Collaboration, G. Aad *et al.*, "Search for charginos nearly mass degenerate with the lightest neutralino based on a disappearing-track signature in pp collisions at $\sqrt{(s)}$=8TeV with the ATLAS detector," *Phys.Rev.* **D88** no. 11, (2013) 112006, arXiv:1310.3675 [hep-ex]. 107

[174] T. Cohen, M. Lisanti, A. Pierce, and T. R. Slatyer, "Wino Dark Matter Under Siege," *JCAP* **1310** (2013) 061, arXiv:1307.4082. 107

[175] J. Fan and M. Reece, "In Wino Veritas? Indirect Searches Shed Light on Neutralino Dark Matter," *JHEP* **1310** (2013) 124, arXiv:1307.4400 [hep-ph].

[176] A. Hryczuk, I. Cholis, R. Iengo, M. Tavakoli, and P. Ullio, "Indirect Detection Analysis: Wino Dark Matter Case Study," *JCAP* **1407** (2014) 031, arXiv:1401.6212 [astro-ph.HE].

[177] M. Low and L.-T. Wang, "Neutralino dark matter at 14 TeV and 100 TeV," *JHEP* **1408** (2014) 161, arXiv:1404.0682 [hep-ph].

[178] M. Cirelli, F. Sala, and M. Taoso, "Wino-like Minimal Dark Matter and future colliders," *JHEP* **1410** (2014) 033, arXiv:1407.7058 [hep-ph]. 107

[179] R. D. Peccei and H. R. Quinn, "CP Conservation in the Presence of Instantons," *Phys. Rev. Lett.* **38** (1977) 1440–1443. 111, 117, 118

[180] F. Wilczek, "Problem of Strong p and t Invariance in the Presence of Instantons," *Phys. Rev. Lett.* **40** (1978) 279–282. 111, 118

[181] S. Weinberg, "A New Light Boson?," *Phys. Rev. Lett.* **40** (1978) 223–226. 118, 124

[182] J. E. Kim, "Weak Interaction Singlet and Strong CP Invariance," *Phys. Rev. Lett.* **43** (1979) 103. 119, 141

[183] M. A. Shifman, A. Vainshtein, and V. I. Zakharov, "Can Confinement Ensure Natural CP Invariance of Strong Interactions?," *Nucl.Phys.* **B166** (1980) 493. 119, 141

[184] A. Zhitnitsky, "On Possible Suppression of the Axion Hadron Interactions. (In Russian)," *Sov.J.Nucl.Phys.* **31** (1980) 260. 119, 141

[185] M. Dine, W. Fischler, and M. Srednicki, "A Simple Solution to the Strong CP Problem with a Harmless Axion," *Phys.Lett.* **B104** (1981) 199. 111, 119, 141

[186] C. Vafa and E. Witten, "Parity Conservation in QCD," *Phys. Rev. Lett.* **53** (1984) 535. 111, 118

[187] G. G. Raffelt, "Astrophysical axion bounds," *Lect. Notes Phys.* **741** (2008) 51–71, `arXiv:hep-ph/0611350 [hep-ph]`. [,51(2006)]. 111, 127

[188] A. Arvanitaki, S. Dimopoulos, S. Dubovsky, N. Kaloper, and J. March-Russell, "String Axiverse," *Phys. Rev.* **D81** (2010) 123530, `arXiv:0905.4720 [hep-th]`. 111, 127

[189] A. Arvanitaki and S. Dubovsky, "Exploring the String Axiverse with Precision Black Hole Physics," *Phys. Rev.* **D83** (2011) 044026, `arXiv:1004.3558 [hep-th]`.

[190] A. Arvanitaki, M. Baryakhtar, and X. Huang, "Discovering the QCD Axion with Black Holes and Gravitational Waves," *Phys. Rev.* **D91** no. 8, (2015) 084011, `arXiv:1411.2263 [hep-ph]`. 111, 127

[191] J. Preskill, M. B. Wise, and F. Wilczek, "Cosmology of the Invisible Axion," *Phys.Lett.* **B120** (1983) 127–132. 111, 126, 128, 147

[192] L. Abbott and P. Sikivie, "A Cosmological Bound on the Invisible Axion," *Phys.Lett.* **B120** (1983) 133–136.

[193] M. Dine and W. Fischler, "The Not So Harmless Axion," *Phys.Lett.* **B120** (1983) 137–141. 111, 126, 128, 147

[194] P. Sikivie, "Experimental Tests of the Invisible Axion," *Phys. Rev. Lett.* **51** (1983) 1415–1417. [Erratum: Phys. Rev. Lett.52,695(1984)]. 112, 128

[195] L. Krauss, J. Moody, F. Wilczek, and D. E. Morris, "Calculations for Cosmic Axion Detection," *Phys. Rev. Lett.* **55** (1985) 1797. 112, 128

[196] **ADMX** Collaboration, S. J. Asztalos *et al.*, "A SQUID-based microwave cavity search for dark-matter axions," *Phys. Rev. Lett.* **104** (2010) 041301, arXiv:0910.5914 [astro-ph.CO]. 112

[197] E. Armengaud *et al.*, "Conceptual Design of the International Axion Observatory (IAXO)," *JINST* **9** (2014) T05002, arXiv:1401.3233 [physics.ins-det]. 112, 128

[198] D. Horns, J. Jaeckel, A. Lindner, A. Lobanov, J. Redondo, and A. Ringwald, "Searching for WISPy Cold Dark Matter with a Dish Antenna," *JCAP* **1304** (2013) 016, arXiv:1212.2970 [hep-ph].

[199] D. Budker, P. W. Graham, M. Ledbetter, S. Rajendran, and A. Sushkov, "Proposal for a Cosmic Axion Spin Precession Experiment (CASPEr)," *Phys. Rev.* **X4** no. 2, (2014) 021030, arXiv:1306.6089 [hep-ph]. 128

[200] A. Arvanitaki and A. A. Geraci, "Resonantly Detecting Axion-Mediated Forces with Nuclear Magnetic Resonance," *Phys. Rev. Lett.* **113** no. 16, (2014) 161801, arXiv:1403.1290 [hep-ph]. 112, 128

[201] S. Weinberg, "Phenomenological Lagrangians," *Physica* **A96** (1979) 327–340. 112, 120, 129

[202] J. Gasser and H. Leutwyler, "Chiral Perturbation Theory to One Loop," *Annals Phys.* **158** (1984) 142. 121, 131, 136, 176

[203] J. Gasser and H. Leutwyler, "Chiral Perturbation Theory: Expansions in the Mass of the Strange Quark," *Nucl.Phys.* **B250** (1985) 465. 112, 120, 129, 132, 140, 176, 177, 178

[204] M. I. Buchoff, M. Cheng, N. H. Christ, H. T. Ding, C. Jung, *et al.*, "QCD chiral transition, U(1)A symmetry and the dirac spectrum using domain wall fermions," *Phys.Rev.* **D89** no. 5, (2014) 054514, arXiv:1309.4149 [hep-lat]. 112, 129, 150

[205] A. Trunin, F. Burger, E.-M. Ilgenfritz, M. P. Lombardo, and M. Mller-Preussker, "Topological susceptibility from $N_f = 2 + 1 + 1$ lattice QCD at nonzero temperature," *J. Phys. Conf. Ser.* **668** no. 1, (2016) 012123, arXiv:1510.02265 [hep-lat]. 112, 129, 153

[206] G. 't Hooft, "Computation of the Quantum Effects Due to a Four-Dimensional Pseudoparticle," *Phys. Rev.* **D14** (1976) 3432–3450. [Erratum: Phys. Rev.D18,2199(1978)]. 116

[207] R. J. Crewther, "Effects of Topological Charge in Gauge Theories," *Acta Phys. Austriaca Suppl.* **19** (1978) 47–153. 116

[208] S. L. Adler, "Axial vector vertex in spinor electrodynamics," *Phys. Rev.* **177** (1969) 2426–2438. 116

[209] J. S. Bell and R. Jackiw, "A PCAC puzzle: pi0 –¿ gamma gamma in the sigma model," *Nuovo Cim.* **A60** (1969) 47–61.

[210] W. A. Bardeen, "Anomalous Ward identities in spinor field theories," *Phys. Rev.* **184** (1969) 1848–1857.

[211] T. A. collaboration, "Search for Diphoton Events with Large Missing Transverse Momentum in 8 TeV pp Collision Data with the ATLAS Detector,".

[212] C. A. Baker *et al.*, "An Improved experimental limit on the electric dipole moment of the neutron," *Phys. Rev. Lett.* **97** (2006) 131801, `arXiv:hep-ex/0602020 [hep-ex]`. 117

[213] R. D. Peccei and H. R. Quinn, "Constraints imposed by CP conservation in the presence of pseudoparticles," *Phys. Rev. D* **16** (Sep, 1977) 1791–1797. `http://link.aps.org/doi/10.1103/PhysRevD.16.1791`. 117, 118

[214] A. E. Nelson, "Naturally Weak CP Violation," *Phys. Lett.* **B136** (1984) 387–391. 117

[215] A. E. Nelson, "Calculation of θ Barr," *Phys. Lett.* **B143** (1984) 165–170.

[216] S. M. Barr, "A Natural Class of Nonpeccei-quinn Models," *Phys. Rev.* **D30** (1984) 1805.

[217] S. M. Barr, "A Survey of a New Class of Models of CP Violation," *Phys. Rev.* **D34** (1986) 1567. 117

[218] S. R. Coleman, J. Wess, and B. Zumino, "Structure of phenomenological Lagrangians. 1.," *Phys.Rev.* **177** (1969) 2239–2247. 119

[219] J. Callan, Curtis G., S. R. Coleman, J. Wess, and B. Zumino, "Structure of phenomenological Lagrangians. 2.," *Phys.Rev.* **177** (1969) 2247–2250. 119

[220] A. V. Manohar, "Effective field theories," in *Quarks and colliders. Proceedings, 10th Winter Institute, Lake Louise, Canada, February 19-25, 1995*. 1995. arXiv:hep-ph/9508245 [hep-ph]. 121

[221] A. Pich, "Chiral perturbation theory," *Rept. Prog. Phys.* **58** (1995) 563–610, arXiv:hep-ph/9502366 [hep-ph]. 121

[222] P. Di Vecchia and G. Veneziano, "Chiral Dynamics in the Large n Limit," *Nucl.Phys.* **B171** (1980) 253. 124

[223] M. Huang and P. Sikivie, "The Structure of Axionic Domain Walls," *Phys.Rev.* **D32** (1985) 1560. 125

[224] L. Ubaldi, "Effects of theta on the deuteron binding energy and the triple-alpha process," *Phys. Rev.* **D81** (2010) 025011, arXiv:0811.1599 [hep-ph]. 125

[225] H. Georgi, D. B. Kaplan, and L. Randall, "Manifesting the Invisible Axion at Low-energies," *Phys.Lett.* **B169** (1986) 73. 126

[226] D. J. Gross, R. D. Pisarski, and L. G. Yaffe, "QCD and Instantons at Finite Temperature," *Rev.Mod.Phys.* **53** (1981) 43. 126, 149, 150

[227] E. Berkowitz, M. I. Buchoff, and E. Rinaldi, "Lattice QCD input for axion cosmology," *Phys. Rev.* **D92** no. 3, (2015) 034507, arXiv:1505.07455 [hep-ph]. 130

[228] S. Borsanyi, M. Dierigl, Z. Fodor, S. D. Katz, S. W. Mages, D. Nogradi, J. Redondo, A. Ringwald, and K. K. Szabo, "Axion cosmology, lattice QCD and the dilute instanton gas," *Phys. Lett.* **B752** (2016) 175–181, arXiv:1508.06917 [hep-lat]. 150

[229] C. Bonati, M. D'Elia, M. Mariti, G. Martinelli, M. Mesiti, F. Negro, F. Sanfilippo, and G. Villadoro, "Axion phenomenology and θ-dependence from $N_f = 2 + 1$ lattice QCD," *JHEP* **03** (2016) 155, arXiv:1512.06746 [hep-lat]. 130, 150

[230] M. Spalinski, "CHIRAL CORRECTIONS TO THE AXION MASS," *Z.Phys.* **C41** (1988) 87–90. 131

[231] **TWQCD Collaboration** Collaboration, Y.-Y. Mao and T.-W. Chiu, "Topological Susceptibility to the One-Loop Order in Chiral Perturbation Theory," *Phys.Rev.* **D80** (2009) 034502, arXiv:0903.2146 [hep-lat]. 131

[232] T. Appelquist and J. Carazzone, "Infrared Singularities and Massive Fields," *Phys. Rev.* **D11** (1975) 2856. 131

[233] J. Bijnens and G. Ecker, "Mesonic low-energy constants," *Ann. Rev. Nucl. Part. Sci.* **64** (2014) 149–174, arXiv:1405.6488 [hep-ph]. 132, 176

[234] S. Aoki, Y. Aoki, C. Bernard, T. Blum, G. Colangelo, *et al.*, "Review of lattice results concerning low-energy particle physics," *Eur.Phys.J.* **C74** (2014) 2890, arXiv:1310.8555 [hep-lat]. 132, 176, 177

[235] D. B. Kaplan and A. V. Manohar, "Current Mass Ratios of the Light Quarks," *Phys. Rev. Lett.* **56** (1986) 2004. 133

[236] **RM123** Collaboration, G. M. de Divitiis, R. Frezzotti, V. Lubicz, G. Martinelli, R. Petronzio, G. C. Rossi, F. Sanfilippo, S. Simula, and N. Tantalo, "Leading isospin breaking effects on the lattice," *Phys. Rev.* **D87** no. 11, (2013) 114505, arXiv:1303.4896 [hep-lat]. 133, 175

[237] **MILC** Collaboration, S. Basak *et al.*, "Electromagnetic effects on the light hadron spectrum," *J. Phys. Conf. Ser.* **640** no. 1, (2015) 012052, arXiv:1510.04997 [hep-lat]. 175

[238] R. Horsley *et al.*, "Isospin splittings of meson and baryon masses from three-flavor lattice QCD + QED," arXiv:1508.06401 [hep-lat]. 133, 175

[239] F.-K. Guo and U.-G. Meiner, "Cumulants of the QCD topological charge distribution," *Phys. Lett.* **B749** (2015) 278–282, arXiv:1506.05487 [hep-ph]. 135

[240] R. Kaiser, "Anomalies and WZW term of two flavor QCD," *Phys.Rev.* **D63** (2001) 076010, arXiv:hep-ph/0011377 [hep-ph]. 136, 137

[241] B. Ananthanarayan and B. Moussallam, "Electromagnetic corrections in the anomaly sector," *JHEP* **0205** (2002) 052, arXiv:hep-ph/0205232 [hep-ph]. 136, 140

[242] J. Bijnens, L. Girlanda, and P. Talavera, "The Anomalous chiral Lagrangian of order p**6," *Eur.Phys.J.* **C23** (2002) 539–544, arXiv:hep-ph/0110400 [hep-ph]. 136, 138, 139

[243] J. F. Donoghue, B. R. Holstein, and Y. C. R. Lin, "Chiral Loops in pi0, eta0 —¿ gamma gamma and eta eta-prime Mixing," *Phys. Rev. Lett.* **55** (1985) 2766–2769. [Erratum: Phys. Rev. Lett.61,1527(1988)]. 138

[244] J. Bijnens and P. Talavera, "Pi —¿ lepton neutrino gamma form-factors at two loop," *Nucl.Phys.* **B489** (1997) 387–404, arXiv:hep-ph/9610269 [hep-ph]. 139

[245] G. F. Giudice, R. Rattazzi, and A. Strumia, "Unificaxion," *Phys. Lett.* **B715** (2012) 142–148, arXiv:1204.5465 [hep-ph]. 141

[246] M. Srednicki, "Axion Couplings to Matter. 1. CP Conserving Parts," *Nucl.Phys.* **B260** (1985) 689. 142

[247] J. Kodaira, "QCD Higher Order Effects in Polarized Electroproduction: Flavor Singlet Coefficient Functions," *Nucl. Phys.* **B165** (1980) 129–140. 143, 180

[248] E. E. Jenkins and A. V. Manohar, "Baryon chiral perturbation theory using a heavy fermion Lagrangian," *Phys. Lett.* **B255** (1991) 558–562. 144

[249] **QCDSF** Collaboration, G. S. Bali *et al.*, "Strangeness Contribution to the Proton Spin from Lattice QCD," *Phys.Rev.Lett.* **108** (2012) 222001, arXiv:1112.3354 [hep-lat]. 145, 177

[250] M. Engelhardt, "Strange quark contributions to nucleon mass and spin from lattice QCD," *Phys. Rev.* **D86** (2012) 114510, arXiv:1210.0025 [hep-lat].

[251] A. Abdel-Rehim, C. Alexandrou, M. Constantinou, V. Drach, K. Hadjiyiannakou, K. Jansen, G. Koutsou, and A. Vaquero, "Disconnected quark loop contributions to nucleon observables in lattice QCD," *Phys. Rev.* **D89** no. 3, (2014) 034501, arXiv:1310.6339 [hep-lat]. 177, 178

[252] T. Bhattacharya, R. Gupta, and B. Yoon, "Disconnected Quark Loop Contributions to Nucleon Structure," *PoS* **LATTICE2014** (2014) 141, arXiv:1503.05975 [hep-lat]. 177

[253] A. Abdel-Rehim *et al.*, "Nucleon and pion structure with lattice QCD simulations at physical value of the pion mass," *Phys. Rev.* **D92** no. 11, (2015) 114513, arXiv:1507.04936 [hep-lat]. [Erratum: Phys. Rev.D93,no.3,039904(2016)]. 177

[254] A. Abdel-Rehim, C. Alexandrou, M. Constantinou, K. Hadjiyiannakou, K. Jansen, C. Kallidonis, G. Koutsou, and A. V. Avils-Casco, "Disconnected quark loop contributions to nucleon observables using $N_f = 2$ twisted clover fermions at the physical value of the light quark mass," in *Proceedings, 33rd International Symposium on Lattice Field Theory (Lattice 2015)*. 2015. arXiv:1511.00433 [hep-lat]. http://inspirehep.net/record/1402366/files/arXiv:1511.00433.pdf. 145, 177

[255] T. Bhattacharya, S. D. Cohen, R. Gupta, A. Joseph, H.-W. Lin, and B. Yoon, "Nucleon Charges and Electromagnetic Form Factors from 2+1+1-Flavor Lattice QCD," *Phys. Rev.* **D89** no. 9, (2014) 094502, arXiv:1306.5435 [hep-lat]. 145

[256] N. Yamanaka, H. Ohki, T. Hashimoto, and T. Kaneko [JLQCD Collab.], "Nucleon axial and tensor charges with the overlap fermions," *talk presented at Lattice 2015 on 15-07-2015* . 145

[257] Z. G. Berezhiani, A. S. Sakharov, and M. Yu. Khlopov, "Primordial background of cosmological axions," *Sov. J. Nucl. Phys.* **55** (1992) 1063–1071. [Yad. Fiz.55,1918(1992)]. 147

[258] E. Masso, F. Rota, and G. Zsembinszki, "On axion thermalization in the early universe," *Phys. Rev.* **D66** (2002) 023004, arXiv:hep-ph/0203221 [hep-ph].

[259] P. Graf and F. D. Steffen, "Thermal axion production in the primordial quark-gluon plasma," *Phys. Rev.* **D83** (2011) 075011, arXiv:1008.4528 [hep-ph].

[260] A. Salvio, A. Strumia, and W. Xue, "Thermal axion production," *JCAP* **1401** no. 01, (2014) 011, arXiv:1310.6982 [hep-ph]. 147

[261] P. Sikivie, "Axion Cosmology," *Lect. Notes Phys.* **741** (2008) 19–50, arXiv:astro-ph/0610440 [astro-ph]. [,19(2006)]. 147

[262] P. Sikivie, "Of Axions, Domain Walls and the Early Universe," *Phys. Rev. Lett.* **48** (1982) 1156–1159. 148

[263] A. Vilenkin and A. E. Everett, "Cosmic Strings and Domain Walls in Models with Goldstone and PseudoGoldstone Bosons," *Phys. Rev. Lett.* **48** (1982) 1867–1870.

[264] A. Vilenkin, "Cosmic Strings and Domain Walls," *Phys. Rept.* **121** (1985) 263–315.

[265] R. L. Davis, "Cosmic Axions from Cosmic Strings," *Phys. Lett.* **B180** (1986) 225–230.

[266] D. P. Bennett and F. R. Bouchet, "Evidence for a Scaling Solution in Cosmic String Evolution," *Phys. Rev. Lett.* **60** (1988) 257.

[267] A. Dabholkar and J. M. Quashnock, "Pinning Down the Axion," *Nucl. Phys.* **B333** (1990) 815–832.

[268] G. R. Vincent, M. Hindmarsh, and M. Sakellariadou, "Scaling and small scale structure in cosmic string networks," *Phys. Rev.* **D56** (1997) 637–646, `arXiv:astro-ph/9612135 [astro-ph]`. 148

[269] M. Kawasaki, K. Saikawa, and T. Sekiguchi, "Axion dark matter from topological defects," `arXiv:1412.0789 [hep-ph]`. 148

[270] J. O. Andersen, L. E. Leganger, M. Strickland, and N. Su, "Three-loop HTL QCD thermodynamics," *JHEP* **08** (2011) 053, `arXiv:1103.2528 [hep-ph]`. 148

[271] J. Gasser and H. Leutwyler, "Light Quarks at Low Temperatures," *Phys.Lett.* **B184** (1987) 83. 148, 149

[272] J. Gasser and H. Leutwyler, "Thermodynamics of Chiral Symmetry," *Phys. Lett.* **B188** (1987) 477–481. 148, 149

[273] J. O. Andersen, "Chiral perturbation theory in a magnetic background - finite-temperature effects," *JHEP* **1210** (2012) 005, `arXiv:1205.6978 [hep-ph]`. 148

[274] F. C. Hansen and H. Leutwyler, "Charge correlations and topological susceptibility in QCD," *Nucl. Phys.* **B350** (1991) 201–227. 149

[275] P. Gerber and H. Leutwyler, "Hadrons Below the Chiral Phase Transition," *Nucl.Phys.* **B321** (1989) 387. 149

[276] G. 't Hooft, "Computation of the Quantum Effects Due to a Four-Dimensional Pseudoparticle," *Phys.Rev.* **D14** (1976) 3432–3450. 150

[277] C. W. Bernard, "Gauge Zero Modes, Instanton Determinants, and QCD Calculations," *Phys.Rev.* **D19** (1979) 3013. 150

[278] T. Morris, D. Ross, and C. T. Sachrajda, "Higher Order Quantum Corrections in the Presence of an Instanton Background Field," *Nucl.Phys.* **B255** (1985) 115. 150

[279] A. D. Linde, "Infrared Problem in Thermodynamics of the Yang-Mills Gas," *Phys. Lett.* **B96** (1980) 289–292. 150

[280] A. K. Rebhan, "The NonAbelian Debye mass at next-to-leading order," *Phys. Rev.* **D48** (1993) 3967–3970, arXiv:hep-ph/9308232 [hep-ph]. 150

[281] P. B. Arnold and L. G. Yaffe, "The NonAbelian Debye screening length beyond leading order," *Phys. Rev.* **D52** (1995) 7208–7219, arXiv:hep-ph/9508280 [hep-ph]. 150

[282] K. Kajantie, M. Laine, J. Peisa, A. Rajantie, K. Rummukainen, and M. E. Shaposhnikov, "Nonperturbative Debye mass in finite temperature QCD," *Phys. Rev. Lett.* **79** (1997) 3130–3133, arXiv:hep-ph/9708207 [hep-ph]. 150

[283] O. Philipsen, "Debye screening in the QCD plasma," in *Strong and electroweak matter. Proceedings, Meeting, SEWM 2000, Marseille, France, June 13-17, 2000*, pp. 95–106. 2000. arXiv:hep-ph/0010327 [hep-ph]. http://alice.cern.ch/format/showfull?sysnb=2227150.

[284] **WHOT-QCD** Collaboration, Y. Maezawa, N. Ukita, S. Aoki, S. Ejiri, T. Hatsuda, N. Ishii, and K. Kanaya, "Heavy-quark free energy, debye mass, and spatial string tension at finite temperature in two flavor lattice QCD with Wilson quark action," *Phys. Rev.* **D75** (2007) 074501, arXiv:hep-lat/0702004 [hep-lat]. 150

[285] P. Petreczky, H.-P. Schadler, and S. Sharma, "The topological susceptibility in finite temperature QCD and axion cosmology," arXiv:1606.03145 [hep-lat]. 150

[286] S. Borsanyi *et al.*, "Lattice QCD for Cosmology," arXiv:1606.07494 [hep-lat]. 150

[287] O. Philipsen, "The QCD equation of state from the lattice," *Prog. Part. Nucl. Phys.* **70** (2013) 55–107, arXiv:1207.5999 [hep-lat]. 152

[288] S. Borsanyi, Z. Fodor, C. Hoelbling, S. D. Katz, S. Krieg, and K. K. Szabo, "Full result for the QCD equation of state with 2+1 flavors," *Phys. Lett.* **B730** (2014) 99–104, arXiv:1309.5258 [hep-lat]. 152

[289] **Planck** Collaboration, P. A. R. Ade *et al.*, "Planck 2015 results. XX. Constraints on inflation," arXiv:1502.02114 [astro-ph.CO]. 154

[290] A. D. Linde, "Generation of Isothermal Density Perturbations in the Inflationary Universe," *Phys. Lett.* **B158** (1985) 375–380. 155

[291] J. Hamann, S. Hannestad, G. G. Raffelt, and Y. Y. Y. Wong, "Isocurvature forecast in the anthropic axion window," *JCAP* **0906** (2009) 022, arXiv:0904.0647 [hep-ph]. 155

[292] Y. Yamada, "Gauge dependence of the on-shell renormalized mixing matrices," *Phys.Rev.* **D64** (2001) 036008, arXiv:hep-ph/0103046 [hep-ph]. 169

[293] F. Sanfilippo, "Quark Masses from Lattice QCD," *PoS* **LATTICE2014** (2015) 014, arXiv:1505.02794 [hep-lat]. 175, 176

[294] R. Mawhinney [RBC and U. Collaborations], "NLO and NNLO low energy constants for SU(3) chiral perturbation theory," *talk given at Lattice 2015, Japan, July 2015* . 177

[295] P. A. Boyle *et al.*, "Low energy constants of SU(2) partially quenched chiral perturbation theory from N_f=2+1 domain wall QCD," *Phys. Rev.* **D93** no. 5, (2016) 054502, arXiv:1511.01950 [hep-lat]. 177

[296] G. Altarelli and G. G. Ross, "The Anomalous Gluon Contribution to Polarized Leptoproduction," *Phys.Lett.* **B212** (1988) 391. 180

[297] S. A. Larin, "The Renormalization of the axial anomaly in dimensional regularization," *Phys. Lett.* **B303** (1993) 113–118, arXiv:hep-ph/9302240 [hep-ph]. 180